EVALUATION AND DESIGN OF PERMEABLE REACTIVE BARRIERS AMIDST HETEROGENEITY

by

Carl R. Elder

A dissertation submitted in partial fulfillment of
the requirements for the degree of

Doctor of Philosophy
(Civil and Environmental Engineering)

at the

University of Wisconsin – Madison
2000

ABSTRACT

EVALUATION AND DESIGN OF PERMEABLE REACTIVE BARRIERS AMIDST HETEROGENEITY

Carl R. Elder

Under the Supervision of Professor Craig H. Benson

Permeable reactive barriers (PRBs) are *in-situ* walls constructed from porous media that react with groundwater contaminants which enter the PRB. PRBs provide containment if there is sufficient residence time of contaminants in the reactive media for rate-limited reactions to occur. Currently, PRBs are designed assuming the aquifer and PRB are homogeneous and isotropic. This study investigated the impact of aquifer and PRB heterogeneity on influent and effluent from three types of PRB, a horizontal flow PRB (HFPRB), a funnel and gate PRB (FGPRB), and a caisson PRB (CPRB).

Spatial variability in the reaction rate constant (k_r) and hydraulic conductivity (K_P) of the PRB and variations in the mean (μ_{lnK}), standard deviation (σ_{lnK}), and correlation scale of the logarithm of hydraulic conductivity (lnK) of the aquifer were considered. Spatial variability of k_r and K_P was found to have a minor effect on influent and effluent concentrations. Correlation scale of the aquifer hydraulic conductivity parallel to flow, which describes the length of geologic units, had a modest effect, with larger correlation scales yielding higher effluent concentrations. The log-mean (μ_{lnK}) and log-standard deviation (σ_{lnK}) of

aquifer hydraulic conductivity, which describe the geometric mean and spread of hydraulic conductivity, have the greatest impact on influent and effluent concentrations from a PRB. Decreasing μ_{lnK} (i.e., lowering the hydraulic conductivity) does not affect influent concentrations, but decreases median effluent concentrations and broadens the distribution of effluent concentration due to increased residence time in the PRB. Increasing σ_{lnK} (i.e., increasing the range of hydraulic conductivities of the aquifer) decreases the median influent concentration and broadens the distribution of influent concentrations as a result of additional dispersion in a more heterogeneous aquifer. Larger σ_{lnK} also results in higher median effluent concentrations and broader distributions of effluent concentration.

Recommendations for PRB design are made in the second half of this report. The FGPRB was determined to be the most economical PRB design and the HFPRB the least economical design. Design of PRBs using a plug-flow model and factor of safety of two is sufficient for PRBs in aquifers with $\sigma_{lnK} < 1.0$, but factors of safety greater than ten may be needed in aquifers with $\sigma_{lnK} = 4.0$. Scaling factors to be used with plug-flow models are suggested for all types of PRBs. Scaling factors are similar to factors of safety except they are functions of μ_{lnK}, σ_{lnK} and correlation scale, and allow the designer to incorporate risk into PRB design. Several monitoring systems are tested and the lateral and vertical spacing between well screens that maximize the probability of detection per well screen are recommended for each type of PRB. Also, the ability of gravel zones

adjacent to the influent and effluent faces of the PRB to cause more uniform residence times of groundwater in the reactive media and lower effluent concentrations is assessed. Gravel zones do yield more uniform residence times, but provide a more conductive path for groundwater flow through the reactive media, increasing effluent concentrations for all PRBs except a HFPRB in aquifers with $\sigma_{lnK} < 2.3$.

Given these results, recommendations for future PRB design are to place greater importance on aquifer characterization and PRB selection. The aquifer parameters σ_{lnK} and μ_{lnK} strongly impact effluent concentrations. PRB design should begin with adequate aquifer characterization to choose a PRB type and scaling factor that corresponds to a low risk of failure. Then, economical monitoring systems that verify the proper operation of the PRB and have a reasonable chance of detecting higher effluent concentrations can be used. However, it is unlikely that peak concentrations (i.e., greater then the 95^{th} percentile) will be detected even with dense monitoring.

ACKNOWLEDGEMENTS

I would like to thank Dr. Craig Benson and Dr. Gerald Eykholt for their guidance during the last five years. Craig and Jerry's cooperation, patience, and encouragement exemplify the role of a mentor and I thank them for the knowledge that they have given me. I would also like to thank Dr. Tuncer Edil, Dr. Mary Anderson, and Dr. John Hoopes for serving on my committee and for their contributions to my education in and out of the classroom. Thanks are extended to my past and present colleagues for their insight and entertainment. Finally, my most sincere thanks are expressed to my lovely wife Amy, who over the last five years has been a continual source of inspiration and unwavering support.

Financial support for this study was provided by the Wisconsin Ground Water Research Advisory Council (GRAC), which is administered through the University of Wisconsin System Water Resources Center. The findings and opinions expressed herein are those of the authors and are not necessarily consistent with the policies and opinions of GRAC.

TABLE OF CONTENTS

TABLE OF FIGURES

TABLE OF TABLES

SECTION 1

INTRODUCTION

Permeable reactive barriers (PRBs) are in situ walls of reactive media that are down-gradient of a contaminant plume. Dissolved contaminants are transported toward the PRB by ambient groundwater flow where they are treated as they pass through the barrier (Fig. 1.1) (Blowes et al. 1995). In general, PRBs are aligned perpendicular to groundwater flow and may stand-alone or be used as part of a funnel and gate system. PRBs are considered a containment technology because they restrict the transport of contaminants; however, PRBs do not impede the flow of groundwater because the hydraulic conductivity of the PRB is greater than the hydraulic conductivity of the aquifer.

PRBs usually rely on chemical reactions between the contaminant and a reactive media to transform or immobilize contaminants in the groundwater. In properly designed PRBs, the concentration of effluent from the PRB complies with a groundwater standard or other pre-established target concentration. However, designing PRBs that operate properly in heterogeneous aquifers is difficult and the current design method may be inadequate under some conditions (Eykholt 1997).

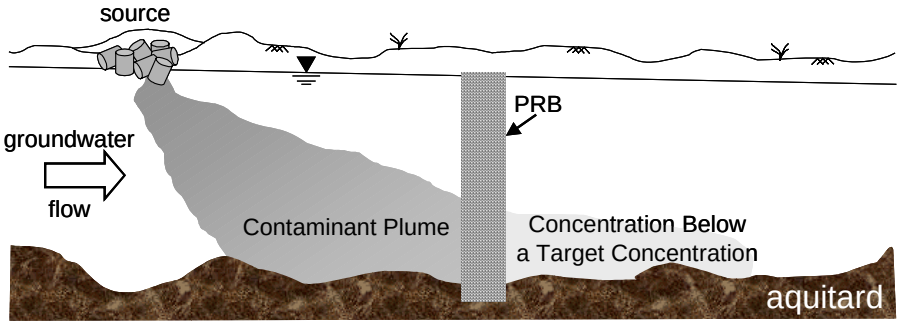

Fig. 1.1 Schematic of a PRB (adapted from Eykholt 1997).

PRBs have been proposed for containment of many contaminants including heavy metals, radioactive waste, petroleum products, industrial chemicals including both LNAPLs and DNAPLs, and fertilizers (Cantrell et al. 1994, Blowes et al. 1995, Shoemaker et al. 1995, Benner et al. 1997). Each contaminant may require a unique reactive media, but the principle of transforming or immobilizing contaminants as they pass through the PRB is the same regardless of the target contaminant.

The advantages of PRBs are that they immobilize or transform contaminants in situ, causing little long-term surface disturbance so that site operations continue while remediation takes place. Also, PRBs treat recalcitrant compounds such as chlorinated solvents, heavy metals, and radionuclides. These are ubiquitous contaminants that are difficult to remove using conventional methods of remediation such as pump and treat. Finally, PRBs are designed to operate passively for several decades. This is perhaps the biggest advantage of PRBs because long-term operation and maintenance costs are minimal and there is no chance of mechanical failures causing the system to shut down.

A disadvantage of PRBs is that there is limited guidance for their design and monitoring. The current design method uses a plug-flow model to estimate residence time of groundwater in the PRB and a first order reaction equation to predict the level of contaminant reduction. A global factor of safety is then applied to account for differences between model assumptions and natural conditions such as variability in groundwater flow and uncertainty in the reactivity of the media.

The purpose of this study was to understand how PRBs operate amidst heterogeneity. The first half of this report assesses how aquifer and PRB heterogeneity affect influent and effluent concentrations from three types of PRBs. Once these factors are understood, the second half of this report suggests a risk-based design method for PRBs and monitoring schemes that account for aquifer and PRB heterogeneity. In particular, the study considers variability in the hydraulic conductivity of the aquifer surrounding the PRB, variability in the hydraulic conductivity of the PRB, and uncertainty in the reactivity of the PRB.

The goals of this study were to identify key parameters that control the reliability of PRBs, evaluate the current method used for designing PRBs, and develop guidelines for uncertainty-based design of PRBs. The anticipated benefits of this project are a better understanding of factors that control the effectiveness of PRBs, and recommend improvements for designing and monitoring PRBs. In addition, components for risk-based analysis of PRBs operation are suggested, which allow designers and regulators to more clearly quantify performance standards for PRBs and incorporate PRBs into exposure models. The outcomes of this research are an advancement to science and engineering because they improve our understanding of the hydraulics of PRBs and suggest design strategies that yield safer, more economical, and more reliable PRBs.

This report is divided into twelve sections. Sections Two and Three are background sections that provide an overview of PRBs and geostatistics, respectively. A summary of reaction mechanisms, design strategies, and the advantages and disadvantages of PRBs is included in Section Two. Section Three

is a review of geostatistics with an emphasis on second-order stationary random fields that can be used to simulate geological heterogeneity. Methods used to simulate flow and mass removal in a PRB are explained in Section Four. The conceptual model for a PRB in a heterogeneous aquifer is also presented in Section Four. Sections Five, Six, and Seven present results of a parametric study on aquifer and PRB heterogeneity for each type of PRB. Section Eight compares the three types of PRBs from a performance and economic perspective. Section Nine is an evaluation of the current design model for PRBs and the introduction of a risk-based design model for PRBs. Section Ten presents recommendations for monitoring PRBs and Section Eleven is a brief discussion of additional design considerations for PRBs. Conclusions for the study are made in Section Twelve.

SECTION 2

PERMEABLE REACTIVE BARRIERS

Permeable reactive barriers (PRBs) are a new technology used for containment of contaminated groundwater. These contaminants may be chlorinated solvents, radioactive isotopes, petroleum compounds, mine waste, or septic discharge (Blowes et al. 1995). Significant laboratory research and some field demonstrations have been performed to assess the usefulness of PRBs as a containment technology. This section provides an overview of this research and discusses the physical and chemical principles of PRBs. Particular attention is paid to PRBs constructed from iron metal that are used for containment of chlorinated ethylene compounds. Additionally, an update of current design, installation, and monitoring methods for PRBs will be covered.

2.1 OVERVIEW OF PERMEABLE REACTIVE BARRIERS

2.1.1 Description of Permeable Reactive Barriers

In 1994, the US had approximately 300,000 to 400,000 hazardous waste sites representing a $750 billion remediation cost over the next 30 years. The most common method of remediation for these sites is pump and treat (NAS 1994). Although pump and treat is common, its effectiveness at achieving groundwater concentrations of organic chemicals in the part-per-billion (ppb) range is uncertain (O'Hannesin and Gillham 1998). The high cost and uncertain effectiveness of pump and treat has spawned the development of innovative new containment and

remedial technologies during the last 20 years (e.g., in-situ air sparging, waste stabilization, and slurry walls).

Permeable reactive barriers are an in situ containment structure that have advanced from an engineering concept to field application during the 1990's (Sims et al. 1991). Permeable reactive barriers consist of a reactive media placed in situ and down gradient of a contaminant source or plume. Composition of the reactive zone may vary; however, the hydraulic conductivity of the zone is designed to be greater than or equal to the surrounding aquifer so that the PRB does not impede groundwater flow.

Figure 2.1 shows a conceptualization of a PRB intercepting an aqueous phase plume. Contaminated groundwater or mobile NAPL is transported into the PRB by natural gradients. Once contaminant enters the PRB, it is removed, immobilized, or transformed by chemical, biological, or physical means. Groundwater which is stripped of the contaminant (to a level that complies with a pre-specified standard such as a MCL) exits the barrier (Gillham 1995, Blowes et al. 1995). In this regard, PRBs differ from other containment technologies because they do not prevent off-site migration of groundwater, only the migration of contaminants. Furthermore, PRBs rely on natural gradients to transport contaminants into an in situ reactive zone where as other remediation methods rely on induced gradients and *ex-situ* treatment (e.g., pump and treat, soil vapor extraction).

Table 2-1 provides a summary of the target contaminants, media used for treating groundwater contaminated with these compounds, and the current level of

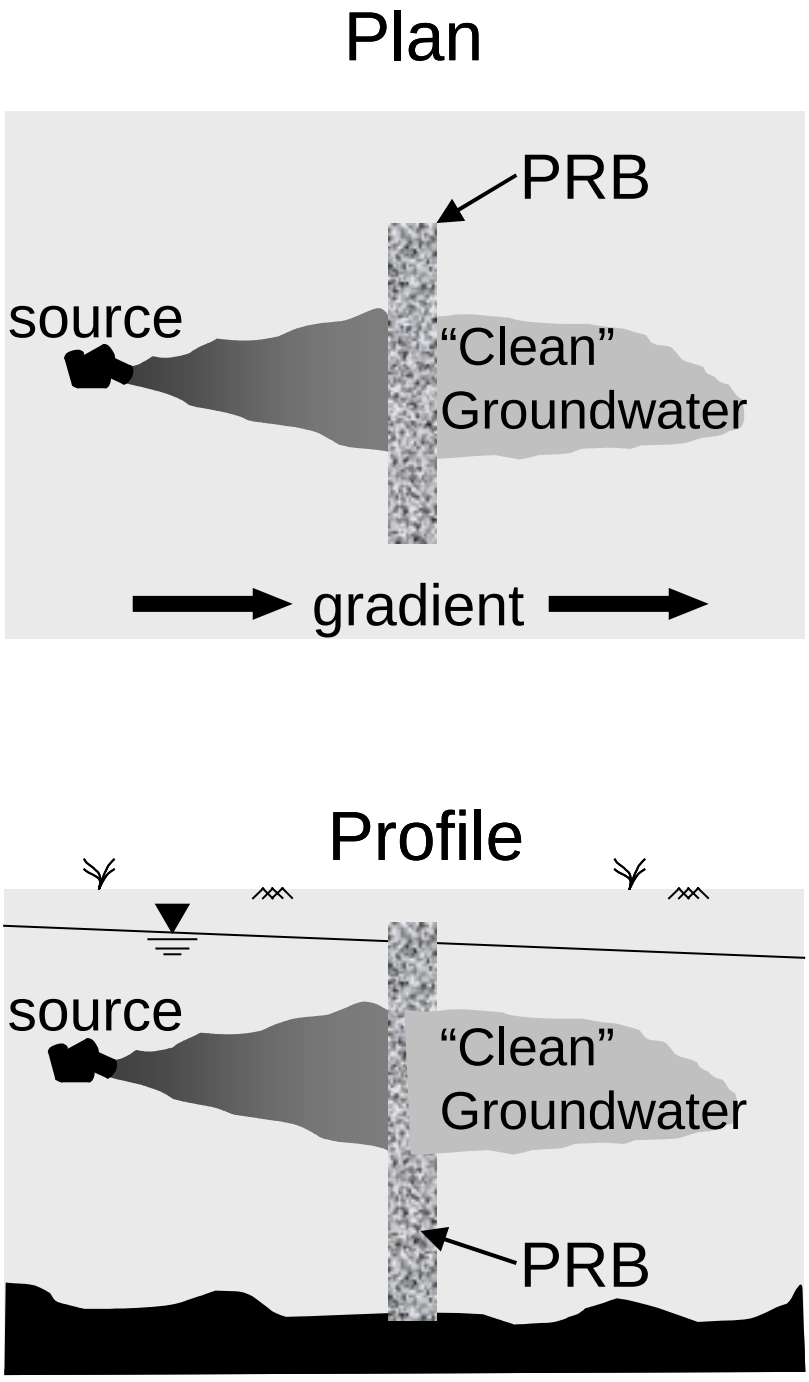

Fig. 2.1 Conceptualization of a PRB Intercepting a Contaminant Plume (adapted from Blowes et al. 1995).

development for each of these combinations (Shoemaker et al. 1995). The most common application of PRBs is for containment of chlorinated ethylene compounds (tetrachloroethylene (PCE), trichloroethylene (TCE), dichloroethylene (DCE), and vinyl chloride) because these contaminants are a ubiquitous and persistent source of groundwater contamination and are difficult to remediate with conventional methods (O'Hannesin and Gillham 1998). However, PRBs have been used for a wide range of groundwater contaminants from acid mine drainage to radioactive isotopes (Farrell et al. 1999, Benner et al. 1997, Charlet et al. 1998, EPA 1999).

Table 2-1 Target Compounds for PRBs, Reactive Media and Level of Development (Adapted from Shoemaker et al. 1995).

Target Compound	Reactive Media	Level of Development
Halogenated Organics (ethylene and ethane)	Metals (Fe, Zn, Mg, Al)	Commercial Market
Inorganics (Cr, TcO_4, UO_4, CrO_4, MoO_4)	Metals (Fe, Zn)	Pilot-Scale Testing
Petroleum Compounds (BTEX)	Peat, Compost, Activated Carbon, Coal, Tire Chips	Field Demonstration
Metals (Mine Waste) (Fe, As, Cd, Cu, Ni, Pb, Zn)	Compost, Wood Chips, Calcium Phosphate	Field Demonstration
Septic Waste (phosphorus, nitrogen)	Air, Oxygen Release Compound	Laboratory Testing
Radioactive Isotopes (Uranium)	Iron Metal	Laboratory Testing

2.1.2 Reaction Mechanisms

Permeable reactive barriers are a versatile containment option because they are a passive means for stripping contaminants from groundwater and they can be

applied to different sites and contaminants by choosing an appropriate reactive media. Reactive media are selected for PRBs based on their effectiveness to treat site-specific contaminants. This section discusses the transformation, immobilization, and removal mechanisms occurring in PRBs, target compounds for these processes, and candidate media.

2.1.2.1 Precipitation

Precipitation is an immobilization mechanism that may be used to remove heavy metals from groundwater. PRBs constructed of media containing slightly soluble salts or sulfate-reducing bacteria are effective at removing heavy metals from groundwater. Salts from the barrier or produced by the bacteria dissolve into the groundwater and form complexes with the aqueous phase heavy metals (McGregor et al. 1998). Heavy metal complexes tend to have a lower solubility than the metal ions and thus precipitate out of groundwater within or down-gradient of the PRB (Shoemaker et al. 1995, Eykholt and Sivavec 1995, EPA 1997).

Another method for inducing precipitation is to alter the pH of groundwater passing through the barrier. This changes the solubility of salts in solution. Benner et al. (1997) report on a PRB constructed from 20% municipal compost, 20% leaf compost, 10% wood chips, and 50% pea-gravel. The PRB is designed to increase the pH of acid mine drainage containing Fe, As, Cd, Cu, Ni, Pb, and Zn. Under more basic conditions, metal salts precipitate. Benner et al. (1997) report greater than 90% removal of metals from groundwater using a 4 m wide barrier with an average groundwater velocity of 0.04 m/d. The barrier has an expected

design life of 15 years, after which excavation and disposal of the zones where the metals precipitated is required for complete remediation (Benner et al. 1997, Hebert et al. 1998).

2.1.2.2 Volatilization and Biodegradation

Volatilization is a removal mechanism and biodegradation is a transformation mechanism that can be used for removing petroleum-based compounds (BTEX) or septic waste (i.e. nitrogen and phosphorus) from groundwater (Blowes et al. 1995, Norris and Wilson 1996, Zwiren and Woodford 1997, Warner et al. 1998). Barriers that rely on volatilization and biodegradation are constructed from coarse-grained media that have air injected through them, or permeable media containing oxygen release compounds (ORCs). For PRBs that have air injected through them, contaminants entering the PRB volatilize into the air stream, and are carried to the ground surface where they are collected or released to the atmosphere (Pankow et al. 1993). Also, oxygen transferred into groundwater from the injected air or released by ORC increases the concentration of dissolved oxygen in the groundwater, which promotes aerobic biodegradation of contaminants within and down-gradient of the PRB (Payne et al. 1996, Zwiren and Woodford 1997).

Zwiren and Woodford (1997) compare the benzene removal rates for PRBs containing ORC to PRBs sparged with air. They conclude that both types of PRBs are effective at removing benzene, but sparged air PRBs are more economical when total petroleum hydrocarbon concentrations exceed 5 mg/L or the average

groundwater velocity is greater than 0.15 m/d (Zwiren and Woodford 1997). An advantage of PRBs that rely of biodegradation and volatilization is that they do not require future excavation and disposal on the media. However, sparged air barriers have higher operation costs than passive PRBs.

2.1.2.3 Sorption

Sorption is an immobilization or retardation mechanism that can be used to reduce the mobility of organic chemicals and metals in groundwater. Potential media are activated carbon, straw, wood chips, peat, coal, shale, paper sludge, and tire chips (Rael et al. 1995, Kershaw and Pamukcu 1997, Moo and Young 1998). The mobility of organic chemicals or metals entering a PRB constructed from these materials is reduced because the contaminants sorb to the media. Final disposal of the sorbed chemicals is designed to occur over time by natural or enhanced degradation (biodegradation, rate-limited reactions, or decay) within the barrier or by excavation of the contaminant laden sorbent (Kershaw and Pamukcu 1997).

2.1.2.4 Oxidation-Reduction

Oxidation-reduction reactions can be used to remove inorganic contaminants or halogenated organic compounds from groundwater. Some inorganic contaminants will precipitate if their valence state is altered (Eykholt and Sivavec 1995, Shoemaker et al. 1995, Farrell et al. 1999). For example, if a PRB is constructed from iron metal, dissolved Cr^{+6} will be reduced to Cr^{+3}. The solubility

of Cr^{+3} is lower than the solubility of Cr^{+6}; thus, a complex of Cr^{+3} will precipitate. Similar reactions occur for TcO_4^-, UO_2^{+2}, CrO_4^-, U(VI) and MoO_4^{-2} when exposed to iron metal (Cantrell et al. 1994, Farrell et al. 1999).

Iron metal can be used for reducing halogenated compounds. Reduction by the metal results in consecutive loss of one halogen atom and replacement by a hydrogen atom. Ultimately, ethylene or ethane are produced as benign products (Roberts et al. 1996, Arnold et al. 1998, Burris et al. 1998). Halogen ions that are removed during the reaction dissolve in groundwater or form mineral salts. Reductive dehalogenation of chlorinated ethylene compounds is the focus of this study because approximately two-thirds of current PRBs are constructed for containment of chlorinated solvents (Jarre and Kociolek 1999).

2.1.3 Requirements, Advantages, and Disadvantages of Permeable Reactive Barriers

2.1.3.1 Requirements

Permeable reactive barriers can be an affordable, long-term strategy for containing groundwater contaminants. However, the effectiveness of PRBs is contingent on several criteria. The media selected for a PRB has to be reactive with the target contaminants but products from the reaction or the medium itself cannot produce toxic effluent (Blowes et al. 1995). The medium also has to be economical, as persistent as the groundwater contaminant, and maintain its reactivity throughout the design life of the PRB (years to decades) (Benner et al. 1997, Shoemaker et al. 1995). Finally, the PRB must be designed such that the

residence time of contaminants in the barrier is adequate for rate-limited reactions to occur (Shoemaker et al. 1995, O'Hannesin and Gillham 1998). For some sites, PRBs are not practical or cost-effective because of excessive depth or groundwater velocity. However, innovative styles of PRBs and developing construction methods are making PRBs viable for a wider range of sites.

2.1.3.2 Advantages

Zero valent metals, particularly zero valent iron (Fe^0), are the most common reactive media for PRBs (i.e., iron-walls). The advantage of PRBs containing iron metal is that they can reduce the concentration of chlorinated ethylene compounds (PCE, TCE, DCE, and vinyl chloride) in groundwater to concentrations in the low part-per-billion (ppb) range. This level of removal is difficult to achieve using conventional methods (O'Hannesin and Gillham 1998). Also, PRBs have lower operation and maintenance costs than most other remedial methods because they rely on natural gradients to carry contaminants into the treatment zone (Rael et al. 1995, O'Hannesin and Gillham 1998). Additionally, commercial grade cast iron metal is an ideal reactive media for reducing halogenated compounds because it is economical, and is believed to maintain its reactivity for several years.

The popularity of PRBs is also leading to faster and cheaper installation methods and less surface disturbance. For plumes containing a mixture of contaminants, PRBs can be built in series or made from a blend of reactive media. This allows several contaminants to be stripped from the groundwater simultaneously (Rael et al. 1995).

2.1.3.3 Disadvantages

Permeable reactive barriers are a reasonable means for containing contaminated groundwater, but they do have limitations and disadvantages. Like any new technology, there is a dearth of long-term data available on reactivity and durability of iron, although current testing is yielding optimistic results that losses are small (O'Hannesin and Gillham 1998, Fort 2000). Also, intermediates and by-products of reduction reactions are halogenated compounds posing some risk and questions about toxicity. For example, two by-products of the reduction of PCE are dichloroacetylene and chloroacetylene, which are toxic. Also, an intermediate in the reduction of PCE, TCE, and DCE is vinyl chloride, which is more toxic than any of the initial compounds (Roberts et al. 1996, Arnold et al. 1998). If incomplete reduction occurs, PRBs can transform influent containing less toxic groundwater into a more toxic effluent containing vinyl chloride. Incomplete reduction can occur if the residence time of contaminant in the barrier is too short or if excessive precipitation occurs on the iron and reduces its reactivity (Rael et al. 1995, Eykholt and Sivavec 1995, Schlimm and Heitz 1996).

Another disadvantage of PRBs is that current construction methods are uneconomical for excavations deeper than 30 m. Thus, PRBs are not well suited for sites with deep water tables or plumes (Blowes et al. 1995). This is a significant limitation since chlorinated solvents tend to have a density greater than one and move downward through an aquifer. Furthermore, PRBs are prone to uncertainty in groundwater flow, reactivity of the media, and hydraulic conductivity of the barrier (Gavaskar et al. 1998, Eykholt et al. 1999). Incomplete reduction can occur

in zones of low reactivity or high flow rate and cause concentrations of vinyl chloride in the effluent to exceed target concentrations (Rael et al. 1995).

2.2 REDUCTIVE DECHLORINATION OF ETHYLENE COMPOUNDS

2.2.1 Reducing Materials

The principle application of PRBs is for containment of PCE, TCE, DCE, and vinyl chloride. Zero valent metals are often used as electron donors for reduction reactions. Metals that have been investigated are aluminum, zinc, magnesium, and iron. Aluminum is the most reactive of the metals, but reactions with aluminum form salts that precipitate on the metal and ultimately lower its reactivity. Zinc shows excellent durability and follows aluminum in order of reactivity, but is seldom used due to its cost and zinc groundwater standard. Magnesium may be used, but it has the lowest reactivity of the metals (Schlimm and Heitz 1996). This leaves iron, which has reactivity between zinc and magnesium and is commercially available in large quantities at a reasonable cost (Roberts et al. 1996). Also, iron is durable enough for PRBs to have a design life of 10 to 15 years (Schlimm and Heitz 1996). These advantages have made iron metal the most common reactive media for containment of groundwater contaminated with chlorinated ethylenes.

2.2.2 Oxidation-Reduction of Chlorinated Species by Metal

Reduction of halogenated organic compounds by a metal (hydrogenolysis, dehydro-halogenation, or reductive elimination) involves oxidation of a metal and

reduction of the halogenated organic and water. Equation 2.1 is the general form of anodic metal dissolution that occurs when a metal donates electrons.

$$M = M^{z+} + z\,e^{-} \qquad (2.1)$$

where M is a metal and z is the number of equivalents of electrons released during the reaction. When iron or zinc is the metal, z equals two. The electrons released by the metal reduce the alkene by the Heyoski reaction:

$$R-Cl \; + \; H^{+} \; + \; 2e^{-} \; \rightarrow \; R-H \; + \; Cl^{-} \qquad (2.2)$$

where R-Cl denotes a chlorinated alkene, R-H denotes a dechlorinated alkene, H^{+} denotes a hydrogen ion (which is assumed to be available in groundwater), and Cl^{-} denotes a chloride ion. Concurrently, water is reduced to yield hydrogen gas and hydroxide ions (Schlimm and Heitz 1996):

$$2H_2O \; + \; 2e^{-} \; \rightarrow \; H_{2(g)} \; + \; 2OH^{-} \qquad (2.3)$$

By-products of these reactions are M^{+2}, Cl^{-}, $H_{2(g)}$, and OH^{-}. The M^{+2} and Cl^{-} ions go into solution. Chloride ions can form salts with naturally occurring minerals in the groundwater and precipitate. Reduction of water yields $H_{2(g)}$, which is released to the atmosphere or dissolves into groundwater. The hydroxide ions remain in

solution, raising the alkalinity of the groundwater (Roberts et al 1996, Arnold et al. 1998).

2.2.3 Reduction of Chlorinated Ethylene Compounds by Iron and Zinc

Roberts et al. (1996) and Arnold et al. (1998) have defined the pathway for reduction of polychlorinated ethylene by iron and zinc metal (Fig. 2.2). Each successive reduction involves oxidation of a metal (Eq. 2.1) and reduction of the alkene and water (Eq. 2.2 and 2.3). Thermodynamically, the most favorable pathway for reduction of PCE to ethylene is through the chlorinated acetylene compounds (Arnold et al. 1998). The most favorable ethane pathway is through TCE, cis-DCE, and vinyl chloride (hydrogenolysis) when iron is the reducing agent and through *trans*-DCE when zinc is the reducing agent (Roberts et al. 1996, O'Hannesin and Gillham 1998, Arnold et al. 1998).

There are three main reaction mechanisms that can occur between the chlorinated ethylene species and the metal: reductive elimination, dehydrohalogenation, and hydrogenolysis. Each reaction is shown in Fig. 2.2. Reductive elimination involves the loss of two halogen ions and an increase in bond order (i.e., double bond to a triple bond). The reactions are an alpha-elimination when halogens are removed from the same carbon atom and a beta-elimination when halogens are removed from separate carbon reactions. Alpha-elimination is not believed to occur during dehalogenation of the ethylene species shown in Fig. 2.2, but beta-elimination is believed to occur, especially when the

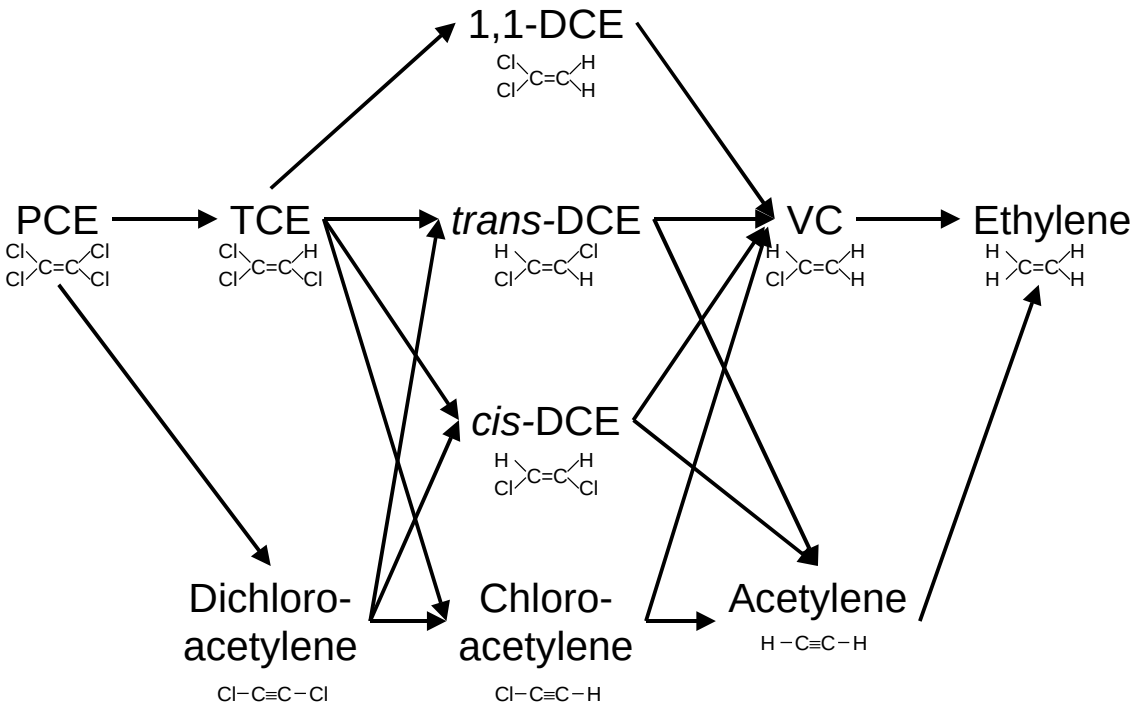

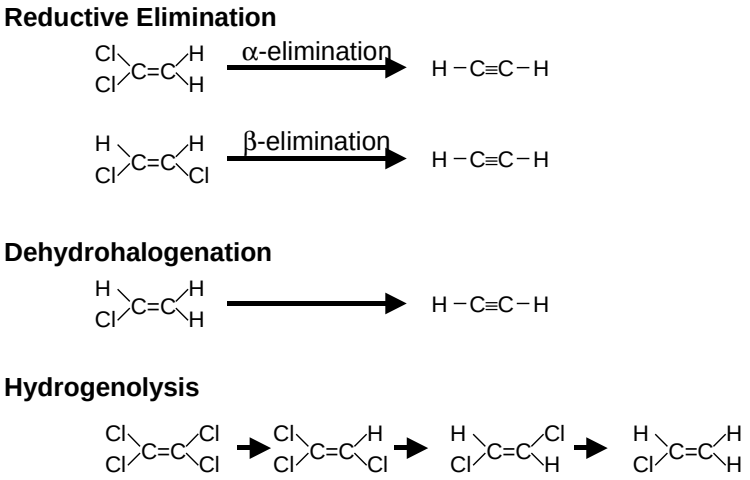

Fig. 2.2 Potential Pathways for the Reduction of PCE to Ethylene (Adapted from Roberts et al. 1996).

oxidant is zinc (Roberts et al. 1996). The acetylene products formed during β-elimination are toxic, but due to their short lifetime and higher reactivity, they are seldom considered when designing a PRB (Arnold and Roberts 1998).

Dehydrohalogenation is similar to reductive elimination in that there is an increase in bond order and loss of a halogen. However, unlike reductive elimination, dehydrohalogenation causes a single halogen to be removed and replaced with a hydrogen. For example, dehydrohalogenation of vinyl chloride yields acetylene. Although dehydrohalogenation is possible, there is no evidence that it occurs (Roberts et al. 1996).

Hydrogenolysis is often assumed to be the reaction pathway for the reduction of PCE to ethylene. Hydrogenolysis is the loss of a single halogen and replacement by a hydrogen ion without a change in the bond order (Eq. 2.2). Hydrogenolysis transforms PCE to ethylene through TCE, DCE, and vinyl chloride intermediates (Roberts et al. 1996, Arnold et al. 1998).

2.2.4 Rate of Dehalogenation

The rate of dehalogenation of chlorinated ethylene species by iron and zinc metal has been studied extensively in the laboratory (Roberts et al. 1996, Gillham and O'Hannesin 1994, Lowry 1995, Mackenzie et al. 1995, Arnold and Roberts 1998); however, predictions of the reaction rate vary and there still exists uncertainty about branching ratios, reaction rates, and the impact of sorption (Charlet et al. 1998, Burris et al. 1998). The difficulty in predicting reaction rates for dehalogenation arises from the low concentrations of contaminants (ppb range),

multiple by-products and intermediates, and uncertainty about reaction pathways and branching ratios. Proper testing should consider a system containing soil, water, reactive material, and contaminant. Working with such systems is difficult because of the number of components and competing reactions such as sorption and volatilization which can skew the results (Charlet et al. 1998). Field testing faces similar problems along with the additional difficulties of scale, representative sampling, and uncertain boundary and initial conditions.

Laboratory and field data indicate that dehalogenation of chlorinated ethylene compounds is first order or pseudo-first order (Gillham 1996, Johnson et al. 1996, Warren et al. 1995, Burris et al. 1998, Arnold and Roberts 1998). First order rates appear to be independent of initial concentration (Gillham and O'Hannesin 1994, Arnold and Roberts 1998) and grade of commercial iron used, although electrolytic iron tends to be more reactive (Gavaskar et al. 1997). Dehalogenation reactions are believed to be surface reactions; thus reaction rates are proportional to the exposed surface area of reactive metal (Gillham and O'Hannesin 1994, Tratnyek et al. 1997). Tratnyek et al. (1997) recommend normalizing reaction rates by the surface area of iron per volume of contaminated fluid, and Burris et al. (1998) recommend correcting temporal data for sorption at non-reactive sites on the surface of the iron. If these corrections are not made, reaction rates determined by different test methods (i.e. batch versus column tests) or between different iron products may be incorrect by an order of magnitude (Johnson et al. 1996). Reaction rates for laboratory experiments (Tratnyek et al.

1997, Arnold and Roberts 1998) and from a 5-year field project (O'Hannesin and Gillham 1998) are given in Table 2-2.

Table 2-2 Reaction Rate for Dehalogenation by Iron.
(Adapted from Tratnyek et al. 1996 and O'Hannesin and Gillham 1998)

Chemical	Symbol	Reaction Rate Constant, $(k_{SA})^1$ (L/m^2-hr)	
		Laboratory Data for Iron[2]	Field Data[3]
tetrachloroethylene	PCE	2.1×10^{-3}	3.6×10^{-3}
trichloroethylene	TCE	3.9×10^{-4}	6.4×10^{-3}
1,1-dichloroethylene	1,1-DCE	6.4×10^{-5}	6.7×10^{-3}
trans-dichloroethylene	*trans*-DCE	1.2×10^{-4}	4.1×10^{-3}
cis-dichloroethylene	*cis*-DCE	4.1×10^{-5}	8.6×10^{-4}
vinyl chloride	VC	5.0×10^{-5}	
tetrachloromethane	PCM	1.2×10^{-1}	
trichloromethane	TCM	9.2×10^{-4}	
tribromomethane	TBM	1.7×10^{-2}	
hexachloroethane	HCA	3.1×10^{-2}	
1,1,2,2-tetrachloroethane	1122TeCA	1.3×10^{-2}	
1,1,1,2-tetrachloroethane	1112TeCA	1.4×10^{-2}	
1,1,1-trichloroethane	111TCA	1.1×10^{-2}	
1,2,3-trichloropropane	123TCP	6.1×10^{-6}	

1 - Reaction rates (k_{SA}) are normalized by the surface area of iron per liter of solution
2 - Tratnyek et al. (1997), Johnson et al. (1996)
3 - O'Hannesin and Gillham (1998)

Significant uncertainty exists on the reaction pathway from TCE to ethene. Originally, hydrogenolysis was believed to be the dominant pathway (Roberts et al. 1996). However, recent batch testing using acid washed zinc suggests that more than 95% of TCE is reduced via a β-elimination (Arnold and Roberts 1998). The predominant β-elimination is from TCE through *cis*- and *trans*- DCE to acetylene (Arnold and Roberts 1998). This pathway is much faster than hydrogenolysis,

explaining why earlier testing detected lower concentrations of acetylene intermediates and had poor mass balance (Roberts et al. 1996). Arnold and Roberts (1998) point out that the β-elimination pathway circumvents the *cis*-DCE to vinyl chloride reaction, the slowest of any reaction in Fig. 2.2, yielding quicker conversion of PCE or TCE to ethene than expected from hydrogenolysis. However, field results may differ because Arnold and Roberts (1998) used acid-washed zinc and batch testing at room temperature, whereas iron in the field has an oxide coating and PRBs are not well mixed reactors that operate at 20°C.

The lowest reaction rate (slowest reaction) for the chlorinated ethylene compounds is for *cis*-DCE. Also, reaction rates determined in the laboratory are generally lower than those observed in the field. This difference is believed to be caused by differences in temperature, water chemistry, and heterogeneity between field and laboratory conditions (O'Hannesin and Gillham 1998). Depletion of the iron during reduction reactions is minimal. In fact, Gillham and O'Hannesin (1994) report that corrosion of iron by dissolution of water is faster than degradation due to reductive dehalogenation. Fort (2000) reports less than a 15% decrease in the reactivity of iron assessed by H_2 measurements during a two-year column test. Common estimates of the design life for granular iron PRBs are 10 to 30 years (Gillham and O'Hannesin 1994, Gaveskar et al. 1998).

2.2.4.1 Column and Batch Testing

Column tests and batch tests are used to estimate reaction rates. These tests tend to yield similar results provided test results are normalized by the surface

area of the iron and the volume of the fluid (Johnson et al. 1996, Tratnyek et al. 1997). Some researchers note a preference toward column testing, stating that column tests are more representative of field conditions (Benner et al. 1997). Other advantages of column tests are that samples can be extruded from *in-situ* PRBs and tested. This preserves some of the heterogeneity and precipitation that occurs in the field while allowing the experimental control of the laboratory (O'Hannesin and Gillham 1994).

Concerns about batch testing are that spatial heterogeneity does not exist and scaling of iron oxides on the reactive media is less likely to occur (Benner et al. 1997). The latter concern is believed to increase the reactive area of the metal and skew test results toward higher reaction rates. Evidence in support of this argument is provided by Warren et al. (1995), who report that the reduction rate of carbon tetrachloride was sensitive to the stirring rate during batch testing. In spite of this evidence, both types of tests are often used to determine the rate of dehalogenation.

2.2.4.2 Factors Affecting Rate of Dehalogenation

There are three principle factors that affect the rate of dehalogenation: availability of surface sites; pH; and dissolved oxygen concentration of the groundwater (Warren et al. 1995, Johnson et al. 1996, Tratnyek et al. 1997, Fort 2000). Of these three factors, availability of surface sites has the most significant impact on reaction rate. Dehalogenation reactions are surface reactions and require direct contact between the metal surface and the contaminant (Johnson et

al. 1996, Roberts et al. 1996). When the surface area of the metal that is available for reaction decreases, the reaction rate also decreases. The surface area of iron or zinc can be reduced if metal oxides build-up on the surface of the metal (scaling) or bio-growth forms on the reactive media (Johnson et al. 1996, O'Hannesin and Gillham 1998, Mackenzie et al. 1999). Site availability can also be limited if the contaminant concentration is high enough to saturate all of the available reactive area (Johnson et al. 1997).

The rate of dehalogenation is also sensitive to pH. At higher pH, fewer hydrogen ions are available to replace the chloride ion removed during the reaction. Warren et al. (1995) report a 10-fold drop in the reaction rate for pH change from 3.5 to 6.5, whereas Matheson and Tratnyek (1994) report a five fold drop in the reaction rate for a pH change from 5 to 10. For reduction of carbon tetrachloride by zinc, the reaction rate was highest between a pH of 2 and 4, decreased approximately and order of magnitude between pH of 4 and 5, and was lowest for pH from 5 to 6 (Warren et al. 1995).

Dissolved oxygen in the pore fluid also affects the reaction rate by increasing the amount of oxide formation on the surface of the metal, which decreases the reactivity (Mackenzie et al. 1999). However, the effect of dissolved oxygen on reaction rate tends to be minor in comparison to changes in the surface area of the metal and pH of the groundwater (Johnson et al. 1996).

2.2.4.3 Uncertainty in the Reaction Rate Constant

There are several factors that cause uncertainty in the reaction rate constant. The most significant of these is in situ aging of the iron and temperature differences between the laboratory and field. Since little data exist on the long-term reactivity of iron, it is not known whether the reaction rate constant will decrease during the design life of the PRB. In particular, the effect of precipitation on the surface of the iron is unknown, but it is expected to decrease the hydraulic conductivity and reactivity of the iron. Current testing indicates that the long-term hydraulic conductivity of iron media is about one-half of the hydraulic conductivity of virgin media when dissolved oxygen of the water is low (Fort 2000). On going research is addressing these issues, but definitive data are not available on the loss of reactivity and hydraulic conductivity during the design life of a PRB. Estimates of the error when measuring the reaction constant in the laboratory are summarized in Table 2-3 (Arnold and Roberts 1998) for each reaction shown in Fig. 2.2, where zinc is the reducing agent.

2.2.5 Models for Predicting Reductive Dechlorination

There are three common techniques for predicting the rate of reduction of PCE, TCE, DCE, or vinyl chloride to ethylene. The simplest method is to assume that all chlorinated ethylene compounds exist as *cis*-DCE (Tratnyek et al. 1997). *Cis*-DCE has the lowest reaction rate of the ethylene species (Table 2-2). Thus, the conversion of *cis*-DCE is the rate limiting step in the reaction pathway. This is a simple and conservative approach (Tratnyek et al. 1997). In fact, Arnold and

Roberts (1998) estimate that PRB thicknesses are overestimated by 41% to 76% when simpler reaction pathways are assumed.

Table 2-3 Reaction Rate for Dehalogenation by Zinc.

(Adapted from Arnold and Roberts1998)

Reaction	Reaction Rate Constant, (k_{SA})[1] (L/m^2-hr)	95% Confidence Limits (number of tests)	Coefficient of Variation[2]
PCE → TCE	0.3	±0.01 (9)	60.0
PCE → dichloroacetylene	4.5×10^{-2}	$\pm 0.7 \times 10^{-2}$ (9)	12.9
TCE → *trans*-DCE	1.5×10^{-3}	$\pm 0.1 \times 10^{-3}$ (5)	30.0
TCE → *cis*-DCE	6.0×10^{-4}	$\pm 1.0 \times 10^{-4}$ (5)	12.0
TCE → 1,1-DCE	6.8×10^{-5}	$\pm 9.1 \times 10^{-5}$ (5)	1.49[3]
TCE → chloroacetylene	9.4×10^{-4}	$\pm 1.2 \times 10^{-4}$ (5)	15.7
trans-DCE → VC	6.4×10^{-7}	$\pm 8.2 \times 10^{-7}$ (2)	1.56[3]
trans-DCE → acetylene	1.3×10^{-5}	$\pm 0.1 \times 10^{-5}$ (2)	26.0
cis-DCE → VC	5.2×10^{-7}	$\pm 1.5 \times 10^{-7}$ (2)	6.93[3]
cis-DCE → acetylene	3.0×10^{-6}	$\pm 0.2 \times 10^{-6}$ (2)	27.3
1,1-DCE → VC	4.1×10^{-5}	$\pm 0.3 \times 10^{-5}$ (3)	27.3
1,1-DCE → acetylene	1.0×10^{-4}	$\pm 0.5 \times 10^{-4}$ (3)	4.00
acetylene → ethene	5.0×10^{-4}	$\pm 1.4 \times 10^{-4}$ (5)	7.14
chloroacetylene → acetylene	6.5	±0.7 (1)	18.6
chloroacetylene → VC	0.50	±0.3 (1)	3.33
dichloroacetylene → *tran*-DCE	20.6	±0.9 (4)	45.8
dichloroacetylene → chloroacetylene	4.4	±0.3 (4)	29.3

1 - Reaction rates (k_{SA}) are normalized by the surface area of iron per liter of solution
2 – Assumes that measurement error is normally distributed so that 95% C.I. correspond to 2σ
3 – Uncertain estimates of k_{SA} due to very low yield during the experiment (Arnold and Roberts 1998)

A second strategy for estimating the reduction of chlorinated ethylene species to ethylene is to convert the concentration of PCE, TCE, and DCE isomers

to equivalent concentrations of vinyl chloride. Although this approach has been suggested in theory, it has not been used in the literature. Usually, the simpler and more conservative approach suggested by Tratnyek et al. (1997) is used.

Another approach for calculating the rate of dehalogenation of chlorinated ethylene compounds to ethylene is presented by Eykholt (1999). Eykholt (1999) provides a method for analytically calculating the concentration of all intermediate species for a network of first order, irreversible reactions. Eykholt's method adds rate constants for each species into a combined rate constant. A matrix of rate coefficients is then constructed from individual and combined rate constants. Rate coefficients in the matrix account for the link between parents, daughters, and ancestors of a species. Concentrations of any particular species in the network can be determined by adding the elements of the rate coefficient matrix corresponding to the species and using a first order decay equation. This method has the advantages of being analytical, fast, and easy to implement. Also, concentrations of all intermediate species are calculated, and first and zero order sinks and sources can be incorporated into the method and each species can have a different retardation (Eykholt 1999, Eykholt and Li 2000).

2.2.6 Characteristics of Effluent from Permeable Reactive Barriers

Detailed monitoring data on the long-term performance of PRBs are scarce. O'Hannesin and Gillham (1998) present the longest available record of PRB performance. They provide pH and concentration data from a five year field test of an iron PRB located at the Borden, Ontario test site. During their test, pH of

groundwater passing through the barrier increased from 8 to 8.7, but returned to 8 down-gradient of the barrier. Groundwater in the PRB was supersaturated with $FeCO_3$ and $CaCO_3$, so it is believed that some scaling occurred on the iron. Scaling was observed on core samples taken from the PRB. Scaling was not observed in core samples taken during the initial two years; however, noticeable precipitate formed in the first few millimeters of the barrier after three years (O'Hannesin and Gillham 1998).

Concentration of ferrous iron (Fe^{+2}) in the effluent was 0.3 mg/L, which exceeds the aesthetic groundwater standard. This result was expected. PCE and TCE concentrations measured directly and estimated from chloride concentration in the barrier were compared. Concentrations of PCE and TCE decreased 90% and 85%, respectively, across the barrier. Estimates of PCE and TCE concentration predicted from Cl^- concentrations were within 5% of measured PCE and TCE concentrations. Based on their results, O'Hannesin and Gillham (1998) conclude that chloride concentration can be a good indicator of the amount of reduction and consequently PRB performance.

2.3 PERMEABLE REACTIVE BARRIER DESIGN AND INSTALLATION

2.3.1 Designing a Permeable Reactive Barrier

A PRB must (1) intercept the contaminated groundwater, (2) have a hydraulic conductivity greater than the surrounding aquifer, (3) be constructed from material that is reactive toward the contaminant of interest, and (4) be sized so that it has a residence time sufficient for rate-limited reactions to occur (Shoemaker et

al. 1995, Warren et al. 1998). Designing a PRB that fulfills these criteria requires accurate characterization of the hydraulic conductivity of the aquifer, hydraulic conductivity of the PRB, and reactivity of the media. In addition, understanding uncertainty associated with each of these parameters is necessary (Shoemaker et al. 1995).

The most common style of PRB is a horizontal flow permeable reactive barrier (HFPRB) (Fig. 2.1), and it is the only type of PRB for which a design method has been suggested (Gavaskar et al. 1998, Powell et al. 1998). When designing a HFPRB, aquifer heterogeneity, diffusion, and the hydraulic conductivity of the PRB are usually ignored. The seepage velocity of the groundwater in the aquifer is estimated (i.e., pumping test data or tests on samples from the field) and estimates of reactivity for the PRB are obtained from the literature (Table 2-2) or from laboratory tests (Gavaskar et al. 1998). Reduction reactions are assumed to be first order, and the required residence time of contaminants in the PRB for the desired degree of reduction to occur is determined. Residence time is expressed in terms of the seepage velocity of groundwater in the aquifer. Accordingly, the minimum thickness of the PRB (L_{PFR}) is:

$$L_{PFR} = \frac{v}{k_r} \ln\left(\frac{C_{in}}{C_e}\right) \qquad (2.3)$$

where v is the seepage velocity of the groundwater, k_r is the reaction rate, C_{in} is the concentration of contaminant entering the PRB, and C_e is the desired steady-state

concentration of the effluent (for example, the MCL for vinyl chloride). If additional data about the PRB are available, such as sorption isotherms and dispersion coefficients (D), Eq. 2.4 may be used rather than Eq. 2.3 for estimating the required thickness of the PRB (L_{disp}).

$$L_{disp} = \frac{2D}{v\left(1-\sqrt{1+4k'D/v^2}\right)}\ln\left(\frac{C_{in}}{C_e}\right) \qquad (2.4a)$$

where k' equals a combined liquid and solid phase reaction rate which includes sorption (van Genuchten 1981). If reactions are assumed to occur on the surface of the iron such that k' equals k, then Eq. 2.3 and 2.4a can be combined to yield a correction factor for dispersion (CF_{disp}) that adjusts L_{PFR} to account for dispersion.

$$\frac{L_{disp}}{L_{PFR}} = CF_{disp} = \frac{\lambda}{\sqrt{1+2\lambda}-1} \qquad (2.4b)$$

where λ equals $2Dk/v^2$ (Eykholt et al. 1999). For design, the product of CF_{disp} and L_{PFR} is the minimum thickness for the PRB (L_{min}), or if no data are available for estimating dispersion in the aquifer, L_{min} is assumed to equal L_{PFR}.

The design thickness for the PRB is obtained by multiplying L_{min} by a factor of safety. The factor of safety accounts for uncertainty in v, C_{in}, and k_r (Eykholt 1997); differences between laboratory and field conditions; heterogeneity of the aquifer; non-first order reactions; and long-term degradation of the PRB (i.e.,

scaling and degradation) (Gavaskar et al. 1998). Common factors of safety are between 1.5 and 2.5 (Gavaskar et al. 1998, Powell et al. 1998, Nav. Fac. 1998), although Eykholt (1997) suggests a factor of safety between one and six may be necessary. Eykholt et al. (1999) show that a factor of safety greater than 3.3 is required for moderately heterogeneous aquifers, and that the factor of safety should increase as the heterogeneity of the aquifer increases.

Potential problems with the plug-flow design method exist. Shoemaker et al. (1995) point out that the method inadequately accounts for heterogeneity in v, k, and C_{in}. Also, long-term data on scaling and loss of reactivity of metal are not available (Schlimm and Heitz 1996), and the direction of groundwater flow can vary seasonally. O'Hannesin and Gillham (1998) report uneven mass loading to sections of their PRB due to a 30 degree seasonal fluctuation in the direction of groundwater. Benner et al. (1998) noted that preferential groundwater flow (and mass loading) through sections of a PRB constructed to contain mine waste depleted the reactive capacity of the barrier and shortened its design life.

There are several additional factors that should be considered during design of a PRB besides its effectiveness at containing contamination at a site. These include future land use, site geology, and settlement of the underlying soil (Eykholt and Sivavec 1995, Warren et al. 1998). In general, PRBs cause less surface disturbance than other methods of remediation, but may be impractical after the trajectory of the plume, and locations of property lines and buildings are considered. Also, heterogeneity of soils at the site of a proposed PRB should be considered (Warren et al. 1998, Eykholt et al. 1999). The additional material costs

resulting from increasing the factor of safety at more heterogeneous sites may prohibit the use of a PRB (Eykholt 1997). Finally, Eykholt and Sivavec (1995) recommend evaluating settlement below a PRB since iron is 2.5 times heavier than soil (Eykholt and Sivavec 1995).

2.3.2 Permeable Reactive Barrier Designs

The most common type of PRB is a horizontal-flow barrier (Blowes et al. 1995). Horizontal-flow permeable reactive barriers (HFPRBs) are vertically oriented walls of reactive media that are installed perpendicular to groundwater flow, down gradient of a contaminant plume or source. Contaminated groundwater flows horizontally through the HFPRB. HFPRBs typically stand-alone, but can be an element of a larger system that includes a cap, or a pump and treat system (Fig. 2.3a). The advantages of HFPRBs are that they rely on conventional methods of installation; they are easy to conceptualize; and there is a design method available for them (Section 2.2.3). Furthermore, their effectiveness has been documented in the literature (e.g. O'Hannesin and Gillham 1998).

Alternatives to the HFPRB are the funnel and gate PRB (FGPRB) and caisson PRB (CPRB) (Porter 1998, Warner et al. 1998). FGPRBs are a shorter HFPRB that is located between the sides of funnels with low hydraulic conductivity. Groundwater is channeled through the PRB gate by the funnels, where it reacts with the medium and is treated. A CPRB system also relies on funnels to channel contaminated groundwater into the reactive barrier; however, unlike the HFPRB and FGPRB, flow through a CPRB is vertical. The advantages of CPRBs are that

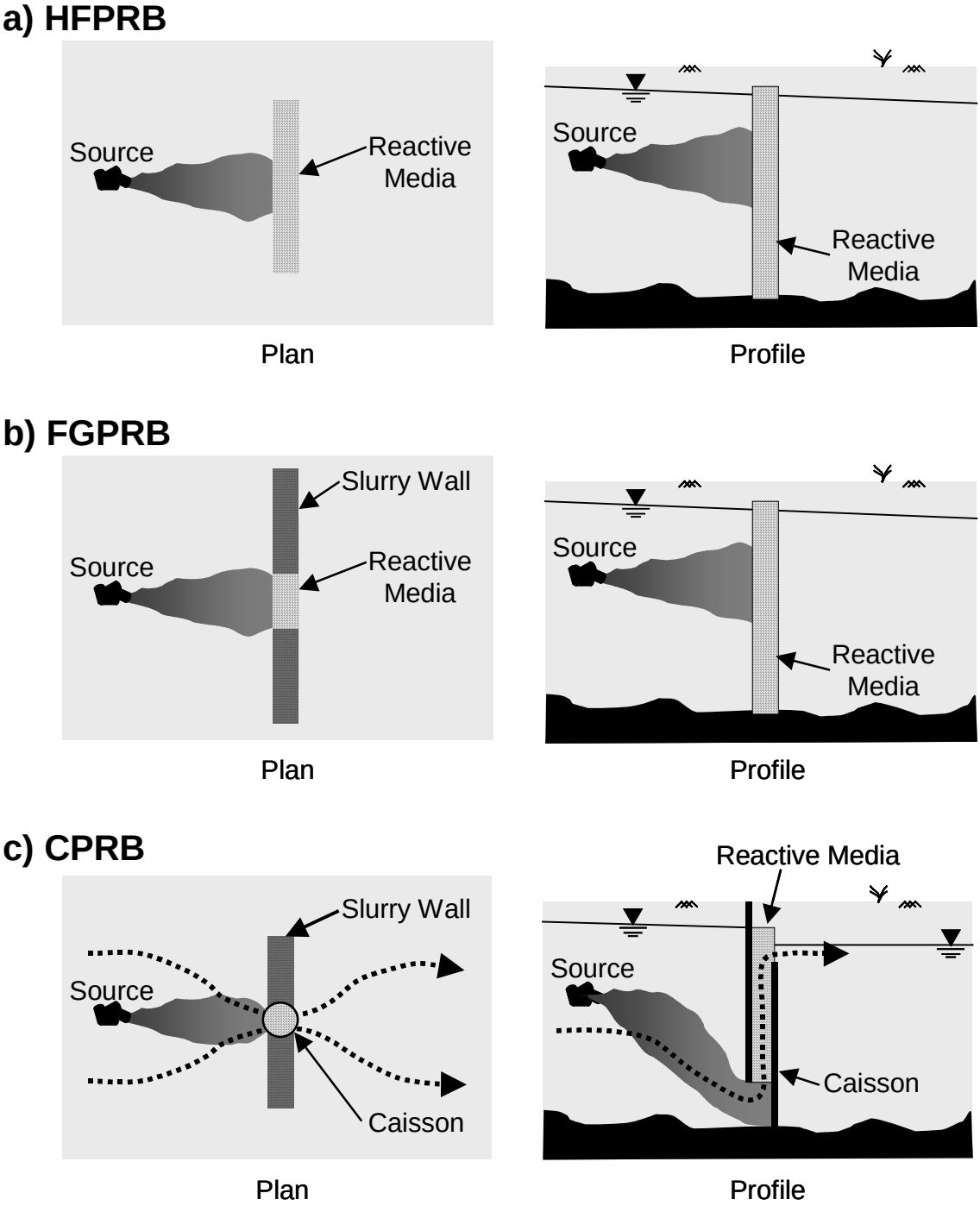

Fig. 2.3 Horizontal-Flow (a), Funnel and Gate (b), and Caisson (c) PRBs.

the upward flow through the reactive media is believed to be more uniform and close to plug-flow. Also, the rigidity of the CPRB allow for easier construction, particularly into existing slurry walls, and the reactive media can be replaced or rejuvenated if necessary (Reinhart et al. 1996). Furthermore, the flow is more focused and expected to be easier to monitor. CPRBs in series have also been suggested for sites with multiple contaminants (Blowes et al. 1995, Shoemaker et al. 1995). All three types of PRB are shown in Fig. 2.3.

2.3.3 Funnel and Gate Systems

Slurry walls or sheet-piling are often used with PRBs to channel groundwater into the PRB and reduce the volume of reactive material required. In these systems, the slurry or sheet piling is referred to as a funnel, and the PRB is the gate (Starr and Cherry 1994). Starr and Cherry (1994) evaluated several funnel and gate configurations. They determined that the largest capture zone using the least material occurs when the funnel is transverse to groundwater flow and the gate is located in the center of the system (Starr and Cherry 1994). Also, the funnel must have a lower hydraulic conductivity than the aquifer and be free of defects (Tachavises 1998) while the gate must have a higher hydraulic conductivity than the aquifer (Starr and Cherry 1994).

An alternative to the low hydraulic conductivity funnel has been suggested by Edwards et al. (1997). They propose an “X” shaped funnel that is constructed from material that is more permeable than the aquifer. The PRB is located at the center of the “X”. Contaminated groundwater enters the funnel and travels through

the funnel toward the gate. Groundwater selects this path because the funnel has lower resistance (higher hydraulic conductivity) than the surrounding aquifer. Contaminated groundwater passes through the PRB located at the center of the "X" and continues traveling through the funnel down gradient of the PRB. Groundwater then returns to the aquifer from the funnel (Edwards et al. 1997).

Funnel and gate systems have the advantage of increasing the volume of water treated without increasing the size of the PRB (Starr and Cherry 1994). Depending on the cost of gate versus funnel construction, funnel and gate systems may be more economical than a PRB alone (Day et al. 1999). FGPRBs have been used effectively at several sites and are often used for larger plumes that require longer PRBs (e.g., the Denver Federal Center has a 366 m long FGPRB that has 4, 12.2 m gates) (McMahon et al. 1999). Figure 2.4 shows funnel and gate systems. Figure 2.4a is a funnel and gate system that has a low hydraulic conductivity funnel (Starr and Cherry 1994), and Fig. 2.4b is a funnel and gate system that has a high hydraulic conductivity funnel (Edwards et al. 1997). The capture zone for the funnel and gate configurations are shown by particle trajectories obtained by the author using MODFLOW (MacDonald and Harbaugh 1988) and Path3D (Zheng 1992).

2.3.4 Permeable Reactive Barrier Installation

Conventional braced cut excavations are often used for constructing horizontal PRBs (Fig. 2.5a). A braced excavation allows inspection of the reactive media and installation of monitoring equipment during placement (Blowes et al.

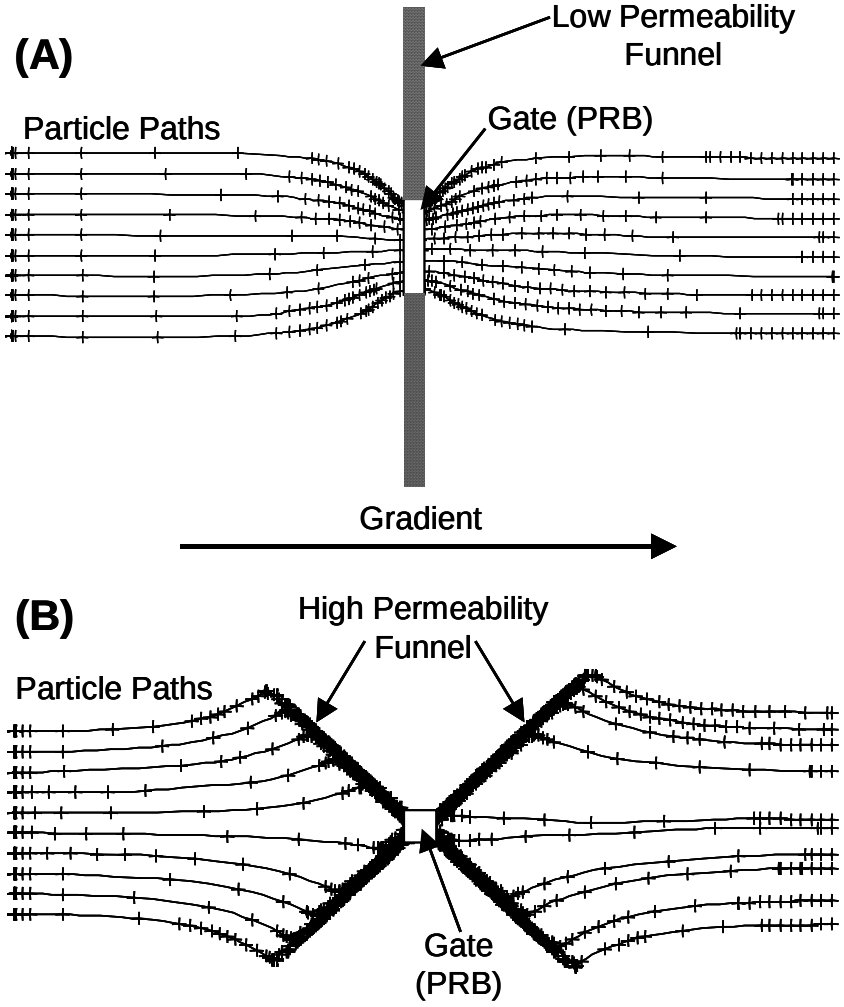

Two-Dimensional, 80 x 80 Element Mesh (1 m spacing)
1 m Thick by 40 m Long System Located in the Middle Half of the Domain
Hyd. Cond. of the Aquifer = 1 x 10^{-5} m/s
Hyd. Cond. of the Slurry Wall = 1 x 10^{-7} m/s
Hyd. Cond. of the PRB and Permeable Funnel = 1 x 10^{-3} m/s
Porosity = 30%
Error Criteria = 0.001, Gradient = 0.01

Fig. 2.4 Particle Paths through a Funnel and Gate: (a) Low Hydraulic Conductivity Funnel, and (b) High Hydraulic Conductivity Funnel.

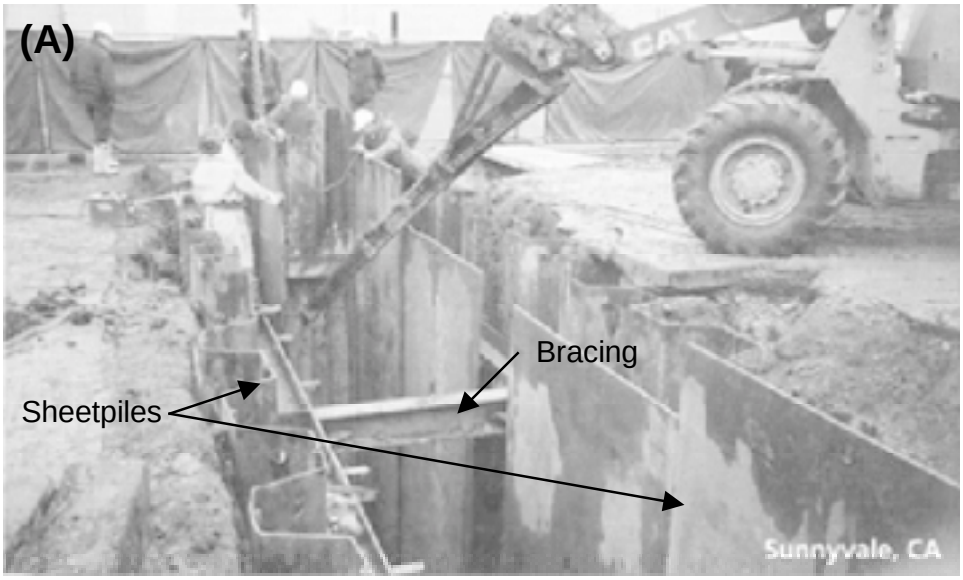

http://www.beak.com/Technologies/ETI/installation.html

http://www.epa.gov/ada/eliz/full.html

Fig. 2.5 Available Methods for Constructing PRBs: (a) Braced Cut and (b) Trenching Machine.

1995, Day et al. 1999). When the trench is open, the underlying strata can be tested for bearing capacity and inspected to ensure that the PRB is keyed into less permeable strata (Tachavises 1998).

Trenching machines are available for constructing PRBs by simultaneously excavating and back-filling the trench with reactive media (Fig. 2.5b). Alternatively, slurry methods can be used where the trench is excavated and kept full of a biodegradable slurry which supports the trench (Day et al. 1999). The reactive media is suspended in the slurry and, as the slurry degrades, the reactive medium remains to form a PRB (Blowes et al. 1995). The disadvantages of continuous trenching and slurry methods are that the underlying strata cannot be inspected and the existence of a key cannot be ensured (Gaveskar et al. 1998). Also, additional work is required to install monitoring equipment, and there is a higher likelihood of high hydraulic conductivity or low reactivity windows occurring in the PRB because there is less control during excavation and placement of the reactive media (Blowes et al. 1995). Furthermore, coring samples from an operational full-scale PRB have shown that PRBs constructed using continuous trenching equipment can compress as much as 25% after they are placed (Puls et al. 1999).

Other installation techniques under development include jet grouting, soil mixing, and installation using a mandrel. During jet grouting, reactive media are suspended in a degradable slurry and injected at high pressure into the subsurface through a pipe. The media displace native soil to form a lens or bulb of reactive material (Hocking et al. 1998, Siegrist et al. 1999). Soil mixing involves

mechanically mixing reactive media with native soil using hollow-stem augers. Alternatively, vertical treatment zones can be pushed into the subsurface using a mandrel. All of these techniques have the same advantages; they are faster and can achieve greater depths than braced excavations or continuous trenching. However, they also have the same disadvantages (i.e., poor control on the location, size, and composition of the reactive zone, and greater disturbance of the surrounding soil) (Shoemaker et al. 1995).

SECTION 3

REVIEW OF GEOSTATISTICS

Geostatistics is a formal technique for spatial and/or temporal parameter estimation (Gelhar 1993). Using geostatistics, data can be estimated between known measurements (kriging), or random fields which are statistically identical, yet random, can be generated for input into existing models (random field generation). People have been using ad-hoc statistical methods for characterizing geologic media for a long time (i.e., averaging and linear interpolation) (Gelhar 1993). Geostatistics, however, is a mathematically rigorous method for applying statistical principles to describe geologic media. These methods yield better estimates than ad-hoc estimates because geostatistics maximizes the use of available data, quantifies the accuracy of the estimate, and can add insight into what future data would be most useful (Georgakakos et al. 1990). Common tasks of geostatistics include integration to estimate total accumulation in space, volume, or time, differentiation for estimating spatial or temporal changes, and interpolation for estimating point measurements (Georgakakos et al. 1990).

Geostatistics combines principles of uncertainty with equations from physics. Geostatistics can be used for solving forward problems and backward problems. In the forward problem, characteristics of the system are defined and statistical distributions of the outcome are predicted. In the backward problem, outcomes are observed, and characteristics of the system are estimated (Georgakakos et al. 1990).

Geostatistics are particularly useful for groundwater modeling because natural processes create variability in hydraulic properties some of which can vary over 13 orders of magnitude (Freeze 1975, Freeze and Cherry 1979). Due to the small scale of variability (i.e., a few meters), direct measure of these aquifer parameters is impractical. Thus, an estimation procedure is necessary for predicting aquifer characteristics between point measurements. When formal procedures are used that have a basis in probability theory, they are called geostatistics. The tools of probability used by geostatistics are spatial correlation, weighting and unbiased conditioning, and averaging (Georgakakos et al. 1990). In other words, the purpose of geostatistics is to use pooled data and unbiased estimators to make "educated guesses" of geologic parameters and variability (Gelhar 1993).

There are four approaches that may be used for modeling groundwater flow across a region with properties of the media that vary spatially. One method is to take point measurements at all locations in an aquifer. With complete knowledge of the aquifer, flow can be predicted almost exactly using Darcy's Law. This method is accurate because there is little uncertainty about input parameters, but the method is susceptible to disturbance caused by sampling (i.e., the Heisenburg Principle) and requires a large quantity of data. A second alternative is to assume large regions of the aquifer are homogeneous. This is a simplification of the real system and ignores the effect of variability of hydraulic properties within the region being modeled. A third approach is to randomly assign hydraulic properties to all locations in the aquifer and solve for flow. Although this approach accounts for

variability in aquifer properties, the spatial connectivity of the data is ignored (Lumb 1974). Finally, approaches two and three can be combined. Zones that have similar properties can be modeled as regions that have small-scale randomness. Randomness in the data are described with distribution functions and the spatial orientation of variability is described using correlation functions. In addition, data within the domain may be conditioned using field measurements (Yarus and Chambers 1994).

The purpose of this section is to summarize principles of geostatistics. In particular, stochastic descriptors, Monte Carlo simulation, and random field generation will be discussed. Topics that will not be discussed are analytical approaches where the governing equations of flow and probability are combined to yield statistical descriptions of flow and kriging techniques for interpolating between point measurements.

3.1 STOCHASTIC DESCRIPTORS

3.1.1 Random Variables

A random variable (**x**) is the outcome of an experiment that has a probability of occurrence described by a probability density distribution (Ross 1997). A random variable can be a function of space and/or time; however, in this report, random variables will be discussed as functions of space since geologic parameters vary extremely slowly over time (Gelhar 1993). Random variables may be continuous or discrete. Continuous random variables are described with density functions, while discrete random variables are described with mass functions (i.e.,

probability density function and probability mass function, respectively). For ease in this report, adherence to the nomenclature is relaxed and “density” is occasionally used when discussing discrete functions.

Distribution functions that describe random variables are the cumulative density function (cumulative mass function), abbreviated cdf (cmf), and probability density function (probability mass function), abbreviated pdf (pmf). A cdf ($F_X(\mathbf{x})$) is a function that describes the probability that a random variable will be less than or equal to a threshold value. For instance, the probability that **x** will be less than or equal to **a** is:

$$F_X(a) = P_X[x \leq a] \tag{3.1a}$$

For continuous random variables, the cdf is described as an integral whereas for discrete random variables, the cmf is described using a summation:

$$F_X(a) = \int_{-\infty}^{a} P_X(x)dx \cong \sum_{i=1}^{a} P_X(x_i) \tag{3.1b}$$

Cumulative distribution functions are equal to unity for **a** equal to infinity and zero for **a** equal to negative infinity. Cumulative distribution functions are also non-decreasing and values of the cdf are additive over non-overlapping ranges. Thus, the P[**a** $\leq$ x $\leq$ **b**] is equal to the difference of $F_X(\mathbf{b})$ and $F_X(\mathbf{a})$ (Grimmett and Stirzaker 1995).

The derivative of the cdf (or cmf) is the pdf (or pmf) ($f_X(\mathbf{a})$) which describes the probability density of a random variable, **a**. The pdf for several common statistical distributions will be described subsequently. Properties of the pdf are that it is always positive and its cumulative sum over all random variables is equal to unity (i.e., $\int_{-\infty}^{\infty} f_X(x)dx = F_X(\infty) = 1$) (Grimmett and Stirzaker 1995).

Two descriptors of the pdf are the mean and variance, the first moment about zero and the second moment about the mean, respectively (Ross 1997). The mean is a measure of the central location of the pdf, based on a weighted sum of all random variables in a distribution (Journel 1989). The mean is equal to the expected value of a distribution (E[X]) and is defined for continuous random variables as:

$$\mu_X = E[X] = \int_{-\infty}^{\infty} x\, f_X(x)dx \qquad (3.2a)$$

The mean for discrete random variables is defined as:

$$\overline{X}_X = E[X] = \frac{1}{N}\sum_{i=1}^{N} x_i \qquad (3.2b)$$

where N is the number of random variables in a discrete data set.

The variance (second moment about the mean) is the expected squared difference of a random variable about the mean. The variance describes the scatter of the data about the central point of the distribution (i.e., the mean) and may be expressed as:

$$\sigma_X^2 = E[(X-\mu)^2] = \int_{-\infty}^{\infty} (x-\mu_X)^2 f_X(x)dx \qquad (3.3a)$$

for continuous distributions and as:

$$S_X^2 = E[(x-\overline{X})^2] = \frac{\sum_{i=1}^{N} (x_i - \overline{X})_i^2}{N-1} \qquad (3.3b)$$

for discrete random variables. The square root of the variance is the standard deviation (σ_x or s_x) of the distribution (Ross 1997). The standard deviation can be normalized by dividing by the mean to yield the coefficient of variation (Journel 1989).

3.1.2 Common Probability Models

3.1.2.1 Uniform (Rectangular) Distribution (U)

The pdf and cdf for a uniform distribution between -5 and -1 (U(-5, -1)) is shown in Fig. 3.1 (Hastings and Peacock 1975). A uniform distribution assigns an equal probability of selecting a random variable between the boundary values (-5

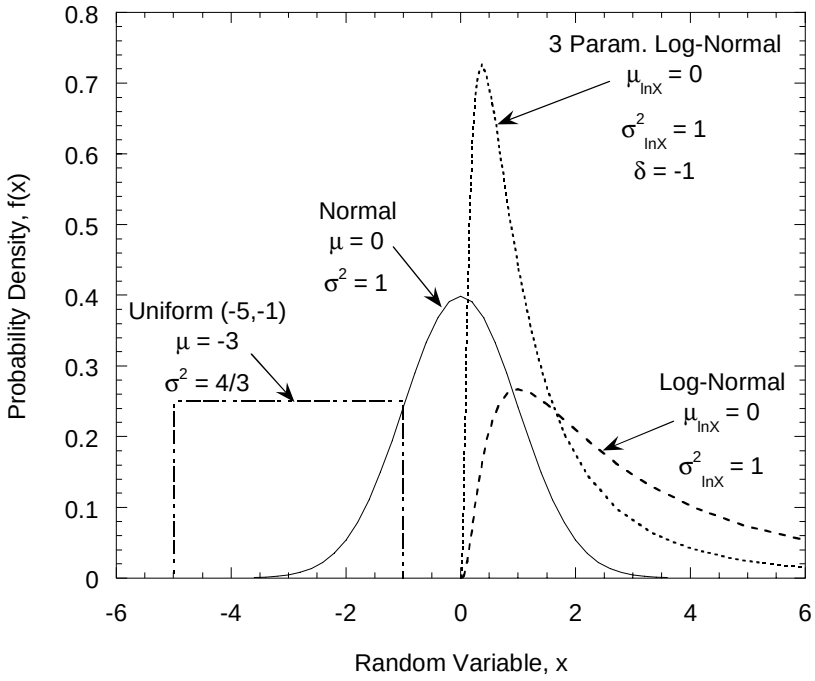

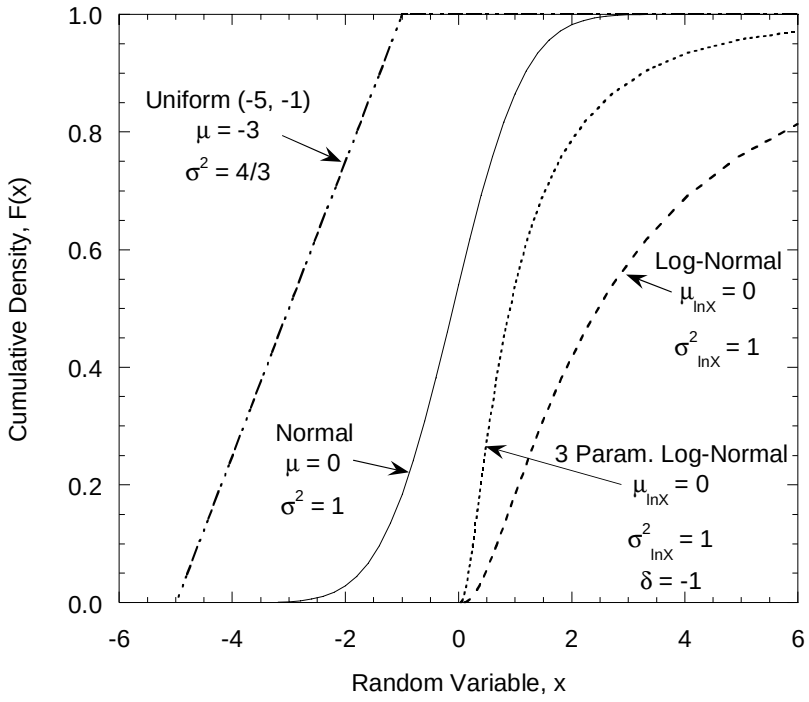

Fig. 3.1 Probability and Cumulative Density Functions for Uniform, Normal, Log-Normal, and Three Parameter Log-Normal Distributions.

and -1 in this case), and zero probability of selecting a random variable outside the boundary values. Uniform distributions are simple, can be converted into normal distributions (Box and Muller 1958), and can be generated easily with automated or manual random number generators (e.g., Press et al. 1992, Whichmann and Hill 1987). Because of these advantages, uniform random variables are widely used in geostatistics.

3.1.2.2 Normal (Gaussian) Distribution (N)

The pdf and cdf for a normal distribution with a mean of zero and variance of one (i.e., standard normal distribution) are shown in Fig. 3.1 (Hastings and Peacock 1975). The pdf for a normal distribution is symmetric about the mean with the mean having the highest probability density. The probability density asymptotically approaches zero as the random variable approaches negative and positive infinity (Grimmett and Stirzaker 1995). A characteristic of normal distributions is that 68% of the mass is located between $\pm\sigma$ of the mean and 95% of the mass is between $\pm 2\sigma$ of the mean (i.e., $F(-\sigma \leq x \leq +\sigma) = 0.68$ and $F(-2\sigma \leq x \leq +2\sigma) = 0.95$) (Journel 1989).

Normal distributions are completely described by their first and second moments (mean and variance respectively). Normal distributions fit many data sets well because the sum of independent, identically distributed random variables approaches a normal distribution by the Central Limit Theorem (Ross 1997). When simulating geologic media, normal distributions that are truncated at zero are often

used to describe water content and porosity (Gelhar 1993), and untruncated normal distributions are used to describe measurement error (Lumb 1974).

3.1.2.3 Log-Normal Distributions (LN)

The pdf and cdf for a log-normal distribution are shown in Fig. 3.1 (Hastings and Peacock 1975). Log-normal distributions are obtained by taking the exponential of normal distributed random variables, or conversely, log-normally distributed random variable are normalized by transforming them using the natural logarithm function (i.e., $X_{LN} = \exp(X_N)$ or $X_N = \ln(X_{LN})$). Log-normal distributions are described using a log-transformed mean (μ_{lnX}) and log-transformed variance (σ^2_{lnX}). These transforms describe the mean and variance of the normal distribution for the log-transformed random variables. The log-transformed mean and variance for the pdf and cdf shown in Fig. 3.1 are zero and one, respectively.

The advantage of log-normal distributions is that they have a positive skew and are always positive (Gelhar 1993, Georgakakos et al. 1990). Moreover, the product of independent, identically distributed random variables form a log-normal distribution since the product of random variables is equal to the sum of their logarithms (Gelhar 1993). Log-normal distributions are commonly used to describe hydraulic conductivity and transmissivity (Freeze 1975, Smith and Freeze 1979, Journel 1989, Gelhar 1993, Benson 1993, Meyer et al. 1997). Nearly homogeneous sandy aquifers have $\sigma^2_{lnK} < 0.5$, moderately heterogeneous aquifers have $0.5 < \sigma^2_{lnK} < 2$, and higher heterogeneity aquifers have $2 < \sigma^2_{lnK} < 4$ (Harter 1998)

A variant of the log-normal distribution is the three-parameter, log-normal (3PLN) distribution. The pdf and cdf for a 3PLN distribution are shown with the log-normal distributions on Fig. 3.1 (Stedinger 1980). The three parameter, log-normal distribution has a third parameter (δ) added to the un-transformed random variable (i.e., $X_{3PLN} = \exp[N(\mu,\sigma)+\delta]$). The third parameter provides additional skew to the pdf. A three parameter log-normal distribution is identical to a log-normal distribution if δ is zero. The pdf and cdf shown in Fig. 3.1 have a mean (μ_{lnK}) of zero, variance (σ^2_{lnK}) of one, and δ of negative one. Stedinger (1980) and Benson (1993) discuss methods for determining δ. Benson (1993) argues that 3PLN distributions can be better descriptors of the hydraulic conductivity than log-normal distributions because of their greater positive skew.

3.1.2.4 Bivariate Normal Distribution (BVN)

The pdf for a bivariate normal distribution (joint normal distribution) is shown in Fig. 3.2. A bivariate normal distribution describes the distribution of two related (correlated) random normal variables (Lumb 1974). For instance, a bivariate distribution may describe inches of rainfall and corn yield per year. When rainfall is high, corn yield is also high and when rainfall is low, corn yield is also low. In this sense, rainfall and corn yield are correlated (Kachigan 1982). Bivariate normal distributions are described using two means (μ_X and μ_Y), two variances (σ_X^2 and σ_Y^2), and a correlation function (ρ_{XY}) or variogram (γ_{XY}). The correlation function or

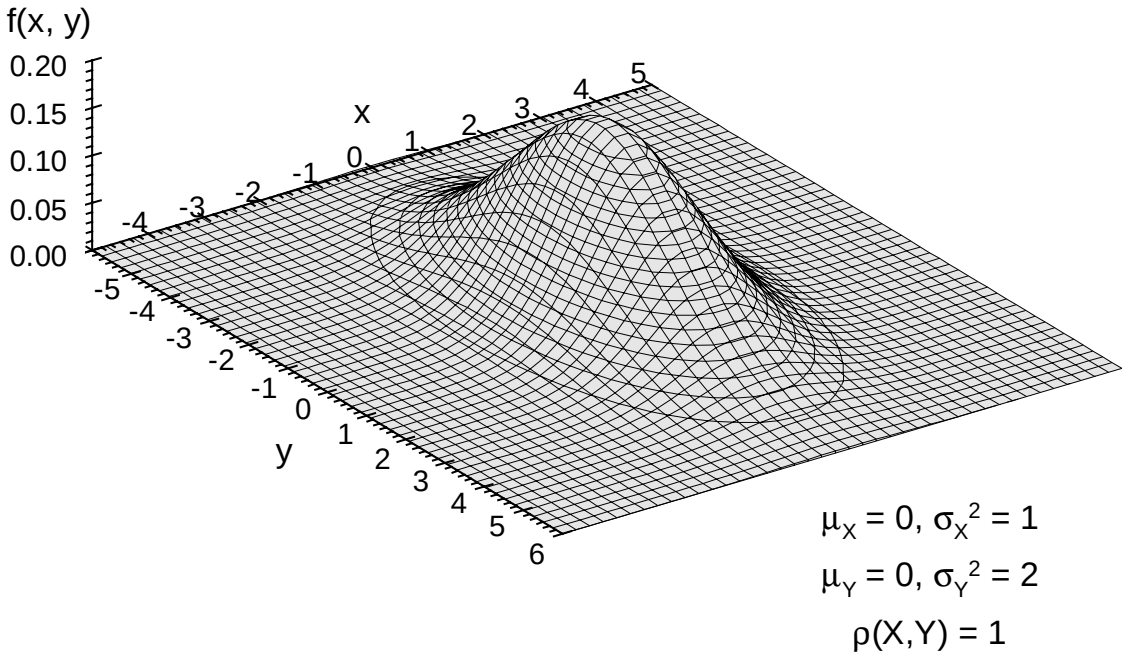

Fig. 3.2 Probability Density Function for a Bivariate Normal Distribution.

variogram describes the correlation between the random variables, **x** and **y** (Lumb 1974, Yarus and Chambers 1994). The bivariate normal distribution shown in Fig. 3.2 has μ_X and μ_Y = 0, σ_X^2 = 1, and σ_Y^2 = 2, and perfect correlation ($\rho(X,Y)=1$). Correlation functions, variograms, and autocorrelation will be discussed below.

3.1.3 Covariance and Correlation

Consider the example for rainfall and corn yield. It introduced a new term, the correlation coefficient (ρ). The correlation coefficient is a normalized covariance for the random variables. The covariance and the correlation coefficient describe the connectivity between the random variables. Simply stated, the covariance is a variance between a pair of data in a bivariate field (Olea 1991, Lumb 1974). Thus, the covariance describes the scatter of the random variables about their means (Ross 1997, Kachigan 1982). The formal definition of covariance for a continuous, bivariate distribution ($F_{XY}(X,Y)$) of random variables **X** and **Y** is:

$$\mathrm{Cov}(X,Y) = \int_{-\infty}^{\infty}\int_{-\infty}^{\infty}(x-\mu_X)(y-\mu_Y)\,f_{XY}(x,y)\,dx\,dy \qquad (3.4a)$$

For discrete random variables, the covariance is:

$$\mathrm{Cov}(X,Y) = \frac{1}{N}\sum_{i=1}^{N}\left[(x-\overline{X})(y-\overline{Y})\right]_i \qquad (3.4b)$$

The covariance can be normalized by dividing by the standard deviation for each of the random variables. This yields the correlation coefficient (ρ) that has no units and a range from negative to positive one.

$$\rho(X,Y) = \frac{\mathrm{Cov}(X,Y)}{\sqrt{\sigma_X^2}\sqrt{\sigma_Y^2}} \tag{3.5}$$

3.1.4 Autocovariance and Autocorrelation

For a spatial distribution of random variables, such as rainfall across an area, the covariance and correlation coefficient describe the expected values of the random variable in space relative to neighboring random variables (Gelhar 1993). Consider rainfall across an area as a two-dimensional random field. Rainfall at nearby locations will not differ drastically. This characteristic is called spatial correlation because it describes the expected variability of a random variables based on the magnitude and location of neighboring random variables (Olea 1991). Similar to the correlation between two random variables, spatial correlation is described using a covariance and correlation coefficient, although the terminology changes to autocovariance and autocorrelation coefficient. Unlike Eq. 3.4, and 3.5, the autocorrelation and autocovariance are calculated for all points at a given separation distance rather than for pairs of random variables at the same location (Yarus and Chambers 1994).

Given a field of discrete random variables (X_p) at locations p, the field will have a mean ($\overline{X}$) and variance (s_x^2). The autocovariance of the field at a separation distance of h is then equal to:

$$\text{Cov}(p,p+h) = \text{Cov}(h) = E\left[\left(X_p - \overline{X}\right)\left(X_{p+h} - \overline{X}\right)\right] = \frac{1}{N_h}\sum_{i=1}^{N_h}\left[(X_p - \overline{X})(X_{p+h} - \overline{X})\right]_i \qquad (3.6)$$

where N_h is the number of points at separation distance h. The autocovariance can be normalized by dividing by the variance of the random field (assuming second-order stationarity) to yield an autocorrelation.

$$\rho(h) = \frac{E\left[\left(X_p - \overline{X}\right)\left(X_{p+h} - \overline{X}\right)\right]}{E\left[\left(X_p - \overline{X}\right)^2\right]} = \frac{\text{Cov}(h)}{s_x^2} \qquad (3.7)$$

Autocorrelation data at several separation distances are shown on Figure 3.3.

Once autocorrelation has been determined for several separation distances, a function is fitted through the data. This function is called an autocorrelation function and describes the relationship between autocorrelation and distance (Olea 1991). Common autocorrelation functions are exponential, spherical, and Gaussian, although any equation which fits the data may be used

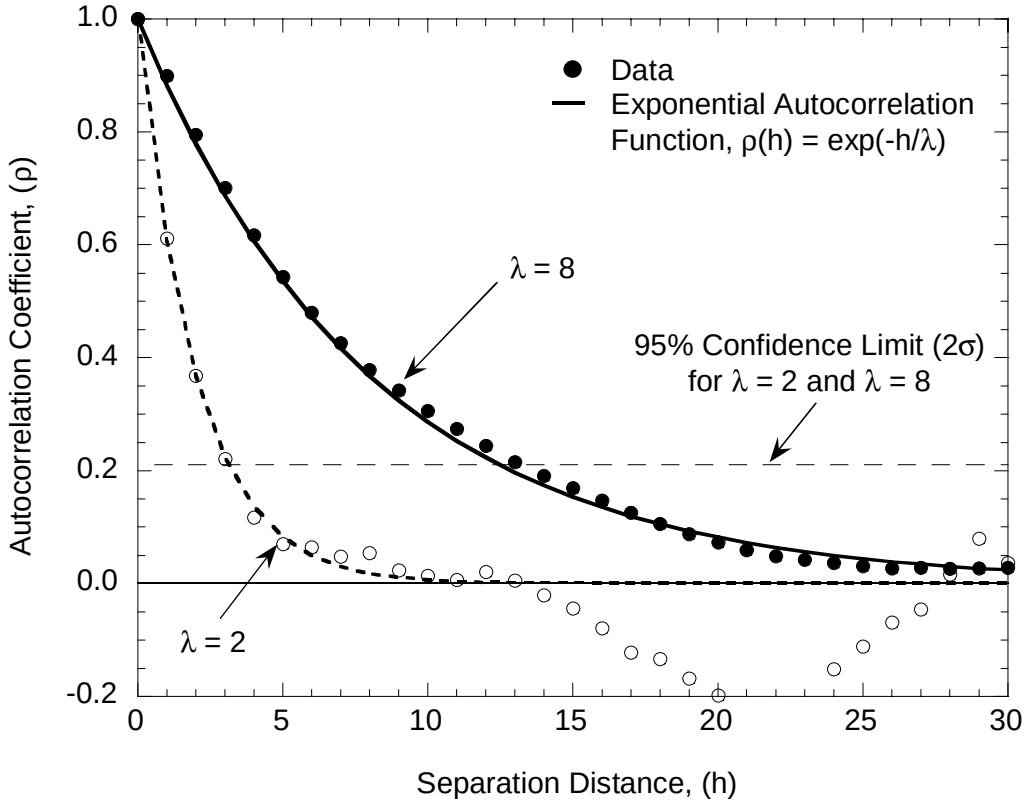

Fig. 3.3 Autocorrelation Data and Autocorrelation Function for Correlated Random Fields with a Correlation Scales of 2 and 8.

(Gelhar 1993, Mantoglou and Wilson 1982). The data shown in Fig. 3.3 are fitted with an exponential correlation function. Exponential correlation functions are of the form:

$$\rho(h) = \exp(-h/\lambda) \tag{3.8}$$

where λ is the correlation scale (Olea 1991). The correlation scale is a measure of the rate of decrease of the autocorrelation function with separation distance (Lumb 1974). The distance over which spatial correlation exists is greater for larger correlation scales.

Although autocorrelation functions are designed to converge to zero at large separation distances, autocorrelation data may fluctuate around zero at larger separation distances (Fig. 3.3). This error is believed to be caused by periodicity in the random field (Olea 1991). To determine if autocorrelation data converge to zero at large separation distances (i.e., determine if the field is ergodic), confidence intervals around autocorrelation equal to zero can be calculated. By assuming that error in autocorrelation is normally distributed, a 95% confidence interval for autocorrelation equal to zero is defined between $\pm 2s_{\rho(h)}$, where $s_{\rho(h)}$ is the standard deviation for the error in autocorrelation at a distance where the autocorrelation is expected to be zero (e.g., $h > 3\lambda$ for exponential autocorrelation functions) (Lumb 1974, Priestly 1981). Autocorrelation data between $\pm 2s_{\rho(h)}$ are assumed to be no different from zero with 95% confidence.

3.1.5 Semi-Variogram

Another descriptor of the autocorrelation between random variables separated in space is the semi-variogram ($\gamma(h)$). The semi-variogram is the second moment of random variables at a given separation distance (Olea 1991, Yarus and Chambers 1994). For discrete random variables, the semi-variogram is:

$$\gamma(h) = \frac{1}{2} E\left[\left(X_{p+h} - X_p\right)^2\right] = \frac{1}{2N_h} \sum_{i=0}^{N_h} \left(X_p - X_{p+h}\right)_i^2 \qquad (3\text{-}9)$$

The semi-variogram has a range from zero to the variance of the random field. The relationship between the semivariance and autocorrelation is obtained by combining Eq. 3.6 and Eq. 3.9:

$$\gamma(h) = \sigma^2 (1 - \rho(h)) \qquad (3.10)$$

Descriptors of a semi-variogram function are the nugget, sill, and range (Fig. 3.4). For stationary, ergodic random fields, the nugget is the semi-variance at zero separation distance, the sill is equal to the variance of the random field, and the range is the minimum separation distance at which the semi-variance equals the sill (Olea 1991).

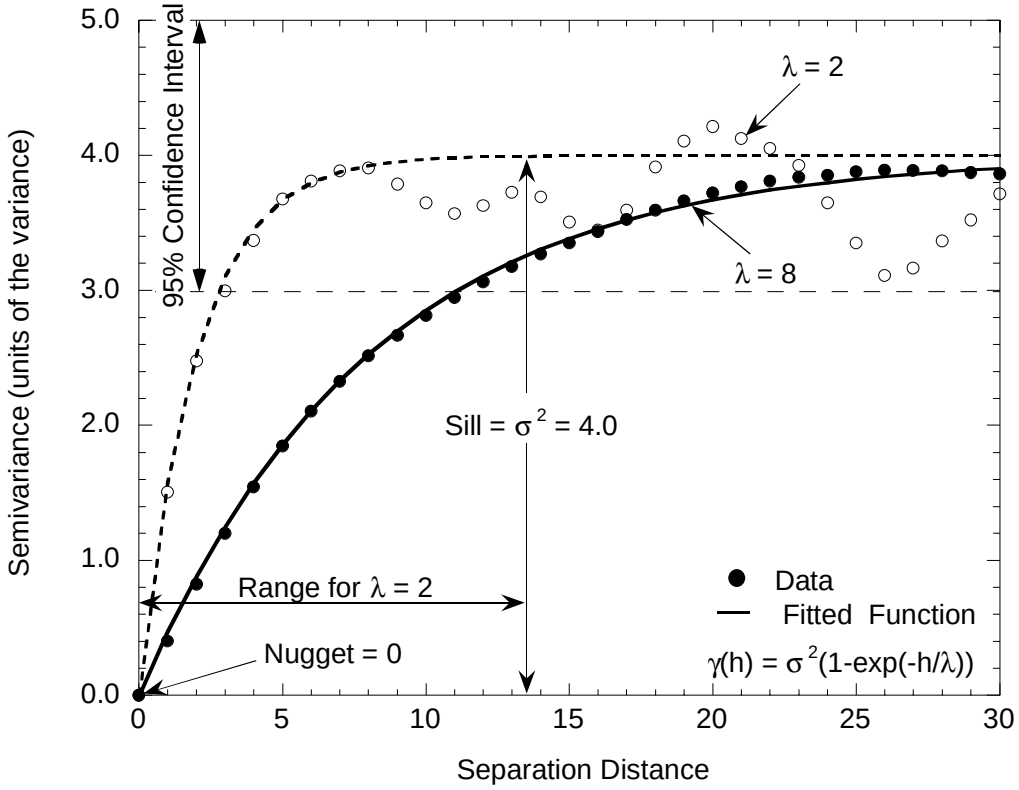

Fig. 3.4 Semivariogram Data and Fitted Exponential Functions for Correlated Random Fields with a Correlation Scales of 2 and 8 (same data as Fig. 3.3).

3.1.6 Common Assumptions of Geostatistical Theory

Several assumptions are made when applying the principles of autocorrelation to describe a random field. First, the field is generally assumed to be second-order stationary, meaning that the first and second moments (i.e., the mean and covariance), do not change in time or space (Gelhar 1993). Thus, the field must be statistically homogeneous such that autocorrelation is only a function of separation distance not location (Journel 1989). Therefore, spatial or temporal trends in the data may need to be removed prior to analysis (Rajaram and McLaughlin 1990). This requirement should not be confused with homogeneous and anisotropic random fields. Second-order stationarity can deal with anisotropic fields (i.e., fields that have different correlation structure in each direction). For heterogeneous fields, autocorrelation may be defined along axes (commonly orthogonal axes x, y, and z) by only considering separation distances parallel to each axis (Mantoglou and Wilson 1982).

3.2 APPLICATIONS OF GEOSTATISTICS

Two common applications of geostatistics will be described in this section, Monte-Carlo simulation and random field generation. A brief overview of Monte-Carlo simulation is discussed and a summary of methods for generating spatially correlated random fields is given. Concluding this section is a discussion of how the two techniques can be used together.

3.2.1 Monte-Carlo Simulation

Monte-Carlo simulation is a statistical tool whereby the outcome of an event is repeatedly predicted for randomly drawn sets of inputs. Monte-Carlo simulation differs from a traditional solution because inputs for the model are not constant. Rather, the inputs are drawn from probability distributions that describe the expected variability of the input parameters. The objective of Monte-Carlo simulation is to perform enough realizations of a problem such that a probability distribution of the outcomes can be constructed (Harter 1998). In essence, numerous samples are taken from probability distributions of the inputs and combined via a model into a probability distribution of outcomes. The number of required realizations depends on the number and variability of the inputs, and the sensitivity of the model. Generally the number of realizations is sufficient when the distribution of outcomes ceases to change with additional realizations (Benson and Daniel 1994). Monte-Carlo simulation of stochastically generated variants of an aquifer is one of the few tools for analysis of contaminant transport in heterogeneous aquifers (Harter 1998).

Eykholt (1997) demonstrates the effectiveness of Monte-Carlo simulation for assessing the impact of variability in reaction rate constant, input concentration, and seepage velocity on the output concentration from a column of reactive media. In his model, the reaction rate constant was characterized using a normal distribution, and the input concentration and seepage velocity were characterized using log-normal distributions. For each trial, 1000 to 10,000 realizations were performed. For each realization, values of reaction rate, input concentration, and

seepage velocity were drawn from their respective distributions. The output concentration from the column was calculated for each realization and the data pooled so that a probability distribution for output concentration could be defined for each trial. From the probability distribution of output concentration, the likelihood of effluent from the column exceeding a prescribed threshold concentration (i.e., maximum contaminant level) was obtained (Eykholt 1997).

3.2.2 Random Field Generation

Three of the common methods for generating spatially correlated random fields are discussed in this section: matrix inversion; turning bands; and local average subdivision (Fenton 1994, Christakos 1992). The aim of each method is to produce equally likely maps of a random field (Journel 1989). All methods assume that the random field is spatially discrete and can be fully described by the mean and covariance (i.e., second-order stationary) (Fenton 1994, Christakos 1992). The following subsection provides a brief theory of each method followed by the advantages and disadvantages of the method. References that provide a more though discussion of each method are noted. The turning bands method is discussed in slightly greater detail than the matrix inversion and local average subdivision methods because the turning bands method was used for generating random fields in this study.

3.2.2.1 Matrix Inversion Method

The matrix inversion method (lower-upper triangle matrix method) is a direct method for generating spatially correlated, random fields (Fenton 1994, Christakos 1992). The method involves creating an autocorrelation matrix that is a^2 by b^2 in size where a and b are the number of points along orthogonal axes of the two-dimensional, random field being generated. The autocorrelation matrix for the random field can be constructed by multiplying a covariance function (i.e., autocorrelation function or semivariogram) by a separation matrix. The separation matrix is ab by ab in size and defines the separation or lag distance between each point in the random field and all other points. The autocorrelation matrix will be a positive definite matrix and can be decomposed into an upper and lower triangular matrix, $\underline{\underline{L}}$ and $\underline{\underline{U}}$ respectively, such that the autocorrelation matrix equals the product of $\underline{\underline{L}}$ and $\underline{\underline{U}}$, and $\underline{\underline{U}}$ equals $\underline{\underline{L}}^T$ (Devroye 1986, Christakos 1992, Alabert 1987). This matrix is often inverted using a Cholesky Decomposition because it is approximately four times faster than other decomposition techniques (Press et al. 1992). Next, $\underline{\underline{L}}$ and $\underline{\underline{U}}$ are multiplied by a vector of independent, standard normal random variables ($\underline{N}$). This yields a covariance matrix ($\underline{\underline{Cov}}$) of standard normal random variables which is a by b in size and has an identical covariance structure as the original autocorrelation matrix since:

$$E\left[\left(\underline{\underline{L}}\,\underline{N}\right)\left(\underline{\underline{L}}\,\underline{N}\right)^T\right] = \underline{\underline{L}}\,E\left[\underline{N}\underline{N}^T\right]\underline{\underline{U}} = \underline{\underline{L}}\,\underline{\underline{I}}\,\underline{\underline{U}} = \underline{\underline{Cov}} \qquad (3.11)$$

where $\underline{I}$ is the identity matrix, which has a mean of zero and variance of one (Devroye 1986, Christakos 1992, Alabert 1987). Then the standard normal covariance can be converted to the desired distribution using a transform function.

Advantages of the matrix inversion method are that it is relatively simple to program and ensures that the random field has the desired covariance (Devroye 1986, Christakos 1992, Alabert 1987). The primary disadvantages of the matrix inversion method are the time needed for inverting the covariance matrix and the rounding error associated with inverting large matrices (Press et al. 1992). For example, consider generating a 100 by 100 node, correlated, random field (i.e., a and b equal 100). The autocorrelation matrix for this field is 10,000 by 10,000. The author attempted to invert a matrix this size using a Cholesky Decomposition but abandoned the process when it had not finished after 10 days of computation time on a HP-9000 workstation with 128 MB of RAM.

3.2.2.2 Turning Bands Method

The turning bands algorithm is used for generating second-order, stationary, correlated random fields of two or more dimensions (Mantoglou and Wilson 1982). The method involves projecting values from several spectral density line processes to discrete points in the random field. The random value at each point is then calculated as the weighted sum of inverted spectra which have been projected to the point from a finite number of spectral line processes (Mantoglou and Wilson 1982).

Given a second-order stationary field, the autocorrelation function can be converted to a spectral density function by taking the Fourier transform of the autocorrelation function. Then, random line processes [N(0,1)] of the spectral density function are constructed around a unit circle (or unit sphere for 3D fields) that has an origin in or near the domain of the random field (Mantoglou and Wilson 1982). Orthogonal projections are made to all points in the random field from each of the spectral line processes (Fig. 3.5). At each point in the random field, a weighted sum of these projections is calculated. This sum is then transformed from a spectral density to a covariance using an inversion method for the Fourier transform (Mantoglou and Wilson 1982, Shinozuka and Jan 1972).

Several variants of the turning bands approach are available (Fenton 1994, Tompson et al. 1989, Mejia and Rodriguez-Iturbe 1974). All of these methods rely on projecting a spectral density to points in the random field, but differ primarily in their strategy for converting from a spectral density to a covariance.

In general, there are two methods for inverting the spectra, a direct approach, where the inverse Fourier transform is approximated by the product of a numerical integral and cosine functions; and a fast-Fourier transform method, in which a standard subroutine is used for the transform. The most common direct approach uses an approximation of the inverse Fourier transform, first suggested by Rice (1954) and modified by Shinozuka and Jan (1972), who approximate the Fourier integral as:

$$Z_i(\zeta) = 2\sum_{k=1}^{m} \sqrt{S_1(w_k)\Delta w}\, \cos(w_k' \zeta + \phi_k) \qquad (3.12)$$

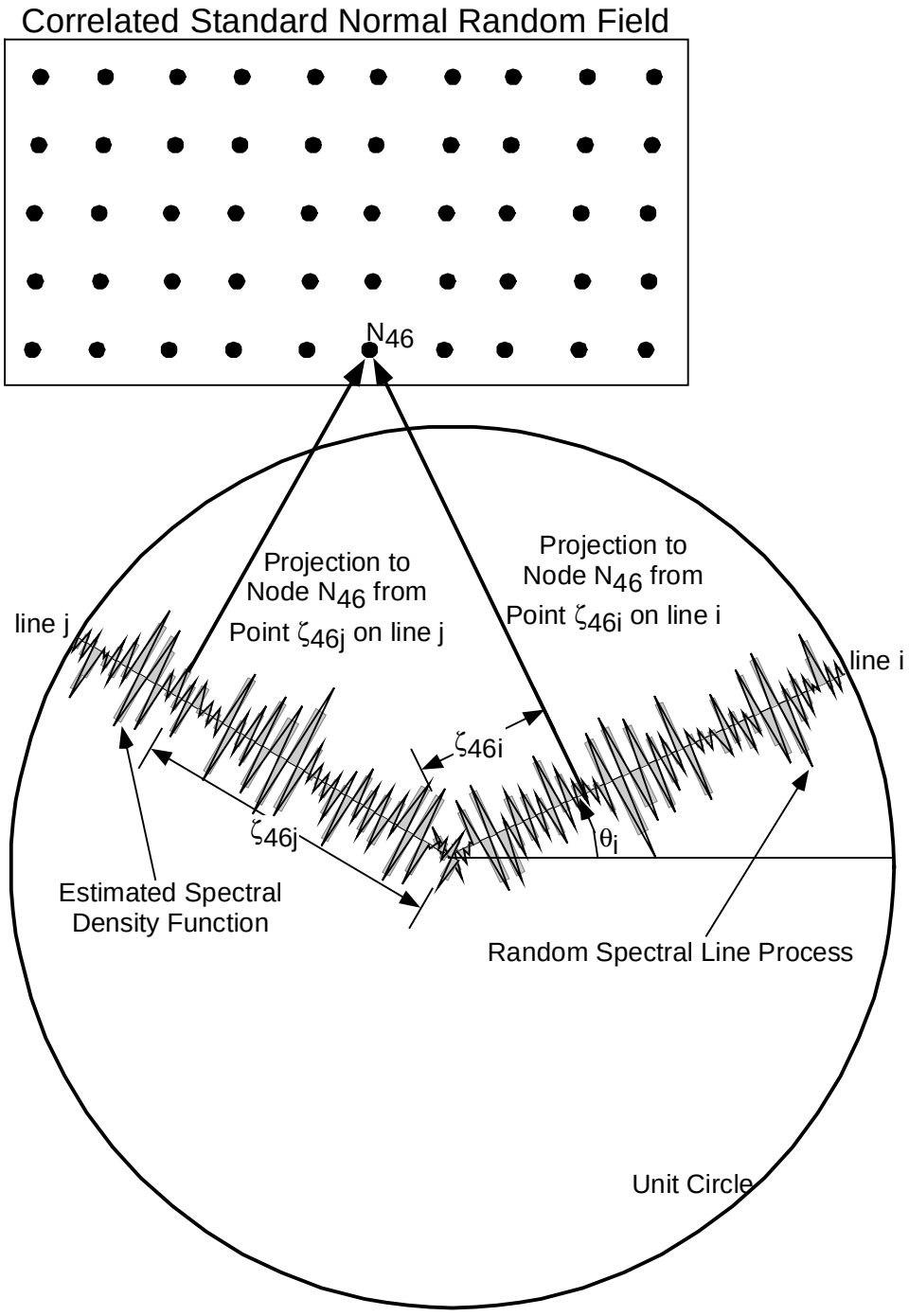

Fig. 3.5 Turning Bands Method for Projecting Points from Line Processes to a Node in the Random Field.

where $Z_i(\zeta)$ is the covariance of a standard normal field at point i in the real domain from a projection of point ζ along the spectral line process, $\sum_{k=1}^{m}\sqrt{S_1(w_k)\Delta w}$ is the numerical integration of the spectral density function ($S_1(w_k)$), discretized into k intervals of differential frequency Δw, w'_k is a frequency shifted by a differential frequency δw to avoid periodicity, and ϕ_k is a random angle [$U(0,2\pi)$]. Typically, the spectral density function is integrated between frequencies of zero and $20/\lambda$, and discretized into at least 100 differential frequencies (i.e., $m \geq 100$) (Mantoglou and Wilson 1982). Mejia and Rodriguez-Iturbe (1974) and El-Kali (1986) propose an equation similar to Eq. 3.12. However, the author could not successfully produce a random field with the desired correlation using their method and computer program.

The advantage of the direct method for inverting the spectral density function is greater flexibility in the choice of variables in Eq. 3.12. The fast-Fourier method is less flexible in this aspect. However, the direct method is two to three times slower than the fast-Fourier method (Tompson et al. 1989).

The alternative to the direct approach for inverting the spectral density function is to use a fast-Fourier transform routine (e.g., Press et al. 1992). When a fast-Fourier transform is used for inverting the spectral density function, the real component of the solution is the covariance at the desired point, and the imaginary component of the solution is discarded (Mantoglou and Wilson 1982). The fast-Fourier transform method is quicker than the direct method and produces random fields with slightly more accurate means. However, it is less flexible in the choice

of parameters for the spectral line process and frequency discretization (Tompson et al. 1989).

Overall, the turning bands method is a robust tool for generating correlated random fields. The mathematical basis for the theory is well established (e.g., Rice 1954, Shinozuka and Jan 1972, Mantoglou and Wilson 1982, and Tompson et al. 1989), the method is capable of producing large random fields in significantly less time than the matrix inversion method (Fenton 1994), and verified and documented source codes are available (e.g., via ftp://s112.es.llnl.gov). Also, since the turning bands method relies on projections between the spectral and real domain, random fields with uneven node spacing can easily be generated. This advantage allows heterogeneous random fields to be produced by simply scaling the size of the random field (and node locations) by a ratio of the correlation lengths in orthogonal directions (Tompson et al. 1989).

Disadvantages of the turning bands method are that it relies on numerical integration and a finite number of line processes. This limitation causes errors in the first and second moments. Tompson et al. (1989) review a number of errors that are inherent to the turning bands method and discuss precautions that can be taken to minimize their effect. One of the most common problems with random fields generated using the turning bands method is streaking. Streaking occurs when too few line processes are used around the unit circle (or unit sphere). The consequence of streaking is bands of lower variance through the random field corresponding to the direction of the line process used for the simulation. Streaking is minimized by increasing the number of line process used for the

simulation (Tompson et al. 1989). The reader is encouraged to review Tompson et al. (1989) prior to using the turning bands method, and refer to Mantoglou and Wilson (1982) for more a detailed discussion of spectral methods.

3.2.2.3 Local Average Subdivision (LAS)

Local average subdivision (LAS) is a method for generating second-order, homogeneous, isotropic random fields by successively subdividing regions of a random field into smaller cells. The basis for the method is to input a "local average" or mean for a region. This "parent" region is subdivided into two "children" for a one-dimensional process and four "children" for a two-dimensional process. The children are assigned correlated random values such that their mean is equal to the random variable of the parent and their variance matches the variance assigned to the random field. Children then become parents, are subdivided into children, and the process repeats. Subdivision of parents to children continues until the desired level of discretization is achieved (Fenton and Vanmarcke 1990).

One of the advantages of the LAS method is that global averages can be assigned across the random field by subdividing the domain into several regions (parents). Each parent is then subdivided to the desired fineness using the LAS method while the global average of the region is maintained. Thus, random fields with statistically dissimilar regions can be generated by assigning the appropriate properties as initial conditions (i.e. parents) for each region. Other advantages of the LAS method are that it ensures the mean of the random field is preserved and

can easily produce random fields with uneven node spacing. Also, the LAS method is well suited for finite element models because element properties can be assigned average properties for adjacent nodes (i.e., equal to the parent random variable). The computational speed of the LAS method is comparable to the turning bands method using fast-Fourier transform and significantly faster than the matrix inversion method (Fenton and Vanmarcke 1990).

There are some significant disadvantages and limitations to the LAS method. The most significant of the limitations is that there is a systematic bias when generating two-dimensional random fields. The bias causes streaking (i.e., lower variance) in a grid pattern at the boundary of all parent cells. The bias is a result of truncating the covariance function of children at the edges of parent cells. Presently, there is no method for eliminating this bias (Fenton 1994). Other disadvantages of the LAS method are that it cannot generate heterogeneous random fields, it is difficult to implement, and it is not widely used (Fenton and Vanmarcke 1990).

3.3 METHODS FOR SIMULATING HETEROGENEOUS AQUIFERS

There are two common methods for generating three-dimensional, random fields that represent the distribution of hydraulic conductivity in an aquifer. One method is to use sedimentary models that distribute facies within a geologic region by considering the lithology and depositional history of a site (Jussel et al. 1994a, Webb 1995, Webb and Anderson 1996, Riemersma et al. 1996). The other method is to use stochastic models that assume hydraulic conductivity is a second-

order, stationary random field that is characterized by a mean and covariance function (Freeze 1975, Smith and Freeze 1979b, Sudicky 1986, Schiebe and Cole 1994, and Moreno and Tsang 1994). In the following section, both modeling approaches will be explained and the advantages and disadvantages of each will be discussed.

3.3.1 Sedimentary Models

Sedimentary models predict the size, location and connectivity of dominant facies within an aquifer and then assign a hydraulic conductivity to each unit (Wu et al. 1973, Jussel et al. 1994a, Webb and Anderson 1996, Fisher et al. 1998). For groundwater flow problems, dominant units are zones of higher hydraulic conductivity (Moreno and Tsang 1994, Webb and Anderson 1996, Fisher et al. 1998); thus, the objective of sedimentary models is to mimic the geological processes that deposit high hydraulic conductivity units.

Several approaches have been used to locate more permeable units within a model domain. Wu et al. (1973), Riemersma et al. (1996), Aiken (1993), and Jussel et al. (1994a) mapped the size and location of facies during site excavations. These data were input directly into a groundwater model (Aiken 1993, Riemersma 1996) or used as representative samples of the site for Monte-Carlo simulation of a larger domain (Riemersma et al. 1996, Wu et al. 1973). For example, Wu et al. (1973) created a network model for predicting seepage under an earth dam by randomly locating oblong sand lenses in an otherwise homogeneous aquifer. The size of the lenses was assigned according to a

probability function that was created from data gathered during a site excavation. Flow between constant head boundaries was assumed to travel through sand lenses and only enter lower hydraulic conductivity soils when passing from the end of a sand lenses to the front of another sand lens. The total resistance for all possible pathways was calculated and seepage through the down gradient boundary was predicted for each realization. Multiple realizations of the aquifer were made so that a distribution of seepage under the dam could be constructed (Wu et al. 1973).

An alternative to randomly locating units of a known size and shape is to use a random walk procedure to assign the location of dominant units within the problem domain (Webb 1995). Webb (1995) created a model that produces an aquifer in layers. For each layer, a random walk procedure steps across the layer and determines the size, location, and branching of channel deposits based on a set of rules in the form of power functions that relate the number and size of channels that flow through the system, and probability functions that determine the likelihood of a channels forking (Webb 1995). Once facies are mapped, geologic units are assigned a uniform hydraulic conductivity (Webb and Anderson 1996) or given a hydraulic conductivity drawn from a variogram for each unit (Riemersma et al. 1996).

Advantages of sedimentary models of hydraulic conductivity are that they use the lithology to describe the distribution of facies within the aquifer and then assign a hydraulic conductivity to each unit. Constructing the lithology prior to assigning hydraulic conductivity, more accurately represents the process by which

the aquifer formed (Webb and Anderson 1996, Riemersma 1996). In addition, sedimentary models allow for sharp contrasts in hydraulic conductivity over short separation distances such as at the intersection of facies (Webb and Anderson 1996).

A disadvantage of sedimentary models is that they often require site data that may not be available. For example, the stream deposit model developed by Webb (1995) requires a bifurcation probability for estimating the probability of channels forking, a sinuosity to describe the tortuosity of channels, an estimate of the number of stream channels within the aquifer, and total flow entering the domain (Webb 1995, Webb and Anderson 1996). Obtaining these data may be difficult and expensive. Another disadvantage of sedimentary models is that present models are for coarse-grained, alluvial deposits (Webb 1995, Webb and Anderson 1996, Jussel et al. 1994a, Riemersma et al. 1996). Models for other types of deposits are not available.

3.3.2 Second-Order Stochastic Models

Second-order stochastic models are an alternative to sedimentary models for generating random fields of hydraulic conductivity that represent an aquifer. Second-order stochastic models differ from sedimentary models by assuming that hydraulic conductivity within the domain (i.e., the aquifer) is a correlated random field that can be described using a mean and covariance function. In this approach, the problem domain is divided into blocks and correlated random values [N(0,1)] are assigned to each block using any of the methods previously mentioned

(Freeze 1975, Tompson and Gelhar 1990, Scheibe and Cole 1994, Moreno and Tsang 1994). Hydraulic conductivity is then calculated for each block by transforming the standard normal random variable [e.g., multiplying the normal random variable by the standard deviation of the log-normal distribution for the hydraulic conductivity (σ_{lnK}), adding the mean of the hydraulic conductivity distribution (μ_{lnK}), and transforming the random variable using a natural logarithm function].

The advantage of the second-order stochastic approach is that only the mean and covariance structure for the simulated hydraulic conductivity fields are required. These data are available for several deposits (e.g., Freeze 1975, Hoeksema and Kitanidis 1985, Sudicky 1986, Hess et al. 1992, Gelhar 1993, Benson and Daniel 1994, Cooke et al. 1995), making this method more versatile than sedimentary models. Table 3-1 summarizes statistical parameters for logarithmically transformed hydraulic conductivity and transmissivity data from several field sites. Another advantage to second-order stochastic models is that random field generators that can produce large fields are readily available and well documented (Mantoglou and Wilson 1982, Tompson et al. 1989, Fenton and Vanmarcke 1990).

A disadvantage of the second-order stochastic approach is that the model assumes that hydraulic conductivity across the problem domain can be described by only a mean and covariance. This simplifying assumption ignores the site lithology and all geologic processes occurring while the deposit formed. One example of this error is the transition between regions of high and low hydraulic

Table 3-1 Stochastic Characterization of Hydraulic Conductivity in Selected Aquifers.

Geology	Mean (μ_{lnK})*	Variance (σ^2_{lnK})*	Correlation Length (ρ)**			Source
			X (m)	Y (m)	Z (m)	
gravel	-2.3	0.94	2.8-5.0	2.8-5.0	0.28-0.5	Jussel et al. (1997a)
alluvium	-0.71^T	1.01^T				Delhomme (1979)
alluvium	2.62^T	1.43^T				Delhomme (1979)
sand/gravel	-2.26	0.41	11-36	7-36	0-1	Riemersma (1997), Aiken (1993)
sand/gravel		3.5	12			Rehfeldt et al. (1989)
sand/gravel		4.6	13		1.6	Rehfeldt et al. (1989)
sand/gravel		3.6	9.5		1.1	Rehfeldt et al. (1989)
sand/gravel		2.1	13		1.5	Rehfeldt et al. (1989)
sand/gravel		1.9	20		0.5	Hufschmied (1986)
sand/gravel		4.5	12		1.5	Boggs et al. (1990)
sand	-4.63	0.38-0.6	2.8	2.8	0.12	Sudicky (1986)
sand		0.9	15			Viera et al. (1981)
sand	-4.62—4.68	0.356-0.261	7.15	2.79	0.160-0.252	Woodbury and Sudicky (1991)
sand	-4.63	0.382	7.50	1.21	0.144	Robin et al. (1991)
sand		0.2-0.5	5.1		0.26	Hess (1989)
sand		0.9	> 3.0		0.1	Byers and Stephens (1993)
sand		1.0	7.6			Gelhar et al.(1983)
sand	-2.26^T	0.69^T				Delhomme (1979)
sand	-1.77^T	2.07^T				Delhomme (1979)
sand	-1.34^T	0.64^T				Delhomme (1979)
sand	-0.48^T	1.91^T				Delhomme (1979)
mixed soils	-0.027					Hoeksema and Kitandis (1985)
silty clay		0.6	0.1			Sisson and Wierenga (1981)
clay liner	-16.8	0.164	-	-	-	Benson (1993)

*ln-normally distributed hydraulic conductivity in cm/s
** X, Y, and Z refer to orthogonal directions parallel to groundwater flow, horizontal and perpendicular to groundwater flow, and vertical respectively
T – transmissivity data

conductivity. Webb and Anderson (1996) point out that large changes in hydraulic conductivity may occur over short separation distances, particularly at the boundary of facies. Second-order stochastic models rely on autocorrelation functions that smooth data by restricting the effective range of random values at short separation distances (Fig. 3.3 and 3.4). This forces transitions between units to be smoother than what might occur in nature (Webb and Anderson 1996).

3.3.3 Comparison of Sedimentary and Second-Order Stochastic Models

Determining which method of generating three-dimensional random fields of hydraulic conductivity is better is difficult since both models have several advantages and disadvantages. Riemersma et al. (1996) and Schiebe and Cole (1994) evaluate the two models on the basis of particle transit times across statistically similar aquifers that were generated using sedimentary and second-order stochastic models (Riemersma 1996). They present cumulative probability distributions of particle transit times for an aquifer generated using each method. Aquifers that have different levels of heterogeneity are evaluated at steady-state conditions with and without a pumping well (Riemersma et al. 1996, Schiebe and Cole 1994).

Distributions of particle travel time across aquifers are nearly identical for aquifers that have a moderate level of heterogeneity and no pumping (Riemersma et al. 1996, Scheibe and Cole 1994). When a pumping well is added or for more heterogeneous aquifers, particle travel times through aquifers produced using a second-order stochastic model were shorter than those in aquifers produced using

a sedimentary model, although initial arrival times were the same (Riemersma 1996, Riemersma et al. 1996). Riemersma et al. (1996) also compared particle travel times for three aquifers generated using a second-order stochastic model to an aquifer generated entirely from measured hydraulic conductivity data (Aiken 1993). Particle transit times were less for aquifers generated using a second-order stochastic model under pumping conditions or at higher levels of heterogeneity, but similar at moderate levels of heterogeneity and without simulated pumping (Riemersma 1996, Riemersma et al. 1996). From these results, it can be implied that the two modeling approaches for generating heterogeneous fields of hydraulic conductivity (aquifers) yield similar pathways for advective transport and dispersion of contaminants, provided the level of heterogeneity is moderate or low, flow occurs under natural gradients, or no pumping is considered. Also, initial arrival times are similar for both methods at all levels of heterogeneity.

SECTION 4

METHOD AND MODEL VERIFICATION

This section explains the method used to assess the effectiveness of PRBs in heterogeneous aquifers and provides verification of the models used for this study. The section is divided into three parts: (1) aquifer simulation, (2) flow simulation, and (2) contaminant transport modeling. Figure 4.1 is a flow chart showing the basic approach used for this study.

Prior to proceeding, two significant assumptions of the method need to be discussed. These assumptions are necessary for the reader to understand the remainder of this section and subsequent sections.

The first assumption is that flow and transport are steady-state. Thus, sources of contamination are assumed to be persistent and flow is assumed to be independent of time. Steady-state flow is reasonable considering the design life for PRBs is 15 to 30 years. Assuming a constant source of contamination is less realistic since concentrations will likely decrease with time; however, the error caused by overestimating concentration is conservative because it yields higher margins of safety. Added conservatism may be desirable given the dearth of data about the long-term durability of iron.

The second assumption is that distributions of hydraulic conductivity can be accurately described using a second-order stochastic model. The advantages and disadvantages of second-order stochastic models were discussed in the previous

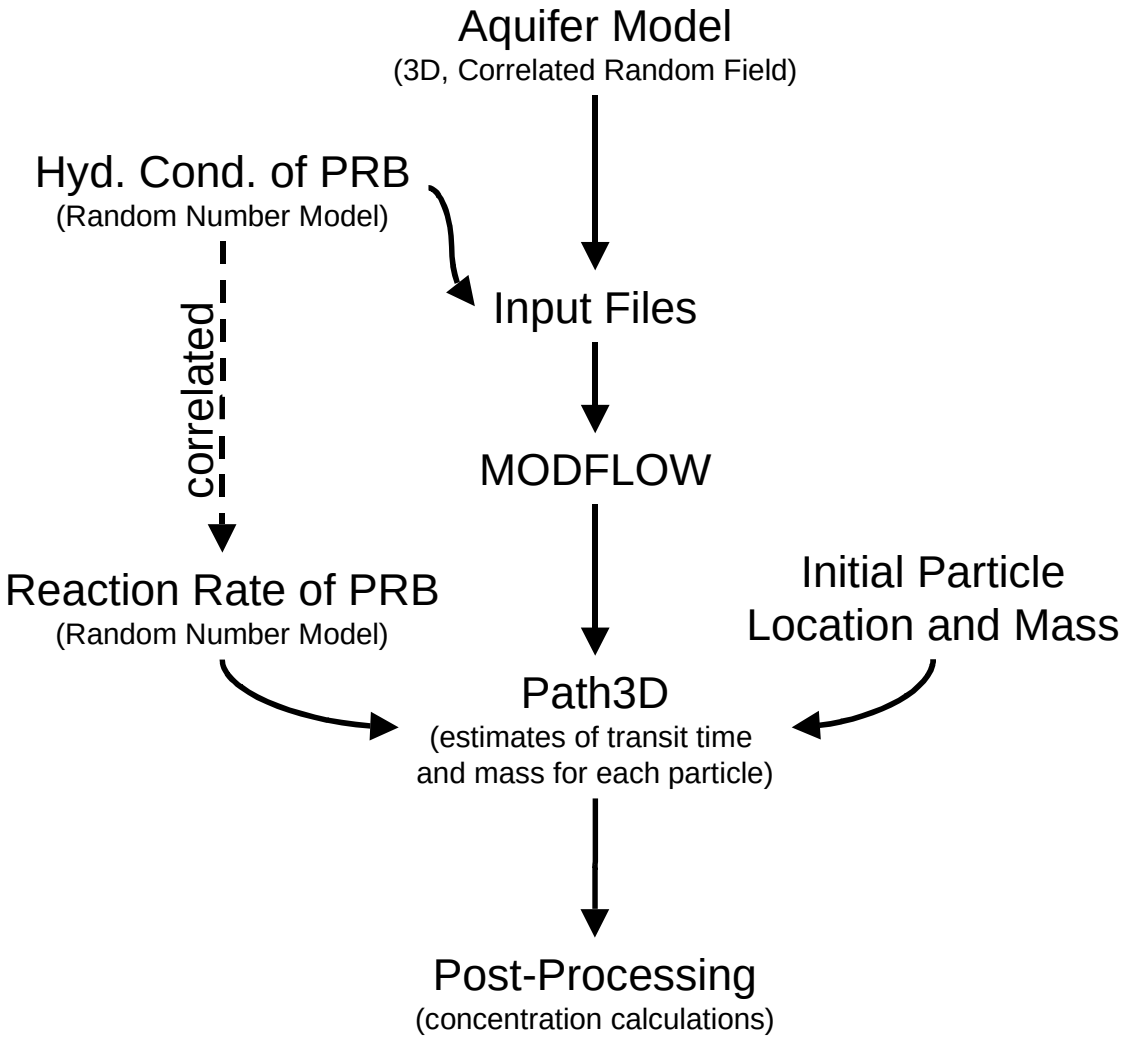

Fig. 4.1 Flowchart of the Method Used for Evaluating the Effectiveness of PRBs Amidst Uncertainty in Flow and Reaction Rate.

section. Additional justification for using a second-order stochastic model is provided in this section.

4.1 AQUIFER SIMULATION

The objective of simulating aquifers is to provide a structure in which to place a PRB. Random fields chosen to represent an aquifer should produce similar boundary conditions for the PRB as a natural aquifer. These conditions include representative flow and concentration entering and exiting the PRB, and a realistic distribution of more permeable units intersecting the PRB. Thus, the aim of using a second-order stochastic approach was not to duplicate flow and contaminants transport in natural aquifers, but rather, to create a domain resembling a natural aquifer for the purpose of studying PRBs.

4.1.1 Random Number Generation and Verification

An essential element of random field generation is the random number generator. Requirements of the random number generator are that it quickly produces random numbers that are independent, random, and have the desired distribution. A linear congruent random variable generator was selected to produce U(0,1) variables for this project. This random number generator was verified for independence, randomness, repeatability, and accuracy.

Linear congruent generators are the most common type of random number generator. Linear congruent generators produce random variables by repeatedly taking the modulus of the previous random variable and a constant that is specified

within the program. Frequently, this involves taking a single modulus but more complex random number generators may use several moduli in series to yield a random variable (e.g., Whichman and Hill 1987). Multiple operations tend to increase the period of the random number string and computation time. For the first call to the generator, the code uses a seed that is provided by the user. For successive calls, a variant of the previous random variable is used as input to the random number generator. In theory, each seed produces a unique and repeatable string of random numbers. This feature is useful when deciphering the impact of randomness within the model from the effects of changing model inputs.

The advantage of linear congruent random number generators is their speed. They produce random variables up to 40 times faster than other methods. The disadvantage of linear congruent generators is that they have shorter cycle lengths than other routines (Press et al. 1992).

The random number generator used for this study was checked for periodicity by generating a continuous string of random variables until the seed for the string was repeated. This test was performed for seeds of 5, 6, 7, 8, and 9. For each trial, the seed was not repeated after 6.2×10^{10} calls to the function. The reported cycle length for similar codes is 2×10^{9}. For this research, 2×10^{9} random variables exceed the expected number of random variables required for generating a random field.

The random number generator was checked for repeatability by producing data sets containing 10 strings of 1000 random variables. The data sets were reproduced three times using the same seed and checked against previous data

sets. The random number generator reproduced each data set exactly to five decimal places.

The random number generator was checked for accuracy at producing U(0,1) random variables using the Kolmogorov-Smirnov Test (Kolmogorov 1933, Smirnov 1939). The Kolmogorov-Smirnov Test evaluates the absolute residual error between two distributions. Ten strings of 1000 random variables were compared against the equation for the CDF of a U(0,1) distribution. The mean, standard deviation, skewness, kurtosis, and D-statistic from the Kolmogorov-Smirnov Test, that measures the probability that the random variables are U(0,1) distributed, are presented in Table 4.1. Table 4.1 also contains the theoretical values for the mean, standard deviation, skewness, kurtosis, and D-statistic for a U(0,1) distribution (Hastings and Peacock 1975).

Table 4-1 Verification for U(0,1) Random Variable Generator.

	Count	Mean	Standard Deviation	Skew	Kurtosis	Kol-Smir. D-Statistic	P(RV are U(0,1))**
Theoretical*	-	0.500	0.289	0.000	-1.200	0.000	-
String 1	1000	0.498	0.289	0.004	-1.197	0.156	>99.9%
String 2	1000	0.501	0.289	-0.008	-1.201	0.092	>99.9%
String 3	1000	0.500	0.289	-0.005	-1.198	0.098	>99.9%
String 4	1000	0.501	0.288	-0.012	-1.187	0.188	>99.9%
String 5	1000	0.500	0.289	-0.012	-1.198	0.141	>99.9%
String 6	1000	0.498	0.289	0.004	-1.198	0.176	>99.9%
String 7	1000	0.499	0.290	0.006	-1.203	0.171	>99.9%
String 8	1000	0.500	0.289	-0.002	-1.204	0.094	>99.9%
String 9	1000	0.499	0.289	0.002	-1.207	0.112	>99.9%
String 10	1000	0.501	0.290	-0.011	-1.208	0.124	>99.9%

* from Hastings and Peacock (1975)
** from Hald (1952)

4.1.2 Random Field Generation and Code Verification

Normally distributed and spatially correlated random fields were generated using a turning bands program by Tompson et al. (1989) (available by ftp at s122.es.llnl.gov in a directory /users/andy/turn). The author modified the code to better suit the needs of this project. These modifications include changing the form in which inputs are entered, format and naming of output files, and grid spacing used by the program. The program was tested to determine if the generated fields are normally distributed, have the correct correlation structure, and are ergodic. Also, the number of lines, discretization of the spectral density function, discretization of frequency, maximum frequency, and maximum correlation scale for the model were varied to determine model parameters that yield satisfactory random fields.

The turning band model was tested at several correlation ratios (correlation length/random field length) to see if the program could accurately produce standard normal random fields. Correlation ratios of 5%, 10%, 20%, and 30% were evaluated for 10 realizations of an isotropic field of 100 by 100 elements. The same seed was used for each set of realizations.

Error in the mean and standard deviation of the random fields increased with correlation ratio. When the correlation ratio was 5%, the absolute residual errors for the mean and standard deviation were 0.03 and 0.038, respectively. At a correlation ratio of 10%, the absolute residual errors for the mean and standard deviation were 0.06 and 0.08, respectively. Random fields with a correlation ratio of 20% had absolute errors of 0.13 and 0.115, while random fields with a

correlation ratio of 30% had errors of 0.18 and 0.21. However, error in the mean and standard deviation decreased when the size of the population was increased by using random values from multiple random fields. For the turning bands method, the mean and standard deviation calculated from all random values from four random fields with a correlation scale of 20% had approximately the same error as the mean and standard deviation calculated using random values from a single random field with a correlation ratio of 10%. The literature recommends a maximum correlation ratio between 10% (Tompson et al. 1989) and 20% (Moreno and Tsang 1994). Given these recommendations and the analysis herein, a maximum correlation ratio of 20% was used.

Autocorrelation data for random fields with correlation ratios of 5%, 10%, 20% and 30% are shown in Fig. 4.2 with the corresponding autocorrelation functions. In addition, 95% confidence limits, calculated using the method of Lumb (1974), have been added around zero autocorrelation. These limits show the ranges of autocorrelation where there is a 95% probability that the autocorrelation is zero.

Data produced using a correlation ratio of less than 30% demonstrate ergodicity within the dimensions of the problem (i.e., $\rho(h) = 0$ as $h \rightarrow 100$) and follow the correlation function well. Autocorrelation data for random fields with a correlation ratio of 30% do not demonstrate ergodicity or match the correlation function well. Based on this result, a correlation ratio of 20% or less was used for this study to ensure random fields are ergodic and have the correct correlation

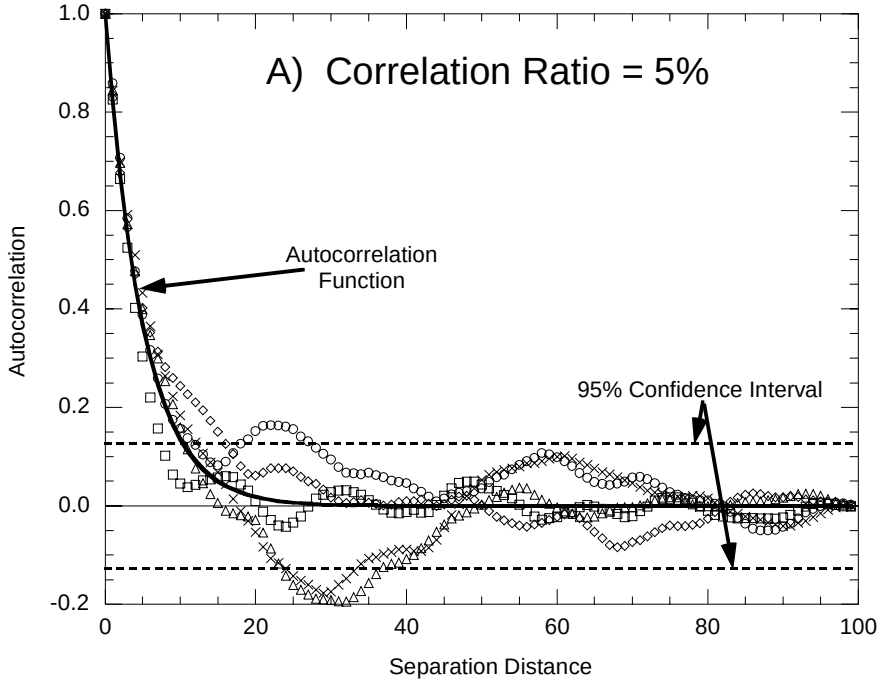
A) Correlation Ratio = 5%
Autocorrelation
Function
95% Confidence Interval
Autocorrelation
Separation Distance
1.0
0.8
0.6
0.4
0.2
0.0
-0.2
0
20
40
60
80
100

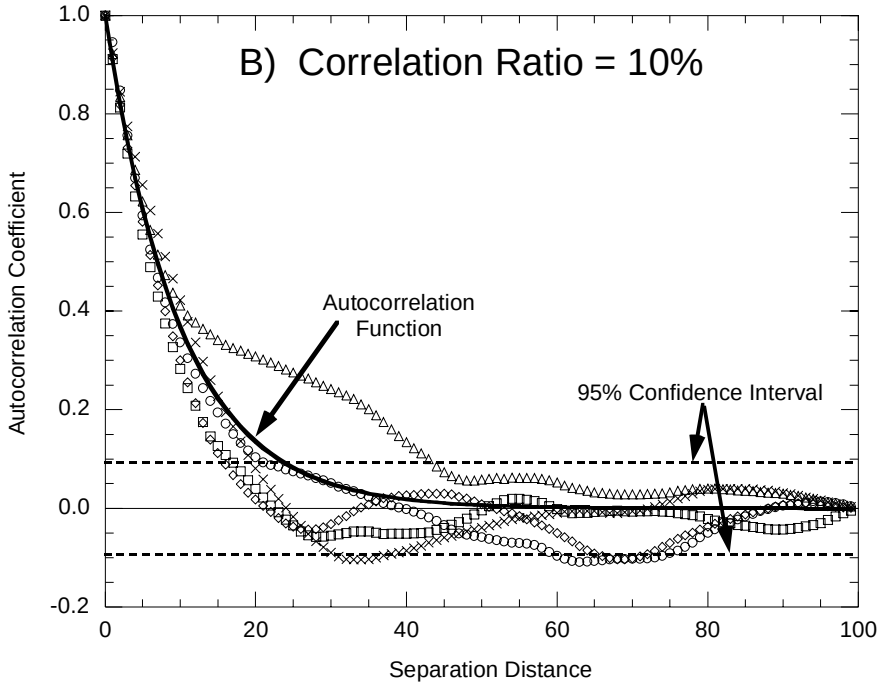
B) Correlation Ratio = 10%
Autocorrelation
Function
95% Confidence Interval
Autocorrelation Coefficient
Separation Distance
1.0
0.8
0.6
0.4
0.2
0.0
-0.2
0
20
40
60
80
100

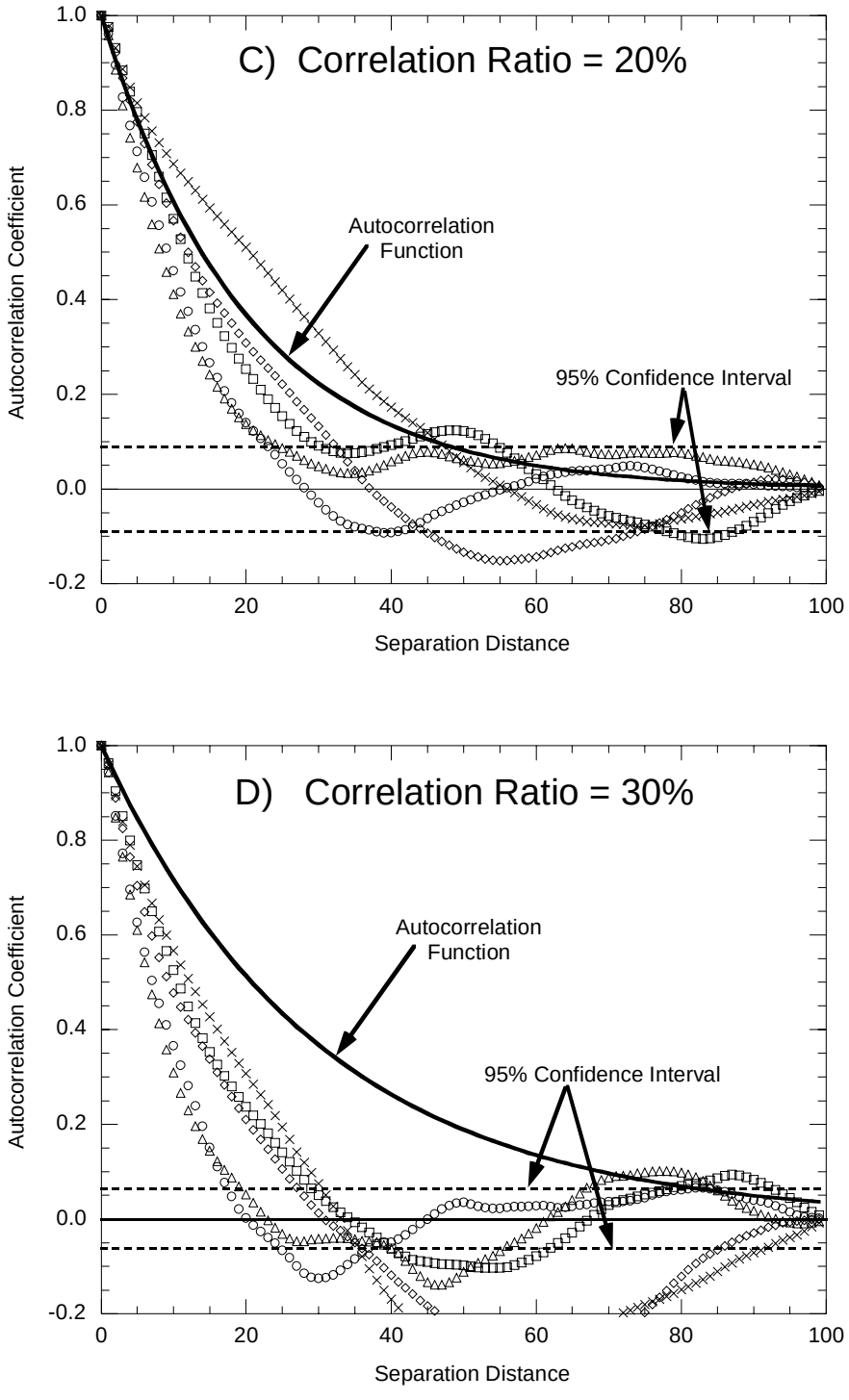

Fig. 4.2 Determination of the Maximum Allowable Correlation Ratio for the Turning Bands Code. Correlation Data and Functions at Correlation Ratios of (a) 5%, (b) 10%, (c) 20%, and (d) 30%.

structure. This criterion is similar to the requirement necessary to achieve the correct mean and standard deviation for the random field.

Normality of the random field was verified using the Kolmogorov-Smirnov Test. The five realizations shown in Fig. 4.2a were tested for normality. For all correlation scales, the probability that the data are normally distributed is greater than 99.9%.

The required discretization of the random field as a ratio of autocorrelation length was investigated. Five isotropic random fields with a correlation ratio of 5% were produced with a ratio of autocorrelation length to grid spacing ($\lambda/\Delta x$) of 10, 8, 6, 4, and 2. These random fields contained 200 by 200, 160 by 160, 120 by 120, 80 by 80, and 40 by 40 cells, respectively. For each random field, five realizations were generated. Autocorrelation data for each realization and the autocorrelation function are shown in Fig. 4.3. Regardless of the discretization that was used, the autocorrelation data differ little from the function and from one another. This implies that any cell width less than one-half of a correlation length is satisfactory. The literature recommends a maximum cell width of one-half of a correlation length (Moreno and Tsang 1994, Ababou et al. 1988) to one-quarter of a correlation length (Tompson et al. 1989), with an optimum cell width of one-tenth of a correlation length (Tompson et al. 1989). Given the data shown in Fig. 4.3, a maximum grid spacing of one-half of a correlation length was used for this study. This criterion allows fewer cells to be used when producing larger fields.

The sensitivity of the mean, standard deviation, and autocorrelation of the random field to changes in the number of lines, discretization of the spectral line

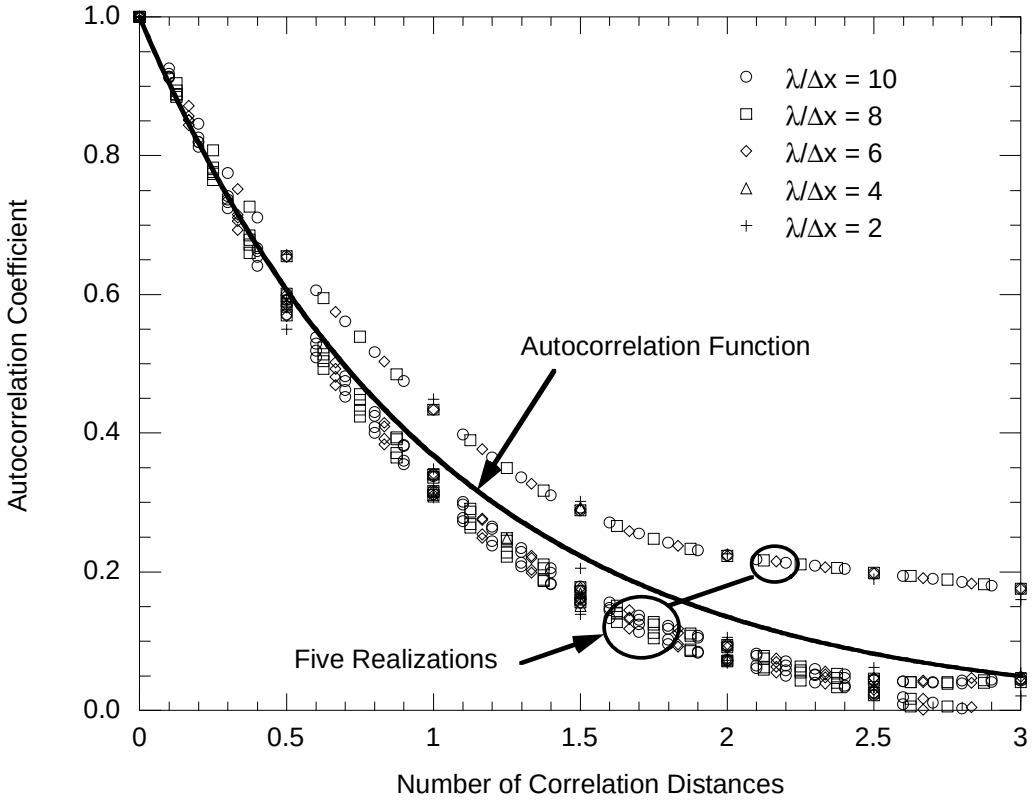

Fig. 4.3 Determination of the Maximum Allowable Grid Spacing for the Turning Bands Code.

process, and upper bound for numerical integration of the spectral density function was investigated briefly. Tompson et al. (1989) fully evaluated the impact of these parameters.

The number of lines projected to each point in the random field was varied between 50 and 500. For each number of lines, five realizations were generated of a 100 by 100 node random field. Changing the number of lines had little effect on estimates of the mean and standard deviation for the random fields, and using more lines only improved the correlation slightly. However, the computation time increased significantly when additional lines were added. Thus, 100 lines were used for all random fields produced for this project. Tompson et al. (1989) also recommends using 100 lines.

The discretization of the spectral line process ($\Delta\zeta$) was reduced from 0.1 to 0.05. This change is consistent with recommendations by Tompson et al. (1989) and allows for a minimum node spacing of 0.05 m rather than 0.1 m. The upper bound for integrating the spectral density function was also fixed at 50 rather than $20/\lambda$. This change ensures that the tail of the spectral density function (i.e., higher frequencies) is properly accounted for during numerical integration.

The turning bands code was modified to produce anisotropic fields by adjusting the node coordinates of the desired anisotropic field such that the autocorrelation length in each direction is the same (an isotropic field). The turning bands method is then used to create an isotropic field for the adjusted coordinate system. Then, the field is “stretched” back to the original coordinates, producing an anisotropic random field. The accuracy of this procedure was verified by

comparing autocorrelation data for an anisotropic, rectangular field (200 x 200 nodes) with a correlation ratio in the X direction equal to 5%, correlation ratio in the Y direction equal to 2.5% with autocorrelation functions. Three realizations of the random field are shown in Fig. 4.4. Autocorrelation data match the appropriate autocorrelation function indicating that the “stretching” procedure works properly.

The final test for the random field is to look for patterns, streaking, and anomalies in the random field. Figure 4.5 shows two realizations of a 200 by 200 node, random field with correlation lengths of 10 and 5, and unit discretization (realizations one and two from Fig. 4.4). There are no unexpected patterns or streaking visible in the fields and there are smooth transitions between lighter and darker regions. Also, locations of darker and lighter regions appear random within each field and different between the two fields indicating that the fields are probably random and independent. The anisotropy of the random fields is apparent in the elongated darker and lighter regions.

Based on the results of the aforementioned tests performed to validate the random field model, the model is believed to produce correlated, normal random fields provided certain criteria are followed. These criteria and constants used for the turning bands code are summarized Table 4.2.

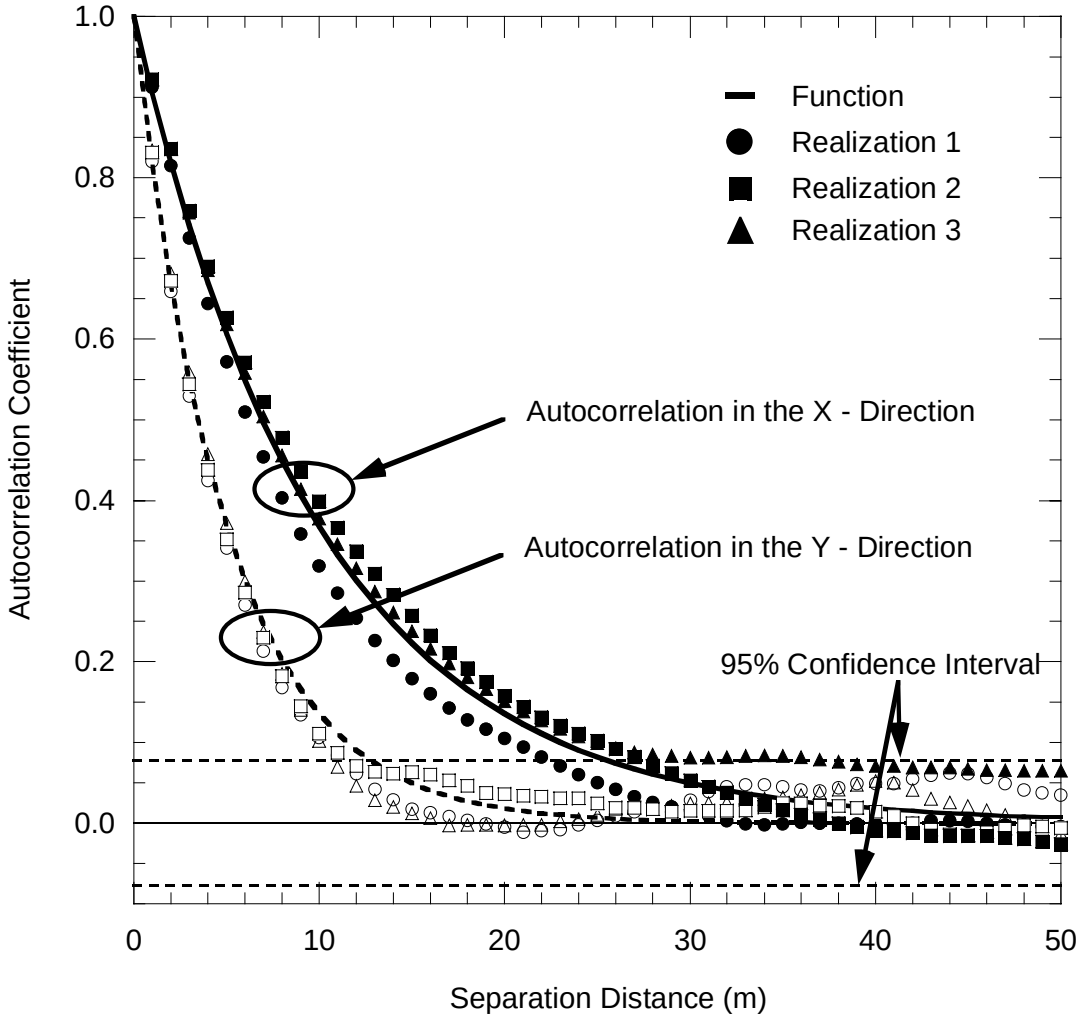

Fig. 4.4 Autocorrelation Functions and Data for an Anisotropic Random Field.

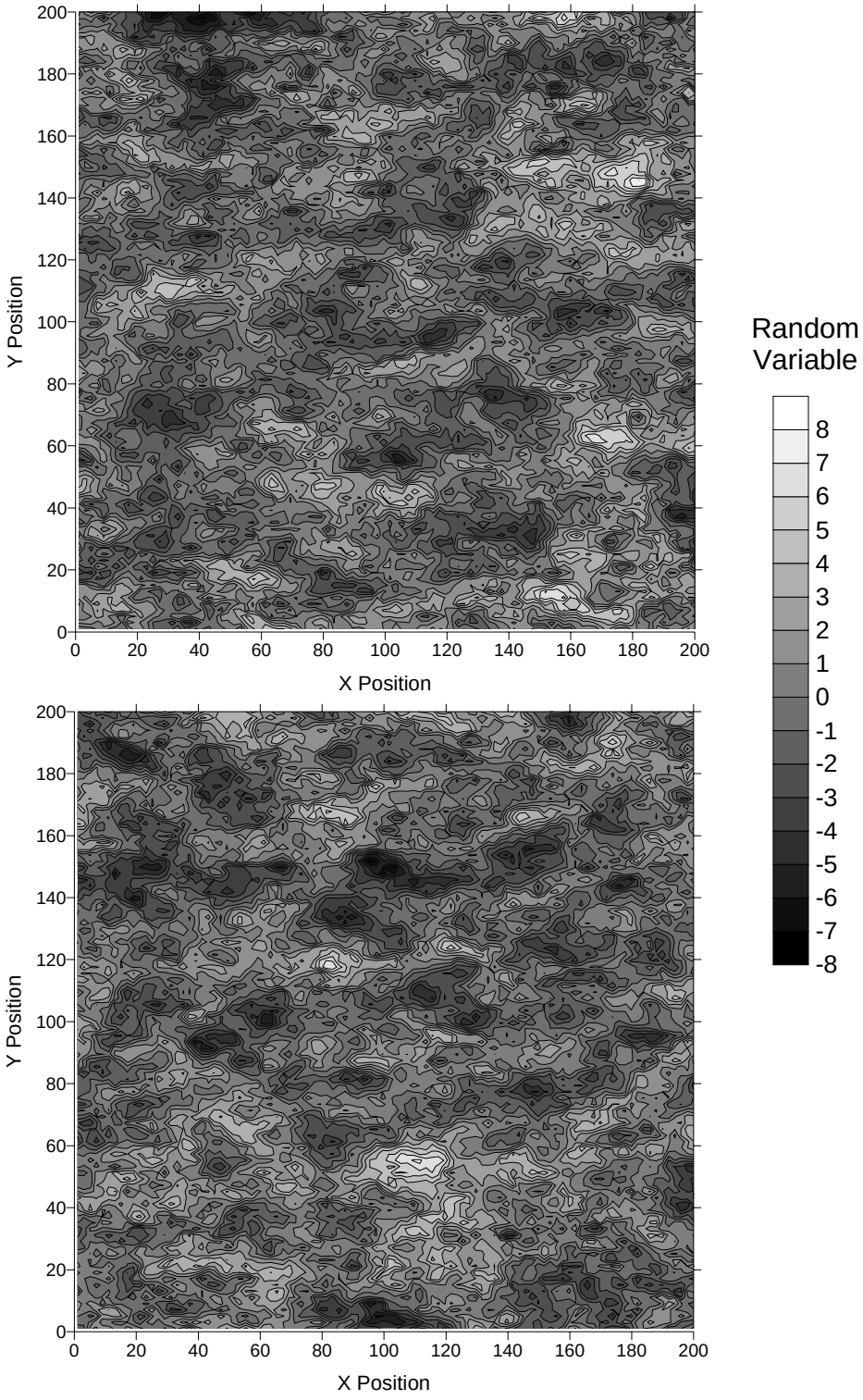

Fig. 4.5 Gray-Scale Images of Two Anisotropic Random Fields (N(0,2), $\lambda_x = 10$, $\lambda_y = 5$, Mesh = 200x200, $\Delta x = \Delta y = 1$, and linear interpolation between data).

Table 4-2 Criteria for Turning Bands Program.

Criteria for Turning Bands Program	
Maximum Correlation Ratio for a Single Random Field	10%
Maximum Correlation Ratio for Four of More Random Fields	20%
Maximum grid size	0.5λ
Number of Lines	100
Discretization of the Spectral Density Function ($\Delta\omega$)	0.1
Maximum Frequency for the Spectral Density Function	50
Discretization of the Unit Line Process ($\Delta\zeta$)	0.05

4.1.3 Stochastic Descriptors of an Aquifer

The random field generator is capable of producing two-dimensional, correlated, standard normal, random fields. These fields are transformed into random fields with the desired distribution and stacked to create a three-dimensional random field of hydraulic conductivity. Since the intent of the random field is to simulate the distribution of hydraulic conductivity in an aquifer, log-normal and three parameter log-normal distributions were investigated. Data for a braided stream deposit reported by Riemersma (1996) were used as representative data for comparison with simulated aquifers.

Determining the appropriate distribution for hydraulic conductivity began by constructing a PDF for the data reported by Riemersma (1996). The best-fit three-parameter log-normal and log-normal distributions were fit to the data. Also, autocorrelation data were calculated and several functions were fit to Riemersma's data. Once the appropriate stochastic functions had been fit to the data, stochastically similar random fields were generated using the turning bands model.

Synthetic aquifers were created from the random fields and the heads at all nodes were calculated using MODFLOW. Transit times for particles to cross the domain were calculated using Path3D. Particle travel times were compared between aquifers created using the second-order stochastic model and those created by Riemersma (1996).

Hydraulic conductivity data reported by Riemersma (1996) for the Stoughton aquifer (Aiken 1992) and a realization from Webb's stream flow model (Webb and Anderson 1996) are shown in Fig. 4.6. Also shown are point values of the three-parameter log-normal and log-normal functions fit to the data. When fitting functions to the data, a better fit was sought for the higher hydraulic conductivity data than for the lower hydraulic conductivity data to better simulate the impact of more permeable units that are believed to strongly affect transport through the aquifer (Riemersma 1997).

The log-normal distribution fit to data for the Stoughton Aquifer has a mean of -6.15 [m/s] and standard deviation of 1.0. The three parameter log-normal function fit the data has a mean of -6.15 [m/s], standard deviation of 1.0, and third parameter of 4.7×10^{-5} m/s. Both functions fit the data with approximately the same accuracy. The three parameter log-normal distribution fit to data from a realization of Webb's stream flow model (a sedimentary model) has a mean of -9.6 [m/s], standard deviation of 2.4, and third parameter of -5.0×10^{-5} m/s. The log-normal function fit to data from a realization of the Webb Stream Flow Model has a mean of -8.85 [m/s] and a standard deviation of 1.71. The three-parameter log-normal

a) Stoughton Aquifer

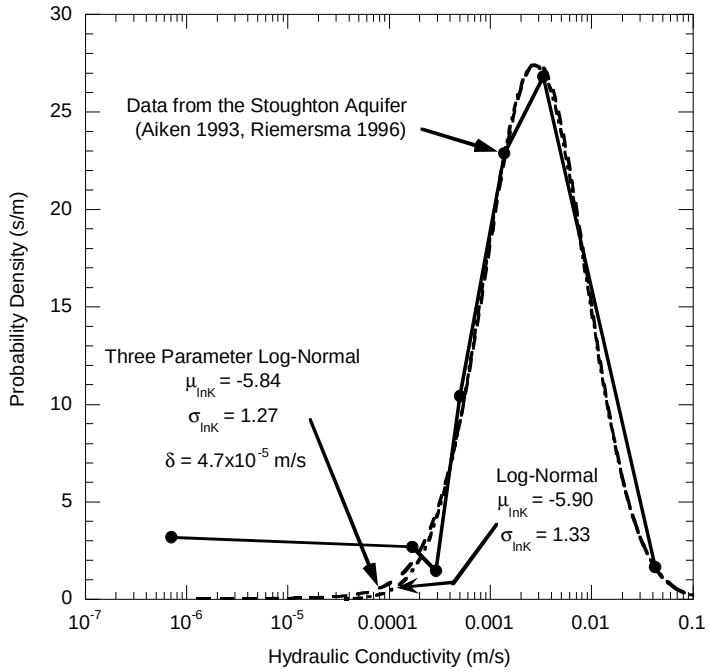

b) Aquifer from Webb Stream Flow Model

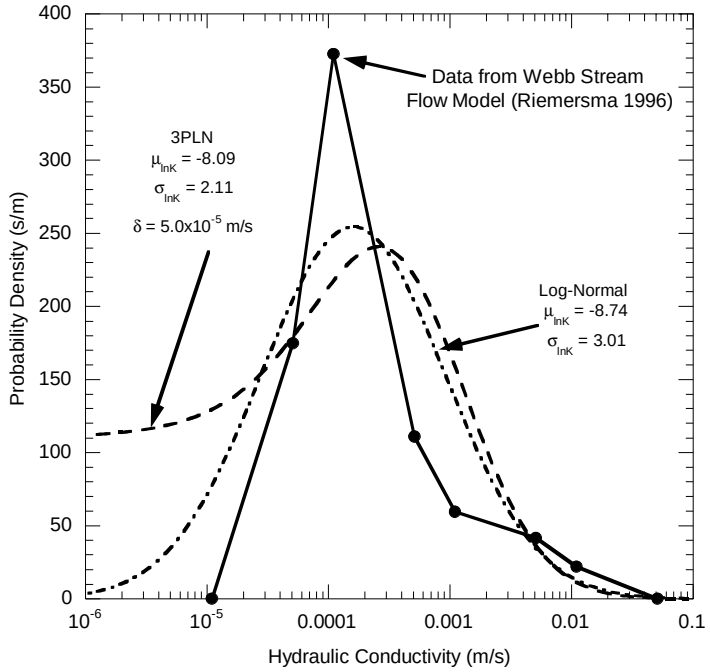

Fig. 4.6 Probability Density Functions Fit to Data from the Stoughton Aquifer (a) and a Realization from the Webb Stream Flow Model (b)

distribution fit data for the stream flow model slightly better (i.e., slightly lower mean-square error) than the log-normal distribution because it represents the higher hydraulic conductivities better.

Sample estimates of the autocorrelation function obtained using the hydraulic conductivity data were fit to exponential, spherical, and double exponential correlation functions. Sample autocorrelation in the horizontal directions were best fit using an exponential function with correlation scales of 30.7 m parallel to the regional gradient and 15.4 m perpendicular to the regional gradient. Vertical hydraulic conductivity is uncorrelated at scales greater than or equal to the vertical discretization. Correlation functions and data for the aquifer are shown in Fig. 4.7.

Several realizations of the Webb stream flow aquifer and the Stoughton aquifer were generated using the turning bands random field generator and three parameter log-normal and log-normal estimates for the hydraulic conductivity field. These aquifers were input into MODFLOW to determine the head at all nodes. Then Path3D was used to calculate the transit time for particles to cross the aquifer. Transit times across the Stoughton aquifer from Riemersma (1996) and the average travel time for five realizations of each stochastic model are shown in Fig. 4.8. Both hydraulic conductivity distributions produce aquifers that yield similar particle transit times as the Stoughton deposit, which suggests that a second-order stochastic model that uses either distribution function can simulate advection through an aquifer.

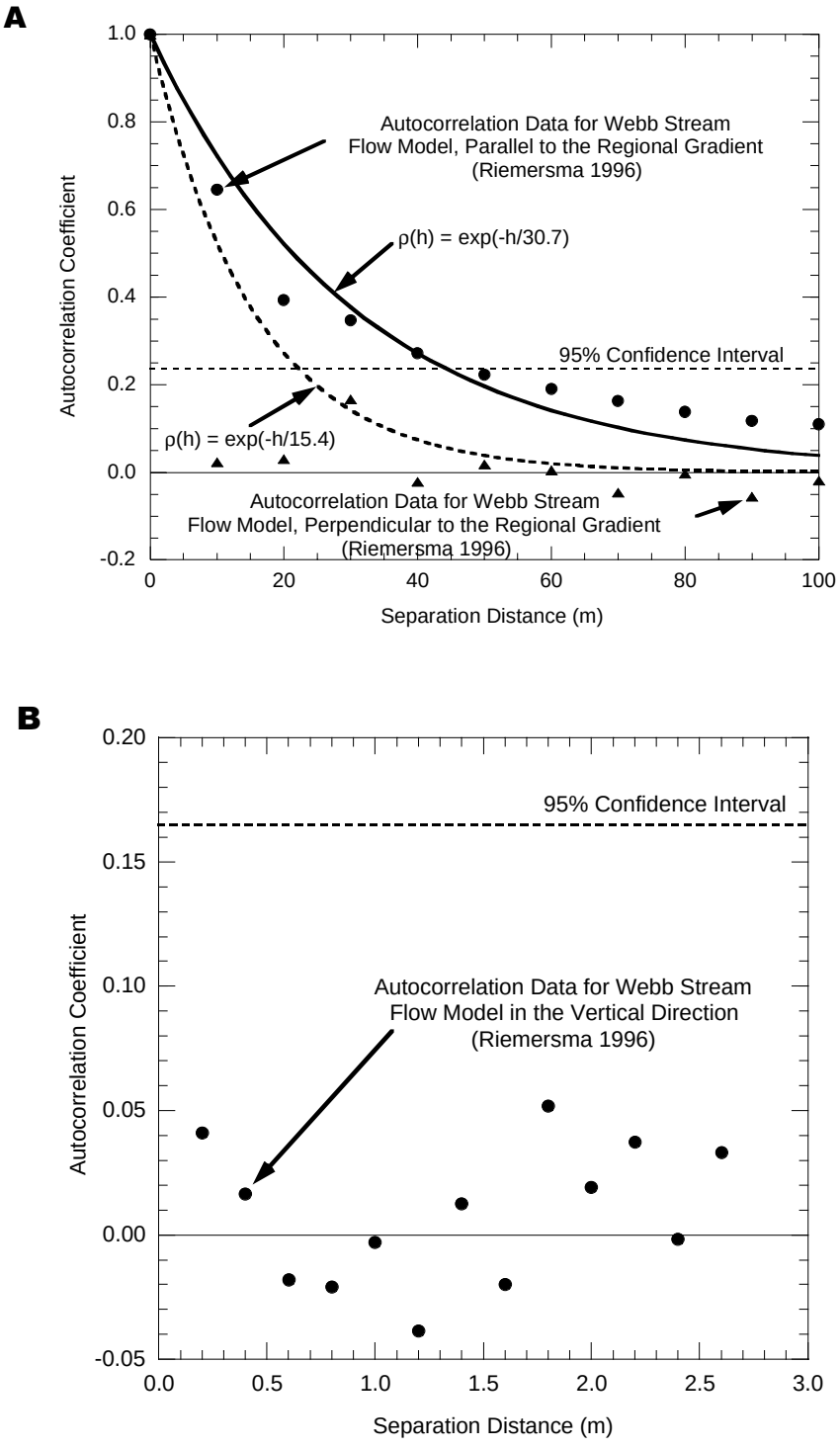

Fig. 4.7 Horizontal (a) and Vertical (b) Autocorrelation Data from a Realization from the Webb Stream Flow Model and Best-Fit Autocorrelation Functions.

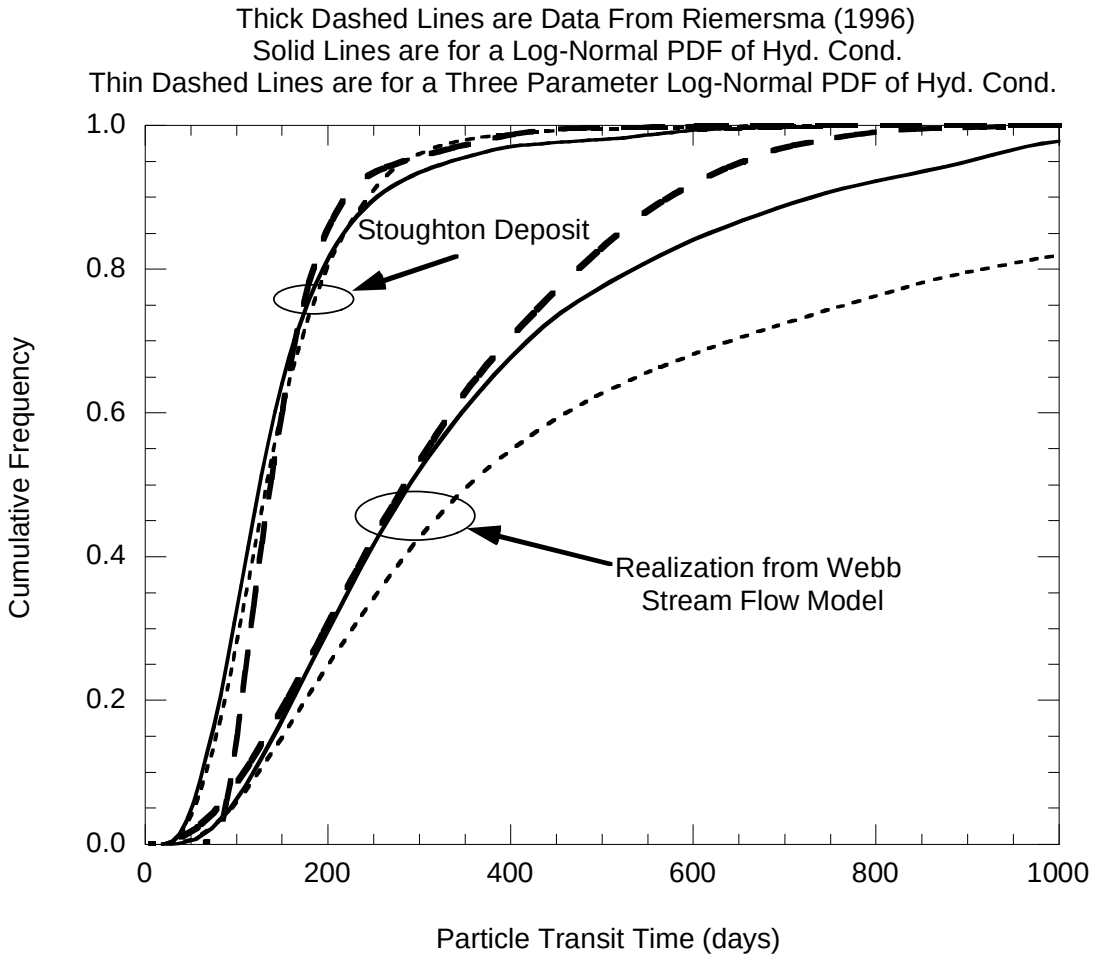

Fig. 4.8 Distributions of Particle Transit Time Across the Stoughton Aquifer and a Realization from the Webb Stream Flow Model.

Distributions of particle transit time for stochastically generated aquifers do not fit the distribution of particle transit time for the Webb Stream Flow model well. Particle transit times predicted for stochastically generated aquifers are longer and more broadly distributed than transit times in Riemersma's realization. Particle transit times from aquifers that are simulated using a log-normally distributed hydraulic conductivity field fit data from the Webb Stream Flow Model better. However, both distributions of hydraulic conductivity yield similar early arrival times as the Webb Stream Flow Model. Early arrival time is more critical for this project than late arrival time because contaminants that travel faster should have the shortest residence time in the PRB. Thus, either distribution function appears satisfactory based on initial arrival times, although the log-normal distribution provides a better overall fit to the data. In the literature, second order stochastic models that use a log-normal function to describe hydraulic conductivity produce reasonable predictions of particle transit time across an aquifer for all but very heterogeneous aquifers or aquifers with a pumping well (Riemersma and Anderson 1996).

A log-normal distribution was used for this study because it matches distributions of particle transit time better than a three parameter log-normal distribution. Also, log-normal distributions have fewer inputs and are used more frequently for describing hydraulic conductivity data than the three parameter log-normal distribution. This is evident in the data shown in Table 3.1, which describe hydraulic conductivity or transmissivity using log-normal distribution functions.

The functions shown in Fig. 4.6 where not used for this study. For convenience, the log-mean hydraulic conductivity was specified as an integer. The baseline simulation uses a log-mean hydraulic conductivity of -10 which corresponds to 4.5×10^{-5} m/s. Standard deviations for the hydraulic conductivity and correlation scale were variables for the parametric study.

4.1.4 Estimating Properties for the PRB

Stochastic descriptors of the hydraulic conductivity and reaction rate of the PRB were obtained from laboratory testing and from the literature. The hydraulic conductivity of Peerless iron filings (+8-50 mesh) was measured in the laboratory using a large-scale constant-head permeameter. Hoban and Vasko (1998) tested pure iron filings and iron filing-sand ratios of 75/25, 50/50, and 25/75. As many as 50 tests were performed on each mixture. Specimens were tested in a 10.2-cm-diameter by 30-cm-long cell, subjected to a hydraulic gradient of approximately 1.6. Specimens were tested at a moderate to high relative density, and tap water was used as the permeant.

Hydraulic conductivity data were grouped and probability density functions were fit to data. The data were best described by a normal distribution. The mean hydraulic conductivity ranged from 2.0×10^{-3} m/s to 8.3×10^{-3} m/s and the standard deviation ranged from 4.1×10^{-4} m/s to 2.6×10^{-5} m/s. For simulation, the PRB was assigned a mean hydraulic conductivity of 2.5×10^{-3} m/s and a standard deviation of 1.0×10^{-4} m/s.

Reaction rate constants for hydrogenolysis of chlorinated ethylene species by pure iron filings were obtained from the literature. The reaction rate constant for the hydrogenolysis of *cis*-DCE by iron metal was used since it is the slowest reaction of the chlorinated ethylene series (Tratnyek et al. 1997, Johnson et al. 1996). Assuming a surface area of 1.0 m^2/mL, the reaction rate constant for *cis*-DCE exposed to iron is 0.98 d^{-1} (Tratnyek et al. 1997, Johnson et al. 1996). The author acknowledges that 1.0 m^2/mL is a low estimate for the surface area of the iron (i.e., surface area ranges from 1 m^2/mL to 3.5 m^2/mL); however, unity is a convenient number from which less conservative designs can be extrapolated (Tratnyek et al. 1997). For modeling, the reaction rate constant was rounded to 1.0 d^{-1} to generalize the solutions from the model and allow the results to easily be scaled to other reaction rate constants.

The spatial variability of the reaction rate constant of the PRB was assumed to be similar to spatial variability in density of soils. The basis for this assumption is that the rate of hydrogenolysis reactions is proportional to the quantity of available iron. Since density is a measure of the quantity of iron per unit volume, variability in density should be proportional to reaction rate constant. This supposition assumes that iron particles are uniformly sized and shaped with a constant reaction rate constant per particle.

Phoon and Kulhawy (1999), Lacasse and Nadim (1996), Kulhaway and Phoon (1996), and Recordon (1977) publish the average coefficient of variation for density of soils as 5%. Given a mean reaction rate constant of $1d^{-1}$, a coefficient of variation of 0.05 yields a standard deviation of reaction rate constant (σ_k) of 0.05 d^{-}

[1]. Thus, reaction rate constant for this study is assumed ~N(1 d^{-1}, 0.05) except for one simulation for each type of PRB in which the reaction rate constant is ~ N(1 d^{-1}, 0.10) to determine the implications of the preceding assumption. In addition, the distribution of reaction rate constant was truncated at zero to avoid mass from being generated in the PRB. This criterion has almost no impact on the distribution for reaction rate because zero is 20 standard deviations below the mean. The model was written so that when a negative reaction rate constant is selected from the distribution it is reset to zero. The PDFs used for simulating hydraulic conductivity and reaction rate constant of the PRB are shown in Fig. 4.9.

4.1.5 Aquifer Generation

Aquifers were created by stacking two-dimensional correlated random fields of hydraulic conductivity. This approach is possible because the autocorrelation scale in the vertical direction is less than the vertical discretization chosen for the problem (Fig. 4.7b). Random fields that contain 300 by 150 nodes were created using the turning bands code. This size field was chosen because 20 layers, each with 300 by 150 nodes, approaches the largest domain that can be solved using MODFLOW. A program named “BCF-builder” was written to create the basic control file (BCF) for MODFLOW. BCF-builder reads the 300 by 150 node hydraulic conductivity field and cuts a sub-field from the center of the field. Sub-fields are stacked to construct a three dimensional aquifer. This approach was chosen because a sub-field of any size can be cut from 300 by 150 node random field as the domain for the problem changes (e.g., HFPRB vs. CPRB). Since BCF-

builder uses sub-fields from the center of a larger random field, the hydraulic conductivity field adjacent to the PRB (i.e., in the center of the model) is identical, regardless of the size of the domain. This procedure allows fair comparisons to be

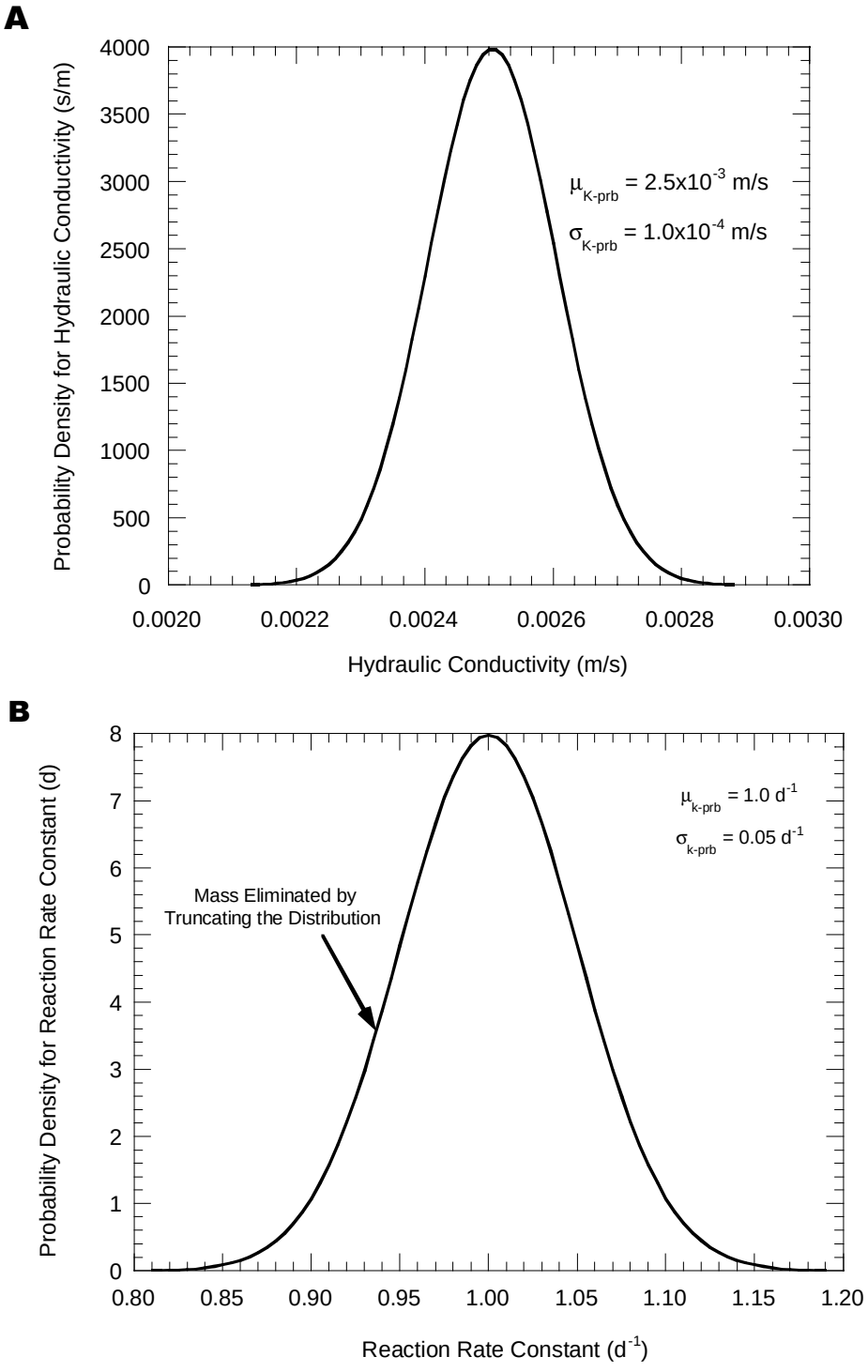

Fig. 4.9 Probability Density Functions Chosen to Represent (a) Hydraulic Conductivity and (b) Reaction Rate Constant for the Permeable Reactive Barrier.

made between problems with different domain sizes amidst heterogeneity.

In addition to writing fields of hydraulic conductivity to a file, BCF-builder also calculates and writes several other variables and arrays to the BCF file. One array that is calculated and written to file by BCF-builder describes conductance between adjacent layers (VCONT). Hydraulic conductivities in finite difference cells are isotropic so that the VCONT calculated between adjacent layers of the aquifers accounts for the vertical component of hydraulic conductivity and causes the vertical correlation length to be less than 0.5 m. BCF-builder writes one fewer VCONT arrays to file than hydraulic conductivity arrays. Each VCONT array is equal in size to the hydraulic conductivity array. BCF-builder calculates VCONT as:

$$VCONT_{x,y,z+\Delta z/2} = \frac{2K_{x,y,z}K_{x,y,z+\Delta z}}{\Delta z\left(K_{x,y,z} + K_{x,y,z+\Delta z}\right)} \qquad (4.1)$$

where $VCONT_{x,y,z+\Delta z/2}$ is VCONT at location x, y and between layers at depths z and $z + \Delta z$, $K_{x,y,z}$ is hydraulic conductivity at position x, y, and depth z, and Δz is center to center spacing between adjacent layers. Equation 4.1 is a simplified form of the vertical conductance equation and assumes that adjacent layers have equal thickness (McDonald and Harbaugh 1998). Additional components of the BCF file such as headers, format statements, and node spacing are also written by BCF-builder. The output from BCF-builder is a BCF file that is input directly into MODFLOW.

BCF files for a homogeneous aquifer and several simple heterogeneous aquifers were created using BCF-builder and ModIME (Zhang et al. 1995). These files were input into MODFLOW and the solutions were compared. The head solutions for both files were identical indicating that BCF-builder calculates and assembles elements of the BCF file correctly (Appendix I).

4.2 FLOW SIMULATION

4.2.1 Governing Equation

MODFLOW (McDonald and Harbaugh 1998) was used to compute the steady-state solution for head across a heterogeneous unconfined aquifer containing a PRB. The head solution was obtained by solving the governing differential equation:

$$\frac{\partial}{\partial x}\left(K_{xx}\frac{\partial h}{\partial x}\right)+\frac{\partial}{\partial y}\left(K_{yy}\frac{\partial h}{\partial y}\right)+\frac{\partial}{\partial z}\left(K_{zz}\frac{\partial h}{\partial z}\right)-W=S_s\frac{\partial h}{\partial t} \qquad (4.2)$$

where K_{xx}, K_{yy}, and K_{zz} are hydraulic conductivities in orthogonal directions x, y, and z, h is total head, W is volumetric flux per unit volume for simulating sources and sinks, S_s is specific storage of the porous media, and t is time. Equation 4.2 requires boundary and initial conditions, which will be described subsequently, and is solved by MODFLOW using a finite difference method. For steady-state simulation, the right-hand side of Eq. 4.2 is equal to zero and initial conditions are not required.

4.2.2 Problem Conceptualization

The initial conceptual model of the problem is an unconfined aquifer that is L_x long, L_y wide, and 10 m thick (Fig. 4.10). The aquifer is composed of 20 layers, each 0.5 m thick and has a fully penetrating reactive barrier located in the center of the aquifer. A hydraulic gradient of 0.01 is applied across the aquifer. A constant head boundary conditions:

$$h\left(x = L_x, 0 \le y \le L_y, 0 \le z \le 10\,m\right) = 10\,m \tag{4.3}$$

is used for the down-gradient boundary, and a constant head boundary condition:

$$h\left(x = 0, 0 \le y \le L_y, 0 \le z \le 10\,m\right) = 10\,m + iL_x \tag{4.4}$$

is used for the up-gradient boundary, where i is hydraulic gradient. The bottom and sides of the model are no flux boundaries such that:

$$\begin{gathered}\frac{\partial h}{\partial z}\left(0 \le x \le L_x, 0 \le y \le L_y, z = 0\,m\right) = \\ \frac{\partial h}{\partial y}\left(0 \le x \le L_x, y = 0 \text{ and } y = L_y, 0 \le z \le 10\,m\right) = 0\end{gathered} \tag{4.5}$$

and the top boundary is an unconfined boundary so that MODFLOW calculates the head in the finite difference cells of the uppermost layer.

A. Horizontal Flow PRB

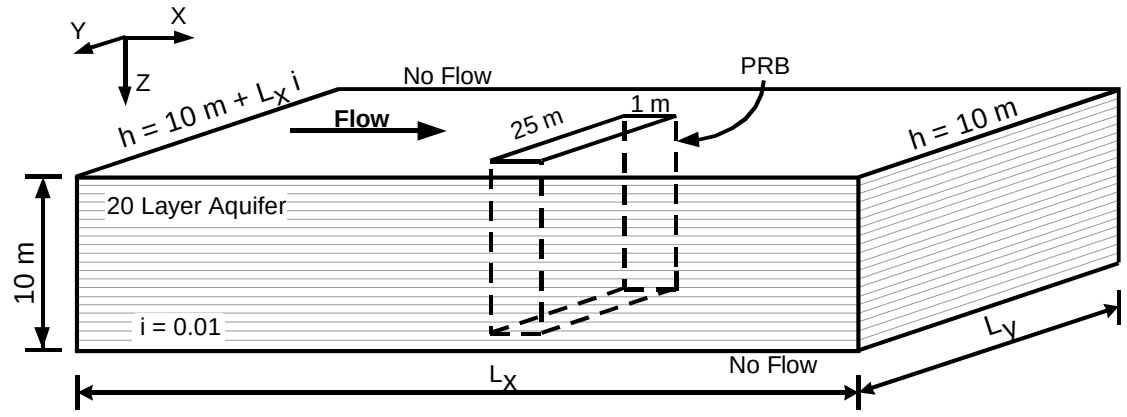

B. Funnel with Gate PRB

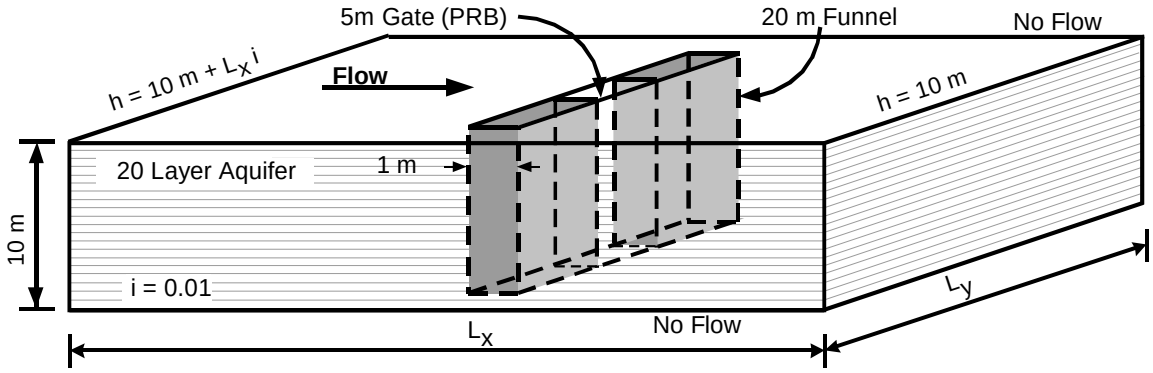

C. Funnel with Caisson PRB

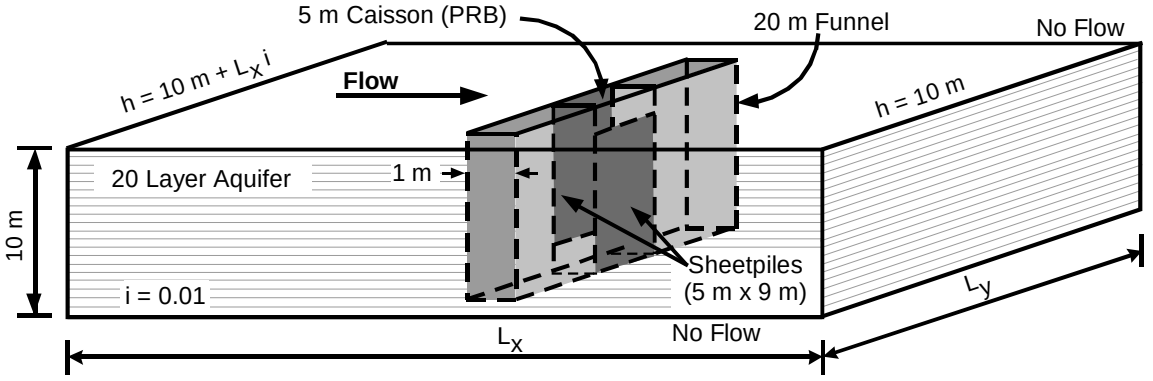

Fig. 4.10 Initial Conceptual Model of Permeable Reactive Barriers Located in the Center of an Aquifer.

4.3 CONTAMINANT TRANSPORT MODELING

4.3.1 Introduction to Path3D

Path3D (Zheng 1992) was used in modeling transport and hydrogenolysis of chlorinated ethylene species in the aquifer and PRB. Path3D is a computer program designed to run in series with MODFLOW and simulate the movement of particles through the model domain. Path3D reads the head solution from MODFLOW along with two other MODFLOW input files and calculates the seepage velocity between cells of the model domain. Path3D then uses a fourth-order Runga-Kutta method to calculate the position of particles at time-steps. The movement of each particle across the aquifer is calculated discretely, and the duration of a time-step is controlled via an error criteria. Path3D reports the coordinates and seepage velocity of each particle at specified increments of time.

Path3D assumes that gravitational forces do not influence the movement of particles and does not account for transport by diffusion. Thus, the trajectory of particles through the domain is solely a result of advection, although retardation can be simulated by increasing the effective porosity. Since diffusion is not considered, mechanical mixing caused by aquifer heterogeneity is the only source of dispersion.

4.3.2 Simulating Contaminant Transport Using Path3D

Path3D was used to simulate contaminant transport using a stream tube approach, similar to that used by Prickett et al. (1981), Hathhorn (1997), Vollmayr et al. (1997), and Hassan et al. (1997). This method is popular for problems where

transport by advection is much greater than transport by diffusion (i.e., Peclet Number > 10) because it is faster than programs such as MT3D, which solve the advection-dispersion equation directly. The method is appropriate for this study because aquifers are predominantly sand so the Peclet Number is greater than 10 and dispersion is inherently accounted for by the heterogeneity of the hydraulic conductivity field.

Advective mass transport from a constant concentration source zone, through the aquifer and PRB, is calculated using a stream tube method. Particles originate in a 15 m wide, 5 m deep source located 20 m up-gradient from the PRB. Path3D calculates particle trajectory and position for a series of time steps, each time step corresponding to a segment of the stream tube. Stream tubes between the source and down-gradient boundary of the model are defined using Path3D.

Each stream tube is assigned a mass flow rate ($\dot{M}_i$) that is calculated from the longitudinal seepage velocity of the particle at the source (v_{xi}), the number of particles per unit volume at the source (N), and the source concentration (C_s) by:

$$N\dot{M}_i = C_s A n v_{xi} \qquad (4.6)$$

where A is the area of the source volume perpendicular to v_x and n is porosity. Mass flow rate for a stream tube is the amount of mass per unit time contributed or removed from a volume of soil by a stream tube that passes through that soil volume.

Once the location, $\dot{M}_i$, and v_{xi} for all stream tubes and positions are defined, the concentration in any block of aquifer (C_{xyz}) is calculated by dividing the total mass existing within the block by the porous volume of the block. The total mass within the block is the cumulative mass existing in segments of stream tubes that are located within the block:

$$C_{xyz} = \frac{\left[\sum_i \left(\dot{M}_i / v_{xi}\right)\right]_{xyz}}{A_{yz} n} \qquad (4.7)$$

where the summation is over stream tubes that intercept a block around location x, y, and z, and A_{yz} is the area of the block perpendicular to v_{xi}.

This method is explained in greater detail in Appendix II. The method was verified by calculating mass flux through six cross-sections of an aquifer containing a funnel and nonreactive gate and by comparison with MT3D. These tests are discussed in Appendix II. The tests verify that mass is conserved and show that the maximum difference in calculated concentrations between the stream tube method and MT3D is 15%, occurring at the edges of the plume. However, the stream tube model runs 500 to 5000 times faster than MT3D.

4.3.3 Simulating First-Order Reactions Using Path3D

First-order loss is simulated using Path3D by assuming particles move by plug flow within a time step. The mass associated with a particle is reduced as:

$$m_j(t+\Delta t) = m_j(t)\exp(-k_{i,j,k}\Delta t) \qquad (4.8)$$

where $m_j(t)$ is the mass of particle j at time t, Δt is the duration of a time step, and $k_{i,j,k}$ is the first-order, reaction rate constant in element i,j,k. To simulate first-order reactions in the PRB but not in the aquifer, $k_{i,j,k}$ for the aquifer ($k_{i,j,k,AQ}$) is equal to zero and $k_{i,j,k}$ for the PRB ($k_{i,j,k,PRB}$) was greater than or equal to zero.

Heterogeneity of the reaction rate constant was incorporated into the model by assigning an independent, standard normal random variable to each finite difference cell. The linear congruent random number generator, mentioned in the previous section, was added to Path3D and the Box-Muller equation (Box and Muller 1958) was used to calculate standard normal random variables. Reaction rate constants in each cell were calculated using the array of standard normal variables. In addition, the reaction rate constant was cross-correlated to hydraulic conductivity in the aquifer by:

$$k_{i,j,k,AQ} = \mu_k + \sigma_k\left\{\rho_{K,k}\frac{\ln(K_{i,j,k,AQ} - \mu_{\ln K})}{\sigma_{\ln k}} + N_{i,j,k}(0,1)\sqrt{1-\rho_{K,k}^2}\right\} \qquad (4.9a)$$

and in the PRB by:

$$k_{i,j,k,PRB} = \mu_k + \sigma_k\left\{\rho_{K,k}\frac{K_{i,j,k,PRB} - \mu_K}{\sigma_k} + N_{i,j,k}(0,1)\sqrt{1-\rho_{K,k}^2}\right\} \qquad (4.9b)$$

where μ_k is the mean reaction rate constant, σ_k is the standard deviation of the reaction rate constant, $\rho_{K,k}$ is the cross-correlation coefficient between hydraulic conductivity and reaction rate constant, $K_{i,j,k}$ is the hydraulic conductivity at location i,j,k, μ_K is the mean hydraulic conductivity, σ_K is the standard deviation in hydraulic conductivity, $N_{i,j,k}(0,1)$ is a standard normal random variable at location i,j,k, and PRB indicates that a variable is for the PRB, while AQ indicates that a variable is for the aquifer. Hydraulic conductivity for the aquifer is transformed using the exponential function to convert it from a log-normally distributed random variable to a normally distributed random variable. Hydraulic conductivity for the PRB and reaction rate constant are normally distributed and only need to be standardized.

Correlating reaction rate constant to hydraulic conductivity (Eykholt 1997) is a more robust method for incorporating heterogeneity into reaction modeling. By selecting a positive correlation coefficient, locations of higher hydraulic conductivity are assigned a larger reaction rate constant. Conversely, by selecting a negative correlation coefficient, locations of higher hydraulic conductivity are assigned a lower reaction rate constant. Hydraulic conductivity and reaction rate constant are independent when the correlation coefficient is equal to zero. Thus, changing the correlation coefficient easily simulates several levels of connectivity between hydraulic conductivity and reaction rate. Using this method, the influence of flow rate on reaction rate constant, which may be related due to scaling on the iron, can be evaluated. The other advantage of spatially assigning the reaction rate constant is that particles passing through the same location are impacted by the same

reaction rate constant. This is important because the reaction rate constant is a property of the media and thus is fixed in space.

4.3.4 Summary of Changes to Path3D

The source code for Path3D was edited significantly for this project. Changes were mostly made within and directly outside the loop that steps through time for each particle. This section is a summary of these edits. The edited source code is lengthy so it is not included, but is available upon request from the author[1].

Path3D was edited to write two new output files and reduce the volume of data written to the default output file. The new output files are a particle mass file and a spatial concentration file. The output written to these files will be discussed subsequently. A flag was also added to the program. This flag is equal to the unit number for the default output file. If the unit number for this file is equal to 16, only a header is written to the default output file. If the unit number is not 16, standard output is reported. This edit reduces the volume of the Path3D output and preserves disk space. The default output file echoes the input files for MODFLOW and Path3D, and may also contain the output for both programs. This file becomes very large when many finite difference cells and particles are used. Thus, standard output files were only written when debugging or verifying the program.

Prior to entering the loop that steps through time, an array equal in size to the finite difference grid is filled with standard normal random variables. The

[1] crelder@students.wisc.edu

purpose of this array is to assign the reaction rate constant to all finite difference cells. The method that was used to cross-correlate reaction rate to hydraulic conductivity was discussed in the previous section.

A variable, “inbar” was added to Path3D. Inbar is a flag that is used to indicate the location of a particle and assign the appropriate reaction rate constant for a time step. If a particle is in the PRB, inbar is equal to one; otherwise inbar is not equal to one. Inbar has appropriate constraints to account for particles that enter the front or sides of the PRB, exit the sides or back of the PRB, exit and re-enter the sides of the PRB, or circumvent the PRB.

Within the loop that calculates particle movement during a time step, Path3D was edited to output $\dot{M}$ of a stream tube at a prescribed X positions (e.g., the front and back of the PRB). At the end of a time step, when the particle position is greater than the desired X position, data for the particle are written to file and saved in memory. Linear interpolation is used to estimate particle velocity, $\dot{M}$, location, and time at the desired X. At the end of the realization, cumulative mass in a specified pore volume (concentration) is calculated. Concentrations on a 1 m by 1m grid at the front and back of the PRB are written to the concentration output file.

The modified version of Path3D was tested for accuracy against an original version of the program. This test verified that the author’s edits did not alter the tracking solution from Path3D (Appendix II).

4.3.5 Inputs for Contaminant Transport Modeling

A 15 m wide, 0.4 m thick, and 5.0 m deep persistent source with an initial concentration of 1000 ppb was used for all simulations. The source zone contains 300 finite difference cells in which four to six particles were initially located randomly within each cell. The source was located 20 m up-gradient of the PRB along the vertical and lateral centerline of the aquifer. The location and size of the source and PRB are shown in Fig. 4.11. Also shown on Fig. 4.11 are the trajectories of 18 particles as they travel across the aquifer.

The error criterion for Path3D was $5x10^{-5}$ m. This results in average time steps of approximately 0.9 days and an average step size of about 12 cm. A smaller time step increases accuracy. Where necessary, interpolation was used to further reduce error in time step discretization. For example, the time when a particle enters the PRB is estimated by linear interpolation between data on either side of the face of the PRB.

4.3.6 Verification of the Ergodic Hypothesis

The ergodic hypothesis states that all parameters of a distribution can be estimated from a single realization. The number of realizations that are required to yield a representative result was determined by performing 20 realizations of a scenario. The CDF of transit time for particles to pass across the PRB for realizations 1 to 10, 11 to 20, and 1 to 20 are shown in Fig. 4.12. Also shown on Fig. 4.12 are two randomly chosen realizations (2 and 9)

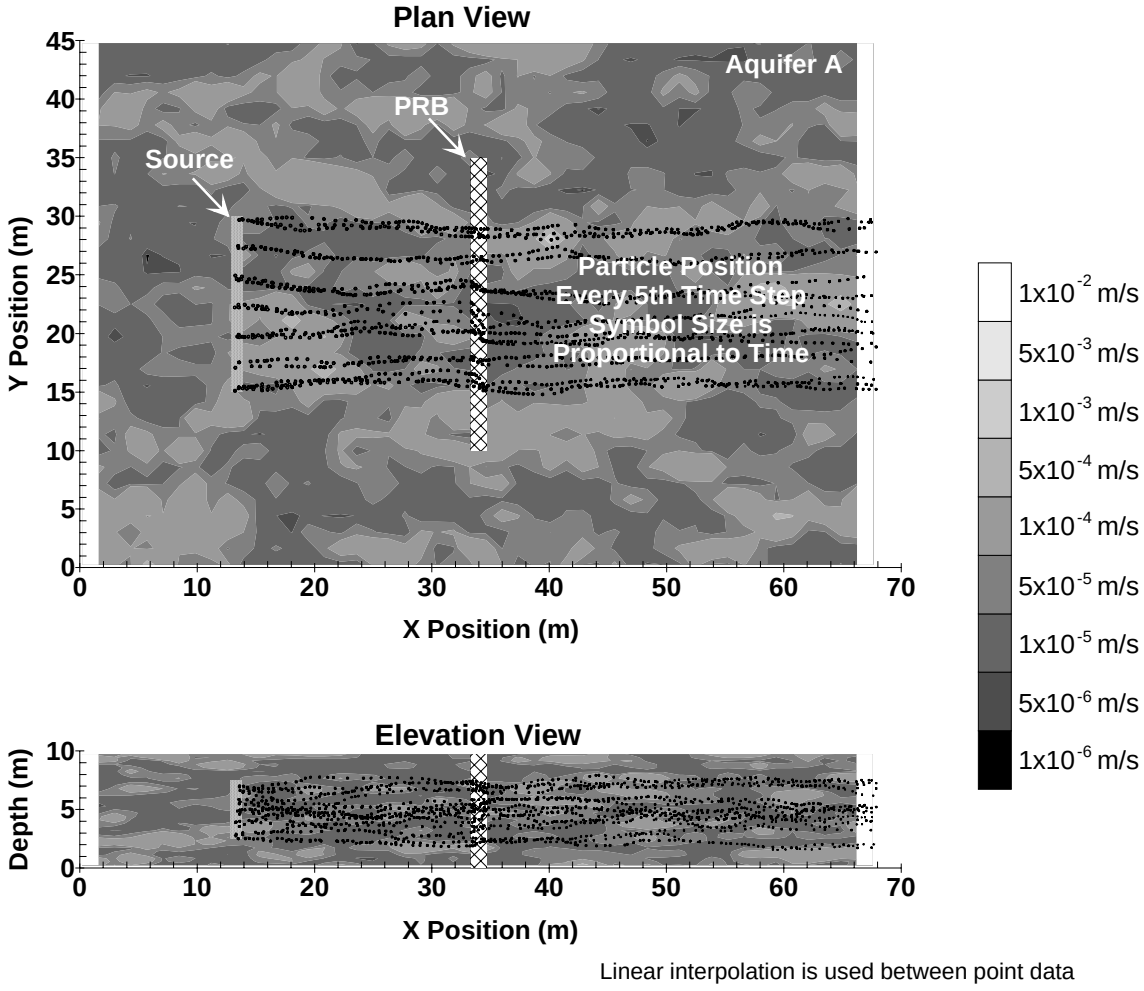

Fig. 4.11 Plan (a) and Elevation (b) View of a Horizontal Permeable Reactive Barrier and Contaminant Source in a Heterogeneous Aquifer. Particle Position are shown for Every 5th Time Step.

Results of individual realizations do not match the pooled results (i.e., the maximum difference is greater than 20%). This indicates that the ergodic hypothesis does not hold for this system and more than a single realization is required to obtain ergodic results. However, the pooled results from two sets of 10 realizations (1-10 or 11-20) are similar and both correspond closely with the pooled data from all 20 realizations (i.e., the maximum difference between all distrubutions is less than 5%). Thus, uncertainty appears to be sufficiently characterized using simulations with 10 realizations. Therefore, all subsequent simulations contained 10 realizations.

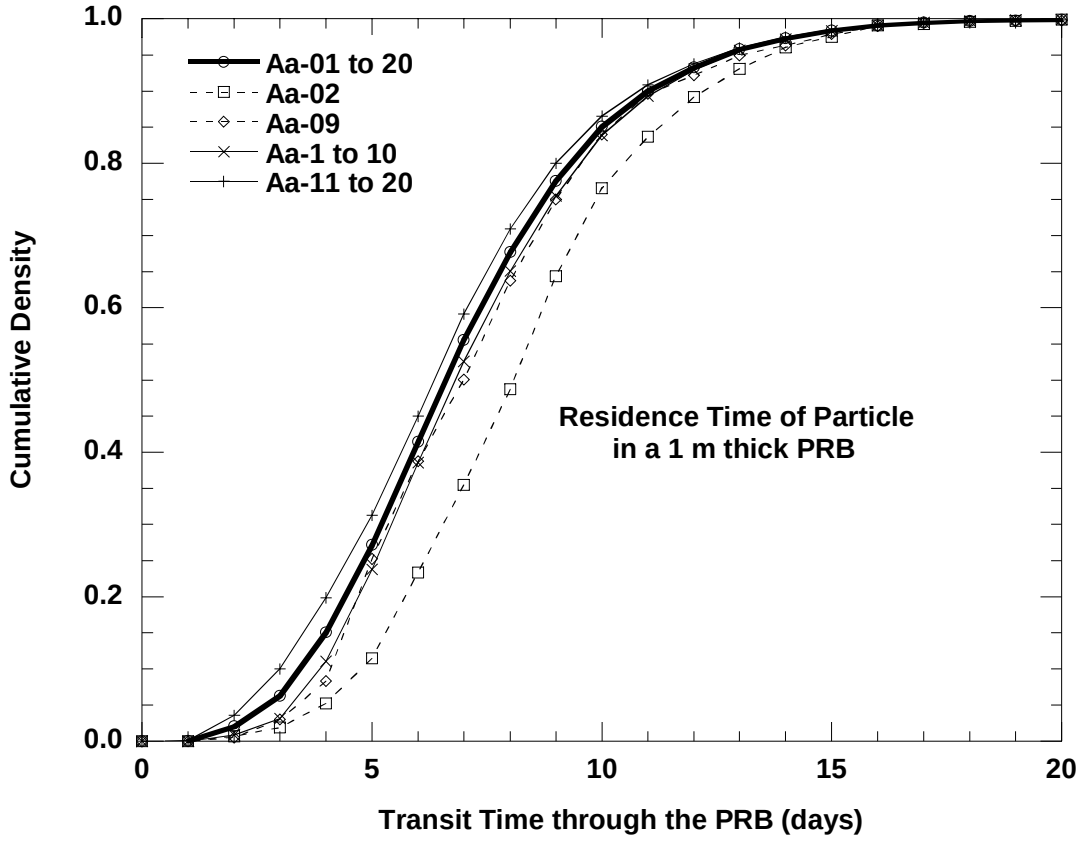

Fig. 4.12 Distribution of Residence Time of Groundwater in a PRB Obtained from Individual Realizations and Pooled Sets of 10 and 20 Realizations.

SECTION 5

RESULTS AND CONCLUSIONS FOR A HORIZONTAL FLOW PRB

5.1 DESCRIPTION OF A HORIZONTAL FLOW PRB

A horizontal flow PRB (HFPRB) is the simplest of the three PRBs considered in this study (Fig. 4.10a). A HFPRB is a trench filled with reactive media that is approximately perpendicular to groundwater flow and down gradient of a contaminant plume. Contaminants are transported into the reactive zone by ambient groundwater flow and pass horizontally through the PRB. HFPRBs are not expected to significantly alter groundwater flow.

The advantages of HFPRBs are that they are easy to conceptualize and there exists some guidance for their design (e.g., Gavaskar et al. 1998, EPA 1995, Powell 1998, Nav. Fac 1998). These advantages have lead to approximately half of the existing full-scale PRBs to be HFPRBs (Jarre and Kociolek 1999). A disadvantage of HFPRBs is that they rely on the breadth of the reactive zone to capture the contaminant plume, thus may be more costly than other styles of PRB. This results in unused portions of reactive media at the edges of the PRB. In addition, HFPRBs are a less redundant type of PRB and more susceptible to defects or non-uniform flow because groundwater passes through the narrowest dimension of the PRB.

5.2 CONCEPTUAL MODEL OF A HFPRB

The conceptual model of a HFPRB is shown in Fig. 4.10a. The HFPRB chosen for this study is a fully penetrating, 1 m thick and 25 m long. This PRB is broad enough to capture the contaminant plume emanating from the source zone.

5.2.1 Verification of Constant Head Boundary Conditions

The distance between the HFPRB and the up-gradient or down-gradient boundary was evaluated to ensure that particles passing through the PRB were not influenced by the location of boundaries. This condition posed a difficult problem given that aquifers are heterogeneous. The approach used was to simulate a larger random field than was expected for the model domain (20 layers, each containing 300 by 150 nodes), and systematically reduce the field size until particle trajectory or velocity through the PRB changed.

A homogeneous PRB was located in the center of the random field. The random field used to simulate the aquifer had a log-mean hydraulic conductivity (μ_{lnK}) of -10.3 (m/s), log-standard deviation of hydraulic conductivity (σ_{lnK}) equal to 3.0, and correlation scales of 10 m and 5 m in the X and Y directions, respectively (λ_x and λ_y). High estimates of the σ_{lnK}, λ_x, and λ_y were used to create aquifers with elongated zones of higher hydraulic conductivity. These units, as discussed by Riemersma and Anderson (1996) and Schreiber et al. (1999), act as preferential flow paths through the aquifer. Boundary conditions that are sufficient for aquifers with larger σ_{lnK}, λ_x, and λ_y, should also be adequate for aquifers with smaller σ_{lnK}, λ_x, or λ_y.

Without knowledge of the appropriate discretization of the problem domain, a reasonable estimate of the grid spacing was chosen. Grid spacing increased symmetrically about the centerline-line of the aquifer at $x = L_x/2$. The smallest grid spacing in the X direction was 0.10 m (located in the center of the aquifer and center of the PRB) and the largest grid spacing in the X direction was 0.60 m (located at the two boundaries). The minimum grid spacing was chosen such that the PRB would be divided into 10 finite-difference cells. This level of discretization allows tortuous flow through the PRB between dominant units on either side of the PRB. The maximum grid size was chosen as 0.6 m so that correlation scales as short as 1.2 m could be simulated yet the problem domain can grow at a reasonable rate so that the boundaries of the problem are several correlation scales from the PRB. The grid spacing increased from 0.10 m to 0.60 m at an expansion ratio of no more than 1.3 between adjacent elements. This is similar to the expansion ratio recommended by Foose (1996) and Tachavises (1998), and less than the ratio recommended by Anderson and Woessner (1992). A discretization of 0.5 m was used for the Y and Z directions.

A homogeneous PRB ($K = 2.5 \times 10^{-3}$ m/s) that was 25 m long, 1 m wide, and 10 m deep was placed in the center of the simulated aquifer as shown in Fig. 4.10a. MODFLOW was used to solve for total head at all nodes within the aquifer and PRB subject to the boundary conditions discussed in Section 4.2.2. The head solution was input into Path3D, and the transit time was calculated for 250 particles to pass through the PRB. Seepage velocities of particles entering and exiting the PRB were also calculated. Particles were initially located 20 m up-gradient of the

PRB ($2\lambda_x$) at 1 m horizontal and vertical spacing. A distance of two correlation scales from a boundary exceeds the distance where head solutions for a bounded domain are identical to the head solution for an unbounded domain (Rubin and Dagan 1989). Based on this conclusion, initially locating particles two correlation scales from the PRB is believed to be sufficiently far from the PRB to allow preferential flow paths to develop prior to particles entering the PRB.

Seepage velocity and particle transit time through the PRB were determined for successively smaller domains. The purpose of this exercise was to determine the minimum distance between the PRB and boundaries such that boundary conditions have no effect on groundwater flow through the PRB. The aquifer was shrunk around the PRB by eliminating elements at the two boundaries (i.e., $x = 0$ and $x = L_x$). An equal number of elements were removed from each boundary to make successively smaller domains; thus, the hydraulic conductivity field in the center of the aquifer surrounding the PRB remained unchanged. Given there was a constant gradient used for the simulations (i.e., constant heads on boundaries varied with the size of the domain), any changes in particle velocity and transit time should be a consequence of changing the location of the boundaries.

Five increasingly smaller problem domains were tested for two heterogeneous aquifers. Conceptual models of these domains are shown in Fig. 5.1. Particle transit times through the PRB and particle velocities entering and exiting the PRB are shown in Fig. 5.2 for the two aquifers. Particle transit time and velocity at the faces of the PRB are similar for all domain sizes except 140

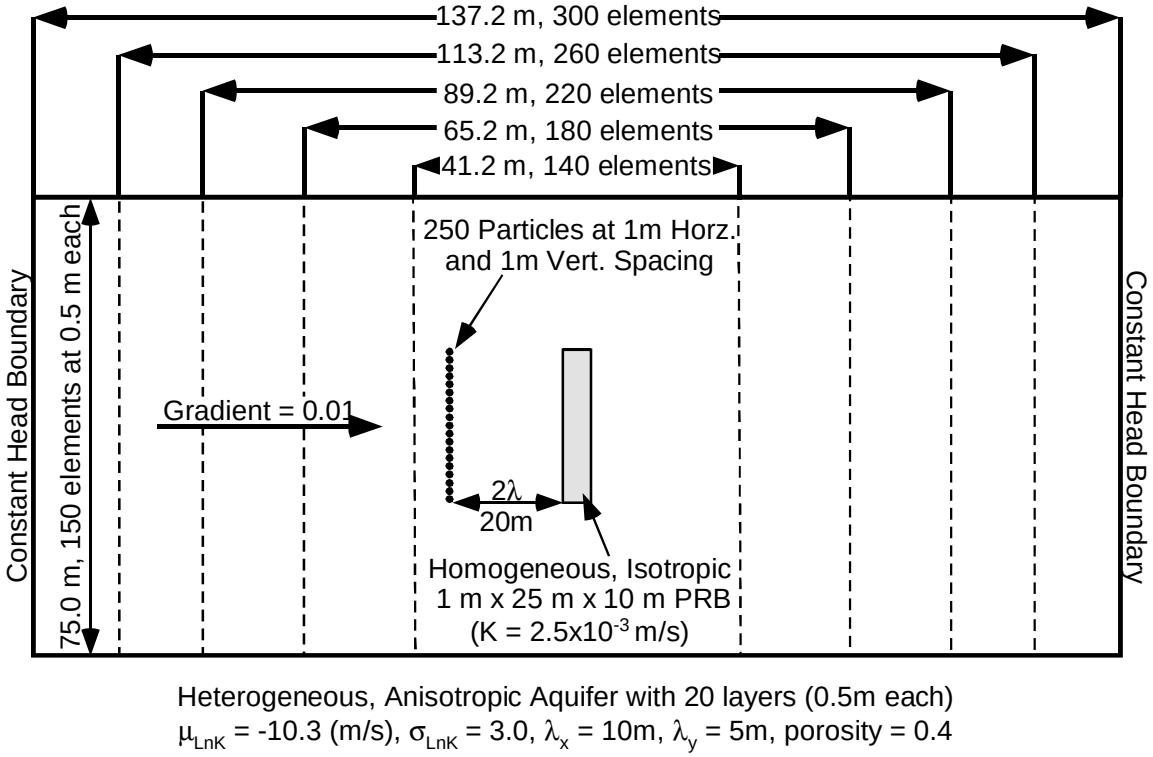

Heterogeneous, Anisotropic Aquifer with 20 layers (0.5m each)
μ_{LnK} = -10.3 (m/s), σ_{LnK} = 3.0, λ_x = 10m, λ_y = 5m, porosity = 0.4

Fig. 5.1 Conceptual Models used to Determine the Appropriate Spacing Between Constant Head Boundaries.

by 150. The smaller domain yields longer transit times and lower particle velocities than the larger domains. Thus, a domain is needed that containing at least 180 elements, which corresponds to a 65.2 m long aquifer. This domain is sufficient to prevent the location of the boundaries from influencing particle transport through the PRB. This criterion corresponds to having the up-gradient boundary and down-gradient boundaries located $3.2\lambda_x$ from the edge of the PRB and $1.2\lambda_x$ upgradient from the source. Rubin and Dagan (1988) show that constant head boundaries influence the distribution of heads only within 2λ of the boundary.

A similar procedure was used to determine the minimum separation distance between the side boundaries of the model and the edge of the PRB. Boundaries were moved successively closer to the PRB until velocity and transit time of particles passing through the PRB changed. The results of simulations using two heterogeneous aquifers are shown in Fig. 5.3. From this analysis, a domain at least 45 m wide is sufficient to prevent the no-flow boundaries from influencing particle transport through the PRB. This corresponds to $2\lambda_y$ between the edges of the PRB and no-flow boundaries. Two correlation scales exceeds the distance where Rubin and Dagan (1989) predict that no flow boundaries will influence flow parallel to a no flow boundary.

5.2.2 Verification Finite Difference Discretization

Having determined proper locations for the boundaries, an appropriate grid discretization scheme was sought. Identical random fields with different grid

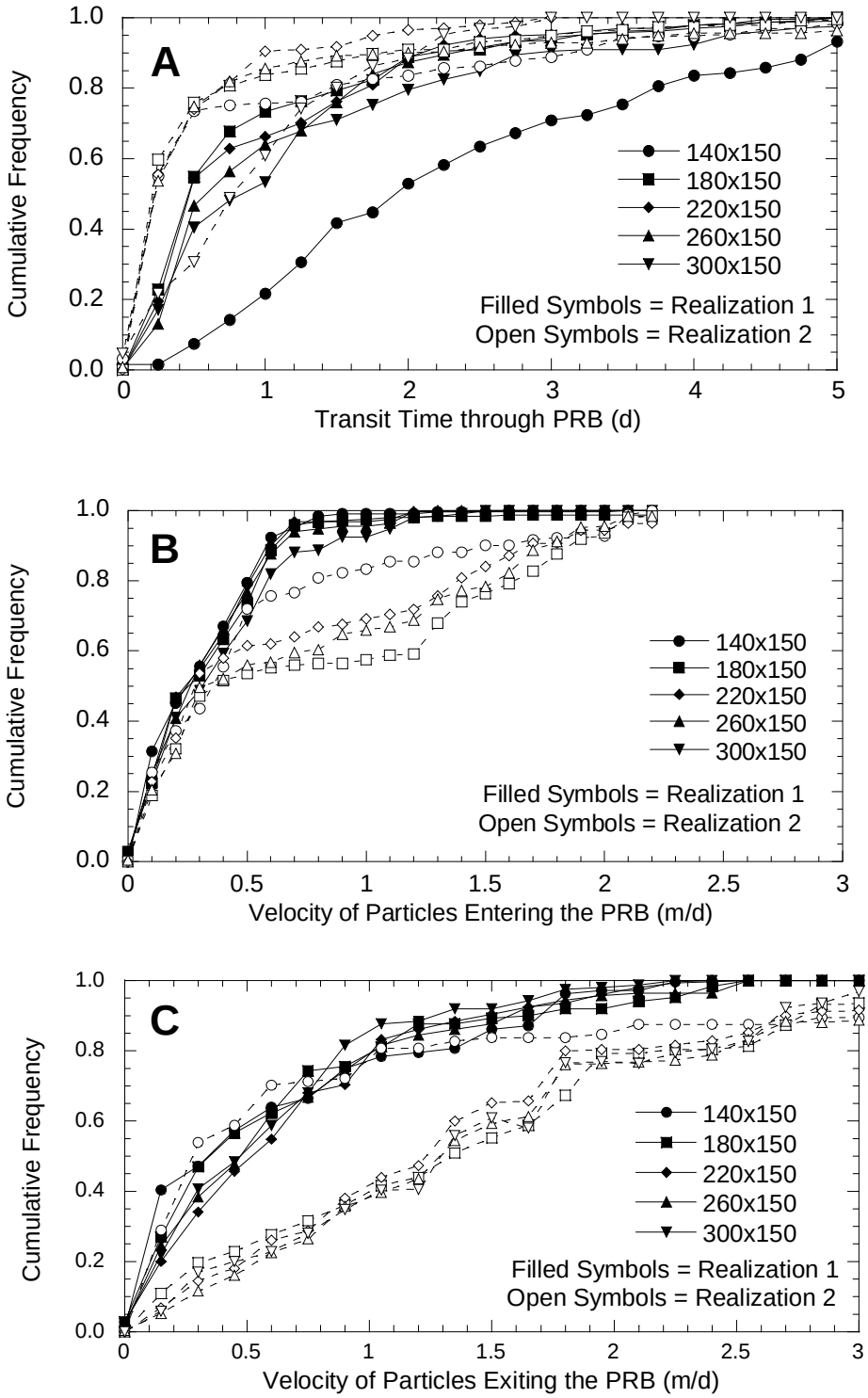

Fig. 5.2 (a) Particle Transit Time through the PRB, (b) Particle Velocity Entering the PRB, and (c) Particle Velocity Exiting the PRB for Five Increasingly Shorter Domains (Two Realizations per Domain).

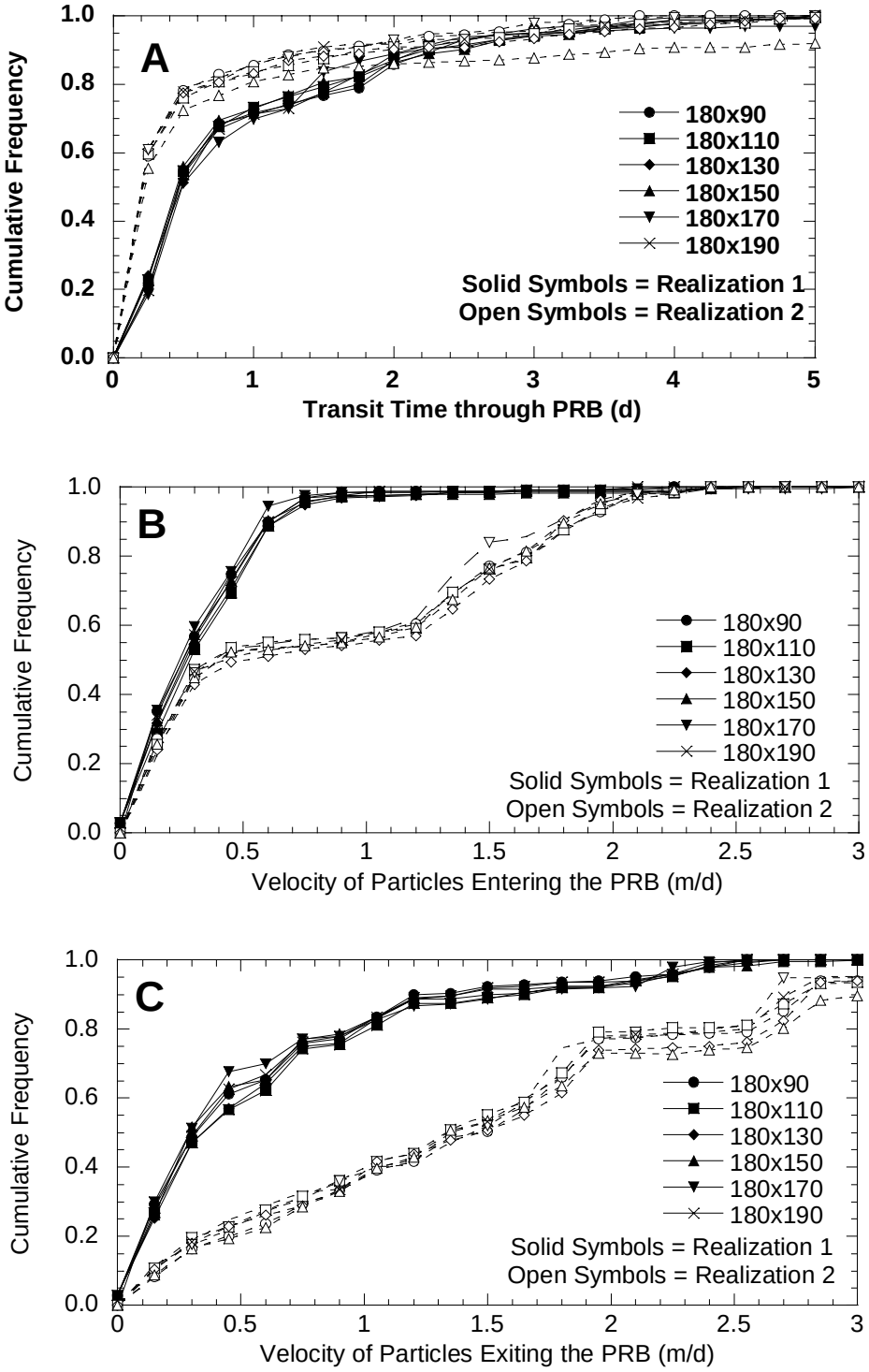

Fig. 5.3 (a) Particle Transit Time through the PRB, (b) Particle Velocity Entering the PRB, and (c) Particle Velocity Exiting the PRB for Five Increasingly Narrower Domains (Two Realizations per Domain).

spacing could not be generated because strings of standard normal random variables are different for random fields of different size. Thus, appropriate discretization was determined for a homogeneous aquifer containing a PRB with the assumption that the same grid would also be sufficient for a heterogeneous aquifer.

Homogeneous aquifers ($K = 3.4 \times 10^{-5}$ m/s) that were at least 65.8 m long, 45 m wide, and 10 m thick were created. A fully penetrating, 25 m long by 1 m wide, homogeneous PRB ($K = 2.5 \times 10^{-3}$ m/s) was placed in the center of the aquifer. The domain was discretized using several schemes. Table 5.1 lists the various discretizations that were used, from the finest discretization (grid 1) to the coarsest discretization (grid 5). There was no general method for selecting potential discretization schemes except the constraint for the random field generator (i.e., $\Delta x = \lambda_x/2$), constraints of MODFLOW (i.e., less than 940,000 elements in the domain), and the expansion ratio constraint ($\Delta x_i/\Delta x_{i+1} \leq 1.5$). Transit time of particles passing through the PRB and velocity of particles entering and exiting the PRB for each alternative are shown in Fig. 5.4.

Grid 3 was selected as the best alternative because it is the coarsest grid that produces results similar to grid 1 (the finest grid). Grids that are coarser than grid 3 yield shorter transit time and higher velocity. Grid 1 and 2 yield similar results to grid 3 and could also be used. However, grids 1 and 2 are finer than grid 3 and require more computational time to calculate a solution. In this respect, grid 3 is a more reasonable choice.

Grid 3 has 230 by 90 elements per layer with a minimum element size of 0.05 m in the PRB and maximum element size of 0.40 m at the boundary. Grid 3 allows the PRB to be divided into 20 columns. The discretization allows minimum correlation scales in the X and Y direction of 0.8 m and 1.0 m, respectively. The size of the domain defined by Grid 3 is 67.8 m by 45.0 m by 10.0 m. This size grid fulfills the criteria for the boundary conditions and has a maximum expansion ratio of 1.2.

Table 5.1 Discretization Schemes Investigated for the Model.

Scheme	Nodes per layer	Domain Size	Discretization from Center of PRB to a Constant Head Boundary (m)
Grid 1 (Finest)	360 x 90	65.2 m x 45 m	20@0.05, 10@0.06, 10@0.07, 10@0.08, 10@0.09, 10@0.11, 10@0.13, 10@0.16, 10@0.19, 10@0.22, 10@0.25, 60@0.30
Grid 2	260 x 90	65.2 m x 45m	20@0.05, 2@0.06, 2@0.07, 10@0.08, 2@0.09, 2@10, 2@0.14, 3@0.18, 3@0.22, 2@0.26, 90@0.32
Grid 3	230 x 90	67.8 m x 45 m	25@0.05, 1@0.06, 1@0.07, 1@0.08, 1@0.09, 1@0.10, 1@0.11, 1@0.13, 1@0.14, 1@0.16, 1@0.19, 1@0.22, 1@0.26, 1@0.31, 1@0.35, 1@0.38, 75@0.40
Grid 4	180 x 90	65.2 m x 45 m	10@0.10, 5@0.12, 5@0.14, 5@0.16, 5@0.18, 5@0.22, 5@0.26, 5@0.32, 5@0.38, 5@0.44, 5@0.44, 5@0.50, 30@0.60
Grid 5 (Coarsest)	88 x 90	65.2 m x 45 m	5@0.20, 2@0.28, 3@0.32, 2@0.36, 2@0.44, 3@0.56, 2@0.62, 2@0.72, 3@0.88, 3@1.0, 15@1.2

5.2.3 Conceptual Model for a Horizontal Flow PRB

The final conceptual model for the HFPRB is shown in Fig. 5.5. The model includes a 25 m long by 1 m wide fully penetrating HFPRB located in the center of a heterogeneous aquifer. The gradient across the domain is 0.01 and flow is from left to right.

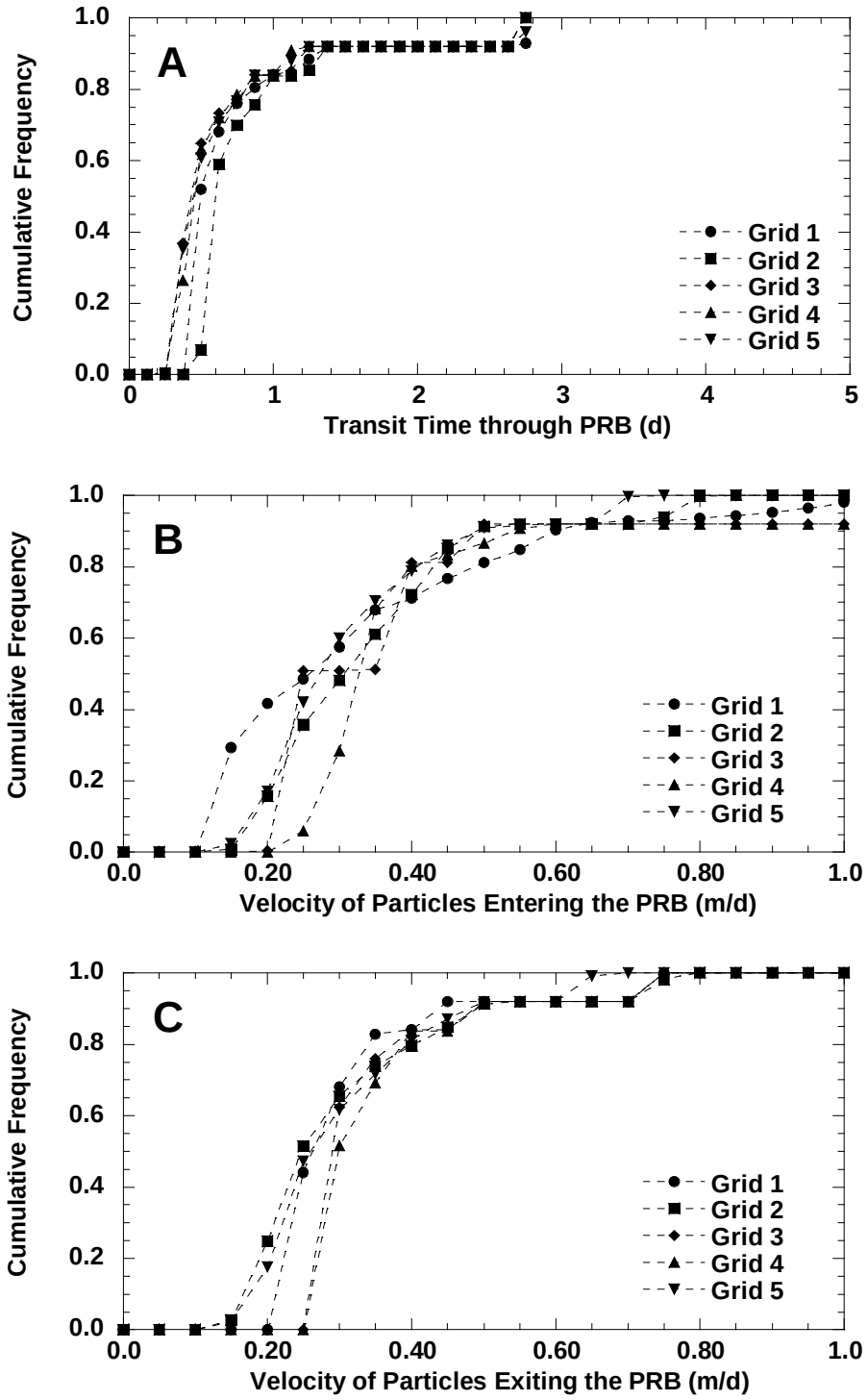

Fig. 5.4 Particle Transit Time through the PRB (a), Particle Velocity Entering the PRB (b), and Particle Velocity Exiting the PRB (c) for Five Increasingly Coarser Discretizations of the Domain.

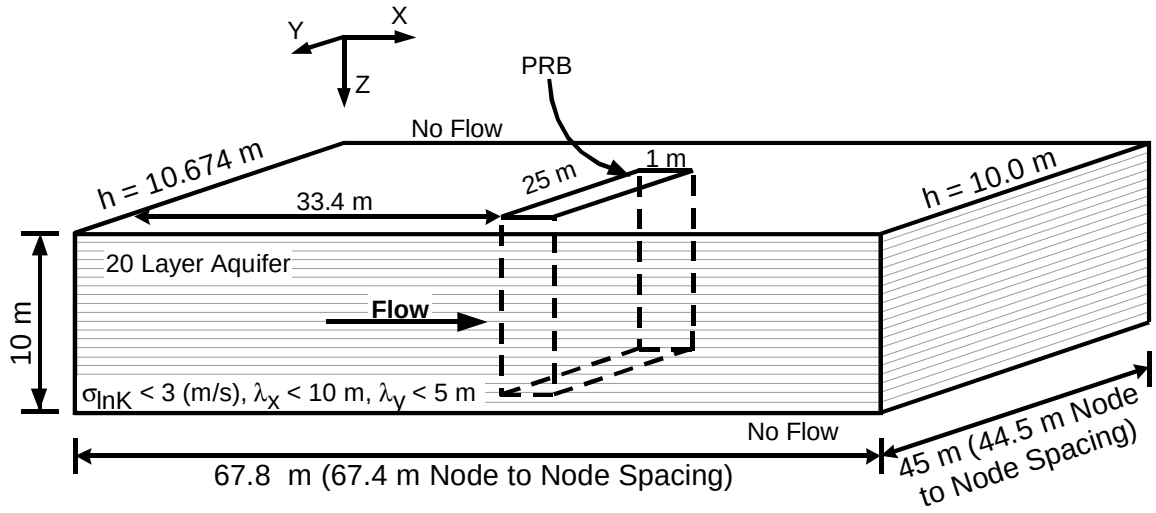

Grid Spacing

Δx = 75 @ 0.40 m | 0.38 m | 0.35 m | 0.31 m | 0.26 m | 0.22 m | 0.19 m | 0.16 m| 0.14 m | 0.13 m | 0.11 m | 0.10 m |0.09 m | 0.08 m | 0.07 m | 0.06 m | 15 @ 0.05 m | 10 @ 0.05 m|
- Center of PRB -
| 10 @ 0.05 m | 15 @ 0.05 m | 0.06 m | 0.07 m | 0.08 m |0.09 m | 0.10 m | 0.11 m | 0.13 m| 0.14 m | 0.16 m | 0.19 m | 0.22 m | 0.26 m | 0.31 m | 0.35 m| 0.38 m | 75 @ 0.40 m

Δy = 90 @ 0.50 m, Δz = 20 @ 0.50 m

Fig. 5.5 Conceptual Model of a Horizontal Flow Permeable Reactive Barrier Located in the Center of a Heterogeneous Aquifer.

5.3 PARTICLE TRAJECTORY THROUGH A HETEROGENEOUS AQUIFER AND PRB

The source for all simulations is 15 m wide by 5 m deep located 20 m up-gradient from the influent face of the PRB. The source contains 1200 particles that are tracked using Path3D until they pass through the PRB. Figure 5.6 is a Y-Z cross section of a realization showing the distribution of concentration at the source, the influent face of the PRB, and the effluent face of the PRB.

The concentration near the source is 1000 ppb as specified for all simulations. There is a lining around the source that appears to have concentrations less than 1000 ppb; however, this is an artifact of the contouring software, caused by linear interpolation between points inside and outside the source.

The influent face of the PRB has concentrations between 1 and 1000 ppb. Higher concentrations occur near the center of the aquifer and lower concentrations occur at the sides, due to dispersion between the source zone and the PRB. The maximum concentration at the influent face of the PRB equals the source concentration.

Concentrations at the effluent face of the PRB are between 0.0001 ppb and 10 ppb. Localized pockets of higher concentration that exist tend to coincide with regions of higher hydraulic conductivity at the influent face of the PRB.

Riemersma and Anderson (1996) claim that contaminants are transported across an aquifer predominantly through zones of higher hydraulic conductivity. To verify this assertion, the distribution of hydraulic conductivity for the aquifer is

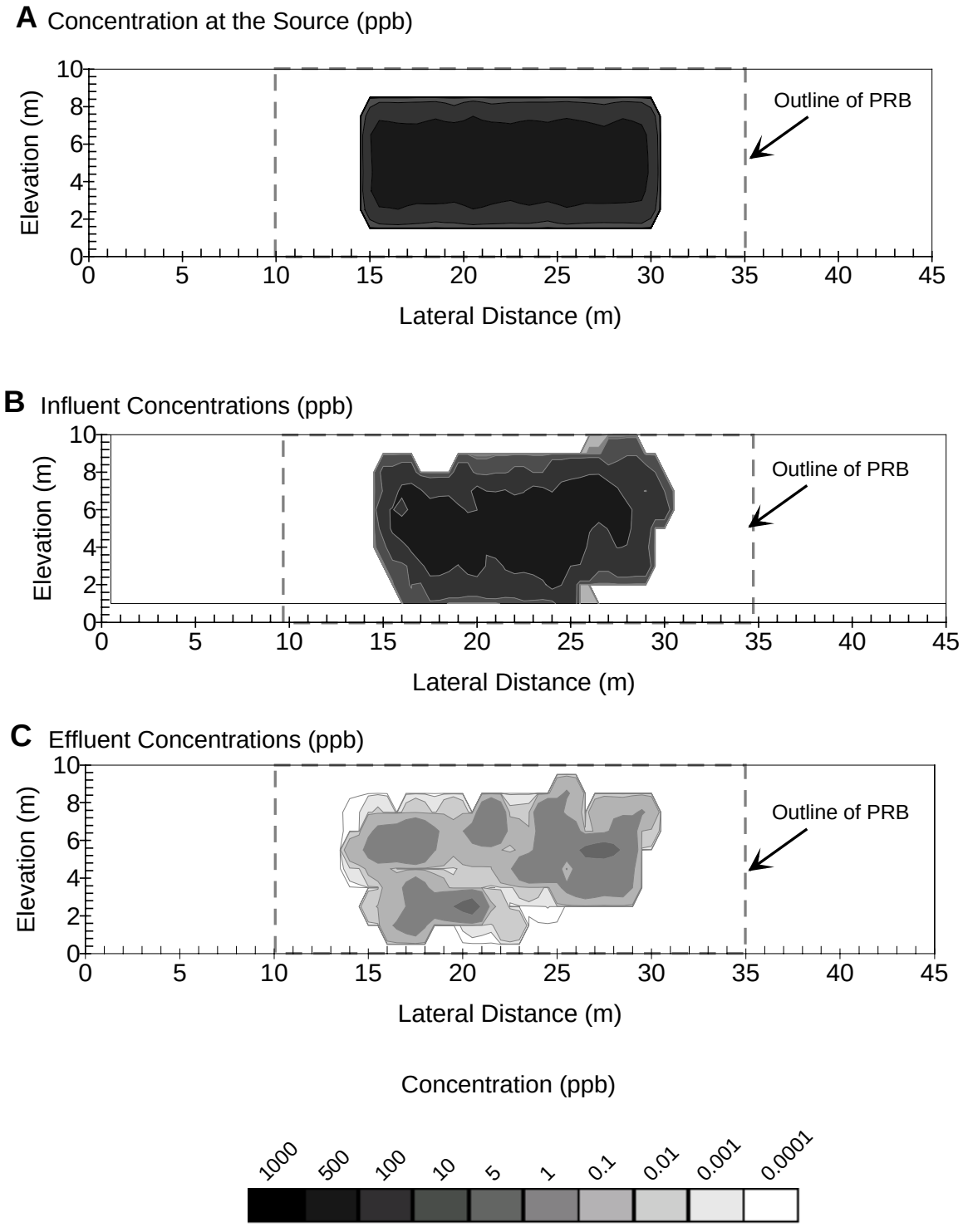

Fig. 5.6 Distribution of Concentration at the Source (a), the Influent Face of the PRB (b), and Effluent Face of the PRB (c). Simulations are for a homogeneous PRB (K_{prb} = 2.5x10^{-3} m/s, k_{rxn} = 1.0 d^{-1}) in an aquifer with μ_{lnK} = -10, σ_{lnK} = 1, λ_x = 3 m, and λ_y = 1 m.

compared with the distribution of hydraulic conductivity for cells in the aquifer that have a particle pass through them. These results are shown in Fig. 5.7. The PDF for the aquifer was generated using hydraulic conductivities from all finite difference cells for a realization of an aquifer with μ_{lnK} = -10, σ_{lnK} = 1, λ_x = 3 m, and λ_y = 1 m. The narrower PDF was created using the hydraulic conductivities for all finite difference cells that had a particle pass through them. Cells that compose the PRB were not included in either PDF.

The PDF for hydraulic conductivity of the aquifer appears as expected; it has a μ_{lnK} of –10 (4.5×10^{-5} m/s) and a σ_{lnK} of 1. The PDF for cells that have particles pass through them has a μ_{lnK} of –9.4 (8.3×10^{-5} m/s), which is nearly double the average hydraulic conductivity for the aquifer, and a σ_{lnK} of 0.24, which is one-quarter of σ_{lnK} for the aquifer. This result indicates that particles pass through higher hydraulic conductivity regions of the aquifer.

The preference for particles (and flow) to pass through more permeable units in the aquifer is shown in Fig 5.8. Figure 5.8 is a plan view of a 10 m by 10 m horizontal slice of the aquifer at an depth of 5.0 to 5.5 m. The magnitude of hydraulic conductivity is indicated by shading, where lighter regions have hydraulic conductivities greater than 4.5×10^{-5} m/s (i.e., $\exp(\mu_{lnK})$) and darker regions have hydraulic conductivities less than 4.5×10^{-5} m/s. Superimposed on the image of hydraulic conductivity are dots that show particle locations within the slice. Dot size decreases with depth between 5.0 m and 5.5 m; particles outside these depths are not shown.

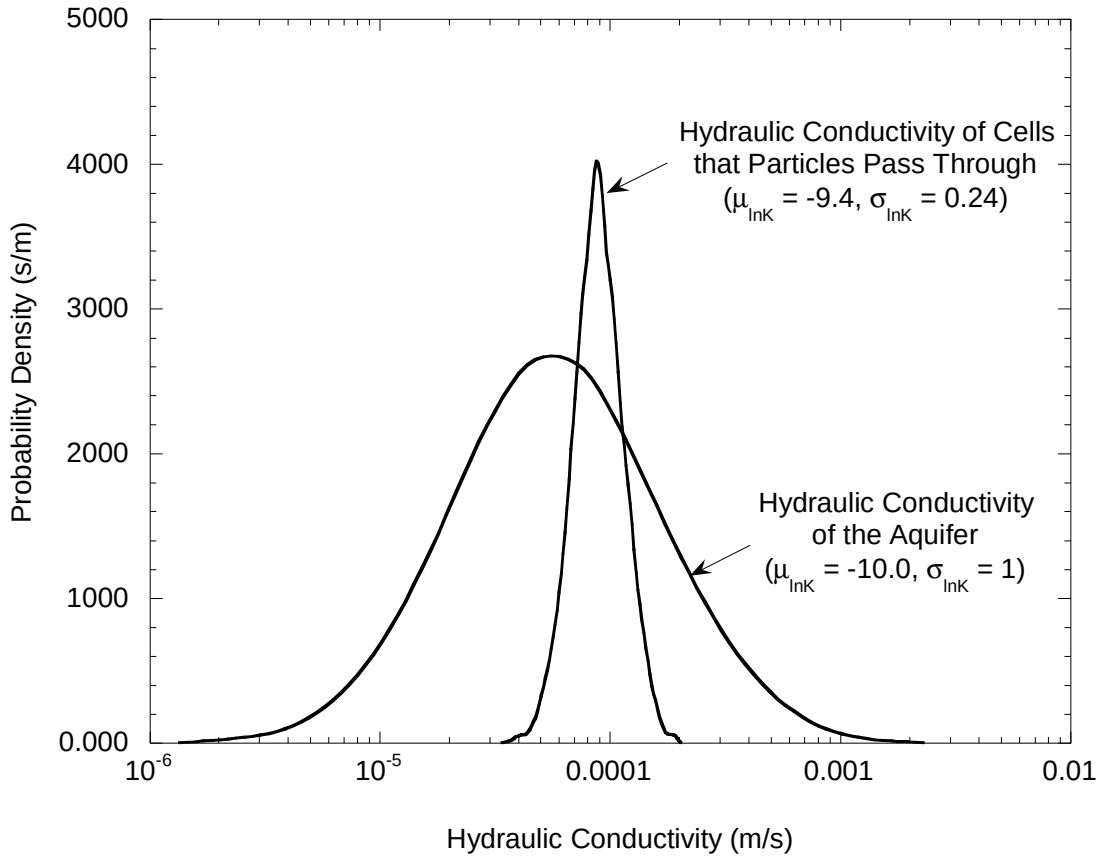

Fig. 5.7 PDFs for Hydraulic Conductivity of the Entire Aquifer and Finite Difference Cells in the Aquifer that Have a Particle Pass Through Them.

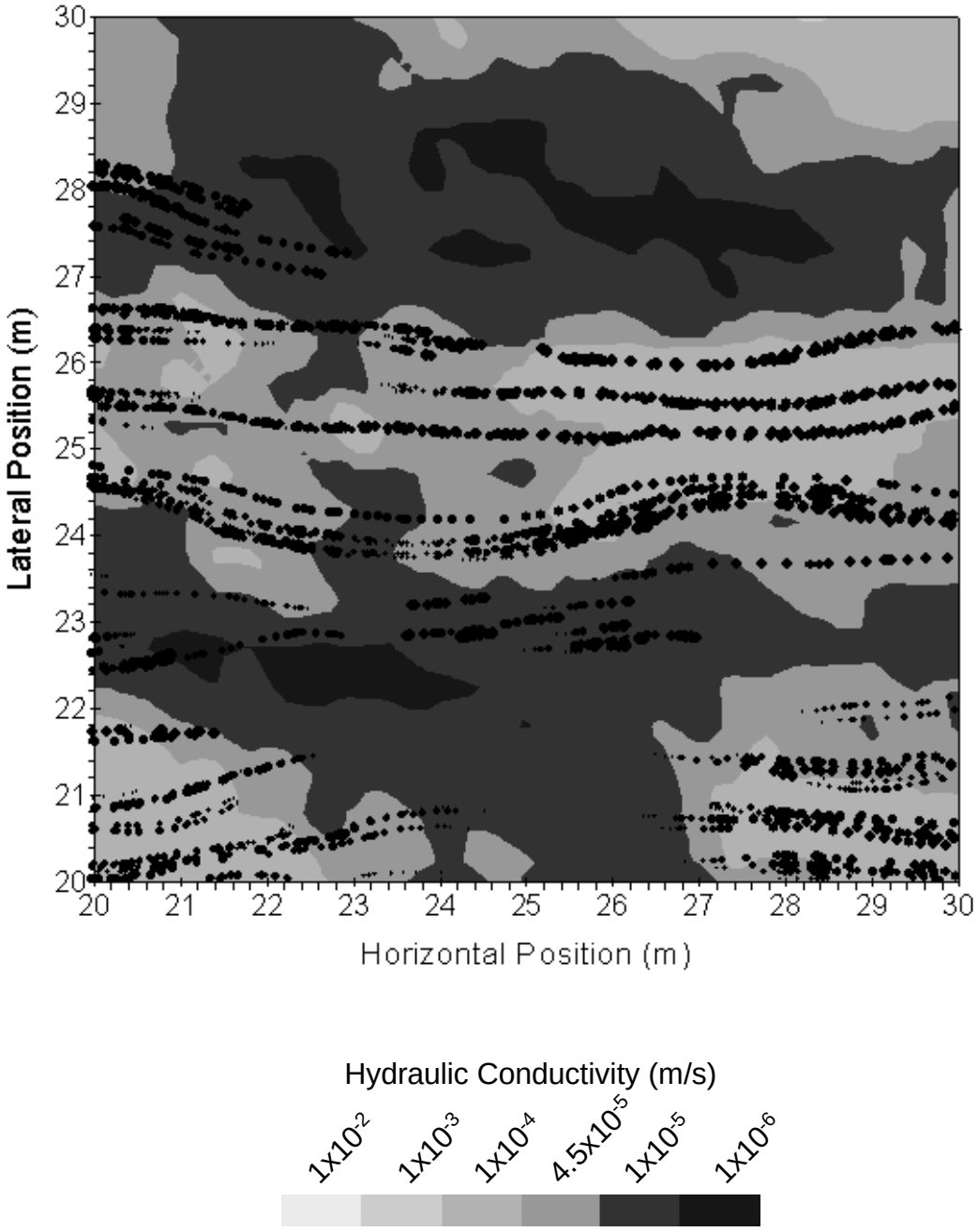

Fig. 5.8 Plan View of a ½ m Thick Slice of Aquifer. Hydraulic Conductivity is Shown by Shading and Particle Paths are Marked with Dots (dot size decreases with depth between 5.0 m and 5.5 m).

Particles pass through regions of higher hydraulic conductivity and avoid regions of lower hydraulic conductivity. Particles bend or move vertically to avoid less permeable units. Figure 5.8 shows the effect of more permeable units on flow through heterogeneous aquifers and supports the conclusion that the location and connectivity of more permeable units govern flow and advective transport through heterogeneous aquifers (Riemersma and Anderson 1996, Schreiber et al. 1999). The locations where these units intercept the PRB is critical because larger mass flux and higher flow rates will coincide with these points.

Eykholt et al. (1999) hypothesized that PRBs connect units of higher hydraulic conductivity that are otherwise discontinuous. Short-circuiting by the PRB causes preferential flow paths to form between more conductive units on either side of the PRB. Evidence in support of this hypothesis is shown in Fig. 5.9, which is a plot of the change in lateral position and elevation of particles traveling at X = 34.4 m relative to their position at X = 33.4 m. Changes in particle position are shown for simulations with and without a PRB.

When a PRB is added to the aquifer, there is more lateral and vertical flow, and groundwater travels a longer distance across the section. Longer flow paths form and flow paths are more tortuous because the PRB has a higher hydraulic conductivity than the surrounding aquifer. Thus, groundwater entering the PRB through a more conductive unit is able to meander through the PRB and exit the PRB through another conductive unit. Without the PRB, significantly more head loss is accrued when groundwater passes between discontinuous units of higher

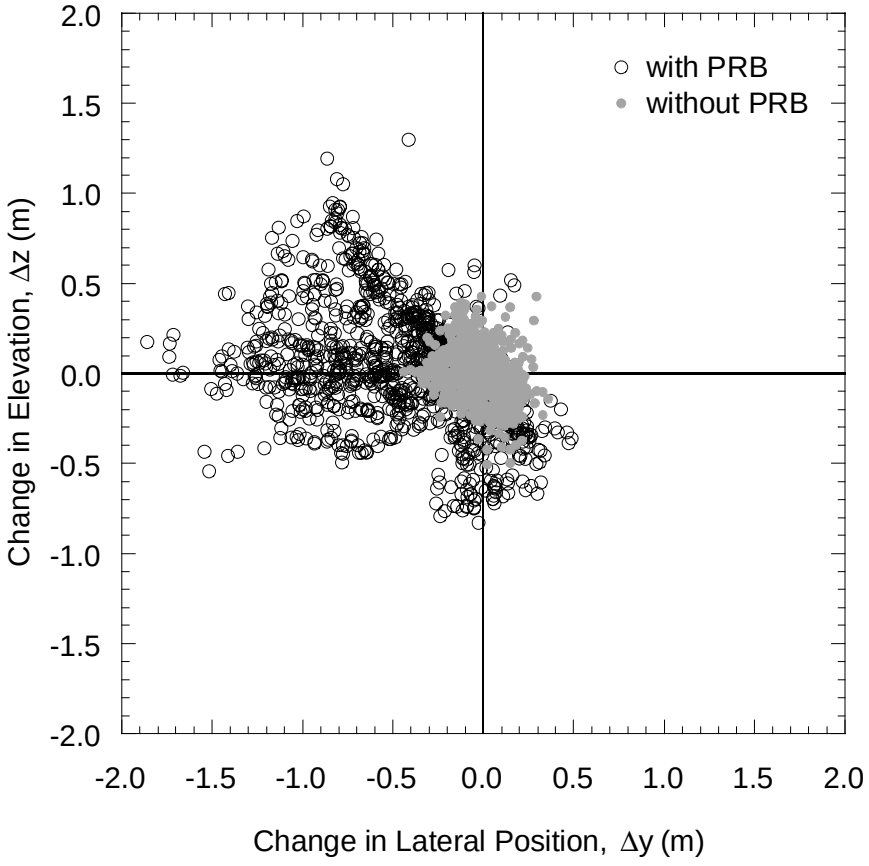

Fig. 5.9 Change in Lateral Position and Elevation Between X = 33.4 m and X = 34.4 m for Aquifers With and Without a PRB (Aquifer: μ_{lnK} = -10, σ_{lnK} = 1, λ_x = 3 m, λ_y = 1 m; PRB: $K_{PRB} = 2.5 \times 10^{-3}$ m/s).

hydraulic conductivity; therefore, particles follow straighter paths through the section.

PDFs of transit time for a particle to pass from 33.4 m to 34.4 m for aquifers with and without a PRB are shown in Fig. 5.10a. PDFs of travel distance between 33.4 and 34.4 m are shown in Fig. 5.10b. Particles have a shorter mean transit time and slightly narrower distribution of transit times when the aquifer contains a PRB. Also, particles travel a longer distance when there is a PRB. Thus, groundwater velocities are faster through the PRB than through a section of aquifer in the same location.

Particles move faster and travel a greater distance when there is a PRB because the PRB offers little resistance to flow due to its higher hydraulic conductivity. When the PRB is not present, head loss is greater per meter of particle travel, and therefore, particles take a more horizontal trajectory between X = 33.4 to 34.4 m. When the PRB is present, resistance between X = 33.4 and 34.4 m is about 50 times less, so particles can move vertically and laterally within the PRB without losing much head. If the gradient across the 1 m section is assumed to be constant, particles are able to travel longer distances through the PRB between conductive units without accruing much additional head loss. When there is not a PRB, particles take shorter and more direct paths because traveling longer distances between conductive zones requires more energy.

Adding a PRB to an aquifer narrows the distribution of transit time and skews it toward shorter residence times (Fig. 5.10a). Transit times become more uniform because the PRB induces greater mixing of groundwater, dampening

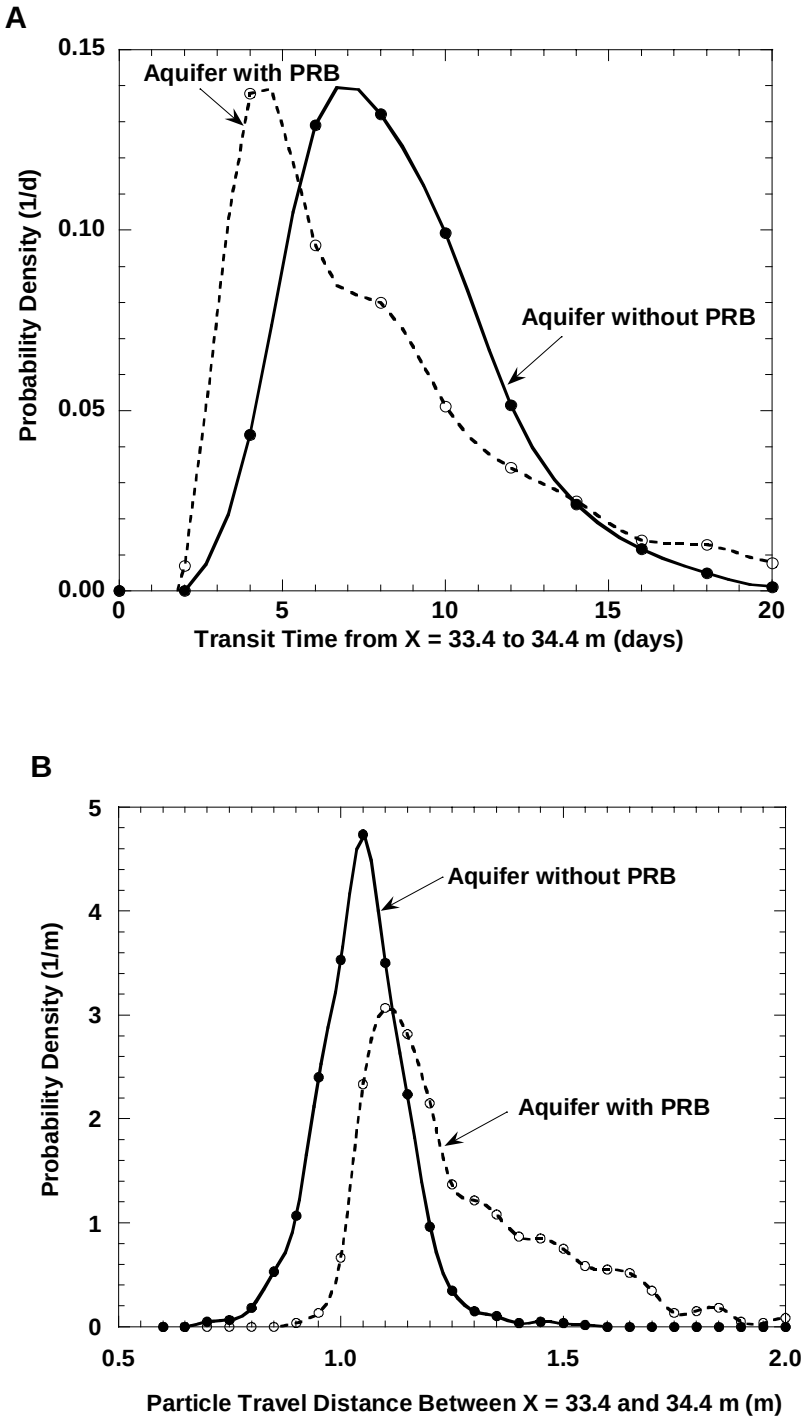

Fig. 5.10 Particle Transit Time (a) and Travel Distance (b) from X = 33.4 m to 34.4 m for Realizations With and Without a PRB (Aquifer: μ_{lnK} = -10, σ_{lnK} = 1, λ_x = 3 m, λ_y = 1 m; PRB: K_{PRB} = 2.5x10^{-3} m/s).

extremes in transit time. Mixing is also shown in Fig. 5.9 by the spreading of particle trajectories when there is a PRB.

5.4 EFFECT OF PRB HETEROGENEITY ON INFLUENT AND EFFLUENT CONCENTRATION FROM A HFPRB

The effects of heterogeneity of the hydraulic conductivity (K_p) and of the reaction rate constant (k_r) for the PRB, and the impact of a uniform change in the K_p and k_r on PRB performance were investigated. Seven PRB configurations were investigated in aquifers with μ_{lnK} = -10 (4.5×10^{-5} m/s), σ_{lnK} = 1.0, λ_x = 3 m, λ_y = 1 m, porosity = 40%, and a gradient of 0.01. Table 5-2 summarizes the parameters describing PRB heterogeneity for these simulations; K_p and k_r are independent for all simulations. Distributions of influent and effluent concentration for these simulations are shown in Fig. 5.11. The 5th, 25th, 50th (median), 75th, and 95th percentiles of concentration are shown in Fig. 5.11. Concentrations below the 5th percentile and above the 95th percentile are omitted for clarity.

Table 5-2 Summary of Input Parameters for Simulating PRB Heterogeneity.

K_p (m/s) (Normally Distributed)		k_r (d^{-1}) (Normally Distributed)	
Mean	Std. Dev.	Mean	Std. Dev.
2.5×10^{-3} *	0	1.0	0
2.5×10^{-4}	0	1.0	0
2.5×10^{-3}	0	0.9	0
2.5×10^{-3}	0	1.1	0
2.5×10^{-3}	1.0×10^{-4}	1.0	0
2.5×10^{-3}	0	1.0	0.05
2.5×10^{-3}	1.0×10^{-4}	1.0	0.05

*Base Case Simulation

a) Influent Concentrations

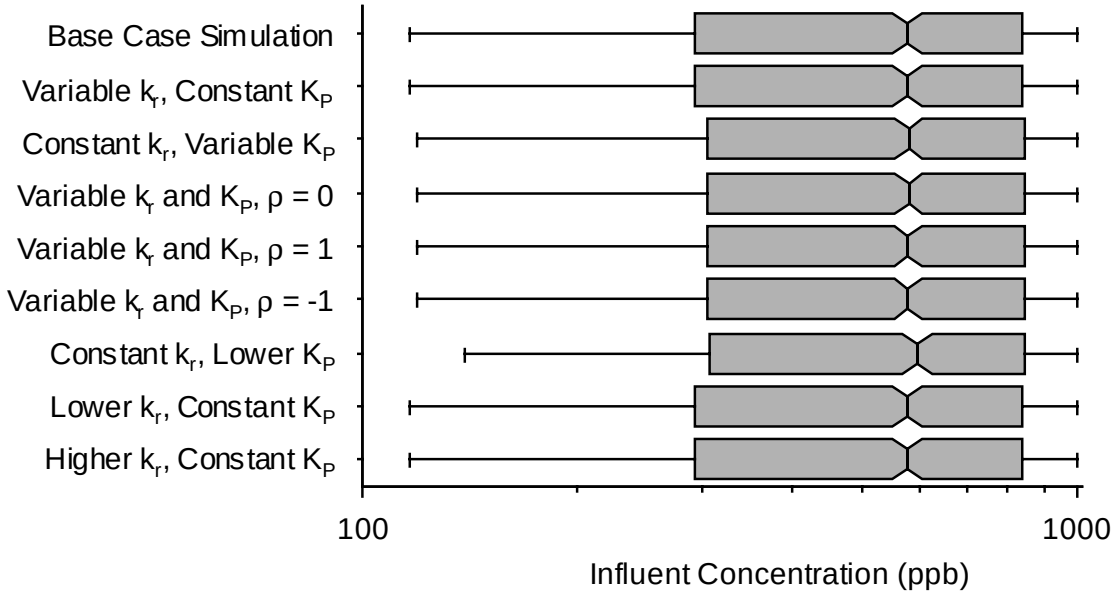

b) Effluent Concentrations

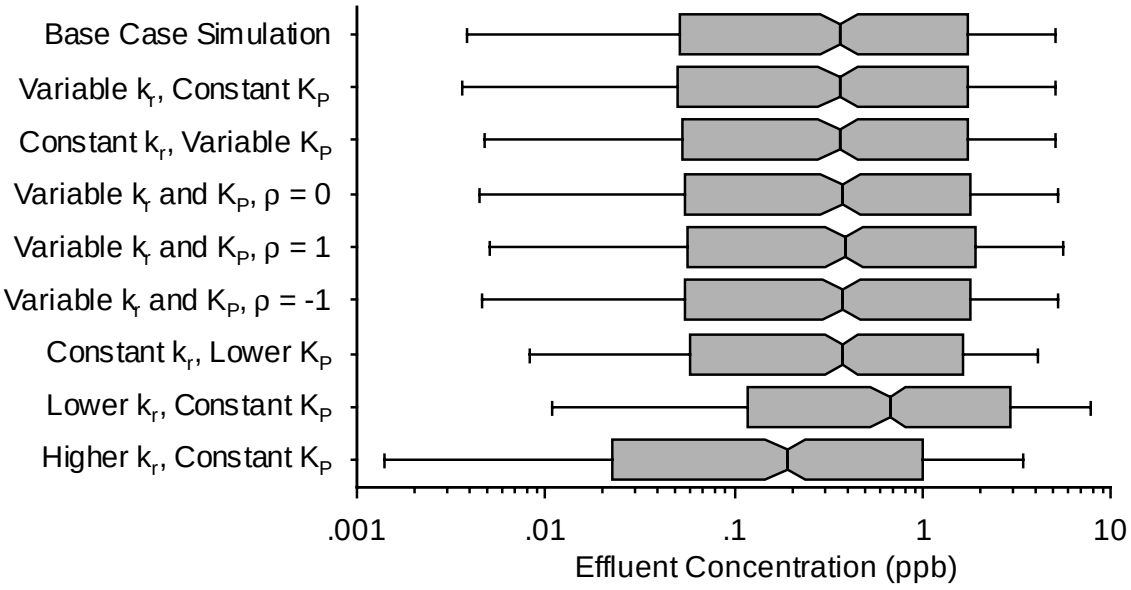

Fig. 5.11 Distributions of Influent (a) and Effluent (b) Concentration for Heterogeneous PRBs (1000 ppb Source, Aquifer with μ_{lnK} = -10, σ_{lnK} = 1, λ_x = 3 m, λ_y = 1 m; PRB; and 1 m PRB).

Most influent concentrations are between 100 ppb and 1000 ppb for all simulations. Distributions of influent concentration are divided into two groups: simulations of HFPRBs with spatially varying or lower K_p and HFPRBs with uniform K_p. HFPRBs with lower or spatially varying K_p yield slightly lower influent concentrations because the flow up-gradient of the PRB is diverted from zones of lower K_p and directed towards zones of higher K_p. Focusing flow through a smaller volume of the PRB increases mixing and dilution at these points, reducing the influent concentration slightly. Variations in k_r have no effect on influent concentration because k_r does not alter flow.

Most distributions of effluent concentration (Fig. 5.11b) are similar to the base case simulation (i.e., homogeneous PRB with k_r = 1.0 d^{-1} and $K_p = 2.5 \times 10^{-3}$). Only simulations with k_r = 0.9 d^{-1} or 1.1 d^{-1} yield different effluent concentrations. These simulations are intended to account for incorrect estimates or changes in the reactivity of PRBs. Poor estimates or changes in reactivity may result from poor interpretation of laboratory data, laboratory data for tests that do not represent field conditions (e.g., incorrect temperature or pH), or temporal changes in the reactivity of the media (aging). The higher and lower bounds for k_r that were investigated represent reaction rate constants at ±2 standard deviations in the distribution of reaction rate constant (Fig. 4.9).

Decreasing k_r to 0.9 d^{-1} shifts the distribution of effluent concentration toward higher concentrations. This is caused by slower reactions in the PRB, such that for a given residence time of groundwater in the PRB (i.e., identical flow fields), less reduction occurs. Conversely, increasing k_r to 1.1 d^{-1} shifts the distribution of

effluent concentration toward lower concentration because reactions occur more quickly (i.e., greater decrease in concentration for a given residence time). Shifts in the distributions of effluent concentration are consistent with the change in concentration predicted using a first-order loss equation (e.g., Eq. 2.3) for equal residence time of groundwater in the PRB. Thus, the consequence of changing k_r, caused by differences in reactivity between the field and laboratory or aging of the media, can be predicted.

Spatial variability in K_p and k_r do not significantly influence effluent concentrations because of the redundancy of the system. If groundwater passes through a region of lower k_r (or K_p), the groundwater is just as likely to then pass through a region of higher k_r (or K_p) so that groundwater has been exposed to average conditions when it reaches the effluent face of the PRB. As a result, effluent concentrations are similar, regardless of the variability in K_p or k_r. This conclusion assumes that the PRB does not contain fully penetrating defects such as stringers of higher K_p or lower k_r, which are unlikely to occur with braced cut or continuous trenching machine construction due to the good quality control and mixing that occurs when placing the media.

An order of magnitude decrease in K_p does not significantly affect distributions of effluent concentration (Fig. 5.11). Provided the HFPRB is more permeable than the aquifer, the degree to which the PRB is more permeable than the aquifer is not important because the flow rate entering and exiting the PRB from the aquifer dictates the residence time of groundwater in the PRB. The PRB

is 5 to 50 times more conductive than the aquifer so that groundwater flow is not restricted by the PRB.

The consequence of lowering K_p on flow entering and exiting the PRB is shown in Fig. 5.12. All aquifers in Fig. 5.12 have μ_{lnK} = -10 ($4.5x10^{-5}$ m/s), σ_{lnK} = 1.0, λ_x = 3 m, and λ_y = 1 m. The K_p's decrease from $2.5x10^{-4}$ m/s to $2.5x10^{-7}$ m/s for the HFPRBs shown in Fig. 5.12a through 5.12d. The HFPRBs in Fig. 5.12a and 5.12b have K_p greater than and slightly smaller than $4.5x10^{-5}$ m/s (i.e., $e^{\mu_{lnK}}$), whereas K_p is significantly smaller than $4.5x10^{-5}$ m/s in Fig. 5.12c and 5.12d. When K_p is approximately equal or greater than $4.5x10^{-5}$ m/s, particles approach and pass through the HFPRB along approximately horizontal paths, and the PRB does not significantly alter the size or shape of the plume. However, when K_p is less than $4.5x10^{-5}$ m/s, the plume widens as it approaches the PRB and at K_p = $2.5x10^{-7}$ m/s, a significant number of particles circumvent the PRB. Based on these results, it can be concluded that HFPRBs with K_p greater than or equal to $e^{\mu_{lnK}}$ do not significantly affect aquifer flow and plume geometry; when K_p is less than $e^{\mu_{lnK}}$, contaminants may pass around the PRB. Thus, HFPRBs should be designed using media that have a hydraulic conductivity greater than or equal to that of the aquifer.

In summary, seven combinations of variability in K_p and k_r were investigated along with five values for K_p. Influent and effluent concentrations are affected little by spatial variability in k_r and K_p, and changes in mean K_p, provided the PRB is more permeable than the aquifer. Effluent concentrations decrease uniformly with

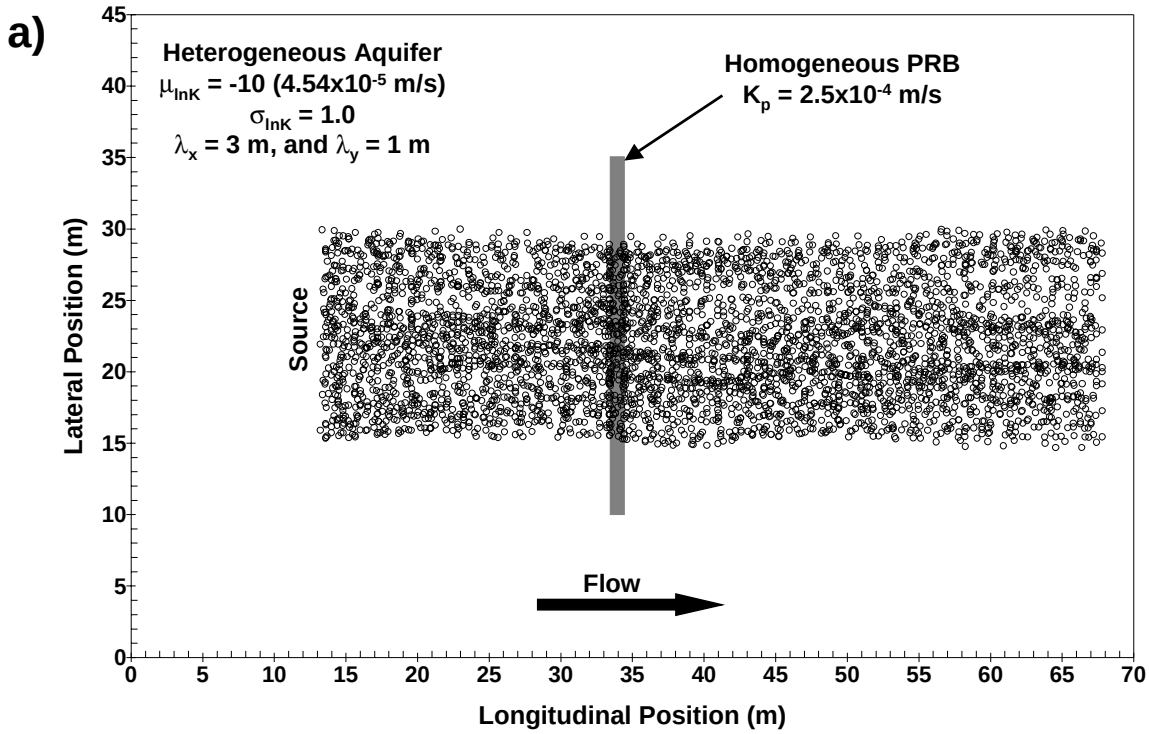
a)
Heterogeneous Aquifer
μ_{lnK} = -10 (4.54x10^{-5} m/s)
σ_{lnK} = 1.0
λ_x = 3 m, and λ_y = 1 m
Homogeneous PRB
K_p = 2.5x10^{-4} m/s
Source
Flow
Lateral Position (m)
Longitudinal Position (m)
0
5
10
15
20
25
30
35
40
45
50
55
60
65
70

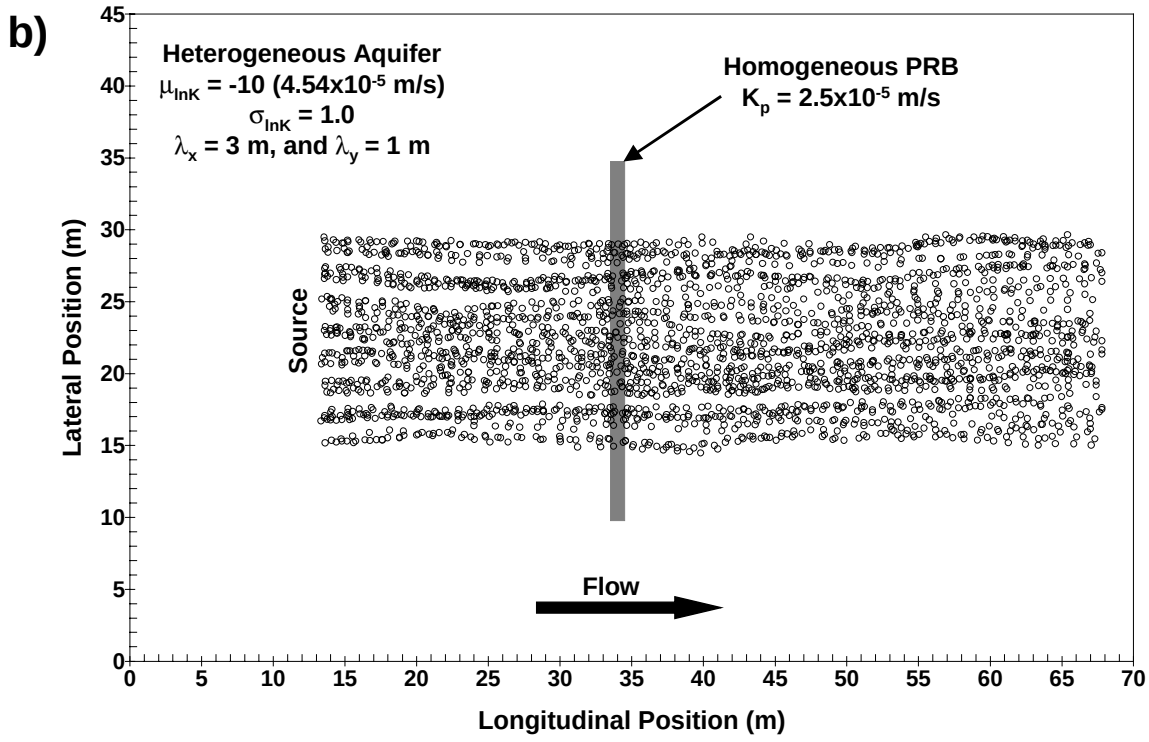
b)
Heterogeneous Aquifer
μ_{lnK} = -10 (4.54x10^{-5} m/s)
σ_{lnK} = 1.0
λ_x = 3 m, and λ_y = 1 m
Homogeneous PRB
K_p = 2.5x10^{-5} m/s
Source
Flow
Lateral Position (m)
Longitudinal Position (m)
0
5
10
15
20
25
30
35
40
45
50
55
60
65
70

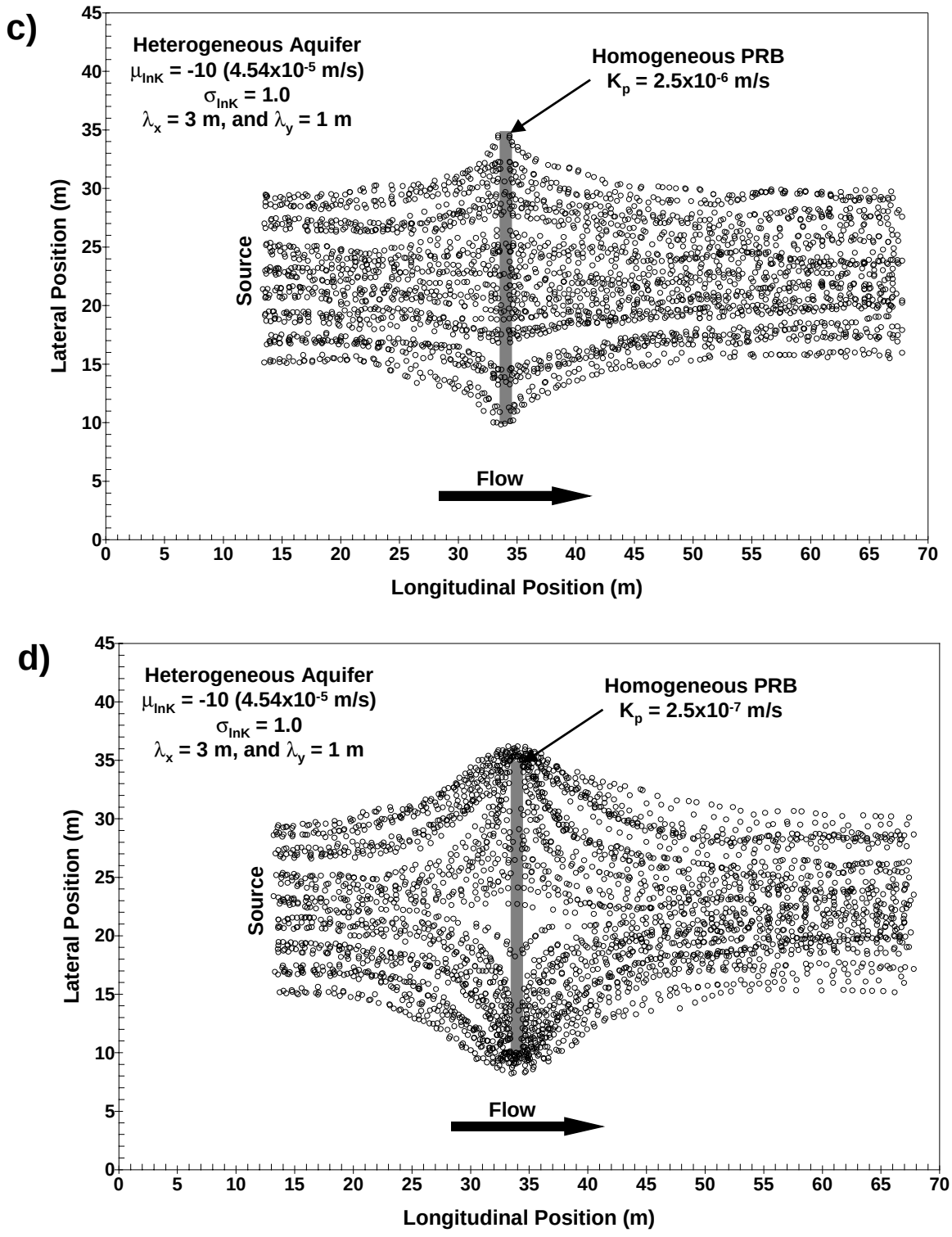

Fig. 5.12 Particle Trajectory for HFPRB that Have $K_p = 2.5x10^{-4}$ m/s (a), $K_p = 2.5x10^{-5}$ m/s (b), $K_p = 2.5x10^{-6}$ m/s (c), and $K_p = 2.5x10^{-7}$ m/s (d). Aquifer have $\mu_{lnK} = -10$, $\sigma_{lnK} = 1$, $\lambda_x = 3$ m, and $\lambda_y = 1$ m.

increasing mean k_r, and effluent concentrations increase uniformly with decreasing mean k_r. Thus, proper estimation of short and long-term reactivity of the media is the most important characteristic of the PRB affecting its performance.

Figure 5.13 shows concentrations for the same aquifer as in Fig. 5.11 but with σ_{lnK} = 4.0 (σ_{lnK} = 1.0 in Fig. 5.11). Distributions of influent concentration are similar in Fig. 5.11 and Fig. 5.13. Distributions of effluent concentration in Fig. 5.13 are shifted toward higher concentrations than in Fig. 5.11 due to the greater mixing at higher σ_{lnK}. Trends in the distributions are similar (i.e., uniform changes in K_p and variability in k_r do not significantly affect influent and effluent concentrations, whereas uniform increases and decreases in k_r shift effluent concentration).

5.5 EFFECT OF AQUIFER HETEROGENEITY ON INFLUENT AND EFFLUENT CONCENTRATION FROM A HFPRB

This section discusses distributions for the influent and effluent concentration from a PRB located in aquifers that have different μ_{lnK}, σ_{lnK}, and correlation scales.

5.5.1 Effect of μ_{lnK}

Effect of μ_{lnK} on distributions of influent and effluent concentration from a HFPRB was investigated by simulating identical HFPRBs (i.e., homogeneous PRB with $K_p = 2.5 \times 10^{-3}$ m/s and $k_r = 1$ d^{-1}) located in aquifers with μ_{lnK} of –9, -10, -11, and -12. These μ_{lnK} correspond to hydraulic conductivities of 1.5×10^{-4}, 4.5×10^{-5},

a) Influent Concentrations

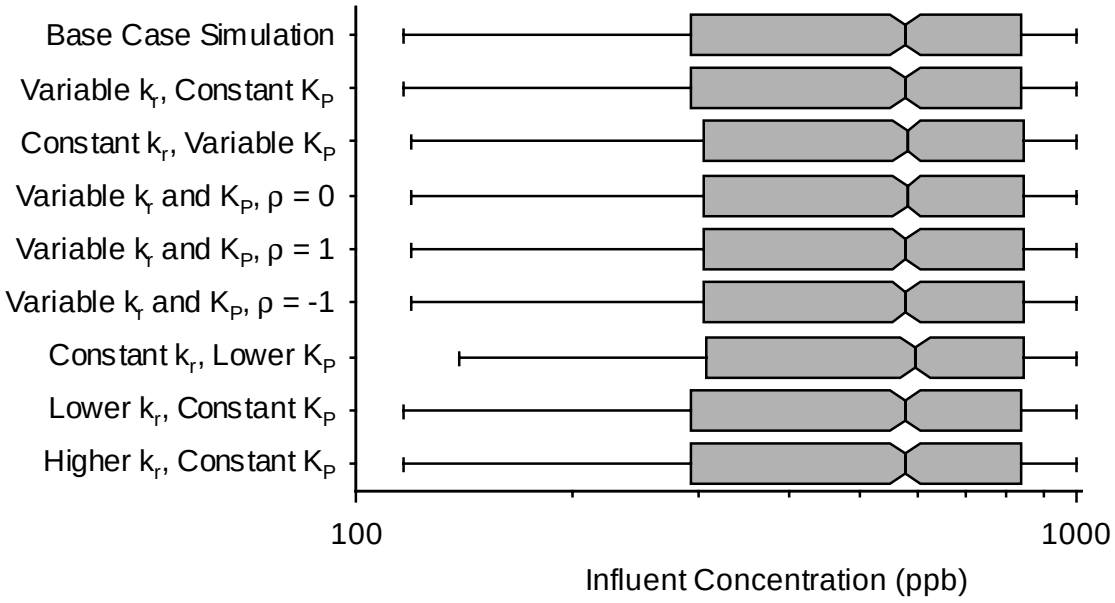

b) Effluent Concentrations

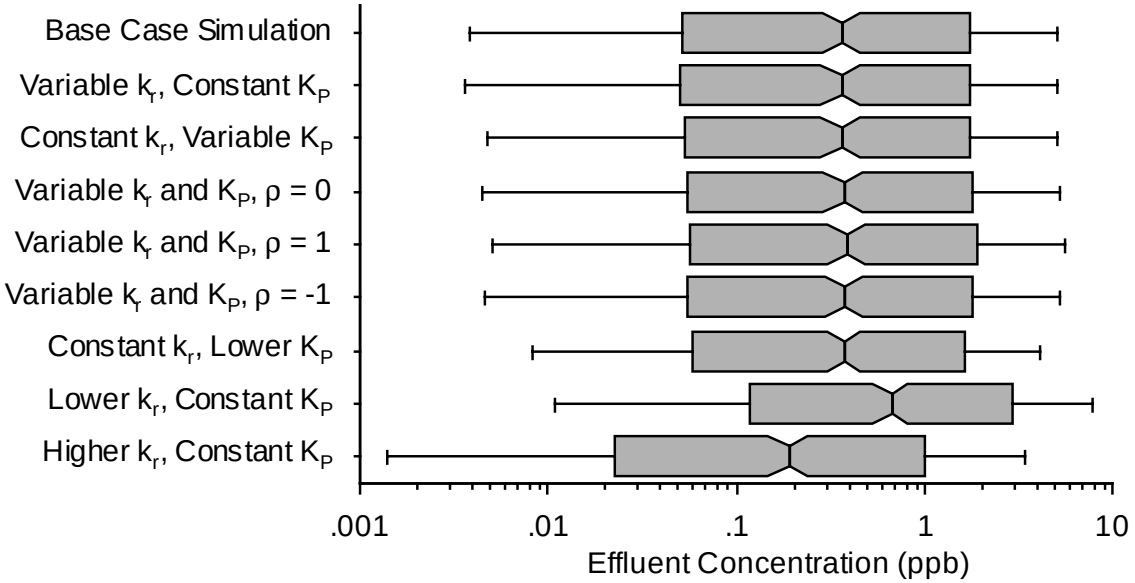

Fig. 5.13 Distributions of Influent (a) and Effluent (b) Concentration from PRBs in Aquifer with μ_{lnK} = -10, λ_x = 3 m, λ_y = 1 m, and σ_{lnK} = 4.0 and Several Combinations of k_r and K_p.

$1.7x10^{-5}$, and $6.1x10^{-6}$ m/s, which cover the range of μ_{lnK} for most natural soil deposits (Table 3.1). For these simulations, $\sigma_{lnK} = 1.0$, $\lambda_x = 3$ m, and $\lambda_y = 1$ m.

Distributions of influent and effluent concentration for the PRB in each aquifer are shown in Fig. 5.14. Distributions of effluent concentrations from a HFPRB in an aquifer with $\mu_{lnK} = -12$ (i.e., $6.1x10^{-6}$ m/s) are not shown because concentrations fall well below the other effluent concentrations (median concentration for $\mu_{lnK} = -12$ was 10^{-17} ppb).

Distributions of influent concentration are not affected by μ_{lnK}. Contaminant may take longer to reach the PRB when μ_{lnK} is lower, but the spatial distribution of concentration entering the PRB will be the same provided σ_{lnK} is the same. In essence, the distributions of hydraulic conductivity for aquifers shown in Fig. 5.14 are identical in all respects except for the magnitude of the hydraulic conductivity. For example, the hydraulic conductivity field for the simulation with a $\mu_{lnK} = -11$ could be obtained by dividing the hydraulic conductivity at all nodes for the simulation with $\mu_{lnK} = -10$ by 2.706 (i.e., e^{-1}). Thus, concentrations entering the PRB are identical because the location and relative magnitude of hydraulic conductivity are identical, regardless of μ_{lnK}. Travel times to the PRB vary with μ_{lnK}, but concentrations entering the PRB do not change because reactions are assumed not to occur in the aquifer ($k_r = 0$ in the aquifer). In nature, some reactions may occur in the aquifer (i.e., bacterial digestion or volatilization), in which case the influent concentration will be lower for lower μ_{lnK} because contaminants take longer to reach the PRB.

a) Influent Concentrations

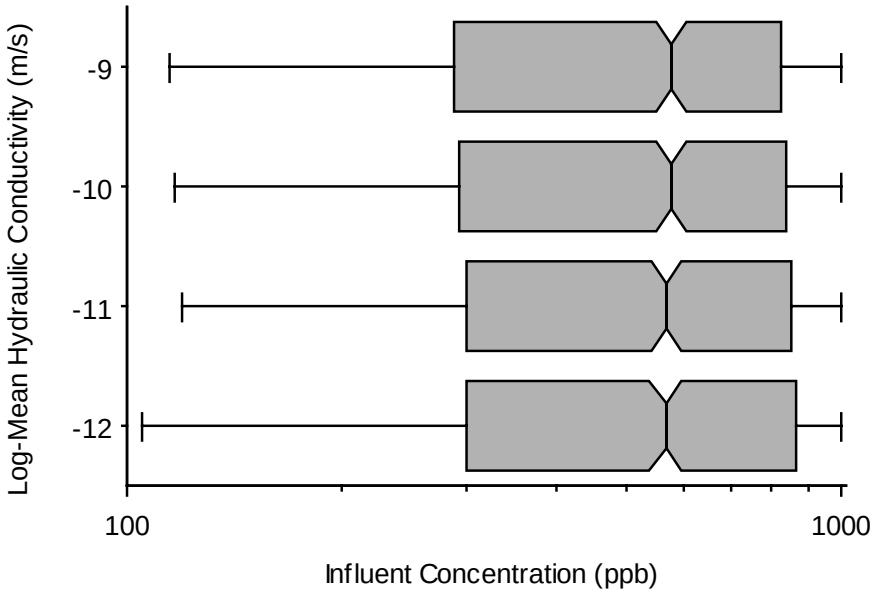

b) Effluent Concentrations

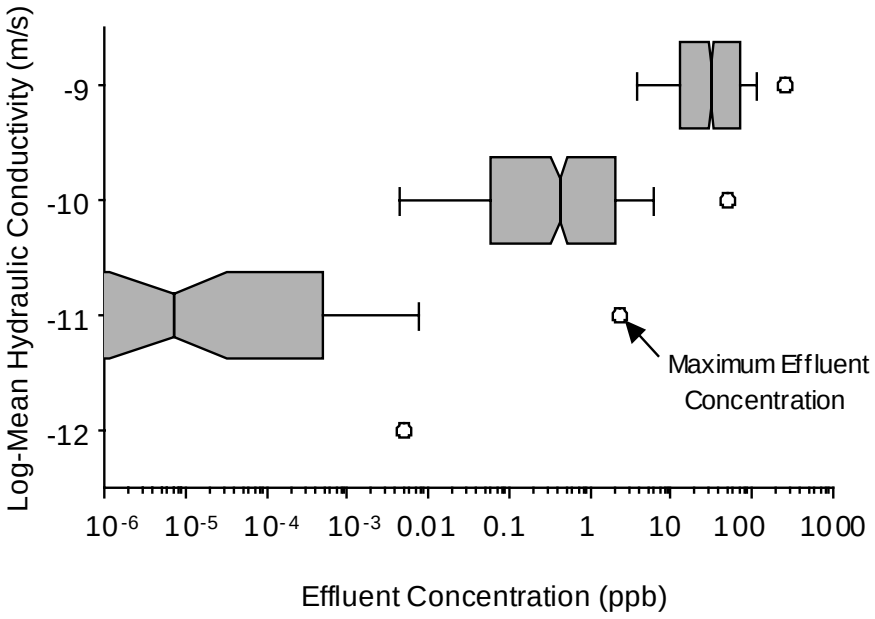

Fig. 5.14 Distributions of Influent (a) and Effluent Concentration (b) for a PRB Located in Aquifers that Have Different μ_{lnK}.

Distributions of effluent concentration shift toward lower concentrations and become more spread as μ_{lnK} decreases, because the seepage velocities are lower in aquifers that have lower μ_{lnK}, all other factors being equal. Lower seepage velocities increase the residence time of contaminants in the PRB and reduce the median effluent concentration.

The residence time of the groundwater in the PRB is proportional to the difference between the distributions of influent and effluent concentration. This difference increases with decreasing μ_{lnK}, indicating longer residence timse for contaminants in PRBs that are located in aquifers with lower μ_{lnK}.

Distributions of effluent concentration are broader when μ_{lnK} is lower because localized zones of higher hydraulic conductivity are present, even at lower μ_{lnK}. Consider the PDFs for hydraulic conductivity shown in Fig. 5.15; as μ_{lnK} decreases, the PDF becomes increasingly skewed toward lower hydraulic conductivities. However, the probability density associated with higher hydraulic conductivities does not change substantially. Thus, the fraction of high permeability units does not change substantially with μ_{lnK}. Additional evidence that higher permeability units exist at all μ_{lnK} is shown in Fig 5.16a and Fig. 5.16b, which are horizontal sections of aquifers with μ_{lnK} = -10 and –11 respectively. Zones having $K > 1 \times 10^{-4}$ m/s are apparent on both images, indicating that more conductive zones exist in aquifers despite differences in μ_{lnK}.

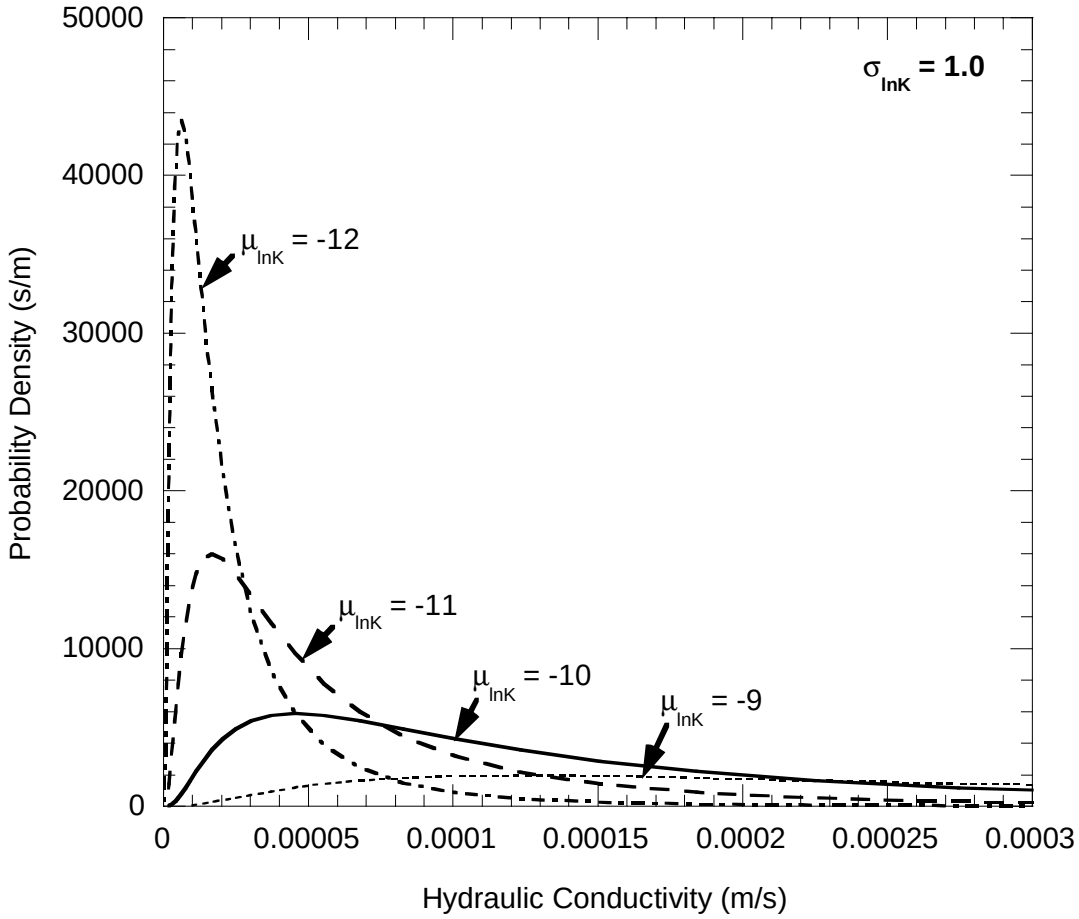

Fig. 5.15 PDFs for Aquifers that Have μ_{lnK} = -9, -10, -11, and –12, and σ_{lnK} = 1.

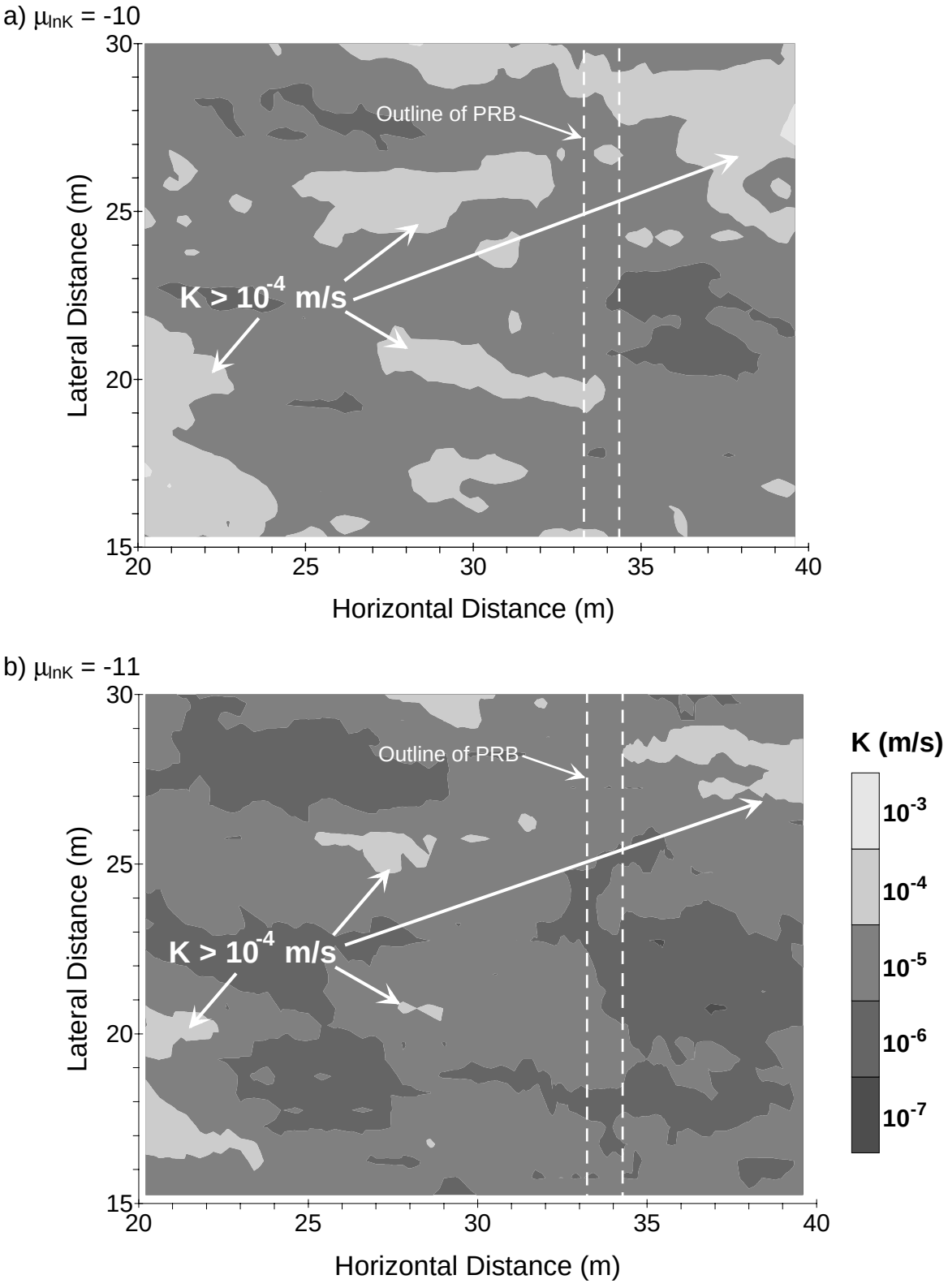

Fig. 5.16 Images of Random Fields that Have μ_{lnK} = -10 (a), and –11 (b).

A shift toward lower median effluent coupled with higher effluent concentrations due to a small fraction of high permeability units, broadens the distribution of effluent concentration at lower μ_{lnK}.

5.5.2 Effect of σ_{lnK}

The impact of varying σ_{lnK} for the aquifer was investigated by simulating PRB-aquifer systems with μ_{lnK} = -10 and low (σ_{lnK} = 0.25), moderate (σ_{lnK} = 1.0), or high (σ_{lnK} = 2.25 and 4.0) heterogeneity (Harter 1998). All simulations had a porosity of 40%, λ_x of 3 m, and λ_y of 1 m. Similar to the previous section, data are shown for a homogeneous PRB ($K_p = 2.5x10^{-3}$ m/s and $k_r = 1\ d^{-1}$). The results of these simulations are shown in shown in Fig. 5.17.

Distributions of influent concentration shift toward lower concentrations and broaden as σ_{lnK} increases (Fig. 5.17). The distribution shifts because there is greater spatial variability in hydraulic conductivity at higher σ_{lnK}. Greater spatial variability results in more mixing (i.e., dispersion) and lower concentrations. Influent concentrations decrease and broaden more for σ_{lnK} = 0.25 to 2.25 than from σ_{lnK} = 2.25 to 4.0, suggesting that mixing between the source and the PRB is strongly affected by low to moderate heterogeneity (σ_{lnK} < 2.25). More mixing occurs from σ_{lnK} = 0.25 to 2.25 because permeable units become more common in this range of σ_{lnK}. PDFs for σ_{lnK} = 0.25, 1.0, 2.25, and 4.0 are shown in Fig. 5.18. Between σ_{lnK} = 0.25 and 2.25, PDFs change significantly; the peak of the PDF decreases and more mass is distributed in the tail. For σ_{lnK} > 2.25, PDFs.

a) Influent Concentrations

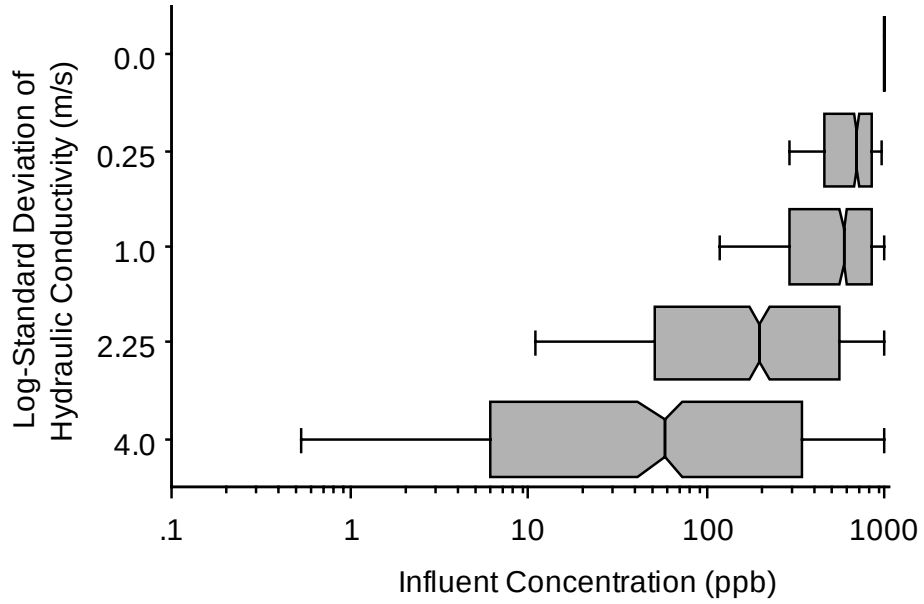

b) Effluent Concentrations

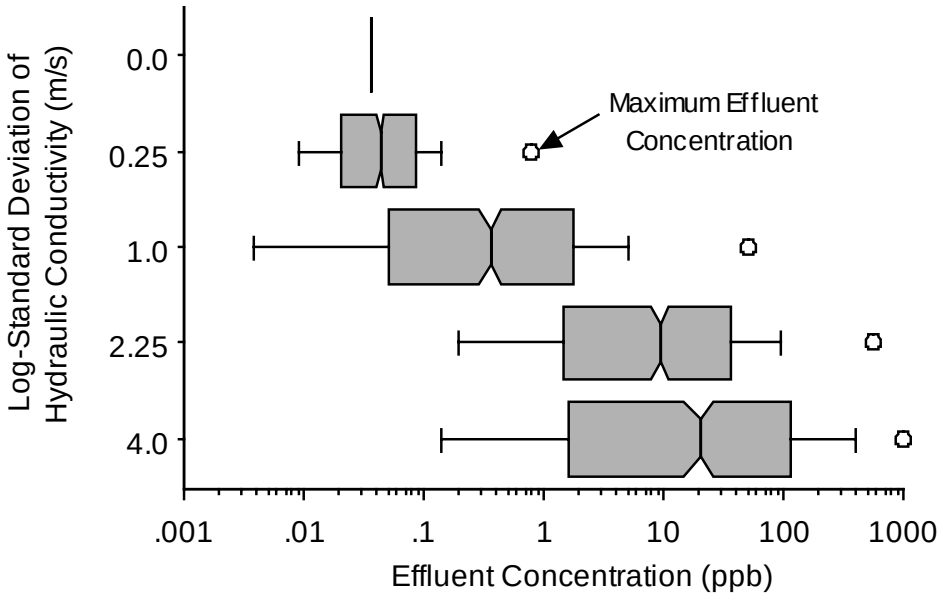

Fig. 5.17 Distributions of Influent (a) and Effluent (b) Concentration for PRB Located in Aquifers that Have Different σ_{lnK}.

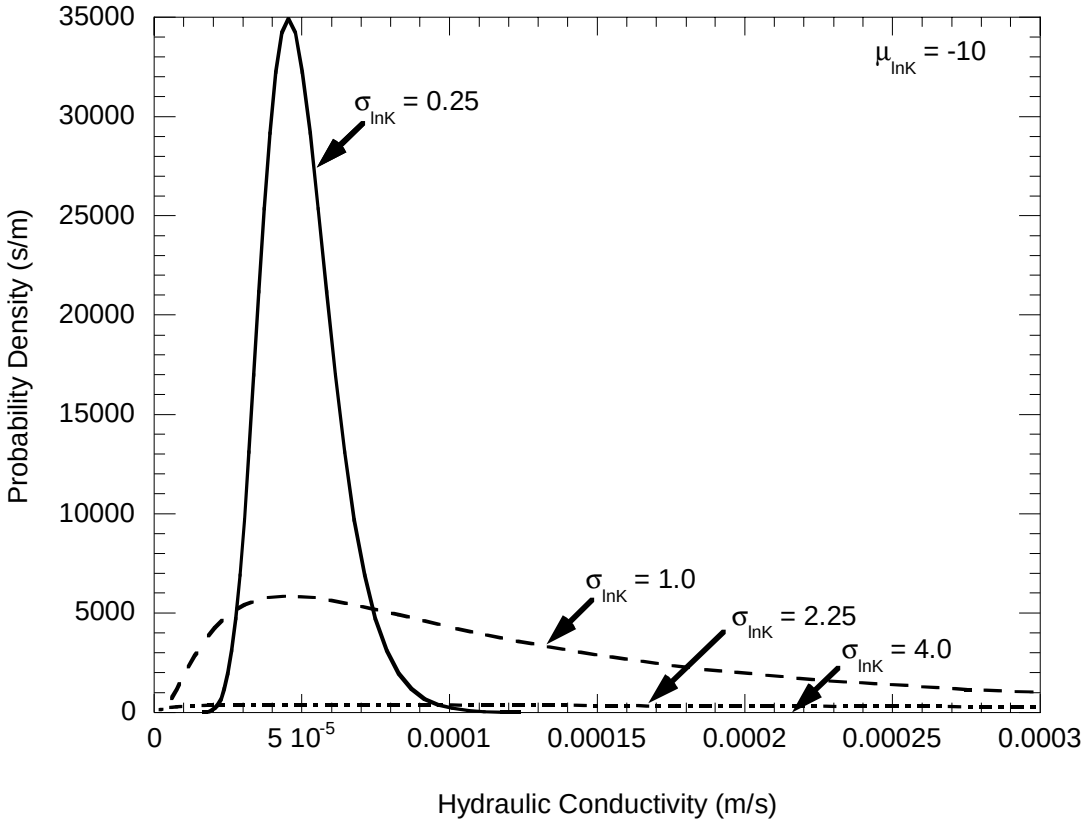

Fig. 5.18 PDFs for Aquifers that Have Different σ_{lnK}.

continue to have lower probability mass at $4.5x10^{-5}$ m/s (i.e., $e^{\mu_{lnK}}$) and more mass in the tail. The large increase in spatial variability of hydraulic conductivity between σ_{lnK} = 0.25 and 2.25 causes mixing and a shift in influent concentration. For σ_{lnK} greater than 2.25, there are smaller increases in spatial variability of hydraulic conductivity in the aquifer and consequently a smaller shift in distributions of influent concentration.

Increasing σ_{lnK} of the aquifer also broadens the distribution of influent concentration. As σ_{lnK} increases, seepage velocities become more variable due to greater spatial variability of hydraulic conductivity in the aquifer, which causes greater mixing (i.e., dispersion) and a larger range of influent concentrations

Effluent concentrations increase with increasing σ_{lnK}. At lower σ_{lnK}, transit times of contaminant in the PRB are more uniform and closer to the transit time predicted using a plug flow model (i.e., C_e in Eq. 2.3). For $\sigma_{lnK} > 0$, effluent concentrations are higher than C_e from Eq. 2.3 because the aquifer contains zones of hydraulic conductivity greater than the geometric mean for the aquifer. As σ_{lnK} increases, effluent concentrations also increase because a larger fraction of the aquifer contains more permeable units, and these units control advective mass transfer through the aquifer. Similar to influent concentrations, shifts in effluent concentration are larger for σ_{lnK} of 0.25 to 2.25 than for σ_{lnK} of 2.25 to 4.0 because the PDFs of hydraulic conductivity change most for $\sigma_{lnK} < 2.25$ (Fig. 5.18). Thus, an error in estimating σ_{lnK} in more homogeneous aquifers (i.e., $\sigma_{lnK} < 2.25$) has a

greater impact on effluent concentration than poor estimates of σ_{lnK} in highly heterogeneous aquifers (i.e., $\sigma_{lnK} > 2.25$).

5.5.3 Effect of Correlation Scale

The effect of correlation scale on the distribution of influent and effluent concentration was investigated by performing simulations with $\mu_{lnK} = -10$, $\sigma_{lnK} = 1.0$, and λ_x and λ_y of 3 m and 1 m, 6 m and 2 m, 9 m and 3 m, 6 m and 5 m, and 6m and 1 m. These λ_x and λ_y are typical correlation scales in sandy aquifers (Table 3.1). Distributions of influent and effluent concentration for these simulations are shown in Fig. 5.19.

Influent concentrations are affected little by varying λ_x or λ_y; however, effluent concentrations increase for larger λ_x. When λ_x is larger, zones of higher hydraulic conductivity tend to be longer. Thus, when a PRB is installed in such an aquifer, it is more likely to bisect a zone of higher hydraulic conductivity, creating two zones of higher hydraulic conductivity that are aligned on either side of the PRB. Influent entering the PRB through a zone of higher hydraulic conductivity bisected by the PRB passes directly through the PRB and exits the PRB into the remainder of the zone, spending minimal time in the PRB. Conversely, when λ_x is lower, the PRB is less likely to bisect a zone of higher hydraulic conductivity. As a result, groundwater flows diagonally across the PRB between unaligned zones of higher hydraulic conductivity. The longer flow path requires more time to traverse the PRB, reducing the effluent concentration.

a) Influent Concentrations

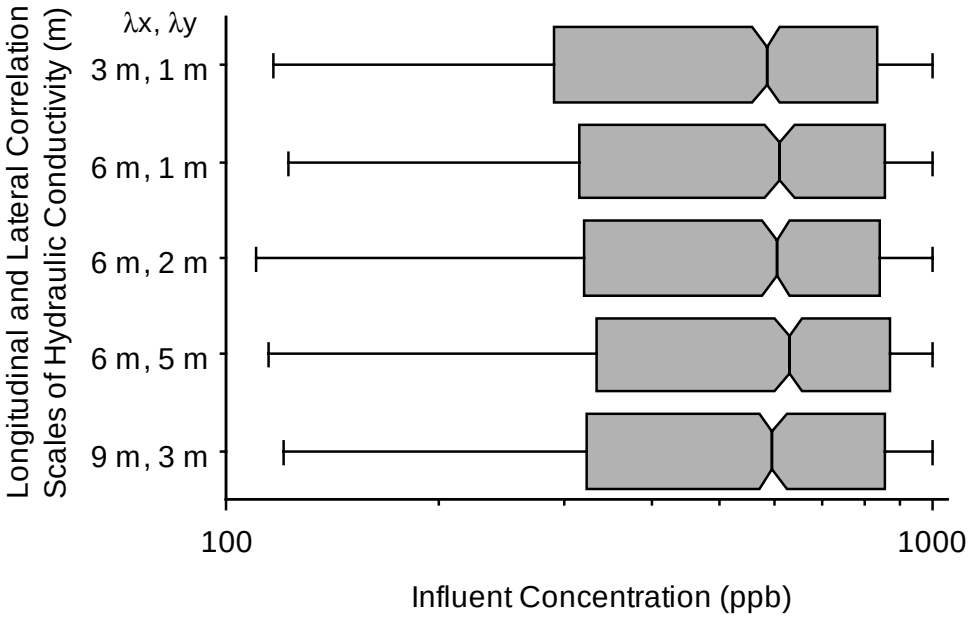

b) Effluent Concentrations

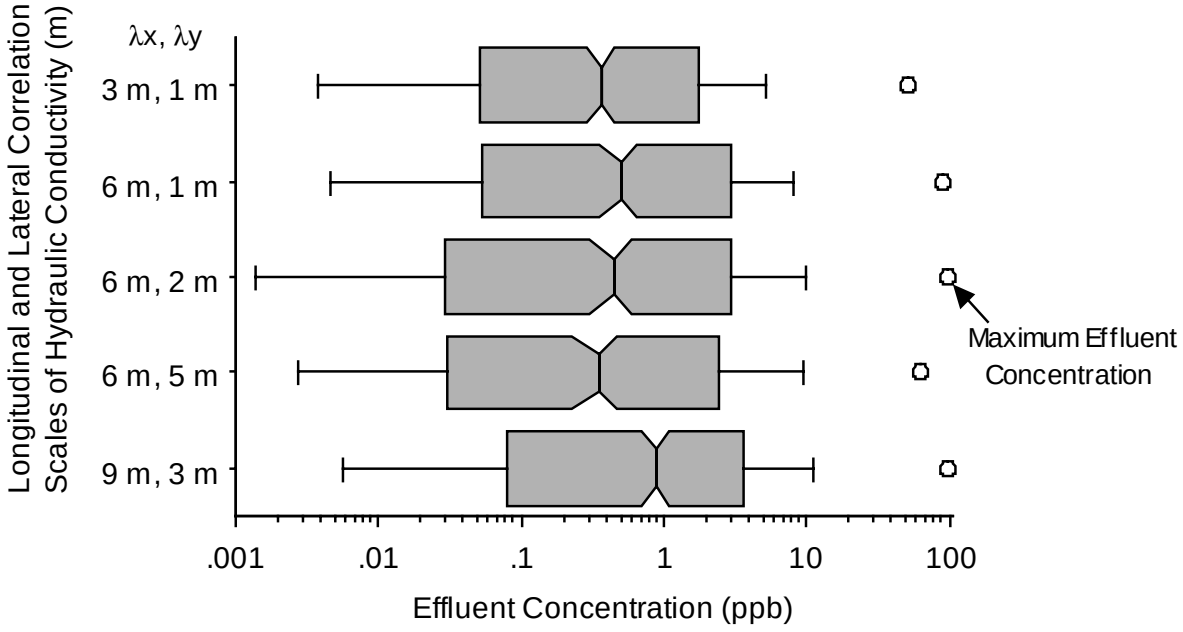

Fig. 5.19 Distributions of Influent (a) and Effluent (b) Concentration for a PRB Located in Aquifers that Have Different λ_x and λ_y.

Hydraulic conductivity fields and stream tubes are shown in Fig. 5.20 for horizontal slices of aquifers at a depth of 5.0 to 5.5 m. In Fig. 5.20a, λ_x = 3 m and λ_y = 1 m, and in Fig. 5.20b λ_x = 9 m and λ_y = 3 m. Zones of similar hydraulic conductivity are longer and exist more often on both sides of the PRB when λ_x is larger. Also for larger λ_x, particle trajectories in the PRB are straighter. At lower λ_x, particles turn after they enter the PRB to avoid exiting the PRB into a less permeable unit (e.g., at a lateral distance of 20 to 23 m).

There is no clear trend between λ_x and the spread of the concentrations (Fig. 5-19). Slight changes in the spread are attributed to differences in the position of permeable zones between random fields having different λ_x. Unlike varying μ_{lnK} and σ_{lnK}, changing λ_x or λ_y alters the relative locations of the more and less permeable units. Thus, slight differences in output are expected. The difference between distributions with changing λ_y is also small (Fig. 5.19). The slight shift in distributions for simulations with λ_y = 1 m to λ_y = 5 m is less than the shift caused by doubling λ_x. Thus, the lateral breadth of units with higher hydraulic conductivity is less important than their length.

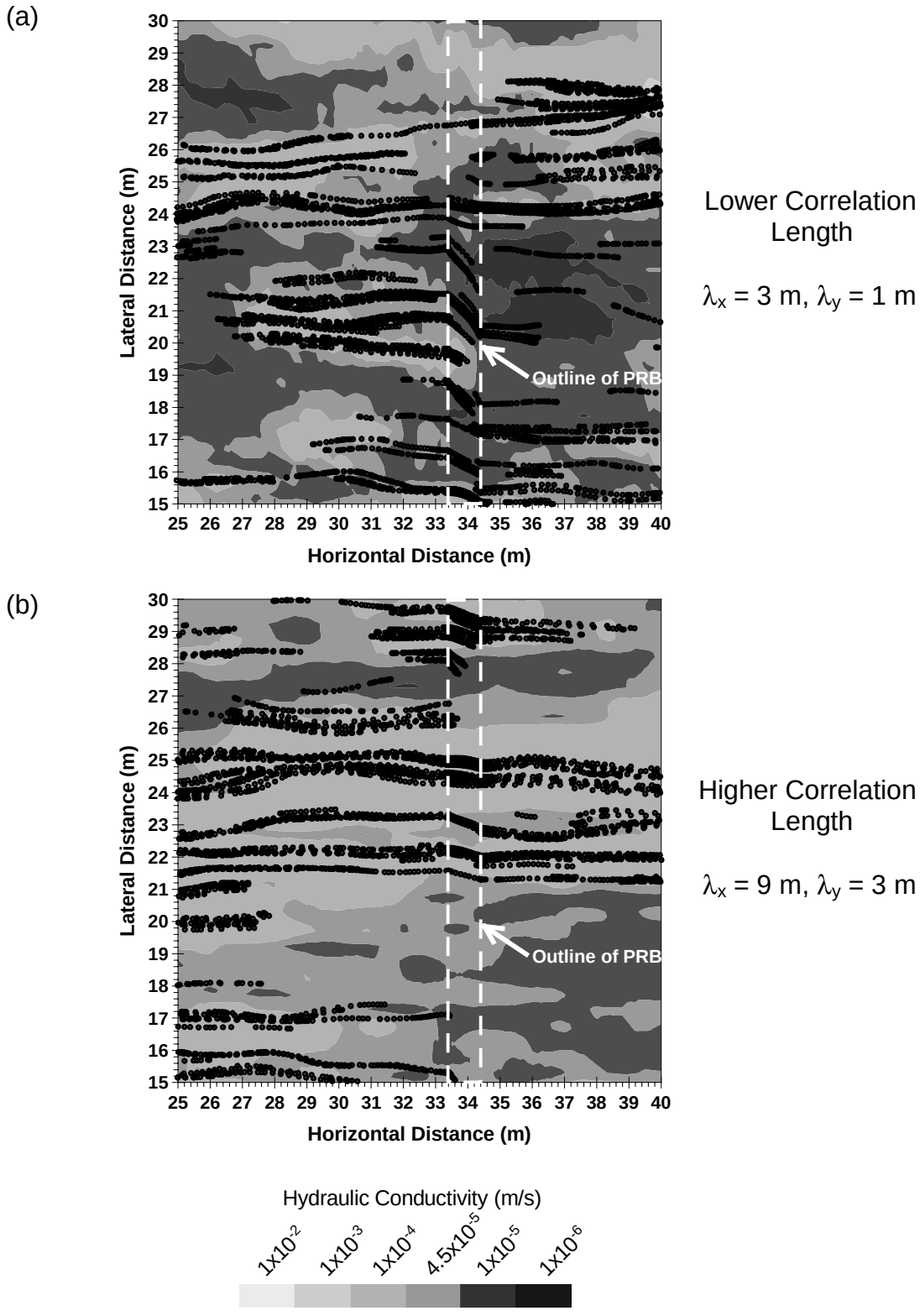

Fig. 5.20 Particle Trajectories Superimposed onto Images of Random Fields with λ_x = 3 m and λ_y = 1 m (a) and λ_x = 9 m and λ_y = 3 m (b).

5.6 A SUMMARY OF THE IMPACT OF PRB AND AQUIFER HETEROGENEITY

This section describes the impact of heterogeneity of the HFPRB and aquifer on influent and effluent concentrations. The effect of changing k_r and K_p, and μ_{lnK}, σ_{lnK}, λ_x, and λ_x on influent and effluent concentration are summarized as follows:

- variability in k_r and K_p, and uniform shifts in K_p (provided $K_p > e^{\mu_{lnK}}$) do not significantly change the distribution of influent or effluent concentration
- increases or decreases in k_r cause a uniform shift in effluent concentration that is consistent with the shift predicted using a first order model
- changing μ_{lnK} does not affect the distribution of influent concentration
- increasing μ_{lnK} shifts the distribution of effluent concentration toward higher concentrations and decreases its spread
- increasing σ_{lnK} shifts distributions of influent concentration toward lower concentrations and increases their spread
- increasing σ_{lnK} shifts distributions of effluent concentration toward higher concentrations and increases their spread
- increasing λ_x or λ_y does not significantly influence the distribution of influent concentration and only causes a slight increase in distributions of effluent concentration

In conclusion, σ_{lnK} was the only parameter that significantly affected distributions of influent concentration, causing lower influent concentrations at higher σ_{lnK}. In general, PRBs located in more heterogeneous aquifers (i.e., aquifers with larger μ_{lnK}, σ_{lnK}, or λ_x) have higher effluent concentrations. Of the parameters that were investigated, μ_{lnK} and σ_{lnK} had the greatest effect on distributions of effluent concentration, λ_x had a small impact, and λ_y and uncertainty in K_p and k_r had little impact on effluent concentration.

SECTION 6

RESULTS AND CONCLUSIONS FOR GATE PRBS WITH A FUNNEL

6.1 GENERAL DESCRIPTION

A funnel and gate PRB (FGPRB) is an in situ structure consisting of a PRB (gate) through which contaminated groundwater is channeled by funnels located on either side of the gate (Starr and Cherry 1994). Typically, funnels have a lower hydraulic conductivity than the surrounding aquifer, such as a soil-bentonite slurry wall; however, highly conductive funnels have also been suggested (Edwards et al. 1997). Contaminants are stripped or transformed in the gate resulting in less contaminated groundwater down-gradient of the FGPRB.

The advantage of a FGPRB is that the breadth of the funnel captures the contaminant plume, whereas the width and thickness of the gate is smaller and designed to only provide adequate residence time for rate limited reactions to occur. This advantage yields more economical systems compared to HFPRBs because the FGPRB is smaller and thus requires less reactive material. Furthermore, by focusing flow through a gate, nearly all of the reactive medium is exposed to contaminants. FGPRBs are particularly well suited for sites with existing containment systems because gates can be inserted into an existing slurry wall to create a FGPRB.

A disadvantage of FGPRBs is that groundwater flows across the smallest dimension of the PRB, a problem that FGPRBs share with HFPRBs. As a result, the performance of FGPRBs can be strongly influenced by the composition of the

aquifer directly up-gradient and down-gradient of the PRB. Also, there are few guidelines for the design and monitoring of FGPRBs. Although nearly half of the current, full-scale PRB systems are FGPRBs (Jarre and Kociolek 1999), most of the analysis for FGPRBs assumes that the aquifer, funnels, and gate are homogeneous (Freeze and Cherry 1994, Edwards et al. 1997) or simple assumptions are made about aquifer heterogeneity (Gavaskar 1998). Based on the results of Section 5, aquifer heterogeneity should affect the performance of FGPRBs. The purpose of this section is to evaluate the impact of PRB and aquifer heterogeneity on the performance of FGPRBs.

6.2 CONCEPTUAL MODEL OF A FGPRB

6.2.1 Establishing the Model Domain Size

The initial conceptual model for a FGPRB is shown in Fig. 4.10b. The system consists of two 20 m wide, 1 m thick, fully penetrating funneling walls (K = $1x10^{-7}$ cm/s) on either side of a 5 m wide, 1 m thick, fully penetrating gate. For all simulations, the funnel is assumed to be homogeneous. The FGPRB system is 45 m wide, which is 20 m wider than the HFPRB described in Section5.2.5. A wider system is necessary to capture contaminants emanating from the source zone (i.e., C_o = 1000 ppb) that is 15 m wide and 5 m deep, located 20 m up-gradient from the PRB.

The appropriate size for the domain was determined using a procedure similar to the method used for the HFPRB. A FGPRB was located in the center of a large domain (290 by 150 elements, 91.8 m by 75 m) and steady-state heads

were determined. One thousand two hundred particles were then released from the source zone and tracked through the FGPRB. This procedure was repeated for domains that were shrunk symmetrically around the FGPRB. The length and width of the domain were reduced until one of the following conditions were met: (1) the transit time of particles passing across the FGPRB changed; (2) the velocity of particles entering the FGPRB changed; (3) the velocity of particles exiting the FGPRB changed; or (4) the boundaries were two correlation scales from the source zone or edges of the FGPRB. The fourth condition is based on the recommendation by Rubin and Dagan (1988, 1989) described in Section 5.5.2.3.

Particle transit times across the FGPRB, particle velocities entering the FGPRB, and particle velocities exiting the FGPRB for domains of different length and width are shown in Fig. 6.1 and Fig. 6.2, respectively. Transit times and seepage velocities do not change significantly as the domain shrinks. Thus, the up-gradient constant head boundary was set 20 m from the source (i.e., double the maximum λ_x), and the no flux boundaries were set 10 m from the edges of the funnel (i.e., double the maximum λ_y). Mesh spacing for the aquifer was identical to the mesh spacing used for simulations of the HFPRB to allow for direct comparison of results for the FGPRB and HFPRB.

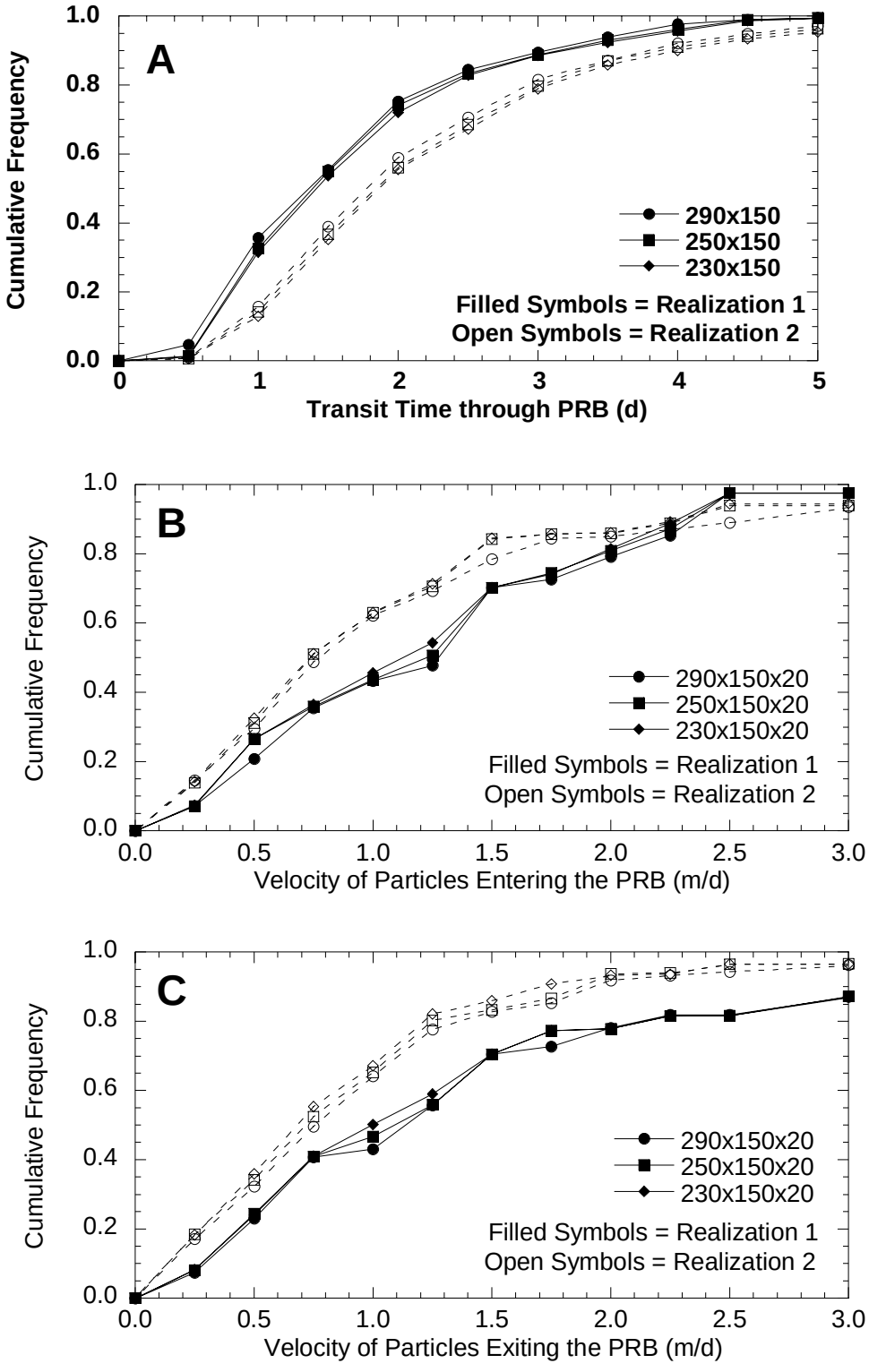

Fig. 6.1 (a) Particle Transit Time through the FGPRB, (b) Velocity Entering the FGPRB, and (c) Velocity Exiting the FGPRB for Increasingly Shorter Model Domains (Two Realizations per Domain).

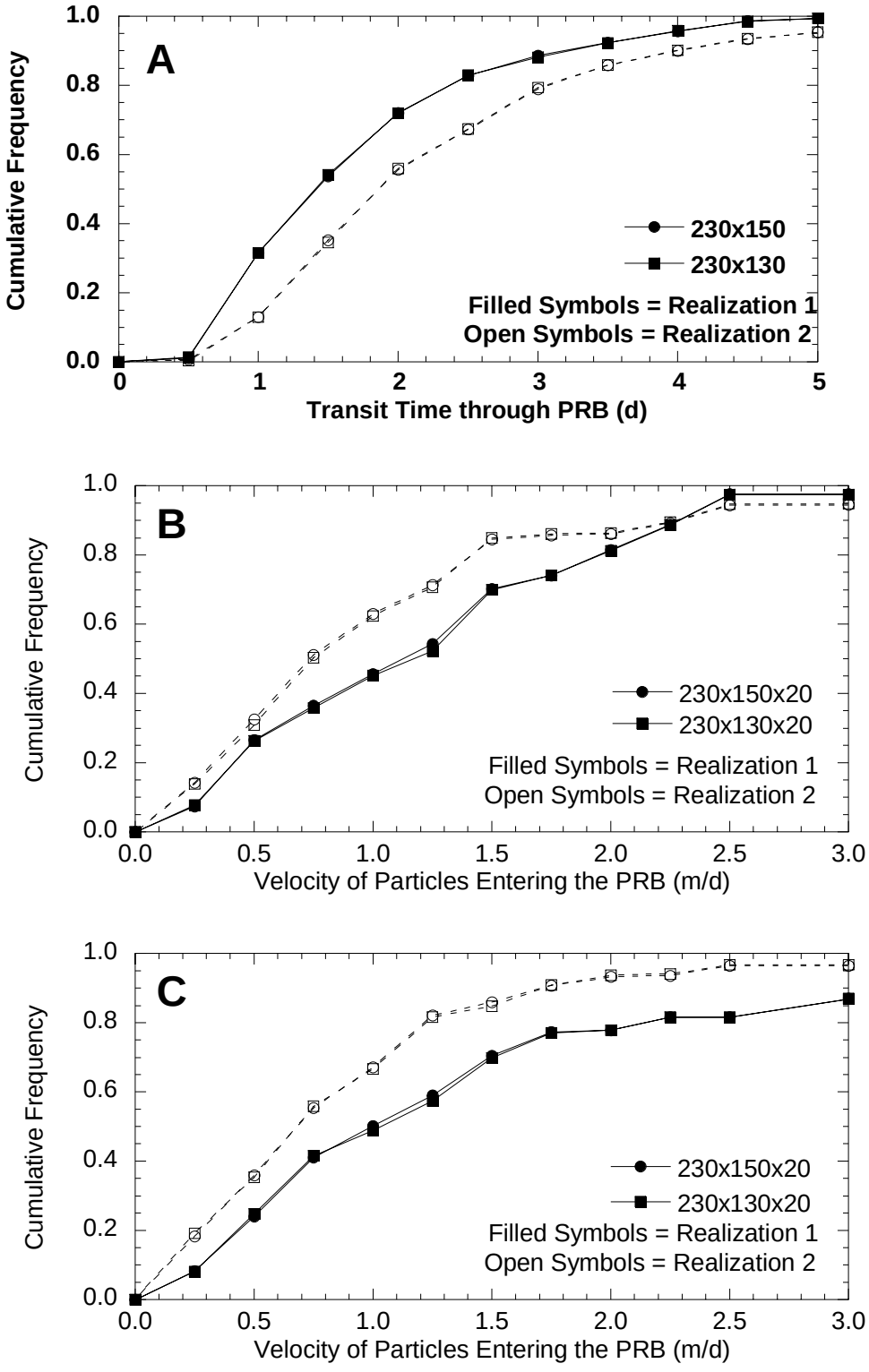

Fig. 6.2 (a) Particle Transit Time through the FGPRB, (b) Velocity Entering the FGPRB, and (c) Velocity Exiting the FGPRB for Narrower Model Domains (Two Realizations per Domain).

6.2.2 Final Conceptual Model of a FGPRB

The final conceptual model of the aquifer and FGPRB is shown in Fig. 6.3. The domain is 67.8 m long (same as the HFPRB), 65 m wide, and 10 m thick. The domain contains 598,000 finite difference cells with a minimum Δx of 0.05 m in the center of the PRB and a maximum Δx of 0.4 m near the boundaries. Size of the finite difference cells increase or decrease with a maximum expansion ratio of 1.2. Lateral (Δy) and vertical cell (Δz) discretization is uniform at 0.5 m. In the center of the domain is a 5 m wide, 1 m thick, fully penetrating PRB (gate). The gate of the FGPRB is composed of 4000 finite difference cells. On either side of the gate are fully penetrating, 20 m wide by 1 m thick homogeneous funneling walls that have a hydraulic conductivity of $1x10^{-7}$ cm/s. A 1000 ppb contaminant source that is 15 m wide by 5 m deep is located 20 m up-gradient of the FGPRB along the lateral and vertical centerline of the aquifer. Flow occurs due to a gradient of 0.01 imposed by constant head boundaries at X = 0 m and X = 67.4 m. The sides (Y = 0 m and Y = 65 m) and bottom of the domain (Z = 0 m) are no flux boundary conditions whereas the top of the aquifer (Z = 10 m) is a variable head boundary (i.e., unconfined aquifer).

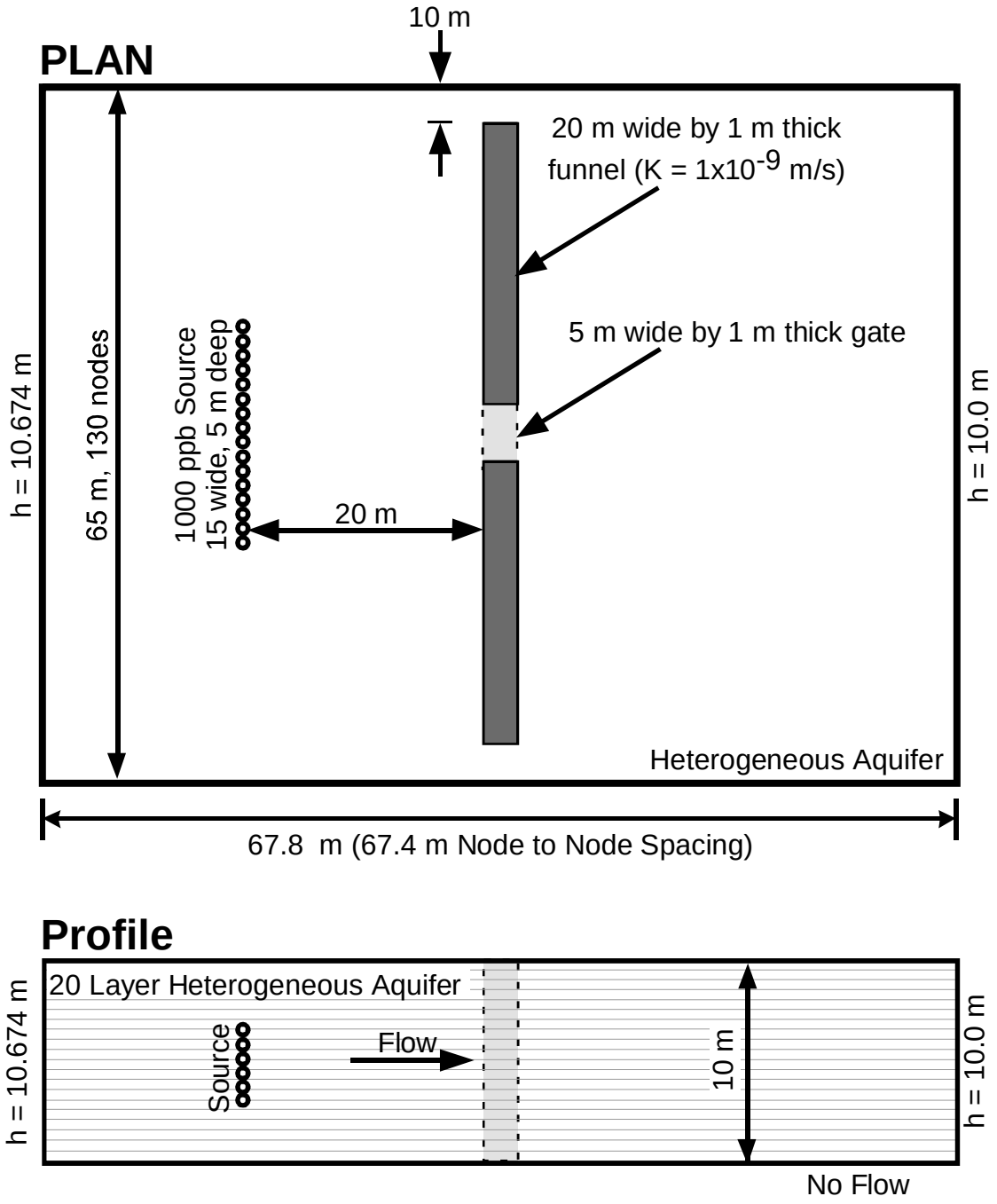

Fig. 6.3 Conceptual Model of a Funnel and Permeable Reactive Gate (FGPRB) Located in the Center of a Heterogeneous Aquifer.

6.3 CONTAMINANT TRANSPORT TOWARDS AND THROUGH A FGPRB

The objective of installing a funnel on either side of a PRB gate is to channel groundwater flow and contaminants through the gate. For most systems, the funnels have lower hydraulic conductivity than the aquifer and are constructed perpendicular to groundwater flow (Starr and Cherry 1994). Groundwater flow is impeded by the funnel and flows around the funnel, either though the gate (in essence a hole in the cut-off wall) or around the ends of the funnel. When developing the conceptual model for the FGPRB, a system equal in width to the HFPRB (25 m) was initially examined. However, this size FGPRB did not capture particles from the 15 m wide source; thus, larger FGPRBs were tried. A 45 m wide system was selected because it captured the contaminant plume. Based on this outcome, designers of FGPRBs should expect FGPRBs to be wider than HFPRBs for identical aquifers and plume size. The additional excavation, labor, and material costs for a larger FGPRB, along with the possibility of the funnels infringing on nearby structures or property lines, may outweigh the benefits of using a smaller amount of reactive media.

Simulated groundwater flow and contaminant transport up-gradient of the FGPRB occur as expected (Starr and Cherry 1994). Particles initially located in the center of the contaminant source move straight towards the gate, pass through the gate, and continue on straight trajectories down-gradient of the PRB. Particles initially located at the edges of the source zone curve toward the gate, pass through the edges of the gate, and then curve outward from the gate down-gradient of the PRB. The trajectory of 150 particles across a homogeneous aquifer, an

aquifer with σ_{lnK} = 1.0, and an aquifer with σ_{lnK} = 4.0 that each contain a FGPRB are shown in Fig. 6.4. All aquifers have a μ_{lnK} = -10 ($4.54x10^{-5}$ m/s), and the heterogeneous aquifers have λ_x = 3 m and λ_y = 1m. The funnel and gate in each aquifer are homogeneous with hydraulic conductivities of $1x10^{-7}$ cm/s and 0.25 cm/s respectively.

Particle paths form an hourglass shape in the homogeneous aquifer and the aquifer with σ_{lnK} = 1.0. Particle paths are densest in the gate and have the greatest spread down gradient of the FGPRB. In Fig. 6.4b, the outline of the particle plume for the homogeneous aquifer (Fig. 6.4a) is shown. The plume in an aquifer with σ_{lnK} = 1.0 is narrower and curves less sharply as it approaches the FGPRB because the heterogeneous aquifer has hydraulic conductivities that are correlated in the longitudinal direction. The correlation structure results in higher hydraulic conductivity zones that are aligned perpendicular to the FGPRB. These zones promote longitudinal transport which narrows the plume.

Particle paths for an aquifer with σ_{lnK} = 4.0 are shown in Fig. 6.4c along with the boundaries for particle plumes in the homogeneous aquifer (Fig. 6.4a) and the aquifer with σ_{lnK} = 1.0 (Fig. 6.4b). Particle paths in Fig. 6.4c are more tortuous than those in more homogeneous aquifers (Fig. 6.4a or 6.4b). At σ_{lnK} = 4.0, particles cluster along the longitudinal axis of the aquifer (and FGPRB). This dense network of pathlines is approximately the same width as the

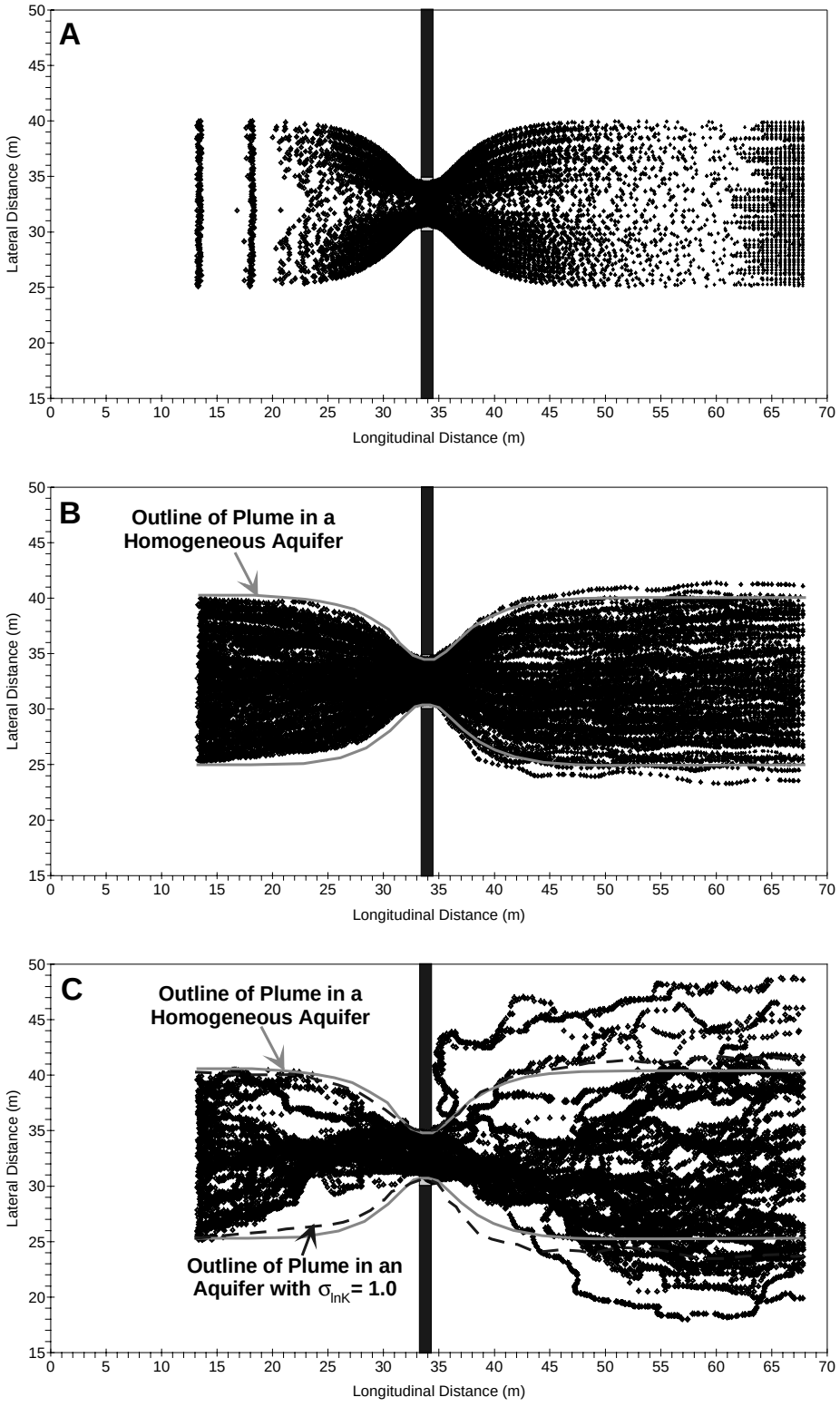

Fig. 6.4 Trajectory of 150 Particles in a Homogeneous Aquifer (a), an Aquifer with σ_{lnK} = 1.0 (b), and an Aquifer with σ_{lnK} = 4.0 (c).

gate and forms about 10 m up-gradient of the PRB. After passing through the gate, particle paths separate, but not symmetrically; rather, particles follow more erratic paths and form a plume that is approximately 75% wider than the plume in the aquifer with σ_{lnK} = 1.0. Since plumes down-gradient of a FGPRB are larger in more heterogeneous aquifers, mass is spread across a larger volume and concentrations decrease.

Flow of groundwater and particles tends to occur through zones of higher hydraulic conductivity, as was shown for the HFPRB in Section 5.3. Zones of higher hydraulic conductivity are preferred pathways for groundwater flow and contaminant transport via advection because they cause lower head loss. A map of hydraulic conductivity and particle paths at a depth of 7.0 to 7.5 m in an aquifer with μ_{lnK} = -10 (4.54×10^{-5} m/s), σ_{lnK} = 1.0, λ_x = 3 m and λ_y = 1 m is shown in Fig. 6.5. Similar to Fig. 5.8, hydraulic conductivities less than 4.54×10^{-5} m/s are darker shades and hydraulic conductivities greater than 4.54×10^{-5} m/s are lighter shades. Also, particle paths are shown in Fig. 6.5 by dots, with larger dots indicating deeper paths.

Particle paths coincide with zones of higher hydraulic conductivity (i.e., lighter regions). They appear to end or start near regions of lower hydraulic conductivity. However, they do not end or start at these locations, but by pass regions of lower hydraulic conductivity by moving vertically to zones of higher hydraulic conductivity located above or below the plane that is shown. The impact that location and connectivity of zones with higher hydraulic conductivity has on transport by advection in heterogeneous aquifers is apparent in Fig. 6.5.

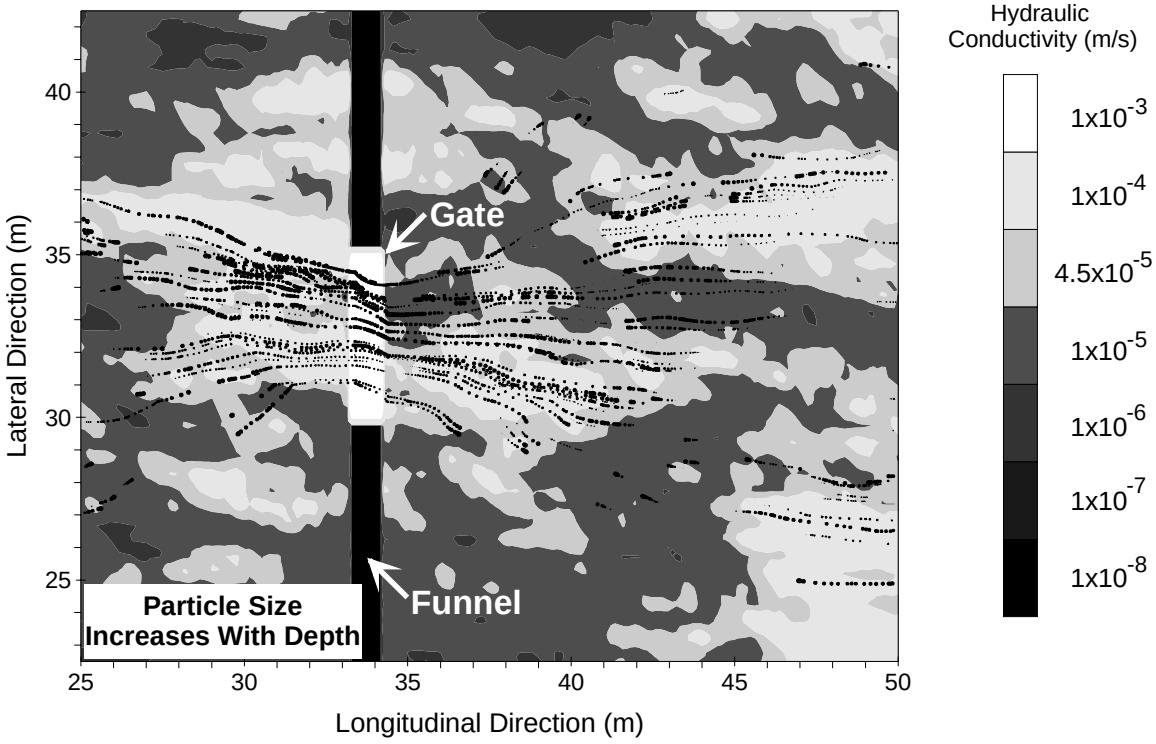

Fig. 6.5 Particle Trajectory and Hydraulic Conductivity at an Elevation of 7.0 to 7.5 m in an Aquifer with μ_{lnK} = -10, σ_{lnK} = 1.0, λ_x = 3 m, λ_y = 1 m.

Concentrations entering a FGPRB in a homogeneous aquifer, an aquifer with σ_{lnK} = 1.0, and an aquifer with σ_{lnK} = 4.0 are shown in Fig. 6.6 (Fig. 6.4 and Fig. 6.6 show the same realizations). Concentrations for the homogeneous aquifer (Fig. 6.6a) are fairly uniform with concentrations between 600 ppb and 800 ppb. Minor differences in influent concentrations are caused by mixing as groundwater is funneled into the gate.

The distribution of concentration entering the gate in heterogeneous aquifers is shown in Figs. 6.6b and 6.6c. When heterogeneity exists, concentrations entering the gate are no longer uniform; rather, pockets of high and low concentration exist. For σ_{lnK} = 1.0, these zones are approximately 1 m^2 in area with most concentrations entering the PRB are between 100 ppb and 300 ppb (i.e., similar to the homogeneous case). For σ_{lnK} = 4.0, the pockets of high or low concentration have smaller areas and lower concentrations.

Another difference between Figs. 6.6a, 6.6b, and 6.6c is that the contaminant plume entering the gate is thicker (i.e., extends over a thicker depth) for larger σ_{lnK}. For example, the plume in a homogeneous aquifer (Fig. 6.6a) is 5 m thick (equal to the thickness of the source). When σ_{lnK} = 1.0 (Fig. 6.6b), the plume is 7.5 m thick and when σ_{lnK} = 4.0 (Fig. 6.6c), the plume entering the gate is 10 m thick. Thus, at higher σ_{lnK}, plumes are larger and there is greater mixing in the vertical direction. The additional dispersion in the aquifer at higher σ_{lnK}, which is apparent by the thicker plumes, causes lower average influent concentrations.

a) Homogeneous Aquifer

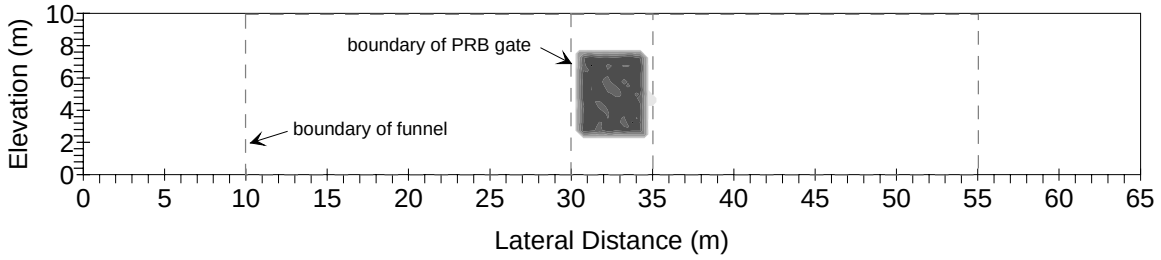

b) Aquifer with σ_{lnK} = 1.0

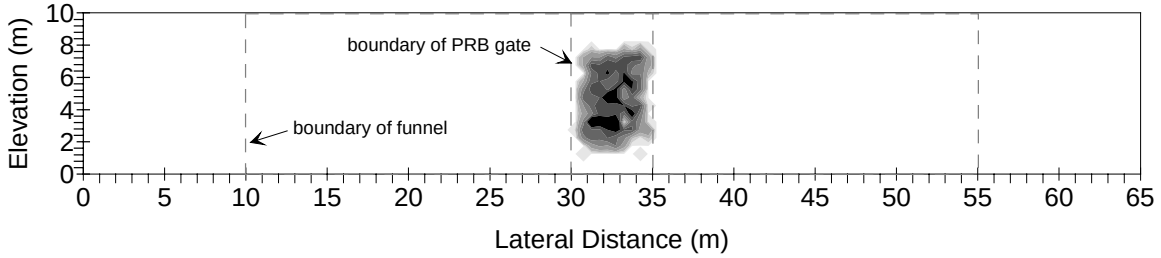

c) Aquifer with σ_{lnK} = 4.0

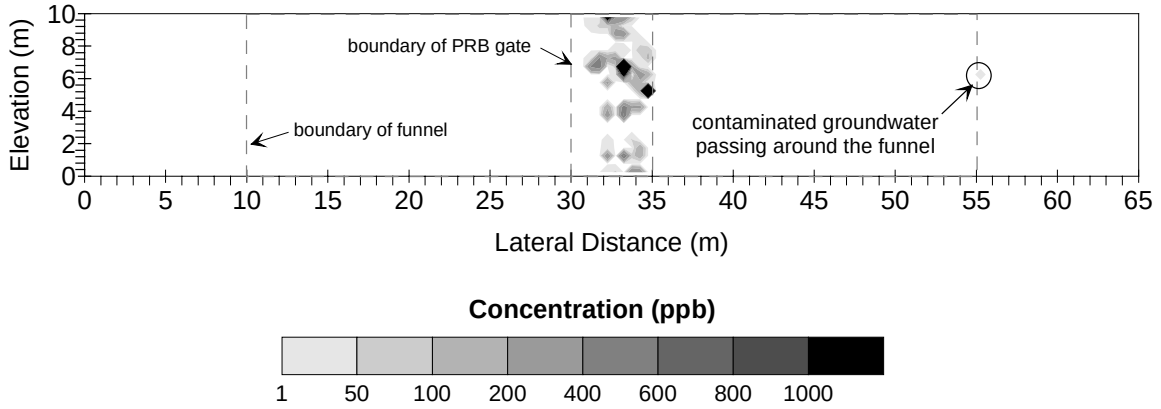

Fig. 6.6 Distributions of Influent Concentration in a Homogeneous Aquifer (a), an Aquifer with σ_{lnK} = 1.0 (b), and an Aquifer with σ_{lnK} = 4.0 (c) (μ_{lnK} = -10, λ_x = 3 m, λ_y = 1 m).

Also shown in Fig 6.6c is a failure of the system at a lateral distance of 55 m. A single stream tube passing around the funnel causes this small pocket of contamination. In the very heterogeneous aquifer, a particle takes an unexpected path around the funnel because this path has less head loss than paths across the front of the funnel and through the gate. This example demonstrates the possibility of FGPRBs failing in very heterogeneous aquifers.

Effluent concentrations are shown in Fig 6.7 for the same realizations that are shown in Fig. 6.6. These distributions are similar in pattern but reduced in magnitude to the influent distributions. In a homogeneous aquifer (Fig. 6.7a), concentrations exiting the gate are uniform except for vertical strips of slightly higher concentration at the edges of the gate, caused by faster flow rates though the edges of the gate as water is pinched between the funnels. The higher flow rates cause contaminants passing through the edges of the gate to have shorter residence times and consequently slightly higher effluent concentrations. In an aquifer with σ_{lnK} = 1.0 (Fig. 6.7b), pockets of high and low concentration exist, particularly along the edges of the gate, but the concentrations are similar to Fig. 6.7a. Also, the effluent plume is thicker for σ_{lnK} = 1.0, approximately 8 m compared to 5 m for the homogeneous case. For σ_{lnK} = 4.0 (Fig. 6.7c), concentrations exiting the gate are distributed into smaller pockets that have a wider range of concentrations. Also, the contaminant plume extends over the entire thickness of the aquifer when σ_{lnK} = 4.0.

a) Homogeneous Aquifer

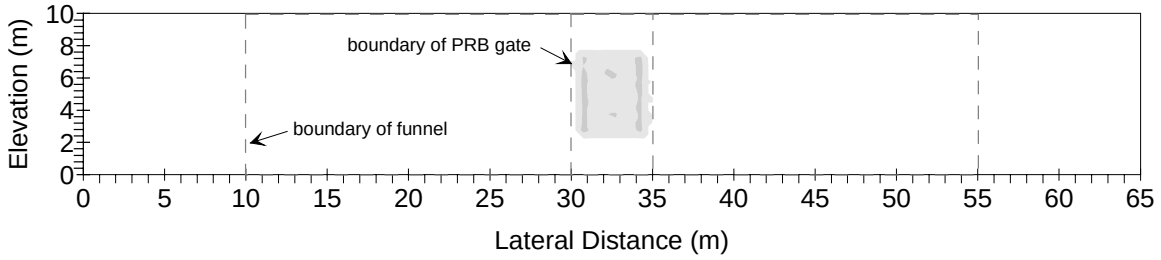

b) Aquifer with σ_{lnK} = 1.0

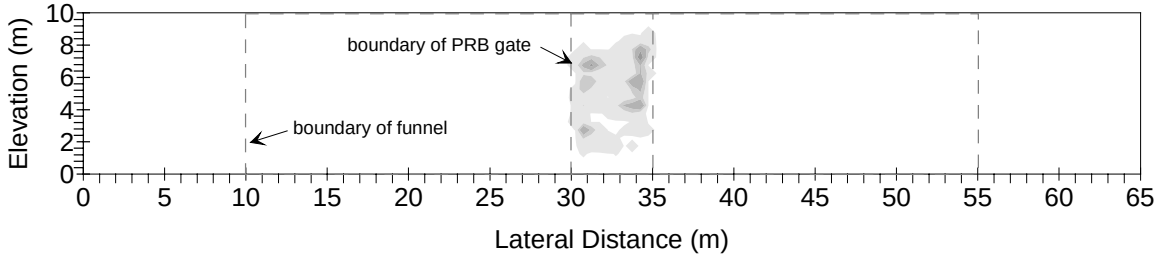

c) Aquifer with σ_{lnK} = 4.0

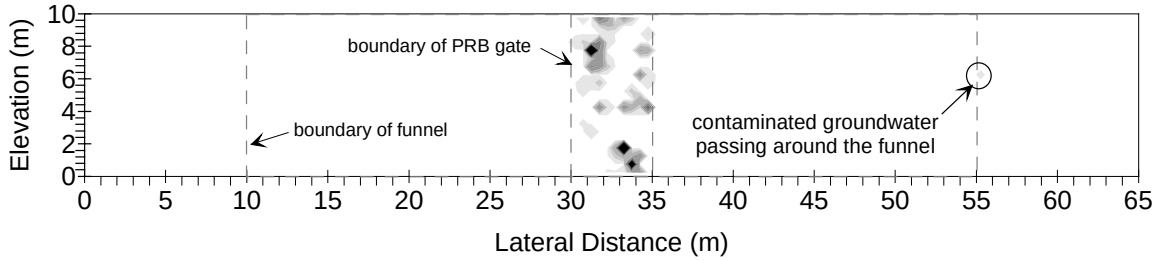

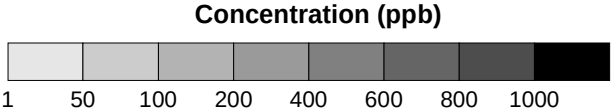

Fig. 6.7 Distributions of Effluent Concentration in a Homogeneous Aquifer (a), an Aquifer with σ_{lnK} = 1.0 (b), and an Aquifer with σ_{lnK} = 4.0 (c) (μ_{lnK} = -10, λ_x = 3 m, λ_y = 1 m).

In summary, FGPRBs appear to operate properly in heterogeneous aquifers. Funnels are effective at channeling most of the contaminated groundwater through the gate, although the necessary width of the funnel will likely be greater than the width of a comparable HFPRB. In homogeneous aquifers, plumes are shaped like an hourglass with their narrowest cross-section at the gate. In heterogeneous aquifers, the plume up-gradient of the FGPRB is narrower and thicker, and funnels toward the gate more gradually. Down-gradient of a FGPRB, the plume becomes wider with increasing σ_{lnK}. Concentrations entering and exiting the gate are uniform in homogeneous aquifers except for strips of slightly higher effluent concentration at the edges of the gate where groundwater velocities are higher. In heterogeneous aquifers, flow and transport by advection occur through zones of higher hydraulic conductivity, causing plumes to be thicker, and influent and effluent concentrations to vary over a wider range as σ_{lnK} increases.

6.4 EFFECT OF PRB HETEROGENEITY

The effect of heterogeneity in the hydraulic conductivity (K_P) and in the reaction rate constant (k_r) of the PRB was investigated by simulating ten funnel and gate systems in aquifers with μ_{lnK} = -10, σ_{lnK} = 1.0, λ_x = 3 m, and λ_y = 1 m. Input parameters for these simulations are given in Table 6.1.

Table 6-1 Input Parameters for Simulating FGPRB Heterogeneity.

K_p (m/s) (Normally Distributed)		k_r (d^{-1}) (Normally Distributed)		$\rho(K_p, k_r)$
Mean	Std. Dev.	Mean	Std. Dev.	
$2.5x10^{-3}$*	0	1.0	0	-
$2.5x10^{-4}$	0	1.0	0	-
$2.5x10^{-3}$	0	0.9	0	-
$2.5x10^{-3}$	0	1.1	0	-
$2.5x10^{-3}$	$1.0x10^{-4}$	1.0	0	-
$2.5x10^{-3}$	0	1.0	0.05	-
$2.5x10^{-3}$	$1.0x10^{-4}$	1.0	0.05	0
$2.5x10^{-3}$	$1.0x10^{-4}$	1.0	0.22	0
$2.5x10^{-3}$	$1.0x10^{-4}$	1.0	0.05	-1
$2.5x10^{-3}$	$1.0x10^{-4}$	1.0	0.05	1

* base case simulation

Distributions of influent and effluent concentration for simulations of a funnel and gate system with varying degrees of heterogeneity are shown in Fig. 6.8. Distributions have a similar shape and trends as those obtained for the HFPRB (i.e., heterogeneity of the PRB has no significant impact on influent concentrations and little influence on effluent concentrations, regardless of $\rho(K_p, k_r)$). Distributions for a homogeneous FGPRB overlap distributions for a FGPRB with variable K_p and k_r. Even for a standard deviation of k_r = 0.22, concentrations still overlap. Distributions also overlap when the hydraulic conductivity for the gate is decreased by an order of magnitude. Thus, as with the HFPRB, provided K_p is equal or greater than the geometric mean hydraulic conductivity of the aquifer, variability in K_p and k_r have little effect on influent and effluent concentrations for a FGPRB.

a) Influent Concentration

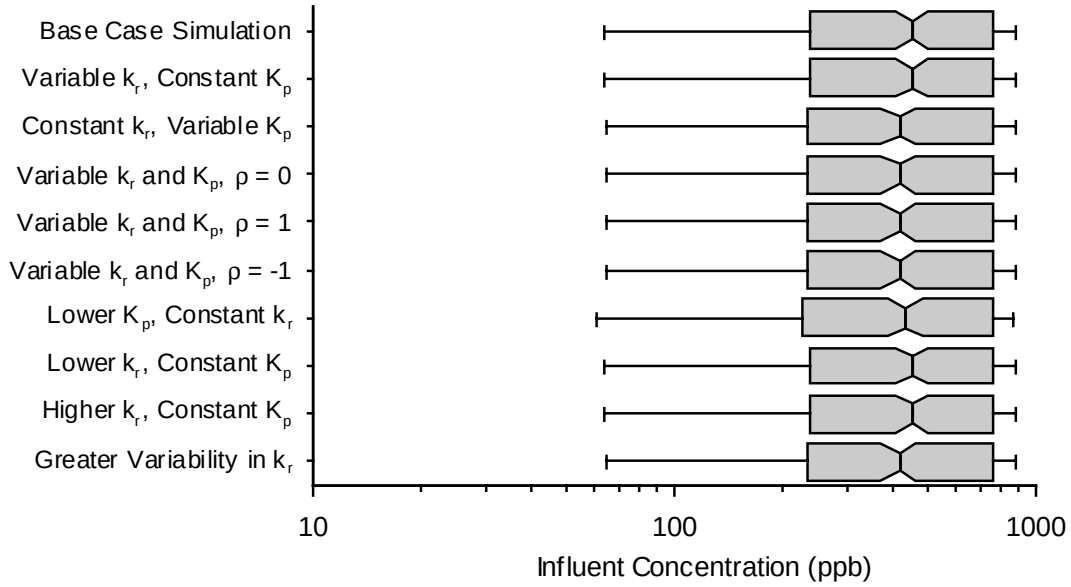

b) Effluent Concentration

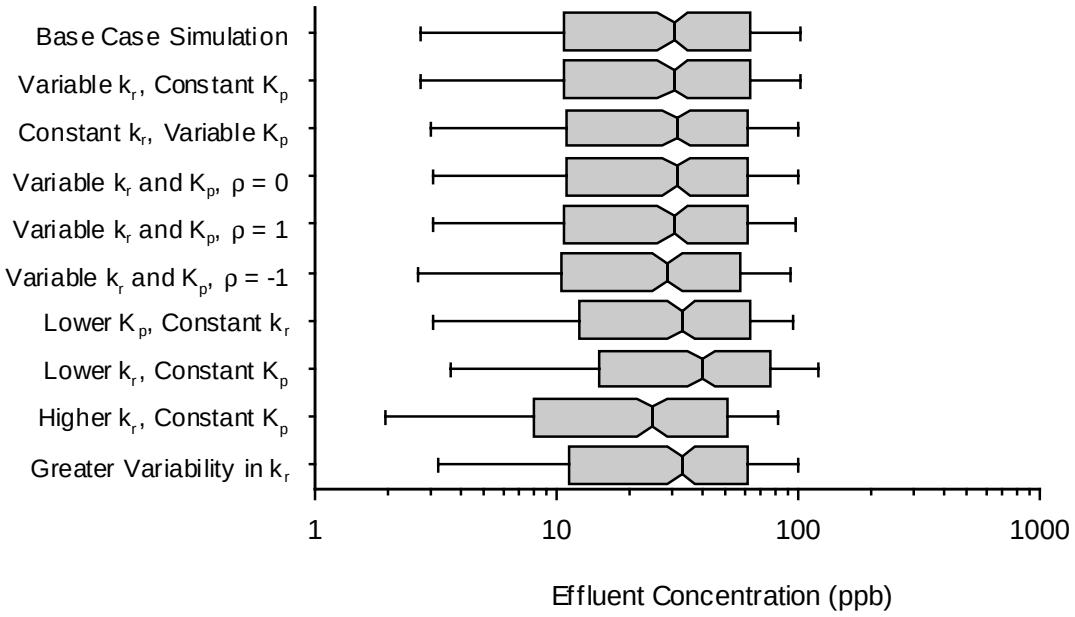

Fig. 6.8 Distributions of Influent (a) and Effluent Concentration (b) for Heterogeneous FGPRBs (5 m wide gate between 20 m homogeneous funnels in an aquifer with μ_{lnK} = -10, σ_{lnK} = 1.0, λ_x = 3 m, λ_y = 1 m).

Two distributions of effluent concentration in Fig. 6.8b are shifted relative to the other distributions. These distributions are for k_r = 1.1 d^{-1} and 0.9 d^{-1} (i.e., k_r 10% higher and lower than other simulations). Changing k_r to 1.1 d^{-1} uniformly decreases effluent concentrations, while changing k_r to 0.9 d^{-1} uniformly increases effluent concentrations. Neither changes the influent concentration. As with the HFPRB, the shift in effluent concentrations is equal to the shift predicted by changing k_r in a first-order loss equation (e.g., Eq. 2.3). For example, the base case simulation has a k_r of 1.0 d^{-1}, a median effluent concentration of 30 ppb, and a median influent concentration of 430 ppb, resulting in an average residence time of 2.66 days. For the same residence time and influent concentration, the effluent concentration predicted for k_r = 0.9 d^{-1} is 39.2 ppb and for k_r = 1.1 d^{-1} is 23.1 ppb, which are equal the median effluent concentrations for FGPRBs with k_r of 0.9 d^{-1} and 1.1 d^{-1}, respectively (Fig. 6.8). Thus, temporal changes in PRB performance can be predicted if long-term changes in k_r due to aging or precipitation are known.

6.5 EFFECT OF AQUIFER HETEROGENEITY

The impact that variability in hydraulic conductivity of the aquifer has on influent and effluent concentrations from a FGPRB is evaluated in this section. Three parameters are discussed in this section, μ_{lnK}, σ_{lnK}, and correlation scale.

6.5.1 Effect of μ_{lnK}

The effect of μ_{lnK} on influent and effluent concentrations from a FGPRB was investigated by simulating a homogeneous FGPRB (k_r = 1.0 d^{-1} and K_p = 2.5x10^{-3}

m/s) in aquifers with σ_{lnK} = 1.0, λ_x = 3 m, λ_y = 1 m, and μ_{lnK} = -9 (1.23×10^{-4} m/s), -10 (4.54×10^{-5} m/s), -11 (1.67×10^{-5} m/s), or -12 (6.14×10^{-6} m/s). Distributions of influent and effluent concentration for these simulations are shown in Fig. 6.9.

Influent concentrations range from 1 ppb to 1000 ppb (i.e., the source concentration) and are unaffected by varying μ_{lnK} of the aquifer because the aquifers are identical in all respects except for the magnitude of hydraulic conductivity. Thus, groundwater and contaminants may take longer to reach the gate in aquifers with lower μ_{lnK}, but since reactions are not simulated in the aquifer (k_r = 0 d^{-1} in the aquifer), the distribution of influent concentrations will be identical. If reactions such as biological digestion or radioactive decay occur in the aquifer, influent concentrations are expected to be lower for lower μ_{lnK}.

Distributions of effluent concentration (Fig. 6.9b) shift toward lower concentrations and broaden as μ_{lnK} decreases. Effluent concentrations decrease because groundwater moves through the aquifer more slowly at lower μ_{lnK}. Consequently, the residence time of groundwater in the gate is longer and more reduction occurs. Distributions of effluent concentration broaden at lower μ_{lnK} because zones of higher hydraulic conductivity exist even in aquifers with a lower geometric mean hydraulic conductivity. Figure 5.14 shows how the probability mass for the upper tail of PDFs for hydraulic conductivity change little with decreasing μ_{lnK}, indicating that zones of higher hydraulic conductivity exist at all μ_{lnK}. These zones are the primary means for advective transport of contaminants

a) Influent Concentration

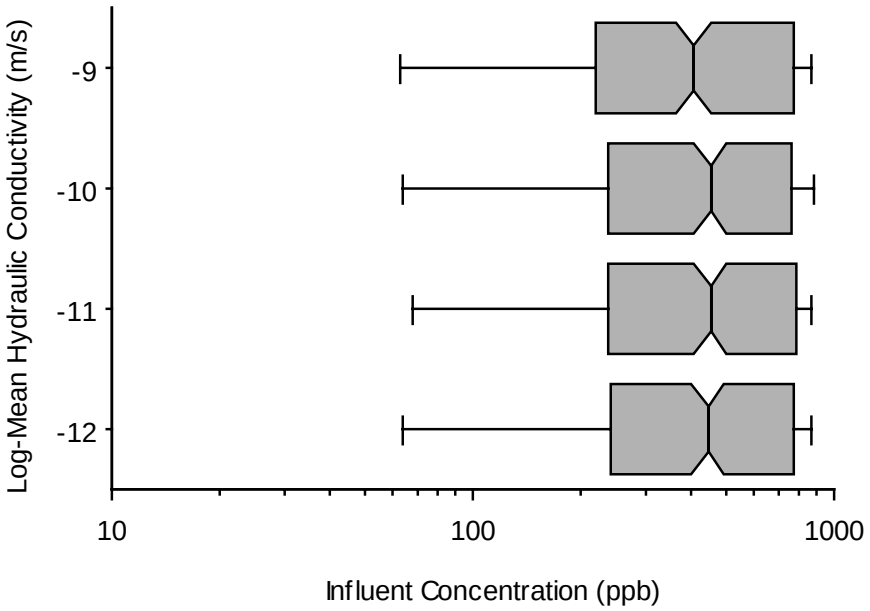

b) Effluent Concentration

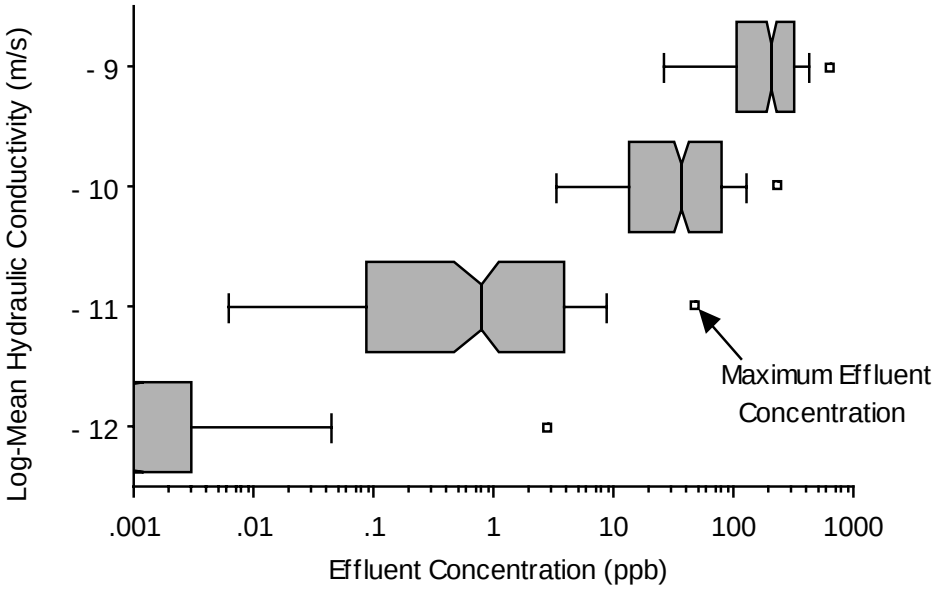

Fig. 6.9 Distributions of Influent (a) and Effluent Concentration (b) for a Homogeneous FGPRB Located in Aquifers with Different μ_{lnK}.

in the aquifer and through the PRB. Higher flow rates occur through these zones and carry a significant fraction of mass to the PRB. The consequence of mass being transported into and through the PRB by units with a higher hydraulic conductivity causes a fraction of the effluent concentrations to be higher. These higher concentrations, when combined with lower median effluent concentration, broaden distributions of effluent concentration at lower μ_{lnK}.

6.5.2 Effect of σ_{lnK}

The effect of varying σ_{lnK} on influent and effluent concentrations from FGPRBs was investigated by simulating a homogeneous FGPRB (k_r = 1.0 d^{-1}, K_p = 2.5x10^{-3} m/s) in aquifers with μ_{lnK} = -10, λ_x = 3 m, λ_y = 1 m, and σ_{lnK} = 0, 0.25, 1.0, 2.25, and 4.0. Distributions of influent and effluent concentration for these simulations are shown in Fig. 6.10.

Influent concentrations decrease and become more broadly distributed as σ_{lnK} increases. Influent concentrations for a homogeneous aquifer (σ_{lnK} =0) are not uniform, but grouped into two ranges. Approximately 60% of the concentrations are between 200 ppb and 500 ppb, and about 40% are between 700 ppb and 1000 ppb (Fig. 6.10a). Approximately one-third of influent have higher concentrations because contaminants directly up-gradient of the gate travel in straight flow-lines toward the gate, mixing little with surrounding groundwater as they travel (Fig. 6.4a). This fraction of groundwater, is approximately equal to the portion of the source zone that is directly up-gradient of the gate (i.e., the gate is 1/3 the width of the source). The limited amount of mixing that occurs as this groundwater

approaches the gate causes influent concentrations to be close to the source concentration. Groundwater initially located in the outer 2/3 of the source is channeled into the gate by the funnel, causing flow-lines to curve as they approach the FGPRB (Fig. 6.4a). More mixing occurs along these flow-lines, and the dilution causes about 2/3 of the influent concentrations to fall into a lower range (i.e., 200 to 500 ppb).

Distributions of influent concentrations for aquifers with σ_{lnK} = 0.25 are also divided into two ranges with approximately 60% between 30 and 600 ppb, and 40% between 600 and 1000 ppb. These ranges are broader than for the homogeneous aquifer and the division between the ranges is not as distinct. Ranges of influent concentration are broader and more continuous because there is more dispersion in the aquifer with σ_{lnK} = 0.25. For σ_{lnK} > 0.25, the distribution of influent concentration is broad and smooth because the wider range of hydraulic conductivities associated with larger σ_{lnK} causes more mixing between the source and PRB, blending concentrations (Fig. 6.4b). As σ_{lnK} continues to increase, the distribution of influent concentration becomes broader because the aquifer contains a wider range of hydraulic conductivities and consequently, groundwater velocities are more varied and there is more dispersion.

Effluent concentrations for the FGPRB follow a similar trend to effluent concentrations for the HFPRB. At higher σ_{lnK}, the median effluent concentration is higher and the distribution of effluent concentrations is broader. The exception to this trend is the aquifer with σ_{lnK} = 0.25, which has effluent concentrations lower

a) Influent Concentration

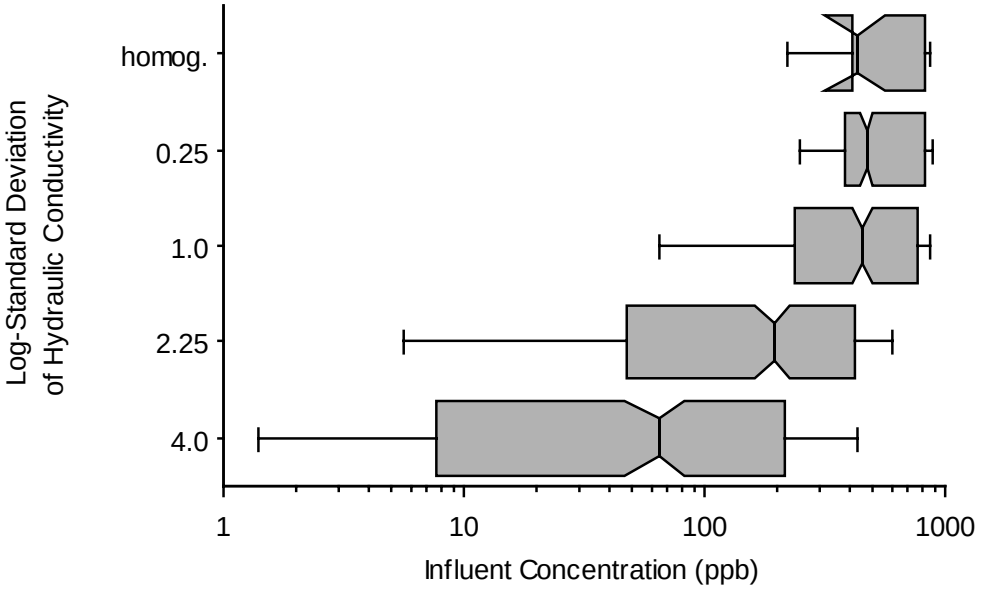

b) Effluent Concentration

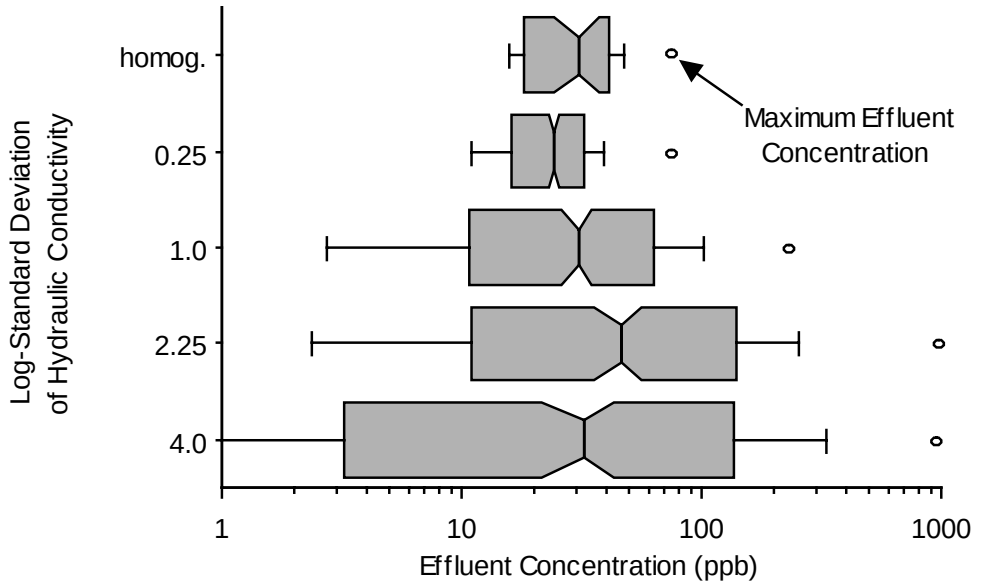

Fig. 6.10 Distributions of Influent (a) and Effluent (b) Concentration for a Homogeneous FGPRB Located in Aquifers with Different σ_{lnK}.

than effluent concentrations for a FGPRB in a homogeneous aquifer. This anomaly will be discussed subsequently.

Median effluent concentrations are higher for aquifers with larger σ_{lnK} because more zones of significantly higher hydraulic conductivity exist in these aquifers. For example, in an aquifer with σ_{lnK} = 1.0, approximately 0.1% of the aquifer contains hydraulic conductivities greater than $1x10^{-3}$ m/s (i.e., $3.09\sigma_{lnK}$ above μ_{lnK}), whereas in an aquifer with σ_{lnK} = 4.0 approximately 22.1% of the aquifer has hydraulic conductivities greater than $1x10^{-3}$ m/s (i.e., $0.77\sigma_{lnK}$ above μ_{lnK}). Knowing that contaminants move faster through regions of higher hydraulic conductivity (all other factors being equal), groundwater and contaminants move faster in aquifers with higher σ_{lnK}. Faster moving contaminants have a lower residence time in the gate and consequently higher median effluent concentrations.

Distributions of effluent concentration are broader in aquifers with larger σ_{lnK} because these aquifers have a larger range of hydraulic conductivity. A larger range of hydraulic conductivities results in a more variable flow field, which increases range of residence times for groundwater passing through the gate and causes effluent from the gate to have a broader distribution.

Similar to the HFPRB, the greatest change in the median and range of effluent concentration occurs for σ_{lnK} less than 2.25. The reason for moderate changes in σ_{lnK} causing larger changes in the distribution of effluent concentration lies in the dramatic change in the shape of log-normal PDFs between σ_{lnK} = 0 and 2.25 (Fig. 5.17). A unit change in σ_{lnK} below 2.25 causes a greater change in the

PDF for hydraulic conductivity than a unit change in σ_{lnK} above 2.25. This occurs because changes in σ_{lnK} below 2.25 add a significant fraction of higher hydraulic conductivities to the aquifer, which causes larger changes in effluent concentration. The same change in σ_{lnK} above 2.25 adds a smaller fraction of higher hydraulic conductivities to the aquifer and consequently causes less change in the distributions of effluent concentration (see section 5.3.2).

A peculiar result in Fig. 6.10b is that the median effluent concentration for a homogeneous aquifer ($\sigma_{lnK} = 0$) is higher than for an aquifer with $\sigma_{lnK} = 0.25$. This difference is a reflection of the slight differences in the distributions of influent concentration, and is accentuated by the log-scale. Approximately 80% of the influent concentrations in an aquifer with $\sigma_{lnK} = 0.25$ are lower than influent concentrations for a homogeneous aquifer. Hence, if flow through the gates for the two aquifers is similar, the aquifer with $\sigma_{lnK} = 0.25$ should have about 80% of its effluent concentrations slightly lower than effluent for the homogeneous aquifer. However, effluent concentrations are uniformly lower when $\sigma_{lnK} = 0.25$, but differences are less than 10 ppb, which is less than the 40 ppb difference in the influent concentrations. These results indicate that flow through the gate in an aquifer with $\sigma_{lnK} = 0.25$ is close but not identical to flow through the gate in a homogeneous aquifer, and that some mixing occurs in the gate when $\sigma_{lnK} = 0.25$. The additional mixing causes effluent concentrations in an aquifer with $\sigma_{lnK} = 0.25$ to be uniformly, but slightly less than effluent concentrations for a homogeneous aquifer.

At σ_{lnK} = 1.0, there is sufficient preferential flow through the gate to cause the median effluent concentrations for a homogeneous and heterogeneous aquifer to be equal, despite lower influent concentrations for the heterogeneous aquifer. At σ_{lnK} greater than 1.0, preferential flow causes the median effluent concentration for heterogeneous aquifers to exceed the median effluent concentration for a homogeneous aquifer.

In summary, influent concentrations decrease and have a greater range as σ_{lnK} increases due to greater dilution between the source and PRB. Distributions of effluent concentration also broaden as σ_{lnK} increases, but shift toward higher concentration with increasing σ_{lnK}. However, the shifts in effluent concentration are less than shifts in influent concentration for σ_{lnK} less than 1 so that effluent concentration when σ_{lnK} is less than 1 lower than effluent concentration for a homogeneous aquifer. Once σ_{lnK} is greater than 1, preferential flow through the PRB causes median effluent concentration to be greater than the median effluent concentration for a homogeneous aquifer due to the reduced residence time.

6.5.3 Effects of Correlation Scale

The impact of varying correlation scales (λ_x and λ_y) on influent and effluent concentrations from a FGPRB are evaluated in this section. Distributions of influent and effluent concentration for a homogeneous FGPRB (k_r = 1.0 d^{-1} and K_p = 2.5x10^{-3} m/s) in aquifers with μ_{lnK} = -10 (4.54x10-5 m/s), σ_{lnK} = 1.0, and varying λ_x and λ_y are shown in Fig. 6.11. Three λ_x (λ_x = 3, 6, and 9 m) and four λ_y (λ_y = 1, 2,

3, and 5 m) were simulated. Three of the simulations have a $\lambda_x/\lambda_y = 3$, one simulation has a $\lambda_x/\lambda_y = 6$, and one simulation has a $\lambda_x/\lambda_y = 1.2$.

Influent concentrations are slightly higher in aquifers with larger λ_x, but nearly identical in aquifers with varying λ_y. Tripling λ_x causes about a 20% increase in influent concentration whereas a five-fold increase in λ_y causes less than a 10% increase in influent concentrations. This is a logical result because aquifers with larger λ_x have longer zones of hydraulic conductivity that are aligned with the regional gradient. In these aquifers, groundwater and contaminants have a more direct path to the PRB than in aquifers with lower λ_x. A straighter path through fewer conductive units will have less mixing between the source and PRB, and consequently higher influent concentrations. Varying λ_y has little impact on influent concentration because most of the flow between the source zone and gate is in the longitudinal direction, whereas changing λ_y affects the lateral dimension of zones of higher hydraulic conductivity.

Distributions of effluent concentration shift slightly toward higher concentrations at larger λ_x but change little with varying λ_y. Tripling λ_x causes a 20% increase in effluent concentration, a similar to the shift in influent concentration for changing λ_x. Similar variability in the distributions of influent and effluent concentration indicate that groundwater flow through the gate is unaffected by varying λ_x. This response is quite different than that observed for the HFPRB. Influent concentrations for the HFPRB doubled when λ_x tripled because a HFPRB is more likely to bisect longer zones of higher hydraulic conductivity that occur with

a) Influent Concentration

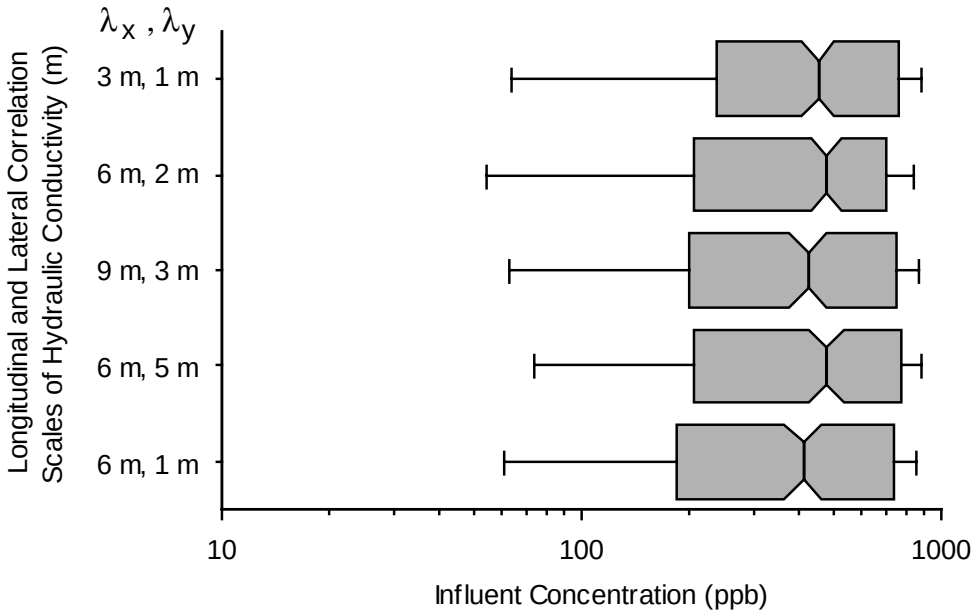

b) Effluent Concentration

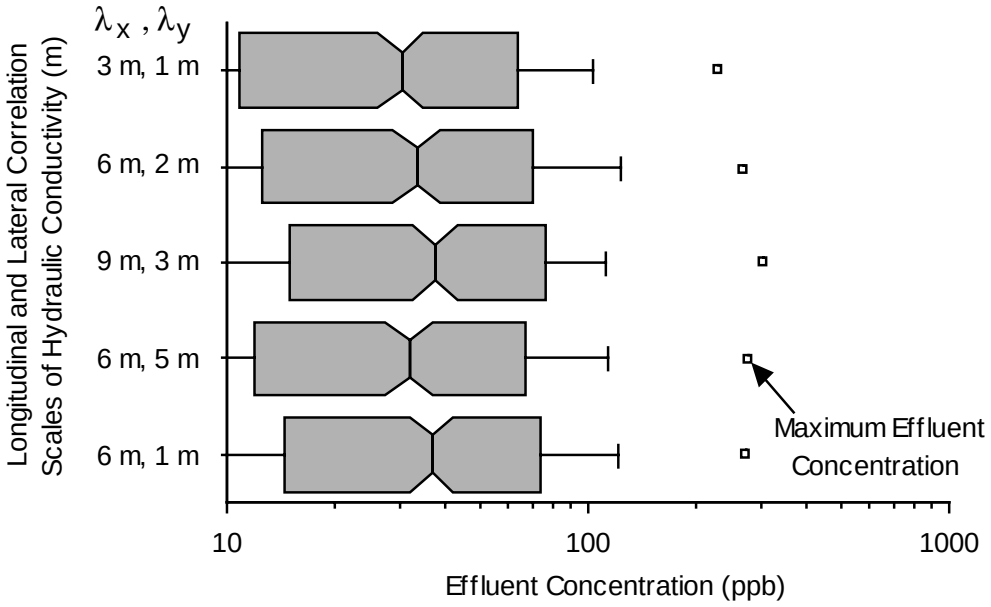

Fig. 6.11 Distributions of Influent and Effluent Concentration for a Homogeneous FGPRB Located in Aquifers with Different λ_x and λ_y.

larger λ_x. In contrast, the up-gradient convergence and down-gradient spreading of the contaminant plume in the FGPRB appears to reduce the influence of λ_x. Unless zones of higher hydraulic conductivity intercept the gate, the more tortuous flow-path that groundwater is forced to take through a FGPRB reduces the impact of λ_x such that the shift in influent and effluent concentration with changing λ_x is only about 20%, one-fifth of the shift observed for the HFPRB.

Differences in influent and effluent concentration may also be attributed to spatial dissimilarity between random fields with different λ_x or λ_y. Unlike changing μ_{lnK} and σ_{lnK} in which the relative magnitude of hydraulic conductivity is consistent between random fields, changing λ_x or λ_y results in a completely new map of hydraulic conductivity, even for random fields with identical seeds. Thus, some of the shift in influent and effluent concentration may be a consequence of the method used for random field generation rather than the impact of changing λ_x or λ_y. Nonetheless, compared to varying μ_{lnK} and σ_{lnK}, changes in λ_x or λ_y have a minor impact on influent and effluent concentrations from a FGPRB.

6.6 COMPARISON OF FGPRB AND HFPRB

Influent and effluent concentrations from a FGPRB and HFPRB are compared in this section. A homogeneous, 5 m wide by 1 m thick FGPRB and 25 m wide by 1 m thick HFPRB that have k_r = 1.0 d^{-1} and K_p = 2.5x10^{-3} m/s are simulated in identical aquifers. Aquifers considered for comparison have σ_{lnK} = 1.0, λ_x = 3 m, λ_y = 1 m, and μ_{lnK} = -9, -10, -11, and –12; or μ_{lnK} = -10, λ_x = 3 m, λ_y = 1 m,

and σ_{lnK} = 0.25, 1.0, 2.25, and 4.0. Only μ_{lnK} and σ_{lnK} are considered because these parameters have the greatest influence on PRB performance.

Distributions of influent and effluent concentrations for homogeneous HFPRBs and FGPRBs in aquifers with μ_{lnK} = -9, -10, -11, and –12 are shown in Fig. 6.12. Influent concentrations are similar for the HFPRB and the FGPRB (approximately 90% between 100 ppb and 1000 ppb and 10% between 1 ppb and 100 ppb). Influent concentrations for the FGPRB are slightly lower than influent concentrations for the HFPRB, because the funnel captures more groundwater from regions outside of the contaminant plume that dilutes contaminants entering the gate and reduces influent concentrations.

Effluent concentrations for the FGPRB are higher than for the HFPRB at all μ_{lnK}, since the flux of water through the FGPRB is much higher than the flux of water through the HFPRB and the thicknesses of the two PRB are equal. The larger groundwater flux through the FGPRB decreases residence times in the reactive media and increases effluent concentrations. Distributions of effluent concentration for the FGPRB coincide with distributions of effluent concentrations for a HFPRB for a unit larger μ_{lnK} (i.e., effluent concentration for a FGPRB at μ_{lnK} = -10 is approximately equal to effluent concentration for a HFPRB at μ_{lnK} = -11). However, this result is coincidental and is not a general characteristic of FGPRBs.

Influent and effluent concentrations for a homogeneous HFPRB and FGPRB in aquifers with μ_{lnK} = -10, λ_x = 3 m, λ_y = 1 m, and σ_{lnK} = 0.25, 1.0, 2.25, and 4.0 are shown in Fig. 6.13. Distributions of influent concentration are similarly shaped for

a) Influent Concentration

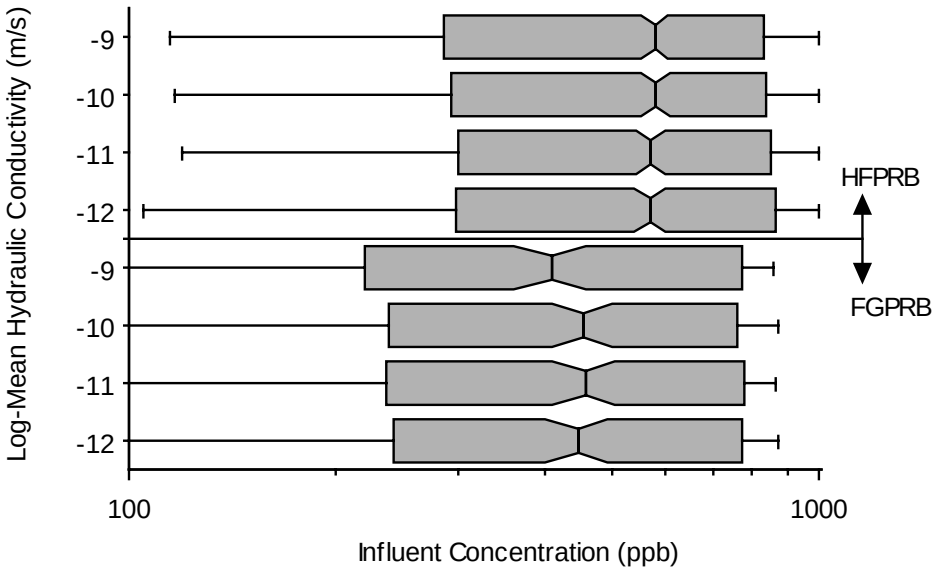

b) Effluent Concentration

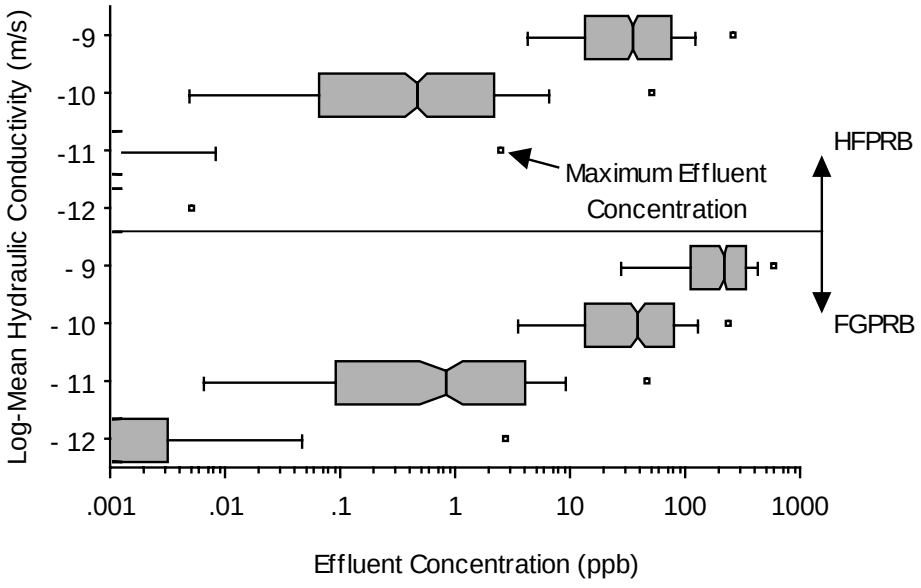

Fig. 6.12 Distributions of Influent and Effluent Concentration for a Homogeneous HFPRB and FGPRB Located in Aquifers with Different μ_{lnK}.

a) Influent Concentration

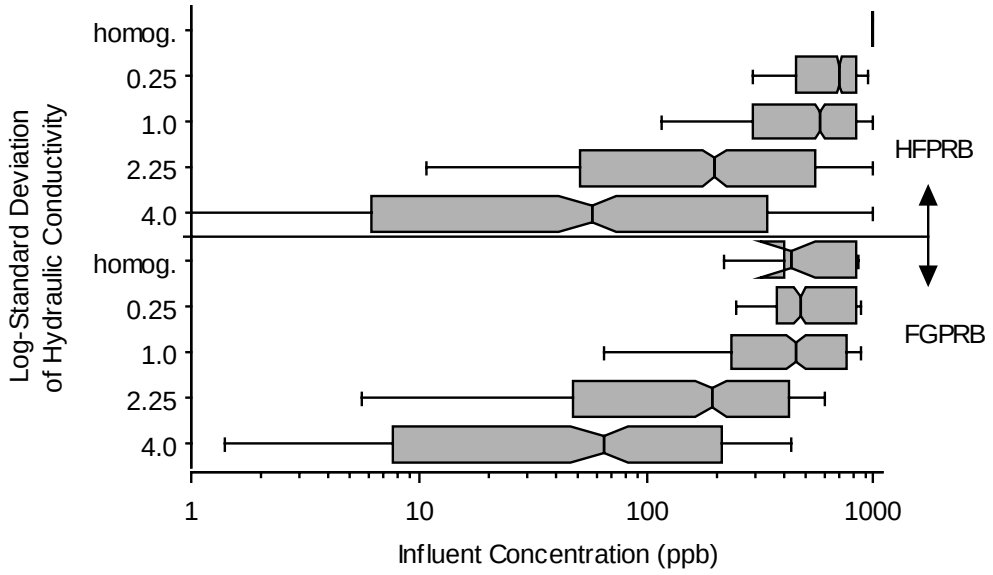

b) Effluent Concentration

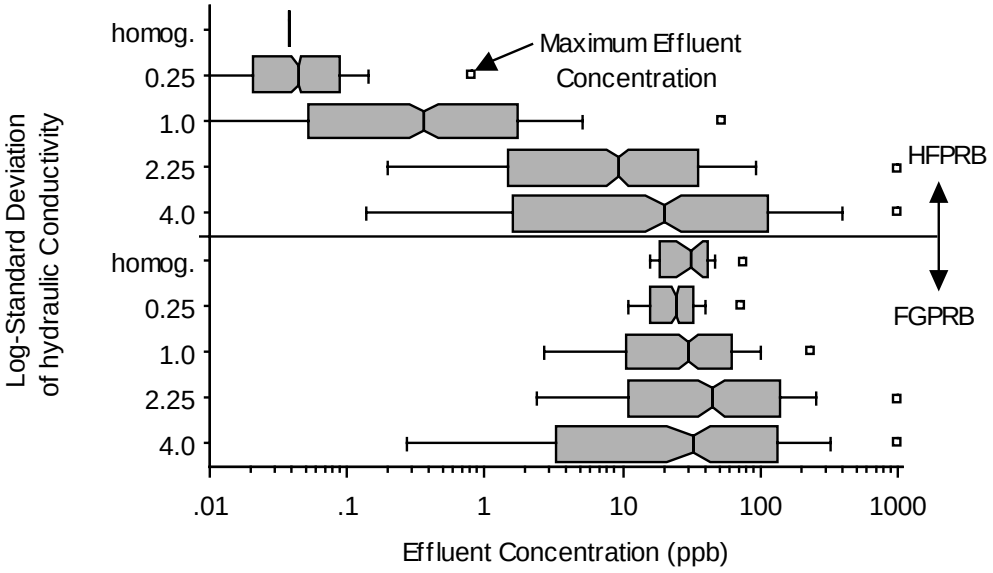

Fig. 6.13 Distributions of Influent (a) and Effluent (b) Concentration for a Homogeneous HFPRB and FGPRB Located in Aquifers with Different σ_{lnK}.

the HFPRB and FGPRB. Also, influent concentration decreases as σ_{lnK} increases for both types of PRB. Influent concentrations are slightly higher for the HFPRB at σ_{lnK} = 0.25 and 1.0 whereas influent concentrations are higher for the FGPRB at σ_{lnK} = 2.25 and 4.0. Influent concentrations are lower for the FGPRB in more homogeneous aquifers because of additional mixing that occurs due to the funnel in the FGPRB. In more homogeneous aquifers (smaller σ_{lnK}), flow-lines approaching a HFPRB are straighter and little dilution occurs as contaminants move from the source to the PRB (Fig. 6.14a). Consequently, concentrations entering a HFPRB are closer to the source concentration. Contaminants also pass directly from the source to the gate of a FGPRB; however, the breadth of the funnel also channels uncontaminated groundwater through the gate. The additional uncontaminated water dilutes contaminated groundwater and reduces influent concentrations for a FGPRB in more homogeneous aquifers.

Mixing also plays a key role in causing influent concentrations for a HFPRB to exceed influent concentrations for a FGPRB in more heterogeneous aquifers (i.e., $\sigma_{lnK} \geq 2.25$). In more heterogeneous aquifers, significant mixing occurs between the source and PRB for both the HFPRB and FGPRB (Fig. 6.4c and 6.14b), causing contaminant plumes to be wider and deeper, and have lower concentrations. However, slightly lower influent concentrations for the FGPRB reflect the additional mixing of contaminated and uncontaminated groundwater that is caused by the funnels.

a) σ_{lnK} = 1.0

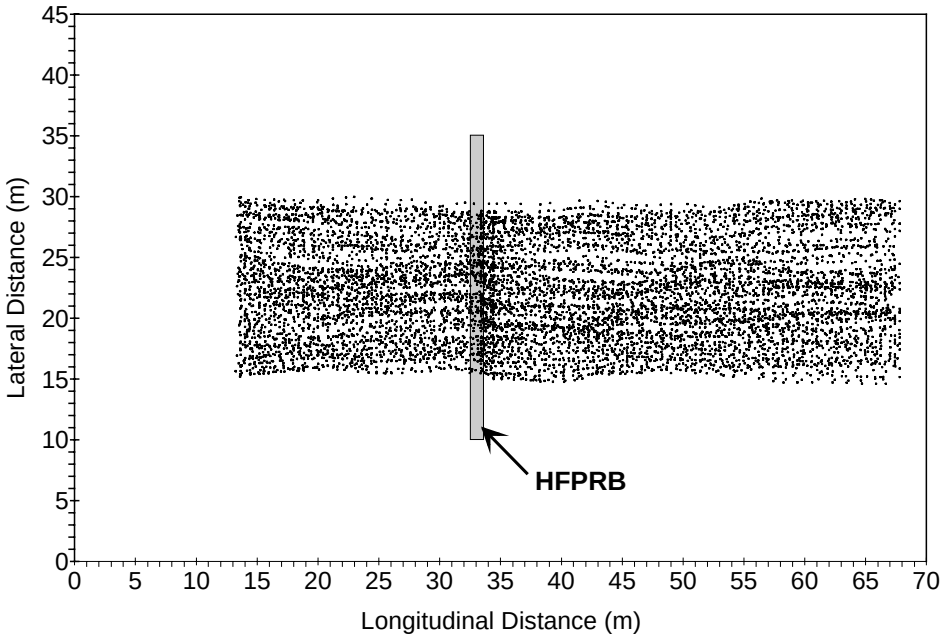

b) σ_{lnK} = 4.0

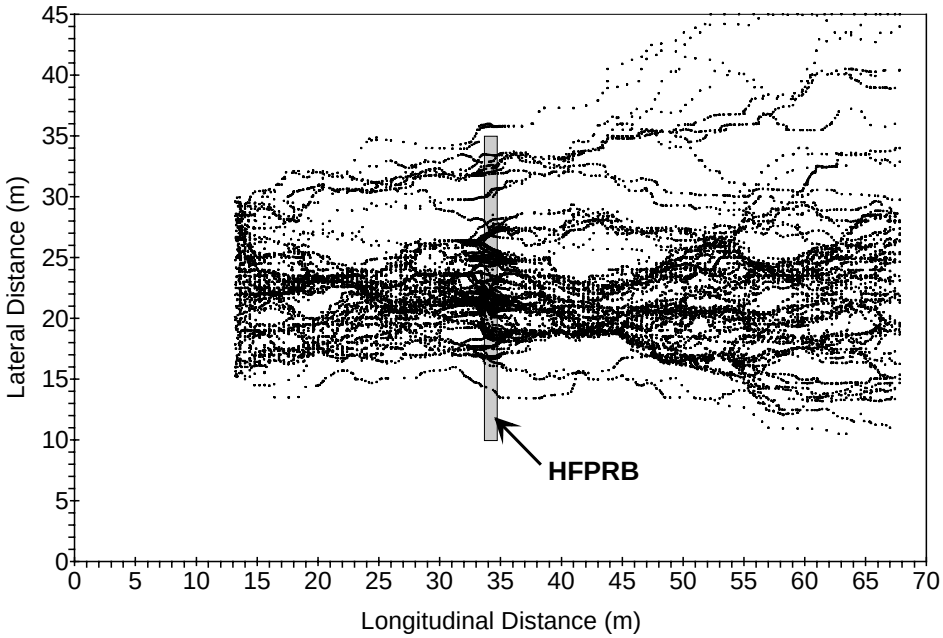

Fig. 6.14 Trajectory of 150 Particle in Aquifers with σ_{lnK} = 1.0 (a) and 4.0 (b) Containing a HFPRB (μ_{lnK} = -10, λ_x = 3 m, λ_y = 1m).

Distributions of effluent concentration for a HFPRB and FGPRB in aquifers with several σ_{lnK} are shown in Fig. 6.13b. Effluent concentrations for a FGPRB are higher than effluent concentrations for a HFPRB due to higher groundwater flow rates through a 5 m wide gate compared to a 25 m wide HFPRB. Faster flow causes residence times to be shorter and effluent concentrations higher for the FGPRB.

Effluent concentrations from a FGPRB also have a smaller coefficient of variation (COV), which is a measure of the range of concentrations relative to the mean. The smaller COV for the FGPRB indicates that flow through the gate is more uniform than flow across a HFPRB. Concentrations are more uniform for a FGPRB because groundwater mixes more prior to entering the PRB and the more tortuous path toward the gate dilutes extremes in concentration.

More uniform effluent concentrations from a FGPRB indicate that smaller factors of safety (FS) is needed for a FGPRB than for a HFPRB. The plug flow model that is often used for PRB design assumes that flow through the reactive media is uniform (e.g., Eq. 2.3). A FS is used with the plug flow model to account for non-uniform flow. Systems that have more varied flow require a larger FS than systems with more uniform flow. Since flow is more uniform through the FGPRB, a smaller FS is needed, resulting in more efficient designs that use less reactive media. Section 9 discusses the required FS for each style of PRB in greater detail.

SECTION 7

RESULTS AND CONCLUSIONS FOR A CAISSON PRB

7.1 GENERAL DESCRIPTION

A caisson permeable reactive barrier (CPRB) is an in situ vertical tube of reactive media that is located at the apex of a low hydraulic conductivity funnel (Fig. 7.1). The funnel is used to channel contaminated groundwater into the CPRB where contaminants are removed from the groundwater. The CPRB is an innovative design because it induces vertical groundwater flow up and down-gradient of the PRB in order to create more uniform influent and effluent velocities, and water is forced to flow across the longest dimension of barrier, which uses the reactive medium more effectively. The funnels and CPRB force groundwater to follow a more tortuous path than the HFPRB or FGPRB. The more tortuous path is intended to cause groundwater to cross zones of varying hydraulic conductivity so that water passes through the PRB more uniformly. Plug-flow through the reactive medium produces more uniform residence times and more efficient use of the reactive medium. In contrast, HFPRBs and FGPRBs experience variable flow rates and have zones that never experience contaminated water, wasting the reactive media. Another advantages of a CPRB is that it has rigid sides so that construction, rejuvenation, or replacement of the reactive media is easier, and monitoring the performance of a CPRB should be easier than monitoring a HFPRB since flow is focused through a smaller area.

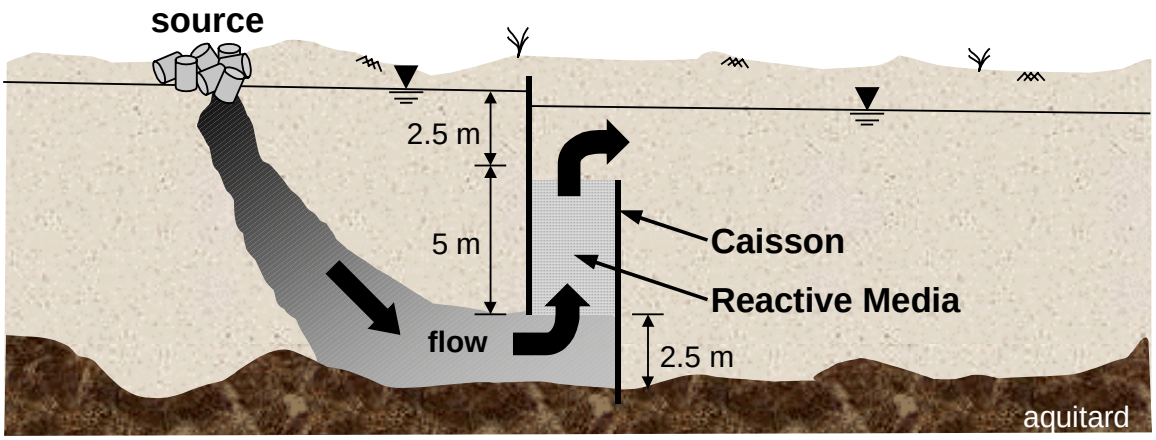

Fig. 7.1 Schematic of a Caisson PRB

This section considers fully penetrating, rectangular CPRBs that are 5 m wide and 1 m thick. The caissons have holes that are 2.5 m tall and 5 m wide located at the bottom of the caisson on the influent face and at the top of the caisson on the effluent face (Fig. 7.1). Holes in these positions are more conducive for DNAPL containment because dissolved plumes of DNAPL will tend to exist at the base of an aquifer where free-phase DNAPL is usually located. For LNAPLs, an influent hole located along the water table and an effluent hole at the base of the caisson is more appropriate. For either arrangement, the caisson is best suited for aqueous-phase contamination because the densities of free-phase DNAPL or LNAPL may prohibit the vertical flow through the reactive medium.

Flow is channeled toward the CPRB by a low hydraulic conductivity funnel. As groundwater approaches the CPRB, it moves downward through the aquifer and enters the up-gradient hole in the CPRB. Groundwater then passes vertically through the reactive media within the caisson and exits through the down-gradient hole (Fig. 7.1). Flow is driven by a difference in total head between the inlet and outlet of the caisson. The path taken by groundwater through the CPRB is longer than for a HFPRB or FGPRB of equal thickness because of the vertical component of flow. Flow along the longest dimension of the PRB is an advantage of the CPRB because there is a longer residence time of contaminants in the media, but the longer flow path also generates more head loss. A CPRB will operate passively only if the head loss for a flow-path around the funnel exceeds head loss through the reactive media. Therefore, CPRBs require longer funnels than a FGPRB of

equal thickness. The required length for funnels will also increase for deeper CPRBs.

The CPRB has two significant disadvantages. First, only one CPRB has been built (Jarre and Kociolek 1999), and this system differs from the one modeled in this report. The only existing CPRB is located in Belfast, Ireland and consists of three caissons, each 1.2 m (4 ft) in diameter and 18.3 m (60 ft) long, that are plumbed together and operate in series. Water enters the first caisson, which is filled with sand, passes through the caisson, and enters the second caisson. The second caisson is filled with reactive media. Groundwater passes through the second caisson, then enters another sand-filled caisson, after which it is released to the aquifer. The feasibility of building the CPRB described in this report is unknown. Problems may occur when driving and aligning the caisson, keying the caisson into an underlying aquitard, or achieving an adequate seal between the caisson and funnel. In light of these potential difficulties, initial CPRBs may be significantly more expensive than equivalent HFPRBs and FGPRBs until construction issues are resolved.

The second disadvantage of CPRBs is that flow is forced to pass through a smaller area (i.e., the influent and effluent holes) when entering and exiting the caisson, making design of the funnels and CPRB more difficult. Focussing flow through holes in the CPRB causes high head loss in the system because the equivalent hydraulic conductivity of the openings is approximately equal to the hydraulic conductivity of the aquifer, not the hydraulic conductivity of the reactive media. This disadvantage is further complicated because head loss is proportional

to the quantity of water captured by the funnel (i.e., the length of the funnel). Thus, openings in the caisson must be chosen carefully so that the head loss is not so large that flow passes around the funnel, but the funnel cannot be so long that there is excessive flow through the PRB. To resolve this problem, either larger caissons (1 to 10 m diameter) are used, or many caissons are needed. If large caissons are used, construction may become more difficult, whereas if many smaller caissons are used, monitoring and maintaining the CPRB becomes expensive. The design of CPRBs will be discussed subsequently.

7.2 CONCEPTUAL MODEL OF A CPRB

The conceptual model for the CPRB is similar to the model for a FGPRB and HFPRB. The model is a heterogeneous aquifer with two fully penetrating caissons separated by a 15 m wall with 10 m walls on either side of the caissons (Fig. 7.2). The two caissons are each 5 m wide, 1 m thick, and have a 5 m tall plug of reactive media. The caissons have 2.5 m tall by 5 m wide holes located on each end as shown in Fig. 7.1 and 7.2. The volume of reactive media in the two caissons is 50 m^3, equal to that for the FGPRB and 20% of that for the HFPRB.

Two caissons are required for the aquifer because head loss through a single caisson was too large. Several systems with a single CPRB were simulated, but the head loss near the entrance of the CPRB was so large that a 15 m caisson with 25 m funnels was unable to channel all particles from the 5 m source through the barrier. Since a larger system is unrealistic, a model with two caissons is used.

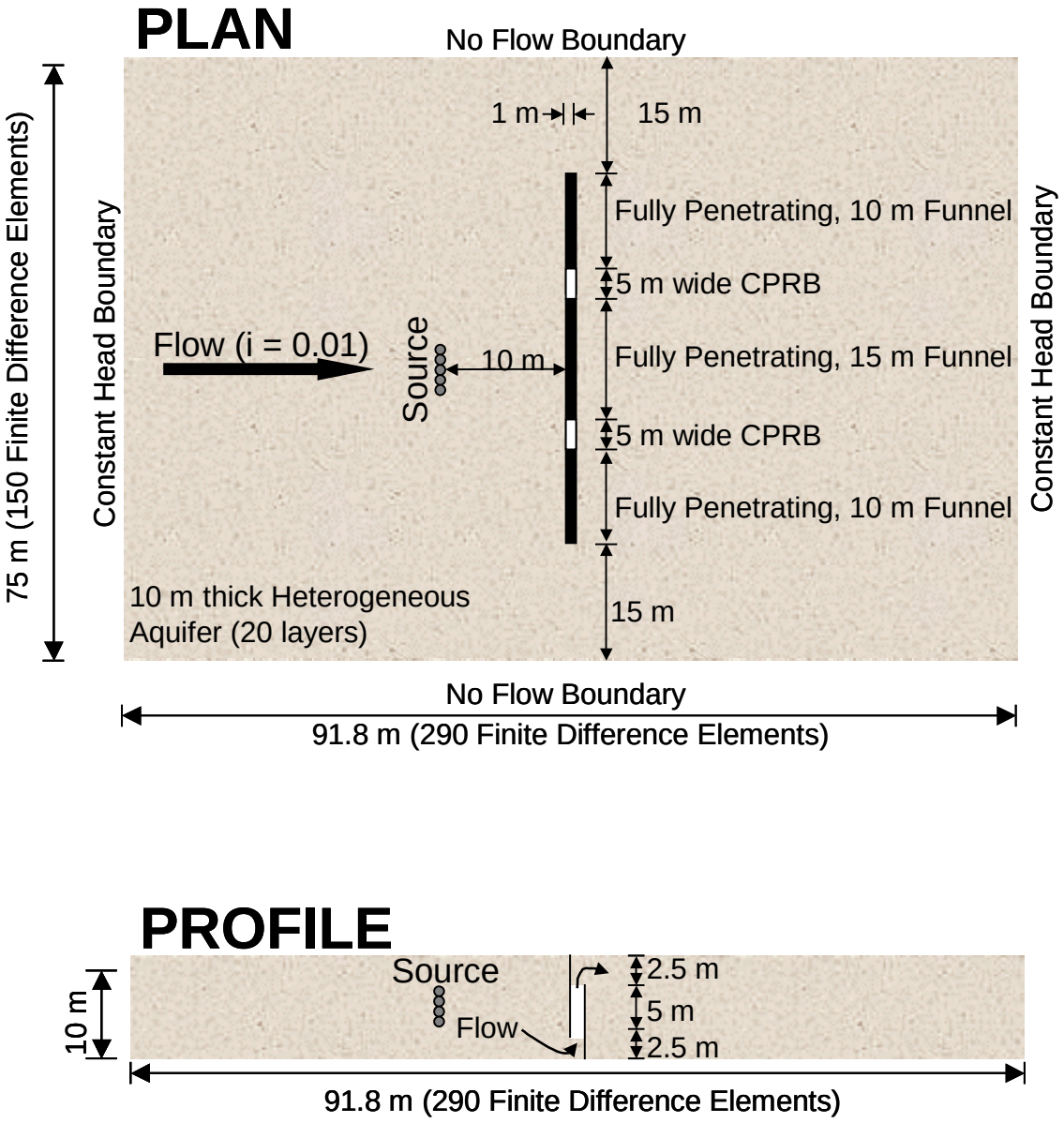

Fig. 7.2 Conceptual Model for CPRBs in a Heterogeneous Aquifer.

Also, the largest funnels were not able to provide containment of a 15 m source in the most heterogeneous aquifer (σ_{lnK} = 4.0). To resolve this, the source was reduced to a 5 m strip with C_o = 1000 ppb. The funnels were able to contain more than 99% of this source in aquifers with σ_{lnK} = 4.0. Greater discussion on the difficulty of providing containment with a CPRB is provided subsequently.

7.2.1 Establishing Size of the Model Domain

Once an appropriate CPRB and source were chosen, the smallest aquifer that does not effect flow through the CPRB was determined. The longitudinal and lateral dimensions of the aquifer were shrunk symmetrically around the system until any of three criteria were met: (1) particle transit times through the PRB changed, (2) velocity of particles entering or exiting the PRB changed, or (4) the boundaries of the domain were within two correlation scales of the funnel. The smallest aquifer that did not satisfy any of these criteria was used for subsequent simulations. A similar procedure was used for the HFPRB and FGPRB.

Distributions of particle transit time, velocity entering the CPRB, and velocity exiting the CPRB in aquifers of varying size are shown in Fig. 7.3. Solid lines are results for one realization and dashed lines are results for a second realization. The smallest aquifer that yields results that are unaffected by the location of the boundaries is 270 by 130 cells (83.8 m long and 65 m wide). Subsequent simulations of CPRBs used this domain.

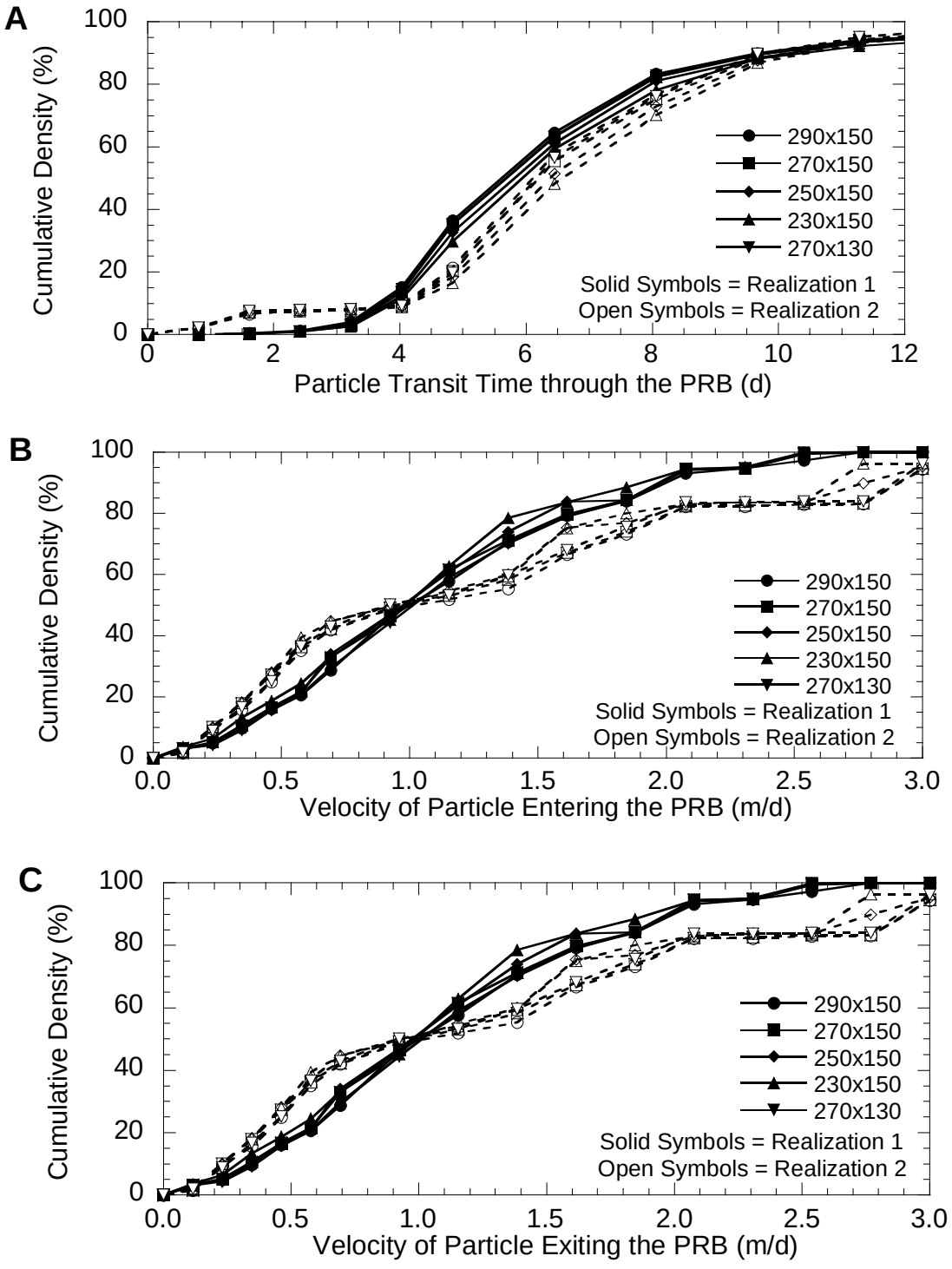

Fig. 7.3 CDFs of Particle Transit Time (a), Velocity Entering the CPRBs (b), and Velocity Exiting the CPRBs (c) for Aquifers of Varying Size.

7.2.2 Final Conceptual Model of a CPRB

The final conceptual model for a CPRB is shown in Fig. 7.4. The aquifer is 83.8 m long, 65 m wide, and 10 m thick. The domain contains 702,000 finite difference cells with a minimum $\Delta x = 0.05$ m in the center of the aquifer (and PRB), a maximum $\Delta x = 0.4$ m at the boundaries, and a constant Δy and $\Delta z = 0.5$ m. Two CPRBs are located at y = 25 to 30 m and 45 to 50 m, each is 1 m thick (x = 41.4 to 42.4 m). Each PRB has a 5 m tall by 5 m wide and 1 m thick plug of reactive media between elevations of 2.5 and 7.5 m. The CPRBs have 2.5 m tall by 5 m wide openings on the influent and effluent sides (Fig. 7.2). Metal casings for the caisson are simulated using a hydraulic conductivity of $1x10^{-30}$ m/s. A 15 m long, 1 m thick funnel ($K = 1x10^{-7}$ cm/s) is located between the CPRBs and 10 m long funnels are located on the outside of the CPRBs.

A 1000 ppb contaminant source, 5 m wide by 5 m deep is located 20 m up-gradient of the PRB along the lateral and vertical centerline of the aquifer. Flow occurs due to a gradient of 0.01 imposed by constant head boundaries at X = 0 m and X = 83.8 m. A no flux boundary condition is imposed on the sides (Y = 0 m and Y = 65 m) and bottom of the domain (Z = 0 m), whereas the top of the aquifer (Z = 10 m) is a variable head boundary (i.e., unconfined aquifer).

7.3 CONTAMINANT TRANSPORT TOWARDS AND THROUGH A CPRB

Funnels are used with CPRBs to capture a plume of contaminated water and channel flow toward the PRB. The objective of the CPRB is to serve as a conduit for vertical water flow through the reactive media. The driving force for the

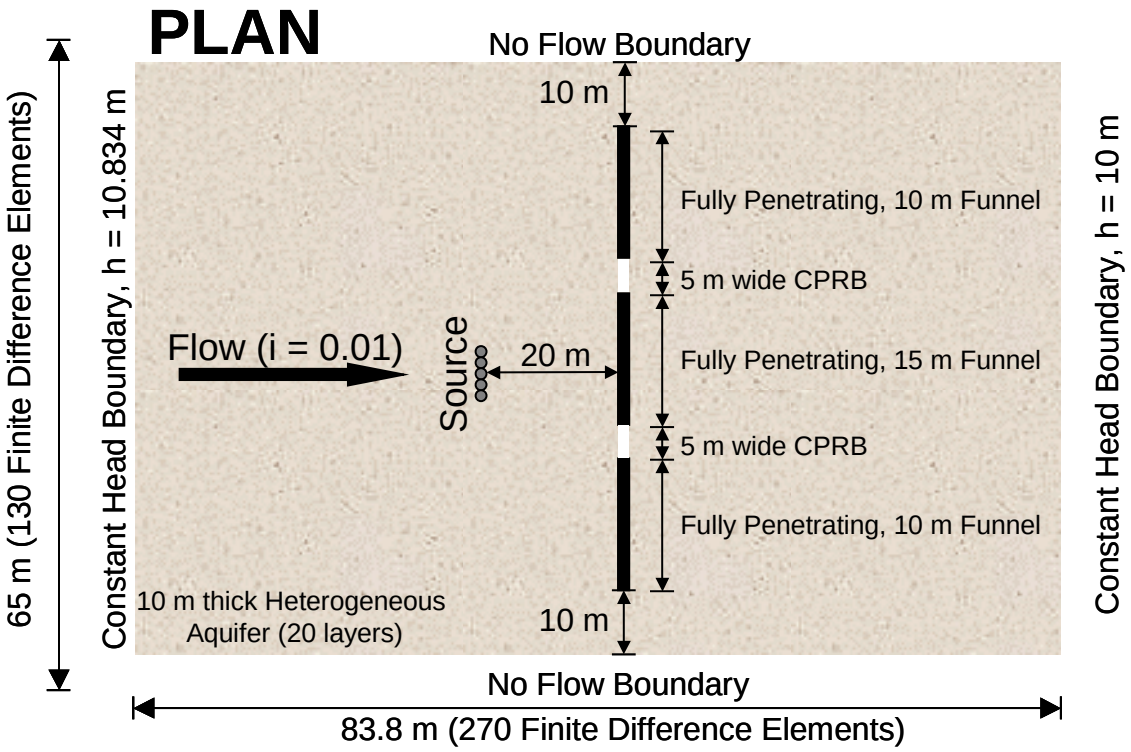

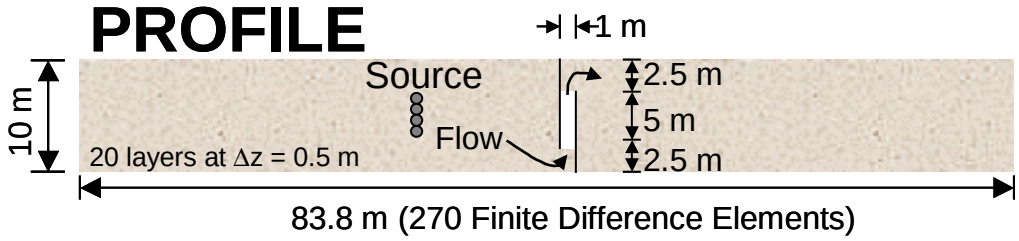

Fig. 7.4 Final Conceptual Model for the CPRBs.

system is a difference in head on either side of the PRB. Funnels are extended laterally to a distance where the minimum head loss along flow paths around the outer edge of the funnel exceeds the maximum head loss through the PRB. This principle is similar to that for the FGPRB.

For a FGPRB, flow captured by the funnel is channeled through a gate. Neglecting resistance within the PRB, because the reactive media has a hydraulic conductivity orders of magnitude greater than the aquifer, the greatest loss in head occurs immediately up-gradient and down-gradient of the PRB where the volumetric flux is highest and hydraulic conductivity is equal to the hydraulic conductivity of the aquifer. The volumetric flux at these locations is the quantity of water channeled through the gate (i.e., captured by the funnels) divided by the cross sectional area of the gate. The same principle holds true for the CPRB. Regions of the aquifer adjacent to the opening of the caisson are the “bottleneck” of the system. At these locations, head loss (Δh) is greatest because the product of cross sectional area for flow (A) and hydraulic conductivity of the aquifer (K_a) is smallest (Eq. 7.1)

$$\Delta h = \frac{-Q\Delta L}{AK_a} \tag{7.1}$$

where Q is volumetric flow rate of water through the CPRB and ΔL is a differential length corresponding to Δh. Thus, the required breadth of funnels is affected by the size of the openings of the caisson since most of the head loss occurs at these points.

7.3.1 Sizing the Caisson

From the previous analysis, several conclusions regarding the design of CPRBs can be made. First, the sensitivity of CPRB performance to hydraulic conductivity at the influent and effluent opening is a significant flaw. If one of the openings coincides with a finer-grained layer, the resistance due to this small region may cause contaminated groundwater to flow around the funnel rather than through the CPRB. The HFPRB and FGPRB are less susceptible to such problems because flow occurs through a larger cross sectional area. To minimize this problem, caissons should be wide and thin rather than narrow and thick; oval or rectangular caissons are a better choice than square or circular caissons. Rectangular or oval caissons allow openings to be larger per vertical meter, reducing head loss at the influent and effluent of the PRB. Narrow caissons that have taller opening may appear to have openings of equal area, but the taller openings reduce the allowable height of reactive media inside the caisson. This is shown using an example.

Two possible CPRBs are shown in Fig. 7.5. Caisson A is 5 m wide whereas Caisson B is 2.5 m wide. Both designs have the same size opening ($A = 10\ m^2$) so that in identical aquifers and with identical funnels, head losses should be the same for the two systems. The reactive media in Caisson A is three times longer than in Caisson B; thus, Caisson B was made six times thicker than caisson A so that both caissons had an equal volume of reactive media (i.e., both CPRBs have 30 m^3 of reactive media). The two CPRBs have the same volumetric flux of groundwater entering them (i.e., identical Q/A) and an equal volume of reactive media. The

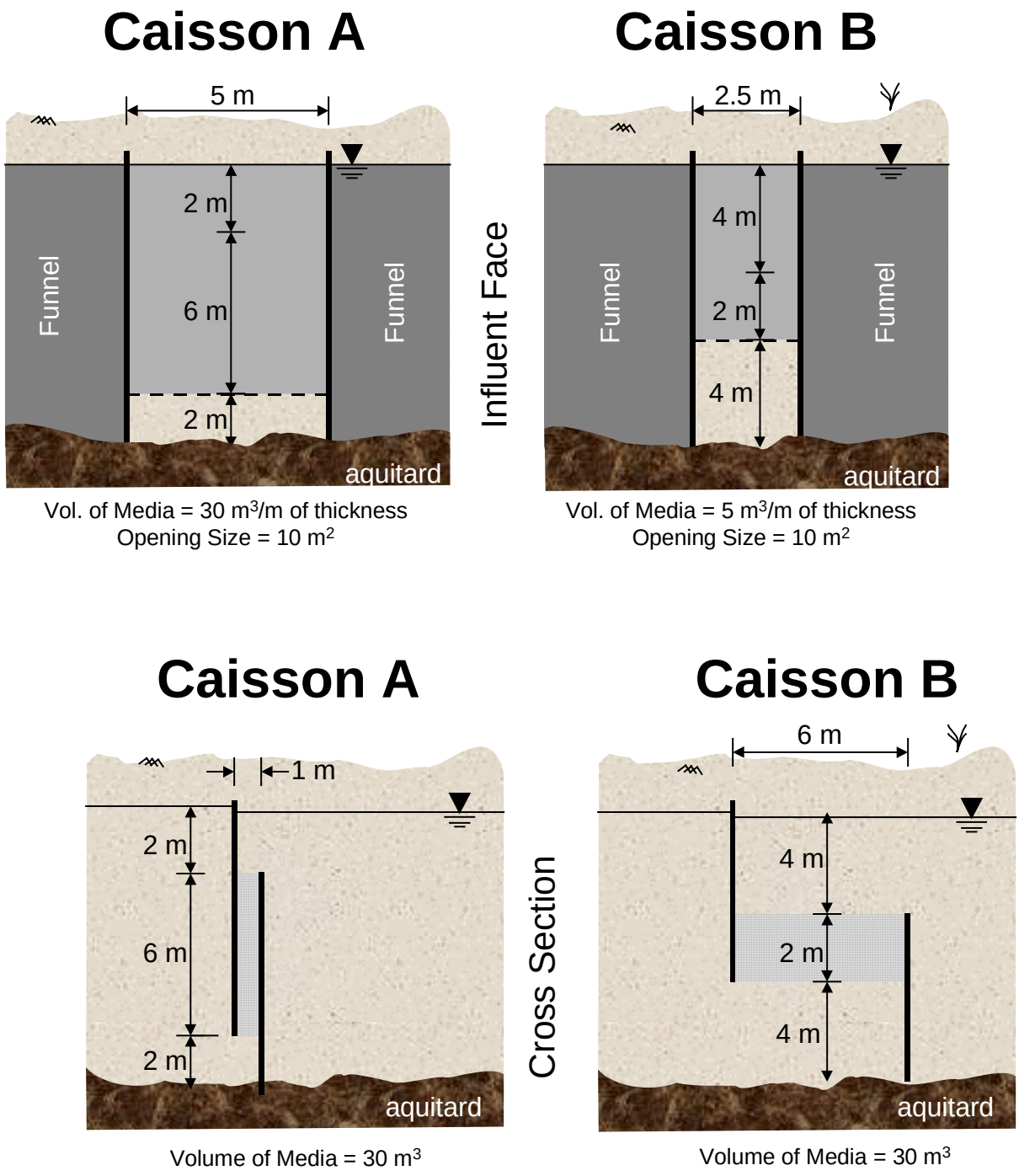

Fig. 7.5 Possible CPRB Configurations, a 5 m Wide CPRB and a 2.5 m Wide CPRB (views of the influent face and cross section are shown for each CPRB).

designs only differ in their width and thickness such that Caisson A is 5 m wide and 1 m thick (i.e., an area of $5m^2$) and Caisson B is 2.5 m wide and 6 m thick (i.e., an area of 15 m^2).

CPRBs A and B might be expected to perform similarly because groundwater should move through Caisson B at one-third of the velocity that it moves through Caisson A (i.e., 5 m^2/15 m^2 = 1/3), yielding equal residence times in the reactive media and thus comparable performance (i.e., Caisson A has 6 m of reactive media and Caisson B has 2 m of reactive media). However, these designs do not yield the same results. Rather, the narrower caisson (Caisson A) yields lower effluent concentrations (Fig. 7.6b). Caisson A performs better because contaminants have a greater residence time in the reactive media (Fig. 7.6a) and consequently, effluent concentrations are lower (Fig. 7.6b). The reason for longer residence times in the narrower CPRB can be explained by observing particle paths through each CPRB.

Particle trajectories through Caisson A and B are shown in Fig. 7.7. Particles enter Caisson A and move vertically upward through the entire volume of reactive media. In contrast, particles move diagonally through the reactive media in Caisson B in a direct path between the openings. Particles do not pass through that portion of the reactive medium that is not along this diagonal and water is stagnant in the top, up-gradient and bottom, down-gradient corners of the caisson. In effect, triangular wedges of reactive media are wasted in Caisson B whereas all of the reactive media is used in Caisson A, resulting in lower effluent concentrations for Caisson A than B. Therefore, the best design for a CPRB is an

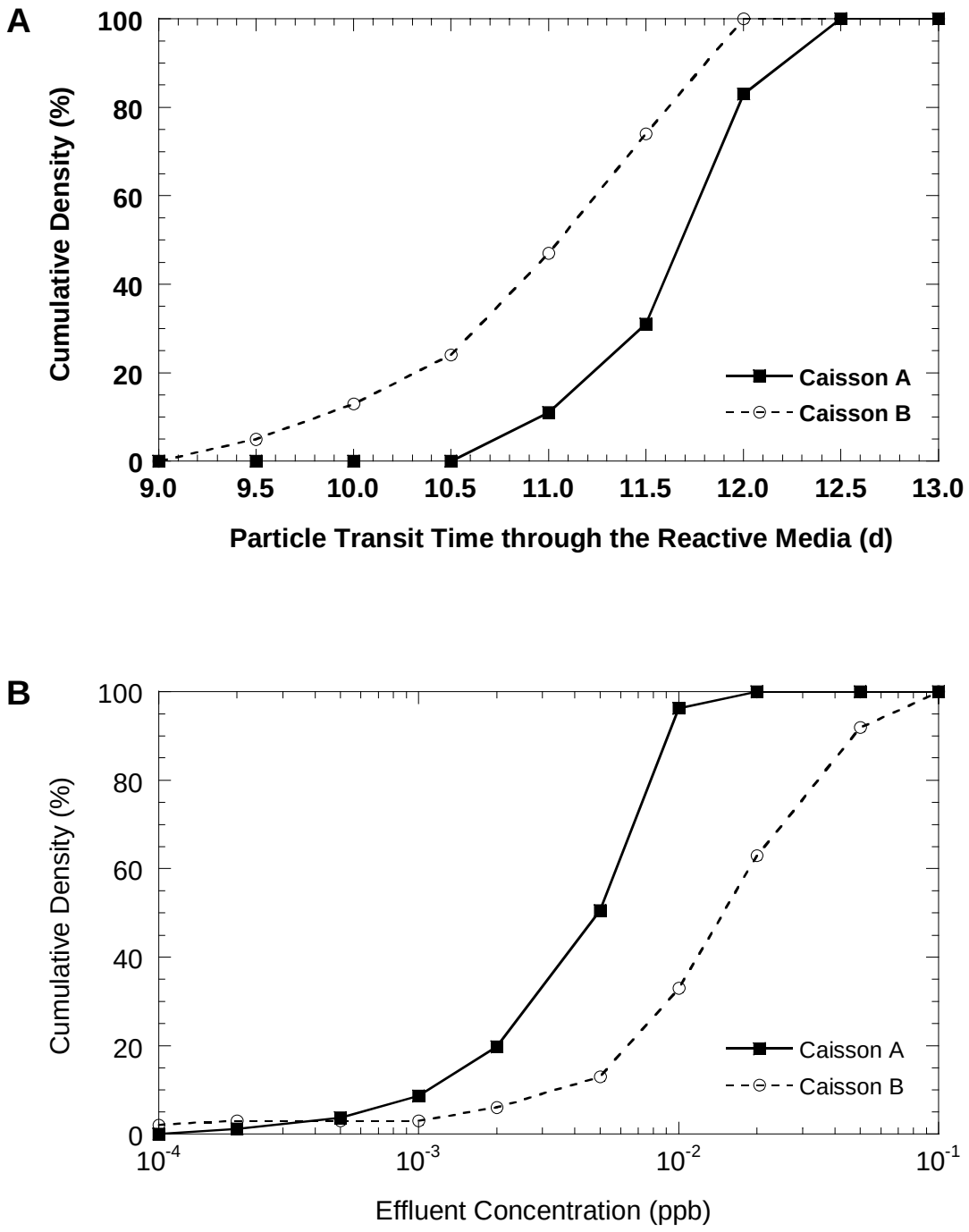

Fig. 7.6 Cumulative Distributions of Particle Transit Time (a) and Effluent Concentration (b) for Caisson Designs A and B.

a) Caisson A (1 m thick CPRB)

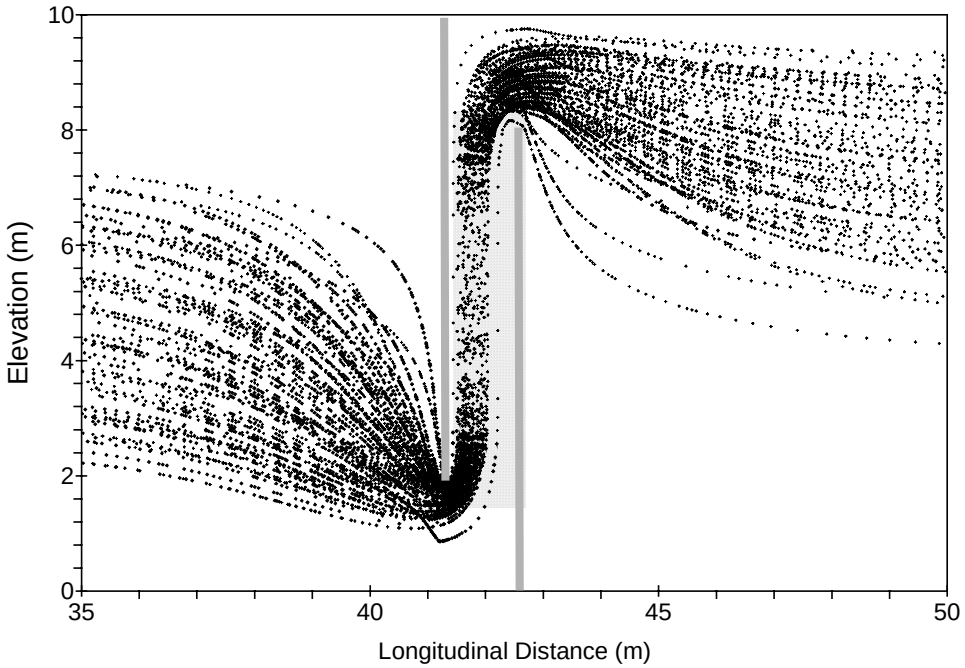

b) Caisson B (6 m thick CPRB)

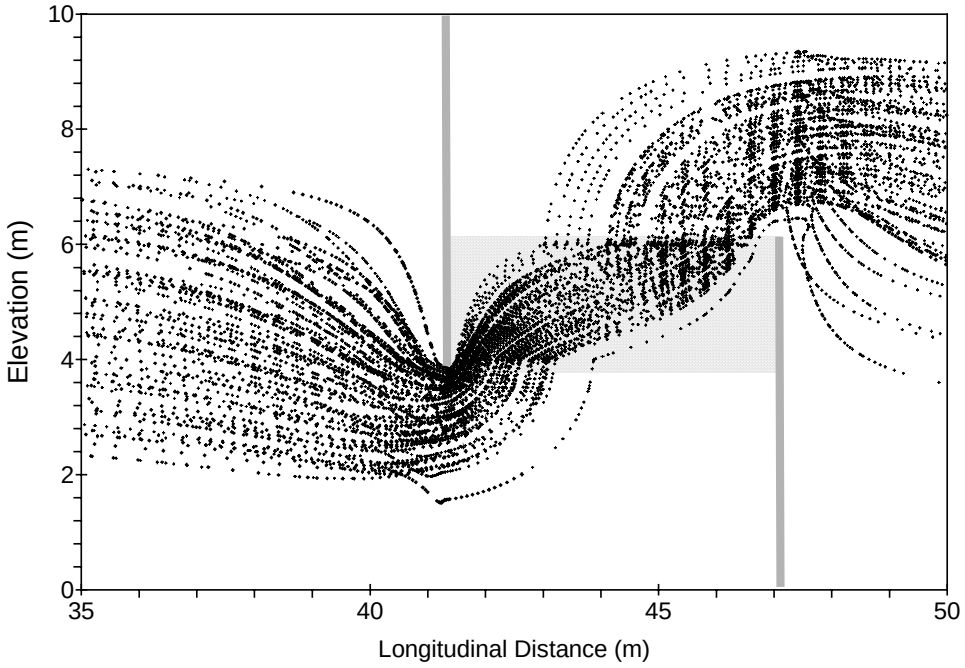

Fig. 7.7 Particle Trajectory Through Caisson Designs A and B.

oval or rectangular caisson that has wide and short openings and a tall, thin plug of reactive media (e.g., Caisson A). This type of CPRB yields lower effluent concentrations because flow passes through all of the reactive media.

7.3.2 Sizing the Funnel

Head loss at the inlet and outlet of a CPRB is proportional to Q (Eq. 7.1), where Q is the volumetric flow rate of water captured by the funnels and entering the PRB. The size of a funnel is selected based on the ability of the funnel to capture the contaminant plume. For wider plumes, a wider funnel is needed; however, a wider funnel channels more water through the CPRB causing greater head loss. As head loss increases, contaminants within the boundaries of the funnel are more likely to take a flow path around the funnel rather than through the CPRB. Thus, the efficiency of a funnel decreases as the funnel gets larger (where efficiency is defined as the additional quantity of water captured for a unit increase in the length of the funnel).

In summary, the design of a funnel for a CPRB poses a difficult problem. The advantage of a CPRB is that it uses reactive media more effectively by channeling groundwater vertically through the caisson. However, if head loss (or Q/A in Eq. 7.1) is too large because of small openings or large funnels, contaminants may pass around the funnels. This condition becomes a greater problem for wider plumes and heterogeneous aquifers. This design problem is a significant disadvantage of CPRBs. The present study examines the effectiveness of CPRBs, but an extensive study on the design of funnels in heterogeneous

aquifers requires a significant amount of attention that is beyond the scope of this report. However, this topic warrants further investigation.

Until the design of funnels in heterogeneous aquifers is better understood, CPRBs are ideal for retrofitting into existing containment systems. CPRBs are well suited for installation in a slurry wall surrounding a contaminated site. A CPRB can be driven across the slurry wall, drilled out, and filled with reactive media. Such a system can then serve as a discharge point for water entering the contaminated site by recharge. For this system, capture would almost be guaranteed and the system would operate passively, replacing the current means for discharging water such as a pump and treat system.

7.4 EFFECT OF PRB HETEROGENEITY

Distributions of influent and effluent concentration for CPRBs with various K_P and k_r in an aquifer with μ_{lnK} = -10 (4.54×10^{-5} m/s), σ_{lnK} = 1.0, λ_x = 3 m, and λ_y = 1 m are shown in Fig. 7.8. Table 7.1 summarizes the K_p and k_r used for these simulations.

Table 7-1 Input Parameters for Simulating CPRB Heterogeneity.

K_p (m/s) (Normally Distributed)		k_r (d^{-1}) (Normally Distributed)		$\rho(K_p,k_r)$
Mean	Std. Dev.	Mean	Std. Dev.	
2.5×10^{-3}	0	1.0	0	-
2.5×10^{-4}	0	1.0	0	-
2.5×10^{-3}	0	0.9	0	-
2.5×10^{-3}	0	1.1	0	-
2.5×10^{-3}	1.0×10^{-4}	1.0	0	-
2.5×10^{-3}	0	1.0	0.05	-
2.5×10^{-3}	1.0×10^{-4}	1.0	0.05	0
2.5×10^{-3}	1.0×10^{-4}	1.0	0.05	1
2.5×10^{-3}	1.0×10^{-4}	1.0	0.05	-1
2.5×10^{-3}	1.0×10^{-4}	1.0	0.22	0

a) Influent Concentrations

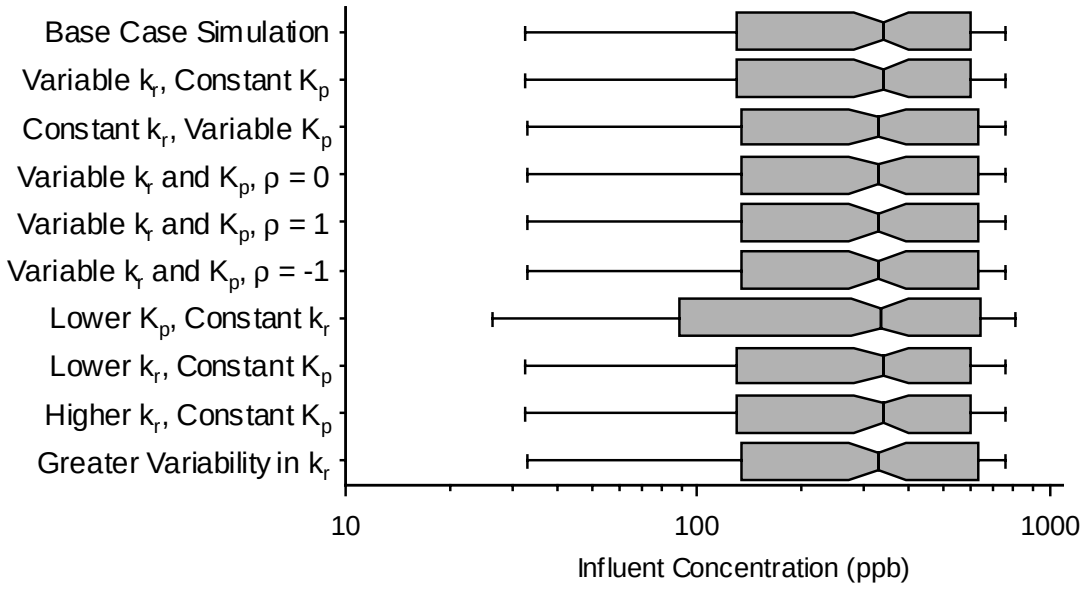

b) Effluent Concentrations

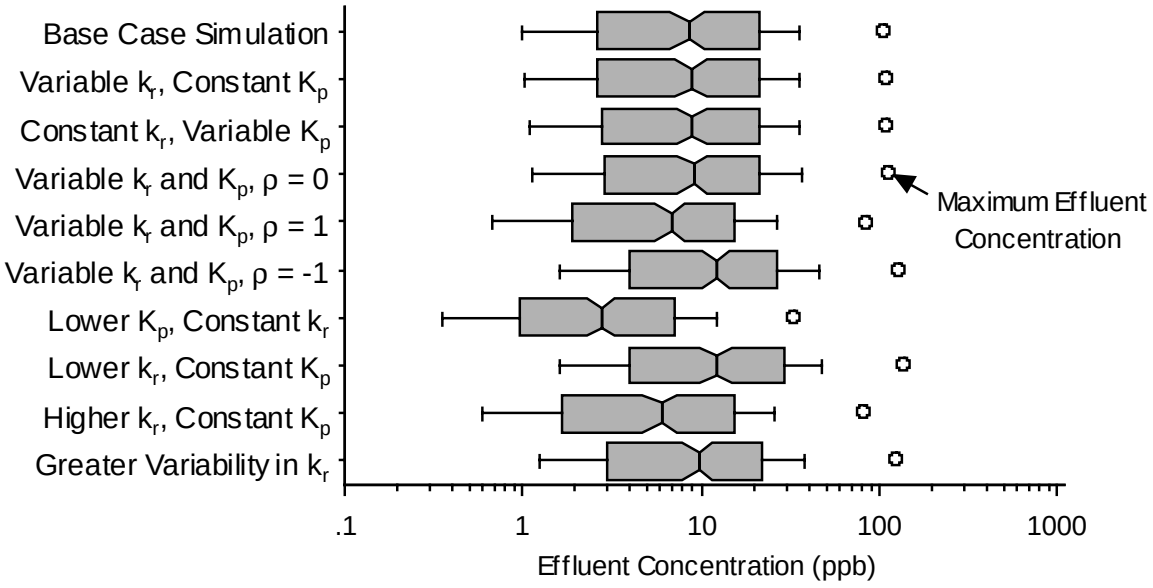

Fig. 7.8 Distributions of Influent and Effluent Concentration for Heterogeneous CPRBs in Aquifers with μ_{lnK} = -10, σ_{lnK} = 1, λ_x = 3 m, and λ_y = 1 m.

Distributions of influent concentration are only slightly affected by variations in K_p, k_r, or uniform changes in k_r. Influent concentrations shift toward lower concentrations when the K_p decreases by an order of magnitude (Fig. 7.8a). When K_p decreases, the higher and lower influent concentrations increase and decrease, respectively. These changes occur because the head loss through the CPRB increases, causing water to build-up behind the PRB. This increases the size and decreases the concentration of the plume, particularly at the edges. Consequently, influent concentrations decrease slightly with decreasing K_p, with the most dramatic change occurring in the lower concentrations that coincide with the edges of the influent plume.

Effluent concentrations are nearly identical for CPRBs that have spatially varying K_p or k_r (Fig. 7.8b). Spatially varying K_p or k_r does not affect effluent concentrations because of the redundancy of the system. Between the influent and effluent ends of the PRB, groundwater passes a sufficient distance so that contaminants are exposed to average conditions before being discharged. Thus, effluent concentrations for heterogeneous and homogeneous CPRBs are nearly identical.

Varying K_p and k_r have little effect on effluent concentrations when K_p and k_r are independent (i.e., $\rho = 0$). However, when K_p and k_r are positively correlated (i.e., when $\rho = 1$, so that higher K_p yields larger k_r), effluent concentrations decrease, and when K_p and k_r are negatively correlated (i.e., when $\rho = -1$, so that higher K_p yields lower k_r) effluent concentrations increase. These results are logical knowing that groundwater and contaminants prefer pathways of higher

hydraulic conductivity. When $\rho = 1$, contaminants are exposed to higher k_r so that more mass is reduced and effluent concentrations are lower. When $\rho = -1$, contaminants are exposed to lower k_r so that less mass is reduced during a given residence time and effluent concentrations are higher.

A 10% decrease in k_r increases effluent concentrations whereas a 10% increase in k_r decreases effluent concentrations (Fig. 7.8b). This response was observed for the HFPRB and FGPRB and occurs because reactions are faster at higher k_r or slower at lower k_r, but the residence time of contaminants in the reactive media is the same. Thus, the change in effluent concentration responds accordingly to the change in k_r predicted by Eq. 2.1. Thus, effluent concentrations for any k_r can be predicted once the distribution of effluent concentration for one k_r is known. This is useful for comparing different reactive media or estimating temporal changes in effluent concentration if the reactive media loses its reactivity.

The most surprising result shown in Fig. 7.8b is that an order of magnitude decrease in K_p caused a 50% decrease in effluent concentrations. Changing K_p did not change effluent concentrations from the HFPRB or FGPRB. The cause for lower effluent concentrations with decreasing K_p is that less water flows through the CPRB and more water flows around the funnel. Decreases in K_p may occur due to scaling or particulate clogging and should affect CPRBs more than the other types of PRsB. Furthermore, the results shown in Fig. 7.8b imply that lower K_p yields lower effluent concentration, but this result is misleading because the capture zone of the funnel also decreases and the likelihood of contaminants flowing around the funnels is greater. Thus, the hydraulic conductivity of the reactive media is more

important to CPRB design than HFPRB or FGPRB design, and there is a greater need for locating monitoring wells at the ends of the funnels for a CPRB system.

7.5 EFFECT OF AQUIFER HETEROGENEITY

7.5.1 Effect of μ_{lnK}

The effect of changing μ_{lnK} on influent and effluent concentrations was evaluated by simulating a homogeneous CPRB ($K_p = 2.5x10^{-3}$ m/s and $k_r = 1.0$ d^{-1}) in aquifers with μ_{lnK} of -9 ($1.23x10^{-4}$ m/s), -10 ($4.54x10^{-5}$ m/s), -11 ($1.67x10^{-5}$ m/s), and -12 ($6.14x10^{-6}$ m/s) with $\sigma_{lnK} = 1.0$, $\lambda_x = 3$ m, and $\lambda_y = 1$ m. Distributions of influent and effluent concentration are shown in Fig. 7.9.

Varying μ_{lnK} has the same impact on the CPRB that it had on the HFPRB and FGPRB. Namely, influent concentrations do not change but distributions of effluent concentration shift toward lower concentration and broaden as μ_{lnK} decreases. Influent concentration is not affected by μ_{lnK} because aquifers with lower μ_{lnK} have lower hydraulic conductivities but the same spatial distribution of hydraulic conductivity. Thus, contaminants travel slower, but the distribution of concentration caused by heterogeneity does not change since reactivity in the aquifer is not simulated. If reactions occur in the aquifer, influent concentrations would be lower for smaller μ_{lnK}.

Effluent concentrations decrease for smaller μ_{lnK} because the hydraulic conductivity of the aquifer is lower, causing seepage velocities in the aquifer and consequently through the PRB to be smaller. As the residence time for

a) Influent Concentration

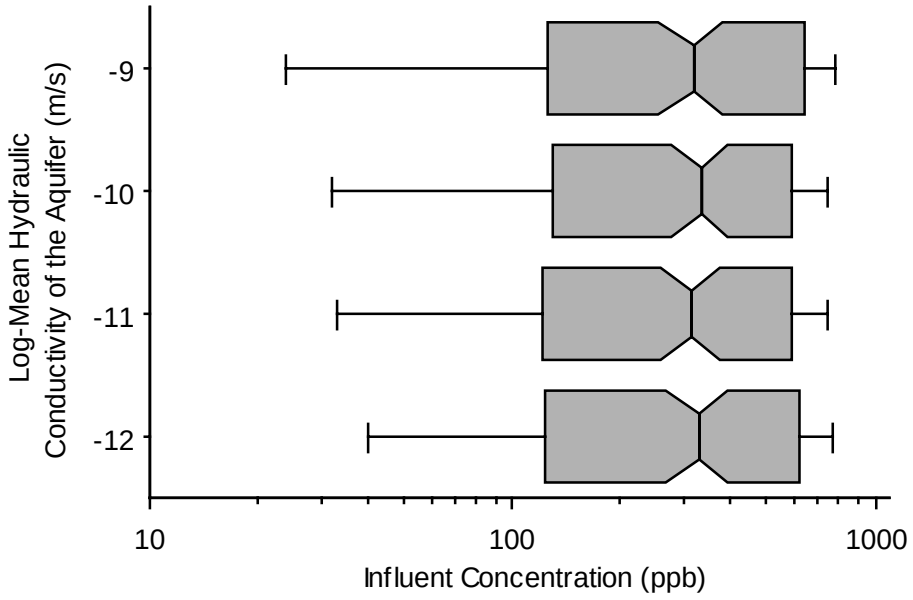

b) Effluent Concentration

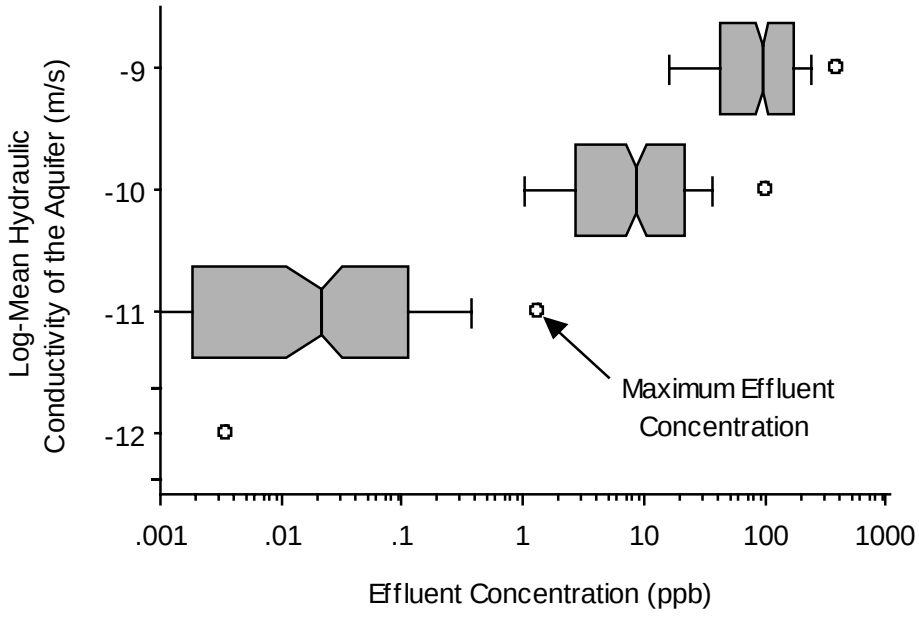

Fig. 7.9 Distributions of Influent and Effluent Concentration for Homogeneous CPRBs in Aquifers with Different μ_{lnK}.

contaminants in the reactive media increases, effluent concentrations are lower. The shift in median effluent concentration is approximately equal to the change in effluent concentration calculated using a first order rate equation and plug flow model. For example, a decrease in μ_{lnK} from -10 to -11 increases the mean residence time of contaminants in the reactive media by 271% (i.e., = e^1).

Distributions of effluent concentration broaden with decreasing μ_{lnK} due to the presence of higher hydraulic conductivity units in the aquifer (Fig. 5.14). These units, which exist even in aquifers with lower μ_{lnK}, have a strong effect on advective transport and cause higher effluent concentrations. The combination of higher concentrations due to a small fraction of more permeable units in the aquifer and decreasing median concentration causes the distribution of effluent concentration to broaden as μ_{lnK} decreases.

7.5.2 Effect of σ_{lnK}

The effect of changing σ_{lnK} on influent and effluent concentrations was evaluated by simulating a homogeneous CPRB (K_p = 2.5x10^{-3} m/s and k_r = 1.0 d^{-1}) in aquifers with σ_{lnK} of 0, 0.25, 1.0, 2.25, and 4.0 with μ_{lnK} = -10 (4.54x10^{-5} m/s), λ_x = 3 m, and λ_y = 1 m. Distributions of influent and effluent concentration are shown in Fig. 7.10.

Influent concentrations decrease and become more spread as σ_{lnK} increases (i.e., more heterogeneous aquifers) because greater mixing at larger σ_{lnK} cause influent plumes to be larger and thus more dilute. A larger change in the

a) Influent Concentration

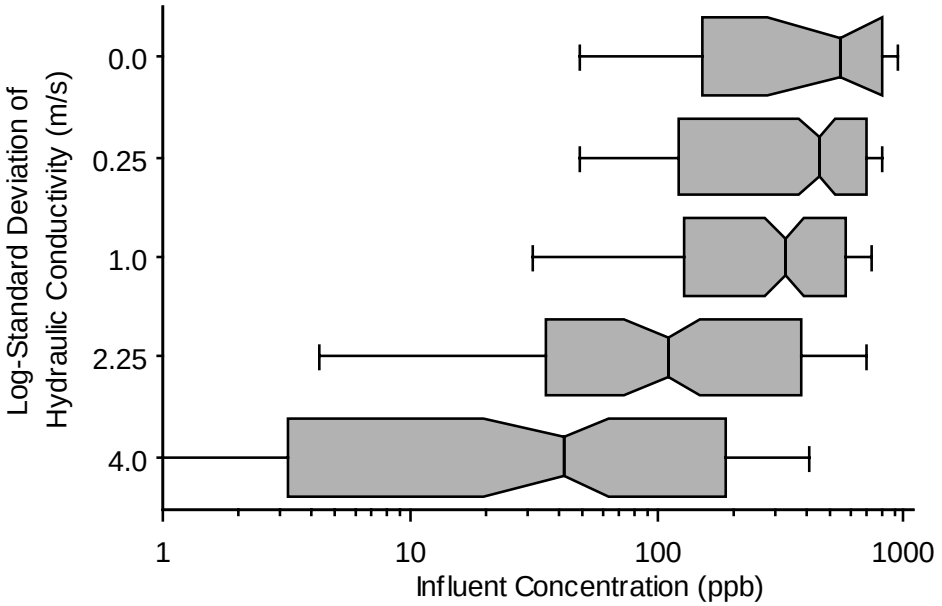

b) Effluent Concentration

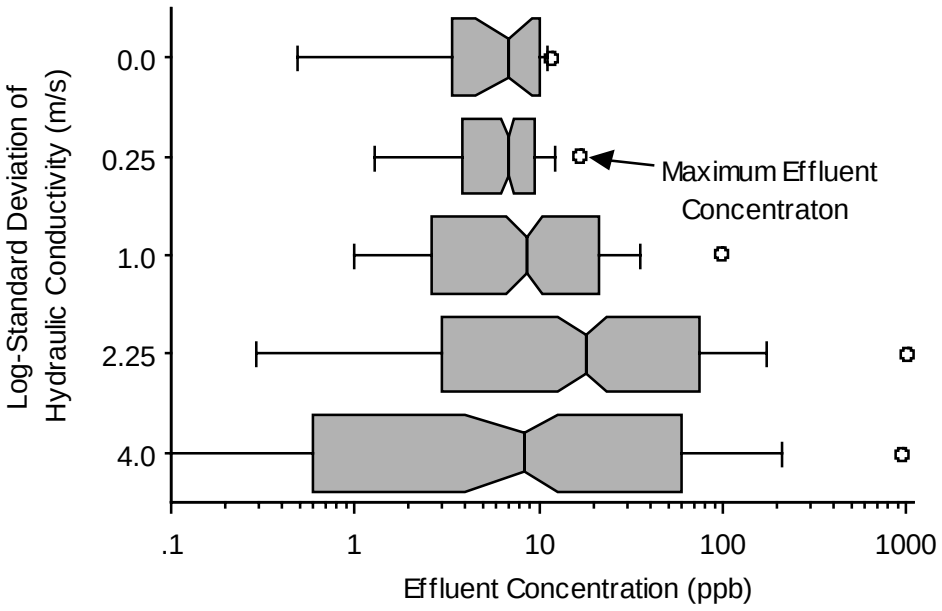

Fig. 7.10 Distributions of Influent and Effluent Concentration for Homogeneous CPRBs in Aquifers with Different σ_{lnK}.

distribution of influent concentrations occurs between σ_{lnK} of 1.0 and 2.25 than for σ_{lnK} less than 1.0 or greater than 2.25. As with the HFPRB, this occurs because more units of higher hydraulic conductivity develop between σ_{lnK} of zero and 2.25 than at σ_{lnK} greater than 2.25 (Fig. 5.17). For $\sigma_{lnK} < 1.0$, zones of varying hydraulic conductivity exist; however, the CPRB forces groundwater flow to converge and move downward, reducing the impact of variations in hydraulic conductivity. are dampened. Not until $\sigma_{lnK} > 1.0$ does the hydraulic conductivity vary to a large enough degree that equivalent hydraulic conductivities along flow paths from the source zone to the CPRB are different enough to spread the distribution of influent concentration. In contrast, the HFPRB does not force groundwater to follow a specific path; thus smaller differences in the distribution of hydraulic conductivity (i.e., $0.25 < \sigma_{lnK} < 1.0$) affect influent concentrations.

Distributions of effluent concentration for a CPRB at different σ_{lnK} resemble effluent concentrations for a FGPRB at different σ_{lnK} (Fig. 7.10b). Distributions of effluent concentration broaden with increasing σ_{lnK}, but median effluent concentrations for all σ_{lnK} vary over small range between 8 and 20 ppb. Unlike the HFPRB and FGPRB, the highest median effluent concentration is for $\sigma_{lnK} = 2.25$, not $\sigma_{lnK} = 4.0$. This appears odd until influent concentrations are considered. Median influent concentration for $\sigma_{lnK} = 4.0$ is 40 ppb but 110 ppb for $\sigma_{lnK} = 2.25$ (Fig. 7.10a), and the median effluent concentration for $\sigma_{lnK} = 4.0$ is 8 ppb but 19 ppb for $\sigma_{lnK} = 2.25$. Thus, on average, a 500% reduction occurs for $\sigma_{lnK} = 4.0$ and 580% reduction occurs for $\sigma_{lnK} = 2.25$. Therefore, the median residence time for

σ_{lnK} = 2.25 is three times longer than for σ_{lnK} = 4.0 (Fig. 7.11), but the longer residence time for σ_{lnK} = 2.25 is not sufficient to compensate for the lower influent concentration at σ_{lnK} = 4.0.

Distributions of effluent concentration also broaden as σ_{lnK} increases due to the increased range of influent concentration and residence times of groundwater in the CPRB. The combined result of more variable influent concentrations and residence times at larger σ_{lnK} is a broader distribution of effluent concentration.

In summary, σ_{lnK} has significant effects on influent and effluent concentrations and on residence times. Influent concentrations decrease and become more spread as σ_{lnK} increases. Once in the CPRB, contaminants have a shorter median and wider range of residence times at lower σ_{lnK}. Differences in median influent concentration are offset by differences in residence time (e.g., lower influent concentration and shorter residence times occur for larger σ_{lnK}) so that the median effluent concentrations at σ_{lnK} between zero and 4.0 are similar. However, the range of influent concentration and variability in residence time causes effluent concentrations to be more distributed at larger σ_{lnK}.

7.5.3 Effect of Correlation Scale

The effect of changing λ_x and λ_y on influent and effluent concentrations was evaluated by simulating a homogeneous CPRB (K_p = 2.5x10^{-3} m/s and k_r = 1.0 d^{-1}) in aquifers with λ_x and λ_y of 3 m and 1 m, 6 m and 2 m, 9 m and 3 m, 6 m and 5 m,

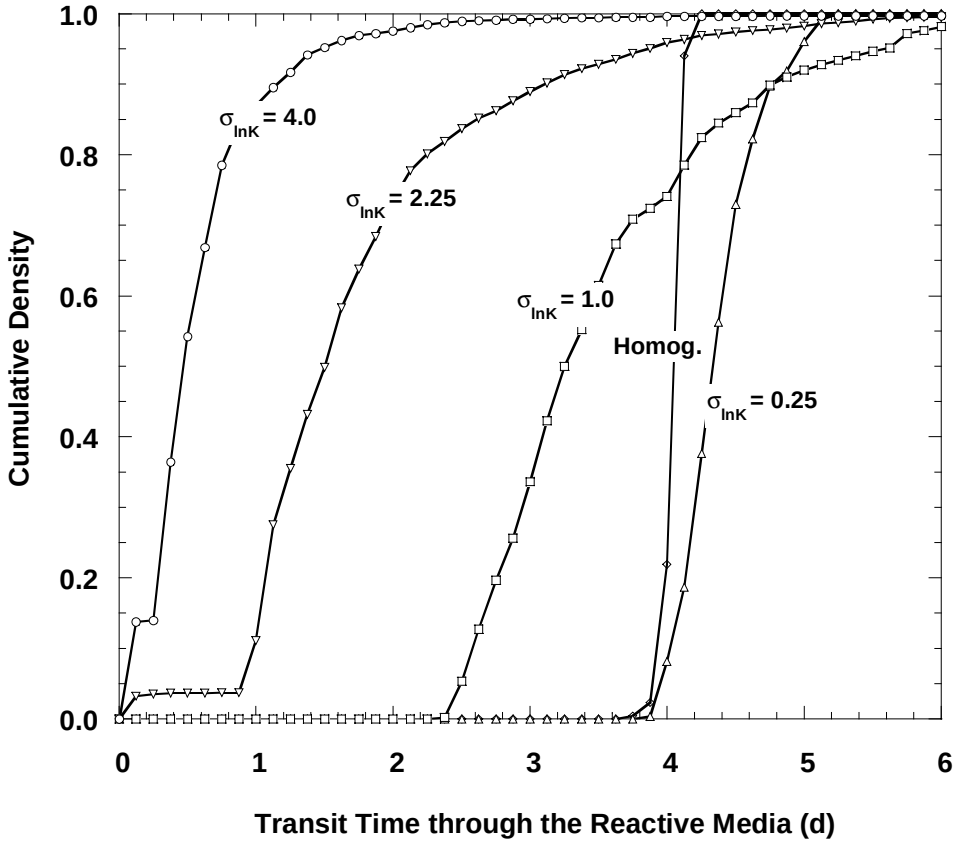

Fig. 7.11 Cumulative Distributions of Particle Residence Time Traversing a Homogeneous CPRB in Aquifers with Different σ_{lnK}.

and 6 m and 1 m. For these simulations μ_{lnK} = -10 ($4.54x10^{-5}$ m/s) and σ_{lnK} = 1.0. Distributions of influent and effluent concentration are shown in Fig. 7.12.

Influent concentrations are affected little by changing λ_x and λ_y. Slight shifts in influent concentration occur, but these appear to be caused by differences in the random fields. Random fields with different λ have different spatial distributions of hydraulic conductivity. In contrast, changing μ_{lnK} or σ_{lnK} scales the magnitude, but not the spatial distribution of hydraulic conductivity.

Changing λ shifts the distribution of effluent concentration slightly. Doubling λ_x results in a 40% decrease in effluent concentration whereas doubling λ_y causes a 25% increase in effluent concentration. However, the net effect of greater correlation (i.e., increasing λ_x and/or λ_y) is less than half an order of magnitude shift in effluent concentrations, which is minor relative to the effect of μ_{lnK}. In summary, increasing λ_x decreases effluent concentration and increasing λ_y increases effluent concentration, but the impact of λ is small relative to the effects of μ_{lnK} and σ_{lnK}.

a) Influent Concentration

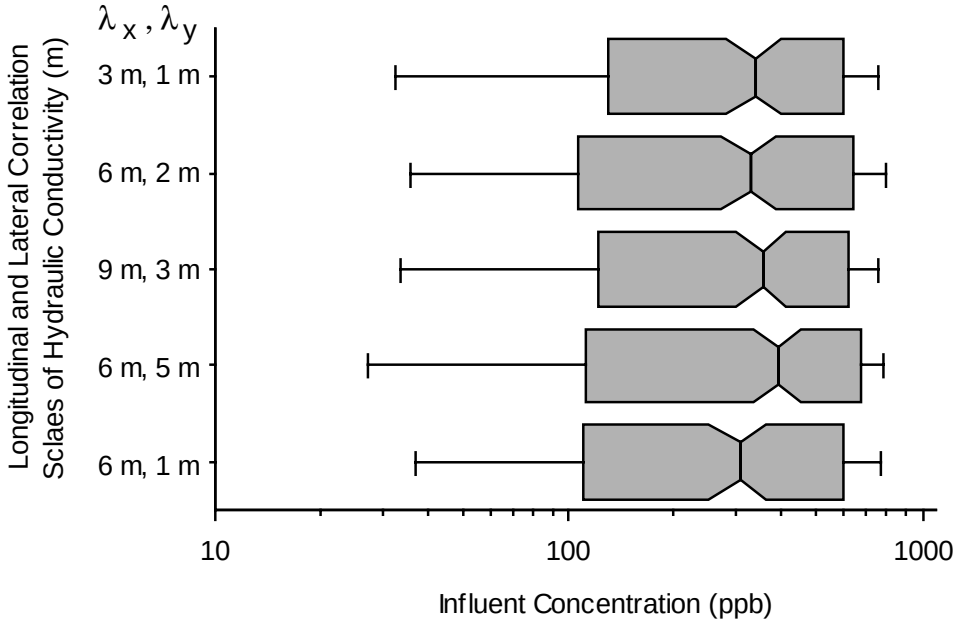

b) Effluent Concentration

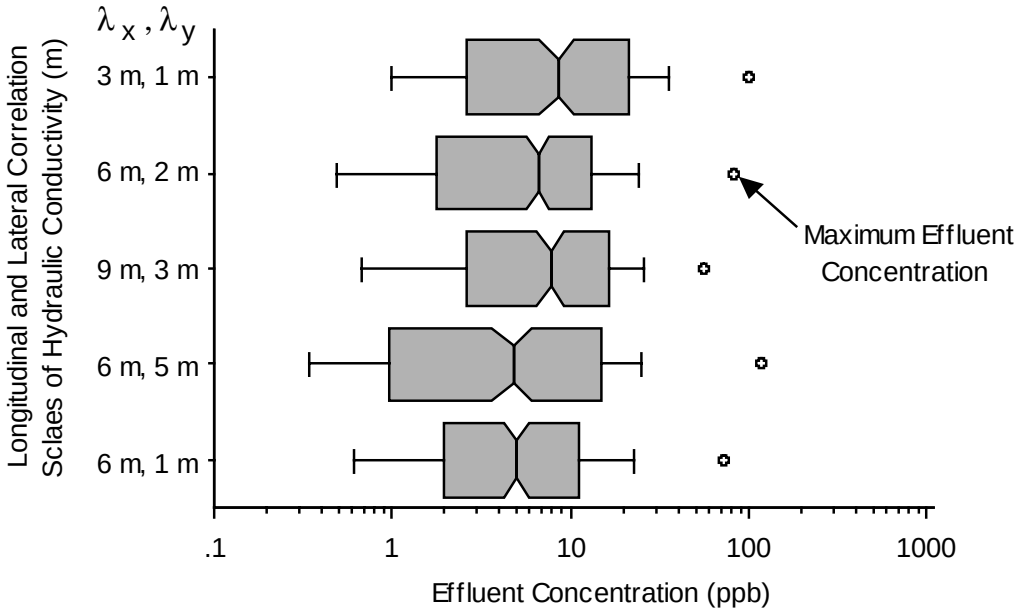

Fig. 7.12 Distributions of Influent and Effluent Concentration for Homogeneous CPRBs in Aquifers with Different λ_x and λ_y.

7.6 COMPARISON OF CPRBs WITH FGPRBs

Influent and effluent concentrations for a CPRB and FGPRB are compared in this section. A FGPRB and HFPRB were compared in Section 6.7, and all three types of PRBs will be compared in Section 8. Distributions of influent and effluent concentration for a FGPRB and CPRB in aquifers with μ_{lnK} = -10 (K = 4.5x10^{-5} m/s) and –11 (K = 1.7x10^{-5} m/s) are shown in Fig. 7.13. For the simulations shown in Fig. 7.13, σ_{lnK} = 1.0, λ_x = 3 m, λ_y = 1 m, and the PRBs are homogeneous (K_p = 2.5x10^{-3} m/s and k_r = 1.0 d^{-1}). The two PRBs each have 50 m^3 of reactive media, although the CPRB has a wider funnel.

Influent and effluent concentrations are lower for the CPRB than for the FGPRB. Influent concentrations are slightly lower because groundwater is diluted more prior to entering the CPRB than the FGPRB. A FGPRB system forces groundwater to converge before entering the PRB; however, the CPRB forces groundwater to converge and move vertically prior to entering the PRB. Vertical flow required by the CPRB causes more head loss and a larger plume up-gradient of the PRB (and also requires longer funnels to be used). Concentrations are more dilute in larger plumes, reducing influent concentrations.

Lower influent concentrations and more effective use of the reactive media cause effluent concentrations from a CPRB to be lower than effluent concentrations from a FGPRB. Difference in effluent concentration between the two types of PRB are greater than the differences expected in influent concentrations, indicating that the CPRB uses reactive media more effectively than

a) Influent Concentrations

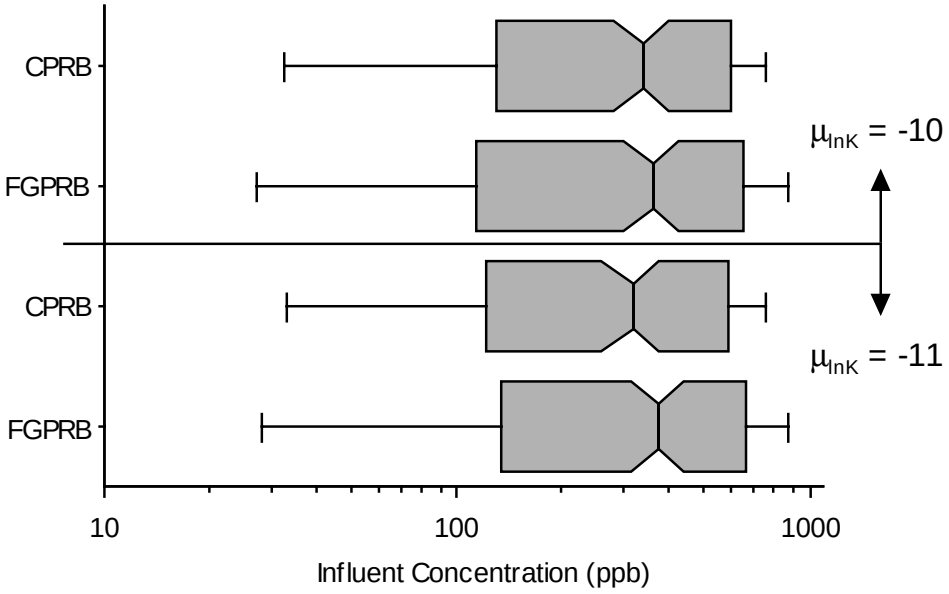

b) Effluent Concentration

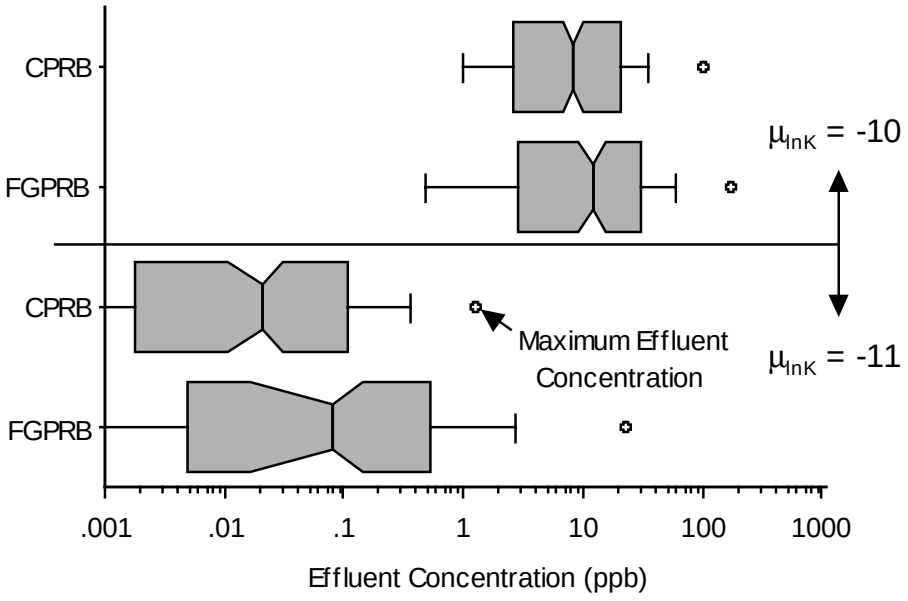

Fig. 7.13 Distributions of Influent (a) and Effluent (b) Concentration for a Homogeneous CPRB and FGPRB in Aquifers with Different μ_{lnK}.

the FGPRB (Fig. 7.7a). This result is consistent with the design of the CPRB, which is expected to use the reactive media more efficiently and have more uniform residence times.

A unit decrease in μ_{lnK} causes a greater decrease in effluent concentration for the CPRB than for the FGPRB (Fig. 7.13b). Thus, CPRBs perform better in less permeable aquifers than FGPRBs due to the differences in flow paths between the two PRBs. Since the CPRB forces groundwater through more zones of different hydraulic conductivity, contaminants flow through the aquifer along paths that have a hydraulic conductivity closer to the geometric mean hydraulic conductivity of the aquifer.

Distributions of influent and effluent concentration for a FGPRB and CPRB in aquifers with σ_{lnK} = 1.0 and 4.0 are shown in Fig. 7.14. Influent concentrations are slightly lower for a CPRB at σ_{lnK} = 1.0, but slightly lower for the FGPRB at σ_{lnK} = 4.0. As the differences are small, the two PRBs are equally effective at diluting influent concentrations. Effluent concentrations are lower for the CPRB than for the FGPRB with a greater difference at larger $\sigma_{lnK.}$ Thus, the CPRB accounts for higher variability in hydraulic conductivity (and flow) better than the FGPRB.

a) Influent Concentration

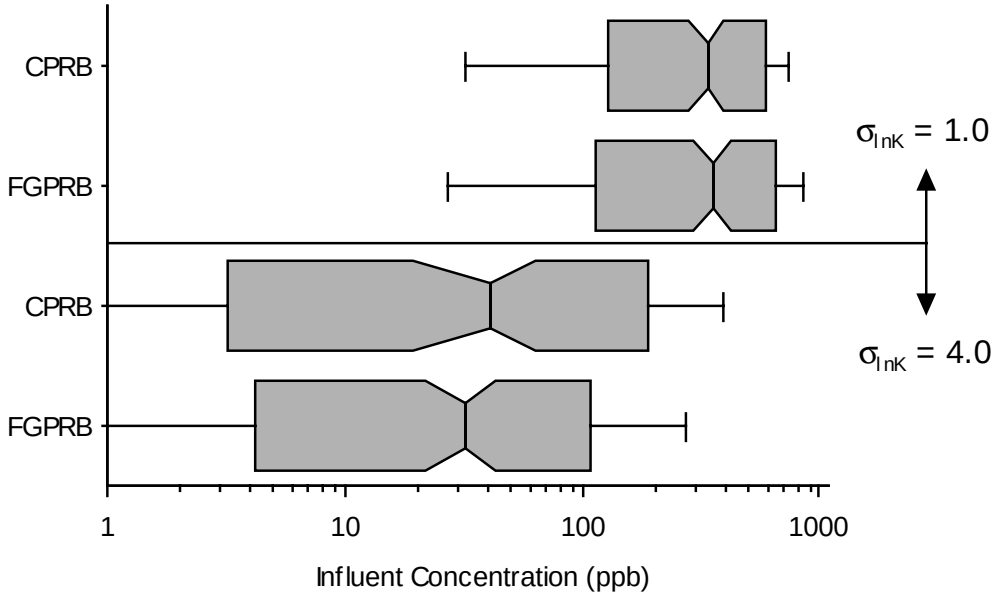

b) Effluent Concentration

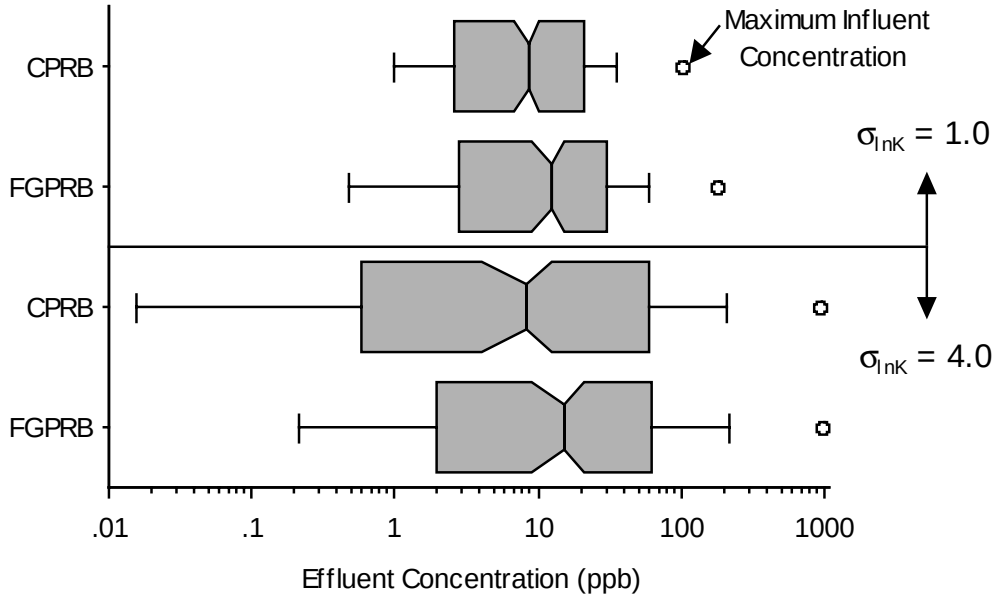

Fig. 7.14 Distributions of Influent (a) and Effluent (b) Concentration for Homogeneous CPRBs and FGPRBs in Aquifers with Different σ_{lnK}.

SECTION 8

COMPARISON OF PRB TYPES

The impact of aquifer and barrier heterogeneity on influent and effluent concentrations for HFPRBs, FGPRBs, and CPRBs was investigated in Sections 5, 6, and 7 using parametric studies. The next four sections evaluate the engineering aspects of HFPRBs, FGPRBs, and CPRBs. Section 8 is a comparison of the three types of PRB on a basis of equal volume of reactive media and cost for equal performance. In Section 9, the effectiveness of current design models is investigated, and a new method that directly considers aquifer heterogeneity and risk is proposed. In Section 10, the likelihood of detecting the median, 75th percentile, and 90th percentile of effluent concentration are calculated, and recommendations are made for the most economical monitoring systems. In Section 11, additional considerations for the design and construction of PRBs are discussed, including the effect of gravel zones at the influent and/or effluent faces of a PRB and several topics for future investigation that pertain to the effectiveness of PRBs, but are beyond the scope of this report.

8.1 CONCEPTUAL MODEL

Influent and effluent concentrations from HFPRBs, FGPRBs, and CPRBs are compared in this section, based on (1) capturing and treating a contaminant plume with PRBs contain 25 m^3 of reactive media, and (2) the cost of PRBs that produce the same effluent concentration regardless of the volume of reactive

media. These simulations use a different aquifer and source than previous simulations to facilitate comparison with previous results. Simulations were performed using an aquifer with μ_{lnK} = -10.5 (K = 2.75x10^{-5} m/s), σ_{lnK} = 1.5, λ_x = 5 m, and λ_y = 2 m. The aquifer is 83.8 m long, 65 m wide, 10 m high, and contains 702,000 finite difference cells. A gradient of 0.005 (0.01 for previous simulations) is imposed across the aquifer using constant head boundaries. Each type of PRBs is positioned in the center of the aquifer, and a 10 m wide by 5 m high strip source is located 20 m up-gradient of the influent face of the PRB. The source is located along the lateral and vertical centerlines of the aquifer and has a constant concentration of 1000 ppb.

8.2 CONSTANT VOLUME OF REACTIVE MEDIA

A HFPRB, FGPRB, and CPRB were designed that fully capture the contaminant plume but contain only 25 m^3 of reactive media. The effective use of reactive media by each type of PRB is measured by comparing effluent concentrations from each design.

Particle trajectories through the aquifer when no PRB is used are shown in Fig. 8.1a. Contaminants move from the source zone (1000 ppb concentration), dispersing as they travel through the aquifer. At X = 41.3 m (location of the influent face of the PRB) the plume is 10 m wide and 9 m high. Concentrations at this distance are between 40 (5th percentile) and 1000 ppb, with a median of 520 ppb.

The HFPRB designed for this plume and aquifer is 20 m wide, 10 m high (fully penetrating), and 0.125 m thick (Fig. 8.1b). The FGPRB designed for this

a) No PRB

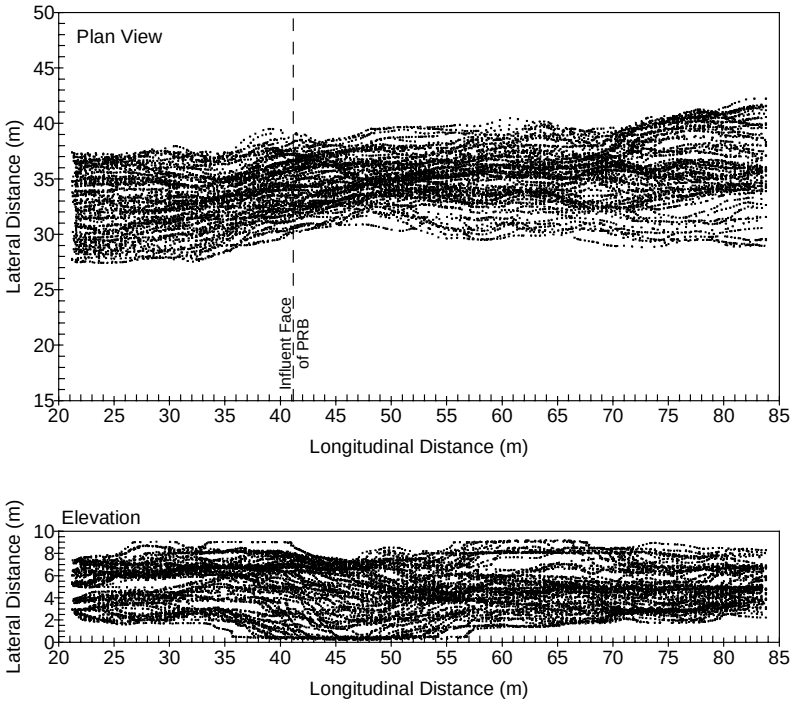

b) HFPRB

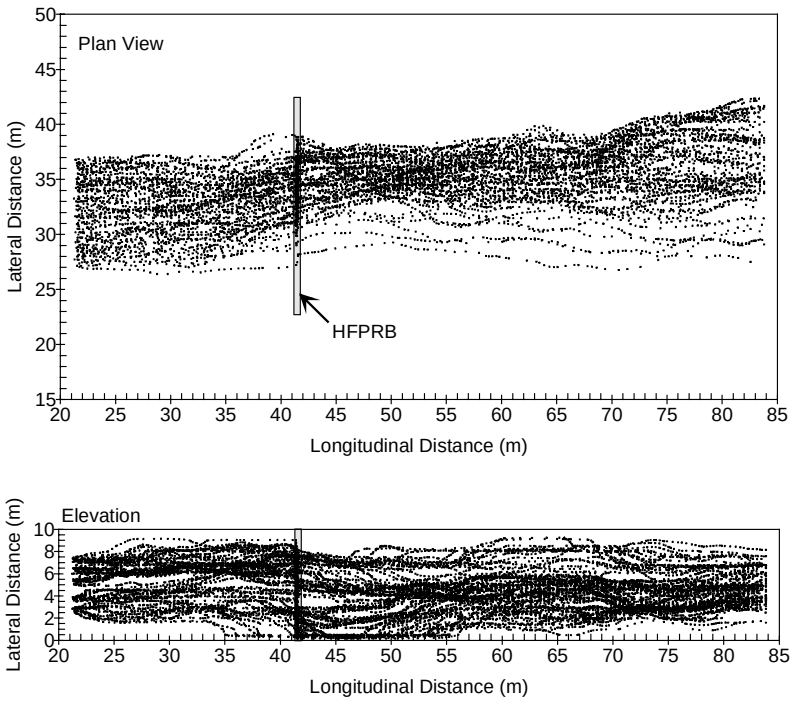

c) FGPRB

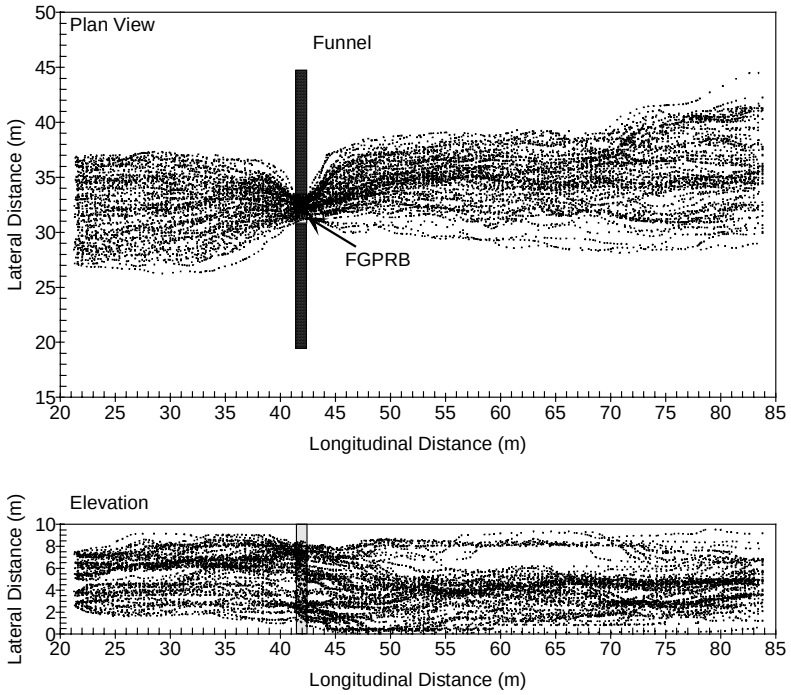

d) CPRB

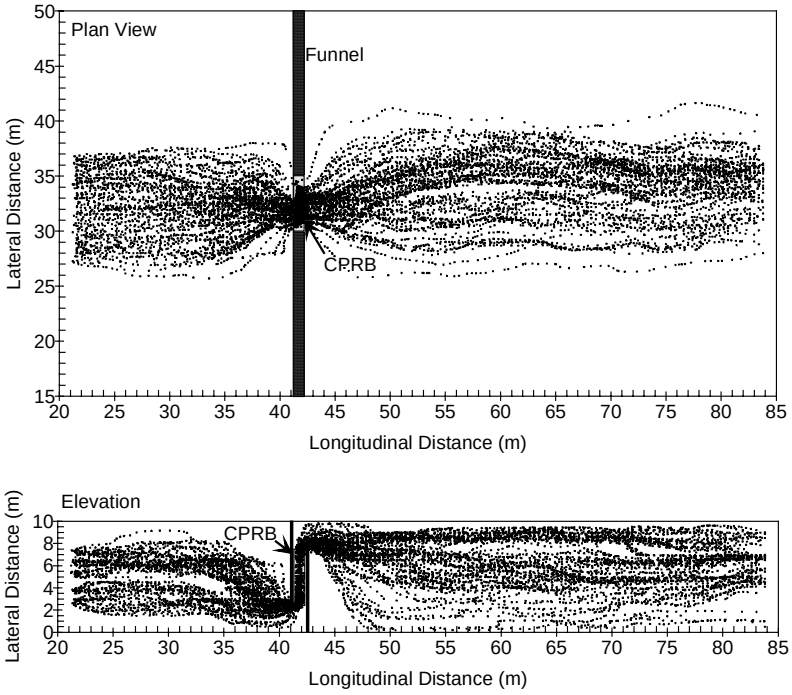

Fig. 8.1 Particle Trajectories Through the Aquifer and Each Type of PRB.

aquifer is 2.5 m wide, 10 m high (fully penetrating), and 1.0 m thick. On either side of the gate are 11.25 m wide by 10 m high funnel walls (Fig. 8.1c). The CPRB designed for this aquifer and plume is a single 5 m wide by 1 m thick caisson. The caisson has 2.5 m high by 5 m wide openings on the influent and effluent faces, and a 5 m tall by 5m wide by 1 m thick plug of reactive media. Groundwater is funneled into the CPRB by 20 m wide by 10 m high funnel walls on either side of the CPRB (Fig. 8.1d).

The HFPRB causes little change in particle trajectory (Fig. 8.1b). The plume is still approximately 10 m wide and 9 m thick when it enters the HFPRB. No particles cross the outer edges or top of the PRB. Within the PRB, some particles appear to move downward, but most particles follow a similar trajectory as shown in Fig 8.1a. The FGPRB and CPRB significantly change the trajectory of particles in the aquifer. The plume on either side of the FGPRB is approximately 12 m wide and 9 m high, while the plume is approximately 15 m wide on the up-gradient side of the CPRB and 23 m wide on the down-gradient side of the CPRB. Groundwater appears to move more diagonally through the FGPRB than the HFPRB, but no particles pass through the top or the bottom of the gate. Vertical flow occurs through the CPRB, and there does not appear to be any regions within the reactive media untouched by particles.

Distributions of influent and effluent concentration from the three PRBs are shown in Fig. 8.2. Influent concentrations for the three PRBs are similar. All have concentrations between 1000 ppb (source concentration) and 10 ppb, with most concentrations >100 ppb. Groundwater concentrations entering the HFPRB and

a) Influent Concentrations

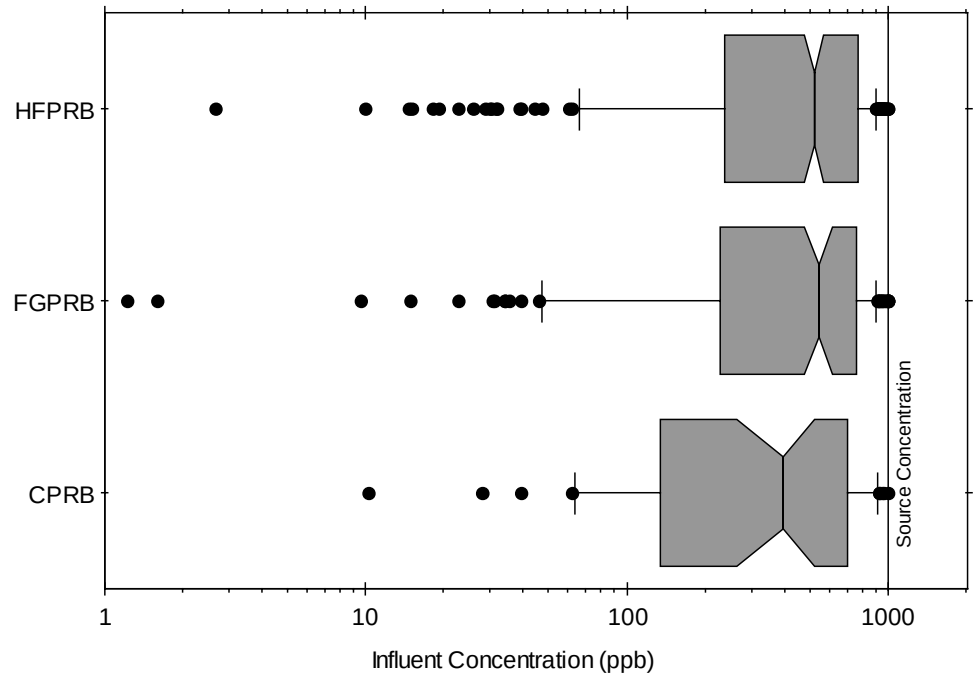

b) Effluent Concentrations

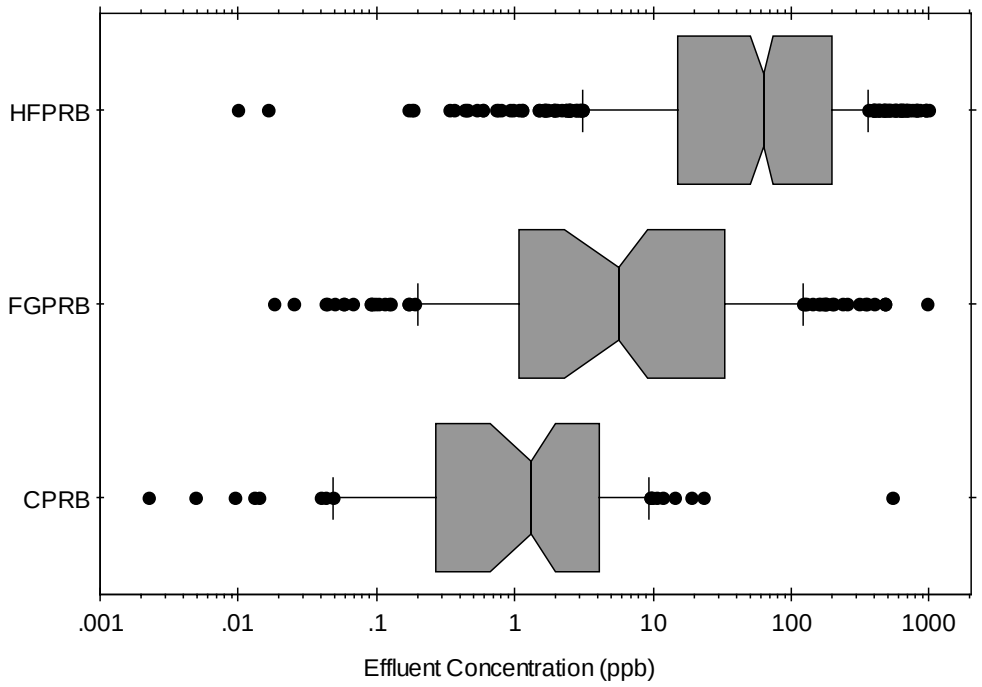

Fig. 8.2 Distributions of Influent (a) and Effluent (b) Concentration for a HFPRB, FGPRB, and CPRB that each have 25 m^3 of Reactive Media.

FGPRB are nearly identical and slightly higher than concentrations entering the CPRB. The CPRB has slightly lower influent concentrations because more water is channeled through the reactive media due to its larger funnel, causing more dilution. Differences in influent concentration between the PRBs are typically less than 30%, which is small relative to differences in effluent concentration. Thus, no type of PRB appears to be significantly more effective at diluting influent concentrations.

Effluent concentrations from the three types of PRB are significantly different. Effluent concentrations are highest for the HFPRB, lowest for the CPRB. Effluent concentrations for the FGPRB are between concentrations for the HFPRB and CPRB.

Effluent concentrations are highest for the HFPRB because it has the thinnest reactive zone (i.e., 0.125 m), compared to 1 m for the FGPRB and 5 m for the CPRB. The HFPRB has such a narrow reactive zone because a 20 m wide by 10 m high PRB is required to capture the containment plume, and the PRB can only contain 25 m^3 of reactive media. Unfortunately mass loadings into the HFPRB are higher in the center of the PRB and lower nearer the edges, causing reactive media at the edges of the PRB to be wasted and reactive media in the center of the PRB to be inadequately thin (Fig. 8.1b). Reactive media in the center of the PRB is so inadequately thin that the maximum effluent concentrations are only slightly lower than influent concentrations, indicating almost complete failure of the PRB.

In summary, a HFPRB design places reactive media as a wide and high, but thin zone in front of the containment plume. Mass loading into a HFPRB is not

uniform because zones of higher hydraulic conductivity dominate flow and mass transport into the PRB, resulting in higher concentrations in the central portion and lower concentrations at the edges, top, and bottom of a HFPRB.

The FGPRB performs significantly better than the HFPRB, yielding effluent concentrations almost an order of magnitude lower than the HFPRB. The FGPRB uses the reactive media more effectively than the HFPRB because the funnel channels lower concentration groundwater into the gate so that the entire lateral dimension of the PRB is exposed to contaminated groundwater (Fig. 8.1c). However, little mass passes through the top or bottom of the FGPRB; thus media in these locations is under-utilized. Nonetheless, the FGPRB attains a reasonable level of performance. The maximum effluent concentration for the FGPRB is approximately 200 ppb, compared to nearly 1000 ppb for the HFPRB and the median effluent concentration is 9 ppb, almost an order of magnitude less than the median effluent concentrations for the HFPRB. In summary, the FGPRB performs better than the HFPRB in heterogeneous aquifers and wastes less reactive media.

The CPRB performs significantly better than the other PRBs, yielding effluent concentrations almost two orders of magnitude less than the HFPRB and an order of magnitude less than the FGPRB. This is not a surprising result because the CPRB is designed to use reactive media more effectively than the other PRBs. The CPRB system forces lateral flow into a reactive gate like the FGPRB, but it also induces vertical flow through the reactive media so that nearly all 25 m^3 of the reactive media is used. Even the maximum effluent concentration is significantly lower for the CPRB than for the HFPRB or FGPRB (i.e., 20 ppb

compared to 200 or 1000 ppb), indicating the CPRB performs better than the other PRBs in heterogeneous aquifers.

The range of the distributions of effluent concentration is narrower for the CPRB than the other types of PRB. This result indicates that residence times and flow through the CPRB are more uniform (i.e., closer to plug flow), which is desirable because reactive media is used more effectively and is more closely approximated by a plug flow model.

8.3 EQUIVALENT PERFORMANCE

A PRB of each type is designed to have an effluent concentration of 10 ppb at the 90^{th} percentile (i.e., 90% of the effluent concentration $\leq$ 10 ppb). The PRBs are designed for the aquifer and source described in Section 8.1. Final designs for the PRBs were obtained by trial and error. These designs are shown in Fig. 8.3. Dimensions and the estimated cost of each are given in Table 8.1. Distributions of influent and effluent concentration for the three PRBs are shown in Fig. 8.4.

The results shown in Fig. 8.3 are not surprising. To attain the same effluent concentration, a HFPRB with 124 m^3 of reactive media is needed, because the HFPRB uses reactive media less efficiently. The same effluent concentrations can be achieved using a FGPRB with about 38% of the reactive media required by the HFPRB. A CPRB that achieves the desired effluent concentration uses the least reactive media (27 m^3), about 22% of the reactive media required by the HFPRB and 56% of the reactive required by the FGPRB. However, the CPRB requires 24

a) HFPRB

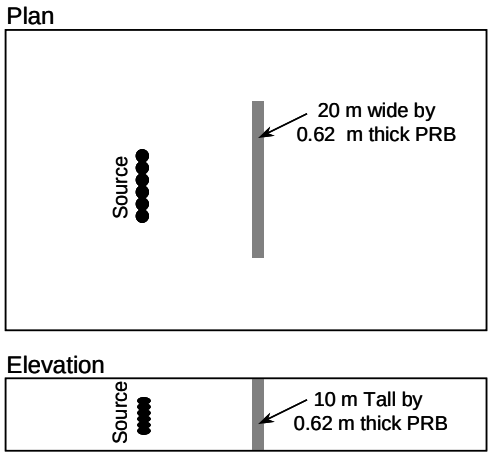

b) FGPRB

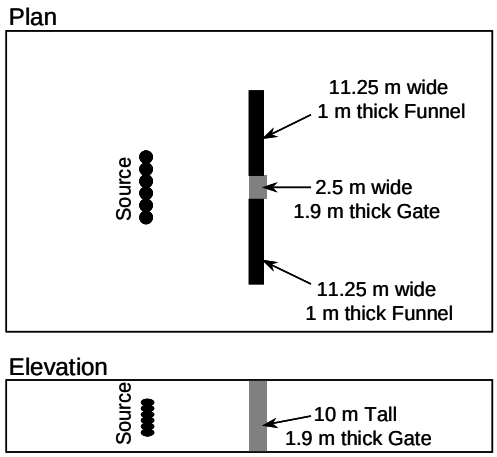

c) CPRB

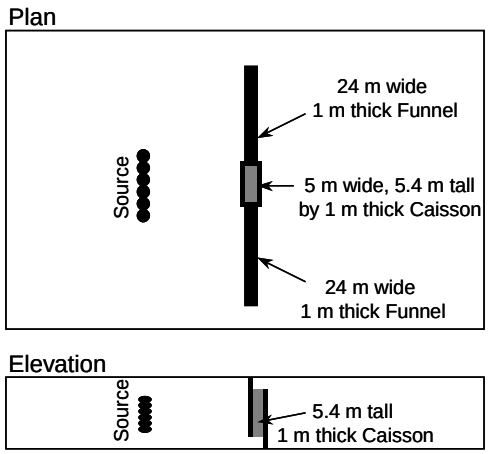

Fig. 8.3 Schematic of a HFPRB (a), FGPRB (b), and CPRB (c) that Each Yield 90% of Effluent below 10 ppb.

a) Influent Concentrations

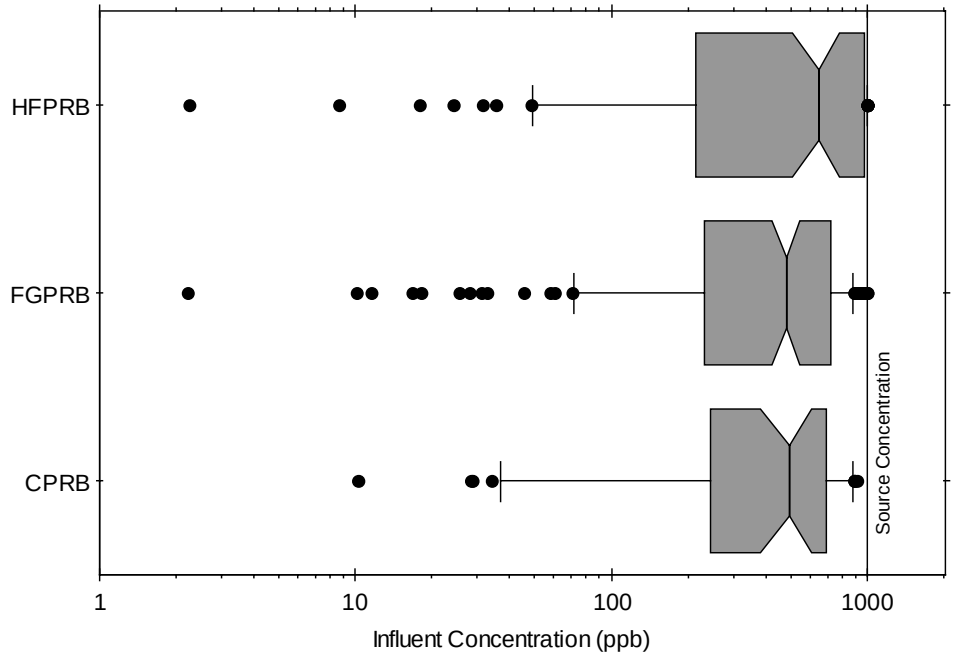

b) Effluent Concentrations

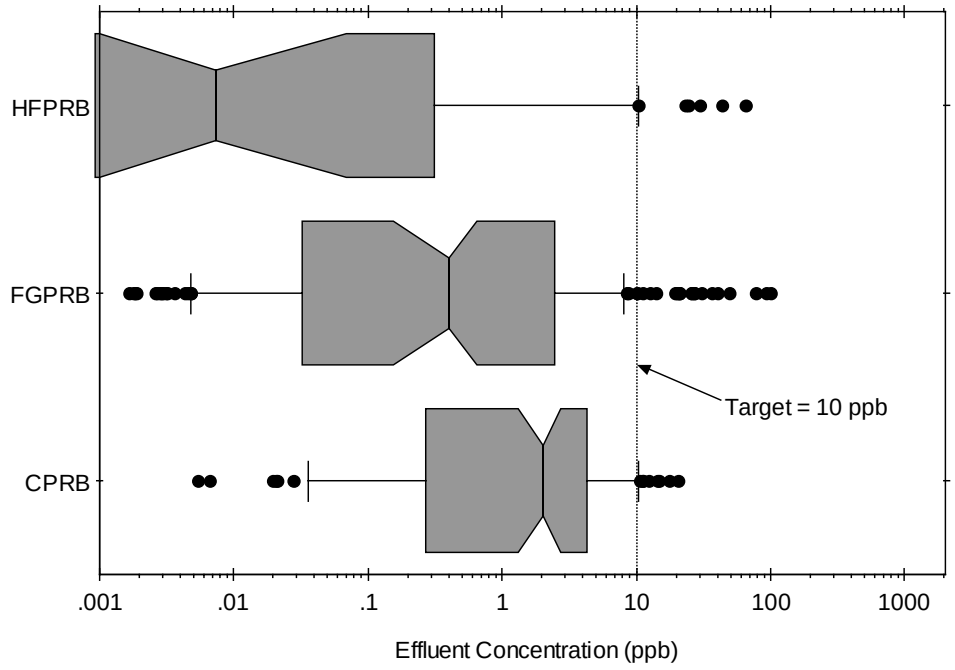

Fig. 8.4 Distributions of Influent and Effluent Concentration for a HFPRB, FGPRB, and CPRB that each Yield the Same Effluent Concentration at the 90th Percentile.

m wide funnel walls (compared to 11.25 m funnel walls for the FGPRB) and a caisson. These additional requirements add to the cost of a CPRB.

Table 8-1 Dimensions and Cost for a HFPRB, FGPRB, and CPRB that have Equivalent Effluent Concentration.

Material, Unit Cost[2], and Dimensions		HFPRB	FGPRB	CPRB
Reactive Media ($1350/m^3)	Width (m)	20	2.5	5
	Depth (m)	10	10	5.4
	Thickness (m)	0.62	1.9	1
	Volume (m^3)	124	47.5	27
Funnel ($65/m^2 + $30^k)	Width (m)	None	22.5	48
	Depth (m)		10	10
Caisson ($375/m^2)	Width (m)	None	None	2@5 x 7.5 m
	Depth (m)			2@1 x 10 m
Total Cost[1] ($)		167,400	108,750	133275

1 – Estimated cost in 1999 US dollars including installation, but not including design, transportation, site preparation, or 15% royalty
2 – Day et al. (1999), Christensen (1999)

8.4 COMPARISON OF COST

The cost for three PRBs that yield equivalent performance is given in Table 8.1. For this analysis, reactive media is assumed to cost $1350/m^3 ($400/ton), slurry wall is assumed to cost $65/m^2 plus $30,000 for mobilization, and sheet piling is assumed to cost $375/m^2 (Day et al. 1999, Christensen 1999). All prices are for installed material but do not include design, transportation, or site preparation costs. As the cost for a caisson was not available, the cost for constructing a 5 m by 1 m box of steel sheet piling was used. A sheet pile caisson

is a reasonable means for constructing a square caisson with the appropriate positioned and sized openings.

The HFPRB is the most expensive alternative, costing $167,400. Although it is more expensive alternative considering materials and construction, the design of HFPRBs is relatively simple. Thus, once design costs are included, cost disparities between the HFPRB and other PRBs should be less. The CPRB is the next cheapest alternative, costing 20% less than the HFPRB. The CPRB saves money by using less reactive media than the other types of PRB; however, the CPRB requires a caisson and larger funnel walls, which add cost. The lower volume of reactive media required by the CPRB saves $27,675 over the FGPRB and $130,950 over the HFPRB, but the caisson costs $35,625 and the 24 m walls cost $61,200. The FGPRB is the cheapest alternative with an estimated cost of $108,750 (35% cheaper than the HFPRB and 18% cheaper than the CPRB). Although the FGPRB uses more reactive media than the CPRB, it does not require a caisson and uses smaller walls. In comparison to the CPRB, the additional reactive media required for the FGPRB adds $27,675, but this cost is offset by not requiring a caisson, saving $35,625. The smaller funnel required for the FGPRB saves an additional $16,575, making the FGPRB the most economic alternative.

A percentile of 90% was chosen arbitrarily as a reasonable level of performance to expect. However, if a probability of failure less than 10% is chosen as a threshold for design, the CPRB may become more economical than the FGPRB because effluent concentrations above the 90^{th} percentile of cumulative density are lower for the CPRB than for the other PRBs (Fig. 8.4).

SECTION 9

DESIGNING PRBs

The purpose of this section is to critique the effectiveness of the current design method for PRBs and to present a new method that accounts for aquifer and PRB heterogeneity more rigorously.

The analysis used for previous sections of this report assumed that complete knowledge of the aquifer exists (i.e., μ_{lnK}, σ_{lnK}, correlation scale are known). However, a designer will not have such information, so this assumption is not made in this section. Rather, pumping tests are simulated on the heterogeneous aquifer. Data from these 'pump tests' are used to estimate the hydraulic conductivity distribution statistics of the aquifer; they are used to evaluate the current design model and to develop a new design method for PRBs. Estimates of hydraulic conductivity obtained from pumping tests are typical of the data available to designers and regulators, and can be different from μ_{lnK} (Dykaar and Kitanidis 1992).

9.1 FIELD ESTIMATES OF HYDRAULIC CONDUCTIVITY

Estimates of hydraulic conductivity that are consistent with data that are available to designers are needed to be fair in evaluating and developing design models for PRBs. Estimates of hydraulic conductivity that are available to designers are usually based on a few laboratory tests or a few field measurements such as slug or pumping test data (Gavaskar et al. 1998, Powell et al. 1998, Wilson

1995). For this study, simulated pumping tests were selected to estimate the hydraulic conductivity of heterogeneous aquifers and typical data used for designing a PRB.

Steady-state pumping tests were simulated in all aquifers using the well option in MODFLOW. A fully penetrating pumping well was located in the center of the aquifer for each realization (X = 33.9 m, Y = 22.5 m) and pumped at a constant rate of 1.44 m^3/d (1.0 L/min) (Fig. 9.1). The gradient across the aquifer was set to zero so that head change throughout the aquifer would only be due to pumping. Heads at eight locations along two orthogonal transects (Fig. 9.1) were used to estimate hydraulic conductivity for the aquifer (namely, 0.25 m, 0.75 m, 1.25 m, and 1.88 m from the pumping well along the X-transect and 2.5 m, 5.0 m, 7.5 m, and 10.0 m from the pumping well along the Y-transect). Heads for all layers of the aquifer were averaged at a given location, as if observation wells were screened across their entire depth. Using pairs of data, hydraulic conductivity was calculated using the Theim equation for an unconfined aquifer (Bear 1979). Hydraulic conductivities along each transect were averaged geometrically to yield an estimate of hydraulic conductivity for the realization. For each aquifer, pumping tests were simulated for ten realizations, and three estimates of hydraulic conductivity were calculated, the geometric mean ($\overline{K}_g$), $\overline{K}_g$ plus one standard deviation (s_{lnK}) above the mean ($\overline{K}_g + \exp(s_{lnK})$), and the maximum measured hydraulic conductivity (K_{max}). The standard deviation (s_{lnK}) was estimated from the hydraulic conductivity 'measurements'.

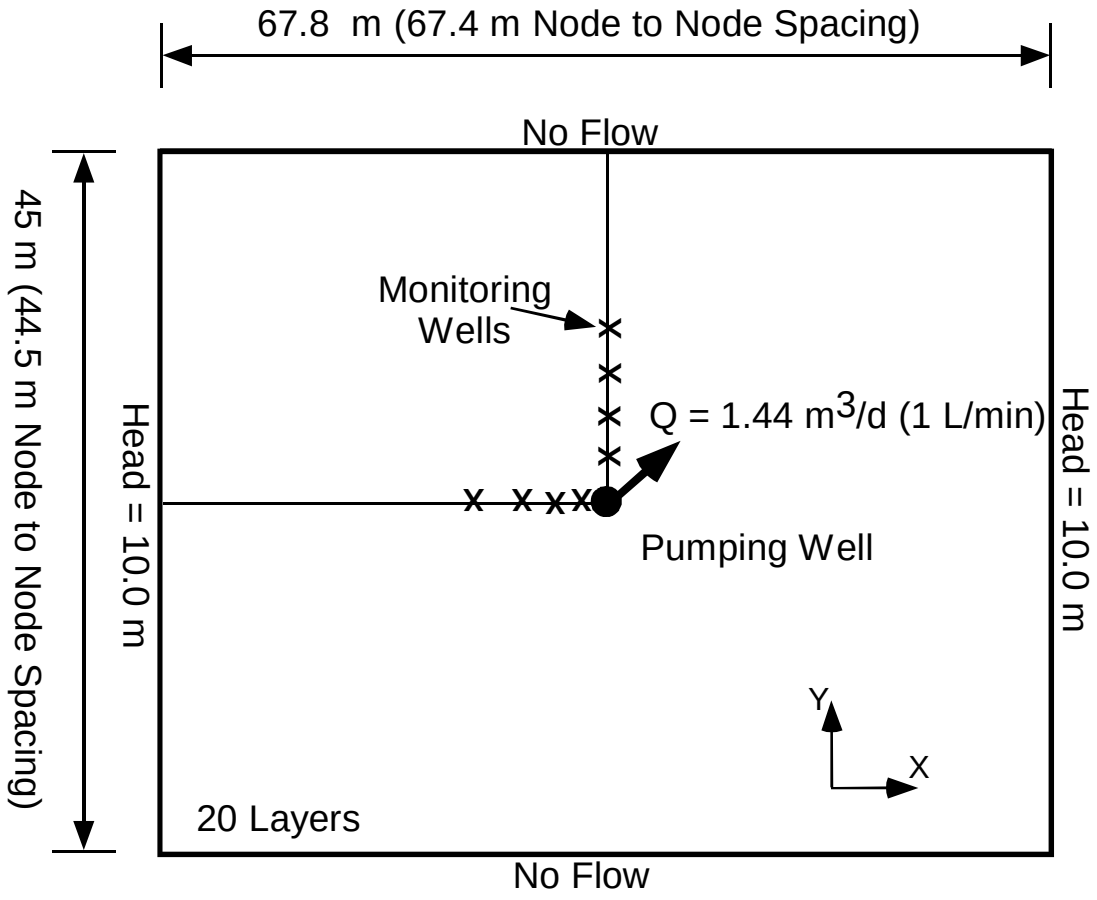

Fig. 9.1 Schematic Showing Location of Pumping Well and Monitoring Wells.

Table 9-1 Estimated Hydraulic Conductivity Obtained from Simulated Pumping Tests.

Aquifer	Input for the Random Field				Hyd. Cond. from Simulated Pumping Tests (m/s)		
	μ_{lnK}	σ_{lnK}	λ_x (m)	λ_y (m)	$\overline{K}_g$	$\overline{K}_g + \exp(s_{lnK})$	K_{max}
Homog.	-10	0	0	0	4.5×10^{-5}	4.5×10^{-5}	4.5×10^{-5}
A	-10	1.0	3	1	5.1×10^{-5}	6.3×10^{-5}	8.5×10^{-5}
B	-10	1.0	6	2	4.7×10^{-5}	6.3×10^{-5}	9.4×10^{-5}
C	-10	4.0	3	1	1.2×10^{-4}	6.7×10^{-4}	1.6×10^{-3}
D	-10	2.25	3	1	6.4×10^{-5}	1.6×10^{-4}	2.6×10^{-4}
E	-10	0.25	3	1	4.5×10^{-5}	5.1×10^{-5}	5.8×10^{-5}
F	-10	1.0	9	3	5.4×10^{-5}	6.8×10^{-5}	8.7×10^{-5}
G	-15	1.0	3	1	6.8×10^{-7}	8.4×10^{-7}	1.5×10^{-6}
H	-11	1.0	3	1	1.9×10^{-5}	2.3×10^{-5}	3.1×10^{-5}
I	-12	1.0	3	1	6.9×10^{-6}	8.6×10^{-6}	1.2×10^{-5}
K	-10	1.0	6	5	5.0×10^{-5}	6.7×10^{-5}	8.5×10^{-5}
L	-10	1.0	6	1	5.0×10^{-5}	6.1×10^{-5}	7.6×10^{-5}
M	-9	1.0	6	1	1.4×10^{-4}	1.7×10^{-4}	2.3×10^{-4}

Hydraulic conductivities are always greater in heterogeneous aquifers than in homogeneous aquifers (maximum difference in $\overline{K}_g$ is 2.6 fold and occurs between a homogeneous aquifer and an aquifer with σ_{lnK} = 4.0 [i.e., aquifer C]). A $\overline{K}_g$ higher than $\exp(\mu_{lnK})$ is consistent with calculations by Dykaar and Kitanidis (1992) and simulations by Fenton and Griffiths (1993). Dykaar and Kitanidis (1992) conclude that $\overline{K}_g$ is approximately equal to $\exp(\mu_{lnK}+\sigma_{lnK}/6)$, which is greater than $\exp(\mu_{lnK})$ because σ_{lnK} is positive. Fenton and Griffiths (1993) used Monte-Carlo simulation to show that $\overline{K}_g$ increases as σ_{lnK} and λ_x increase, with λ_x having a smaller effect than σ_{lnK}.

9.2 CURRENT DESIGN METHOD FOR PRBS

There exists some design guidance for HFPRBs but not for FGPRBs or CPRBs (EPA 1998, Powell et al. 1998, Gaveskar et al. 1998, Nav. Fac. 1998). The design method for HFPRBs assumes plug flow and first-order reactions.

The thickness of a HFPRB is typically calculated using a first-order loss equation and Darcy's Law. Groundwater and contaminants are assumed to move through the PRB by plug flow at the seepage velocity, v_s, given by:

$$v_s = \frac{Ki}{n} \tag{9.1}$$

where K is hydraulic conductivity of the aquifer, i is hydraulic gradient, and n is effective porosity. Concentration in the PRB is assumed to decrease by a first-order reactions such that the ratio of influent to effluent concentration (C_{in}/C_e) is:

$$\frac{C_e}{C_{in}} = \exp(-k_r t) \tag{9.2}$$

where k_r is the rate of the reaction and t is the residence time of contaminants in the reactive media. The minimum residence time to yield a desired C_e for a given C_{in} is obtained by rearranging Eq. 9.2 as:

$$t = \frac{-1}{k} \ln\left(\frac{C_e}{C_{in}}\right) \tag{9.3}$$

Time in Eq. 9.3 can be replaced by the ratio of the minimum PRB thickness (L_{min}) to v_s; substituting $t = L_{min}/v_s$ in Eq. 9.3 with vs given by Eq. 9.1 and solving for L_{min} gives:

$$L_{min} = \frac{-Ki}{nk_r} \ln\left(\frac{C_e}{C_{in}}\right) \tag{9.4}$$

Equation 9.4 is the basis for HFPRB design. Similar equations for FGPRBs and CPRBs do not exist because residence times cannot be calculated using a plug flow model since the flow rate through the PRB depends on the capture zone of the funnels and size of the PRB.

A factor of safety (FS) is often used with Eq. 9.4 to account for variations in hydraulic conductivity caused by heterogeneity, seasonal changes in the direction and magnitude of hydraulic gradient, and differences in k_r due to temperature, scaling, or geochemistry. The FS used with Eq. 9.4 is left to the discretion of the designer, but a typical FS is between one and two. However, numerical simulation has shown that a FS as large as ten may be needed to achieve the desired C_e in more heterogeneous aquifers (Gaveskar et al. 1998, Eykholt 1997, Eykholt et al. 1999).

9.3 EVALUATION OF THE CURRENT DESIGN METHOD

The ability of the current design method for HFPRBs to account for aquifer and PRB heterogeneity is judged by comparing C_e obtained from simulation (i.e., results presented in Sections 5) with C_e calculated using Eq. 9.4. For simplicity, this section will only consider the impact of σ_{lnK} and λ_x for aquifers with μ_{lnK} = -10 (4.5×10^{-5} m/s), since σ_{lnK} has the most impact on effluent concentration and λ_x has a moderate impact.

The current design method for HFPRBs is evaluated by back-calculating the FS needed with Eq. 9.4 to produce a C_e equal to the 90th percentile of effluent concentration from simulation of a 1 m thick PRB in a heterogeneous aquifer (i.e., the PRBs simulated in Section 5). First, the effluent concentration corresponding to the 90th percentile is obtained from the distributions in Section 5. This concentration is set equal to C_e in Eq. 9.4 and L_{min} is calculated assuming n = 40%, i = 0.01, and C_{in} = 1000 ppb. The required factor of safety (FS_{req}) to have 90% of the effluent concentrations less than C_e is then:

$$FS_{req} = \frac{1}{L_{min}} \tag{9.5}$$

with L_{min} in meters. A numerator of one meter is used in Eq. 9.5 because the simulation results are for a 1 m thick HFPRB.

Three estimates of hydraulic conductivity, $\overline{K}_g$, $\overline{K}_g + \exp(s_{lnK})$, and K_{max} are used in Eq. 9.4 to calculate FS_{req}. Any of these hydraulic conductivities could be

used for designing a PRB, but each yields a different FS_{req}. Back-calculated FS_{req} for aquifers with different s_{lnK} and λ_x, and each hydraulic conductivity are shown in Fig. 9.2.

FS_{req} for heterogeneous aquifers exceed FS_{req} for homogeneous aquifers (FS_{req} = 1.0), with many FS_{req} greater than 2.0 when $\overline{K}_g$ is used for design. FS_{req} increases with larger σ_{lnK} and λ_x, but it decreases between $\overline{K}_g$, $\overline{K}_g + \exp(s_{lnK})$, and K_{max}. A larger FS_{req} is needed for designs using $\overline{K}_g$ because $\overline{K}_g$ is the lowest of the three estimates for hydraulic conductivity and does not completely account for the more permeable units that intersect the PRB. Conversely, K_{max}, overestimates the influence of more conductive zones within the aquifer, causing FS_{req} to be lower and even less than unity in some cases.

FS_{req} shown in Fig. 9.2a, increases as s_{lnK} increases for designs based on $\overline{K}_g$, as $\overline{K}_g$ does not account for more permeable units. However, when the design is based on the K_{max}, FS_{req} decreases slightly with increasing s_{lnK} because K_{max} overestimates the effect of more permeable units. FS_{req} back-calculated from $\overline{K}_g + \exp(s_{lnK})$ are between estimates based on $\overline{K}_g$ and K_{max}, and are typically about 1.7 for most s_{lnK}. Thus, FS_{req} = 2 is satisfactory provided K_{max} or $\overline{K}_g + \exp(s_{lnK})$ are used in the design. If $\overline{K}_g$ is used for designing the PRB, a larger factor of safety is needed.

FS_{req} increases as λ_x increases for all hydraulic conductivities (Fig. 9.2b). However, correlation scale has less impact on FS_{req} than s_{lnK} because increasing λ_x

a) Variable s_{lnK}

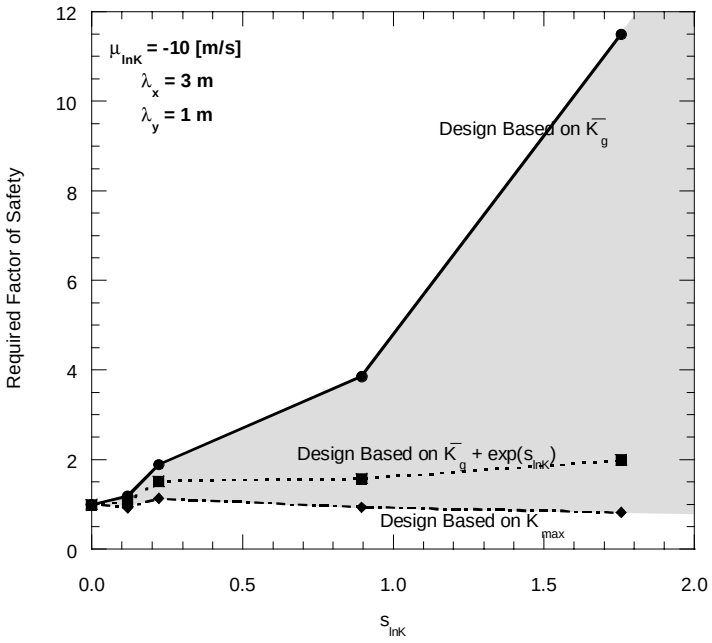

b) Variable λ_x

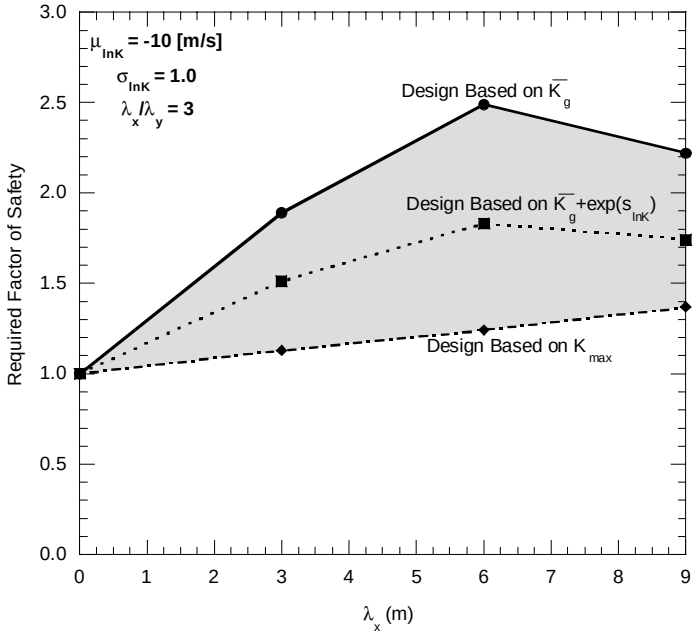

Fig. 9.2 FS_{req} for a HFPRB that Yields 90% of the Effluent Below a Target Concentration. FS_{req} are for a Plug-Flow Model that uses Field Measurements of Hydraulic Conductivity.

causes only moderate increases (10%) in estimated hydraulic conductivity (Table 9-1) and smaller changes in effluent concentration (Section 5.3.3). If $\overline{K}_g$ is used, FS_{req} larger than two may be needed; however, as with s_{lnK}, FS_{req} of two is sufficient provided K_{max} or $\overline{K}_g + \exp(s_{lnK})$ is used.

The FS_{req} shown in Fig. 9.2 indicate that a failure is likely if FS_{req} of one is used. A FS_{req} of two can be used if $\overline{K}_g + \exp(s_{lnK})$ or K_{max} are used for design. However, choosing a higher hydraulic conductivity to compensate for a lower FS_{req} is not a logical design approach and can be overly conservative for more homogeneous aquifers, wasting reactive media and money. A more logical approach is to have larger FS_{req} for more heterogeneous aquifers and smaller FS_{req} for more homogeneous aquifers. The next section addresses this issue by providing empirical equations for calculating FS_{req} as a function of parameters describing aquifer and PRB heterogeneity, and allowable risk.

9.4 ALTERNATIVE TO THE CURRENT DESIGN METHOD

The current design method for HFPRBs was evaluated in the previous section. Based on this analysis, a FS_{req} = 2 and a plug flow model can be used to design PRBs provided higher estimates of hydraulic conductivity for the aquifer are used. Such a method is attractive because it is simple and because it provides adequate designs in more heterogeneous aquifers, but it is overly conservative and uneconomical in more homogeneous aquifers. Additionally, the preceding analysis considered s_{lnK} and correlation scale independently, ignoring the combined impact

of s_{lnK} and λ_x, or PRB heterogeneity. The plug flow model, however, does have the potential to be a satisfactory design tool if FS_{req} can be linked to the PRB and aquifer heterogeneity.

A new design method which predicts a factor of safety as a function of PRB and aquifer heterogeneity is presented in this section. This method introduces a reliability-based scaling factor (F) for each type of PRB that is a function of parameters describing the heterogeneity of the aquifer and PRB.

9.4.1 Calculating Scaling Factors for PRB Design

The premise for the proposed design method is similar to the method used for calculating FS_{req} in the previous section. Distributions of effluent concentration from simulation of PRBs in heterogeneous aquifers are compared with the effluent concentration for a PRB in a homogeneous aquifer. From this comparison, a scaling factor (F) is calculated. This factor can be used with a plug flow model to design a PRB which yields a desired effluent concentration at a specified probability of failure. Effluent concentrations for a HFPRB in a homogeneous aquifer were calculated analytically using Eq. 9.4; however, for FGPRBs and CPRBs, effluent concentrations for a homogeneous aquifer were obtained from simulation.

Cumulative distributions of effluent concentration for the three types of PRB in a homogeneous and a heterogeneous aquifer are shown in Fig. 9.3. Effluent concentration for a HFPRB in a homogeneous aquifer is uniform as predicted from Eq. 9.4. However, effluent concentrations for a FGPRB or CPRB are distributed

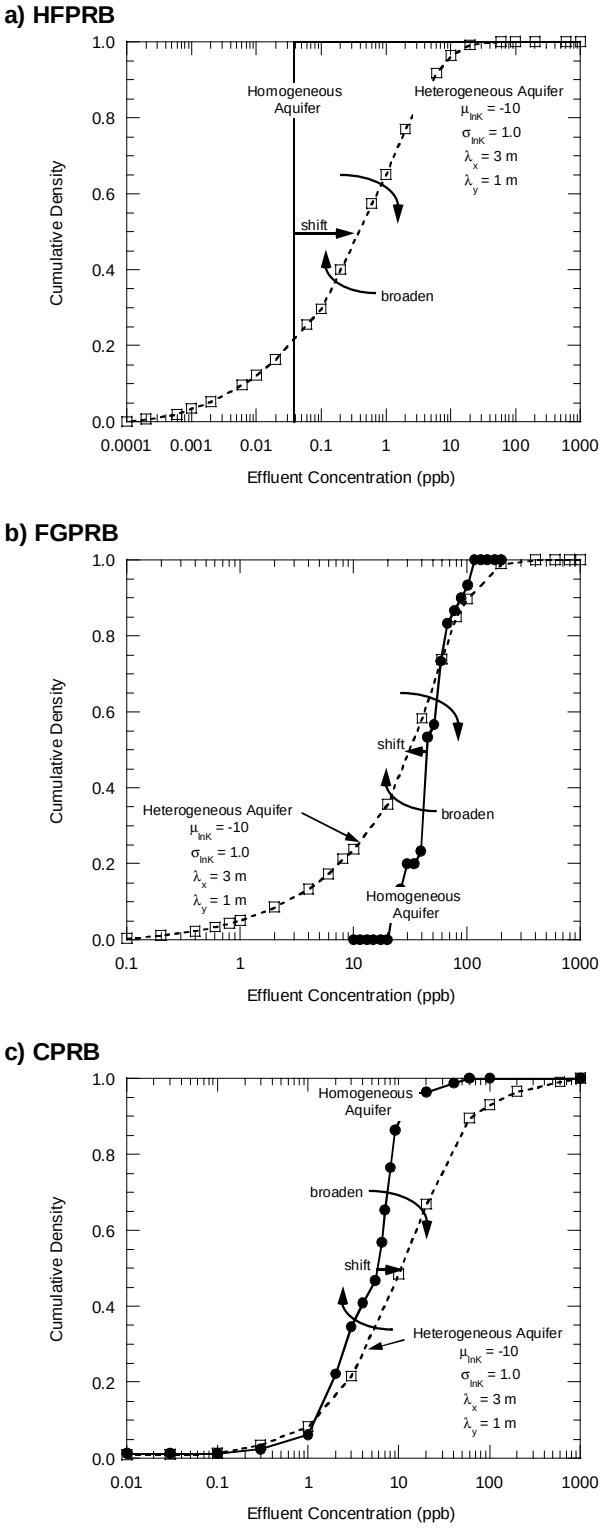

Fig. 9.3 Distributions of Effluent Concentration from a HFPRB (a), FGPRB (b), and CPRB (c) in a Homogeneous and Heterogeneous Aquifer.

because the funnels channel groundwater through the PRB, causing non-uniform flow and increased dilution.

For each type of PRB, distributions of effluent concentration shift and become more spread in more heterogeneous aquifers. The goal of the proposed design model is to characterize the shift and spread of the distributions of effluent concentration caused by heterogeneity. The shift and spread for each type of PRB in a heterogeneous aquifer is compared with median effluent concentrationfrom the same PRB in a homogeneous aquifer to calculate a scaling factor (F). Equations for F are then derived empirically as functions of $\overline{K}_g$, s_{lnK}, λ_x, λ_y, σ_K, and σ_k.

Effluent concentrations from each type of PRB in a heterogeneous aquifer are log-normally distributed. Effluent concentrations presented in Section 5, 6, and 7 proved to be log-normally distributed based on the Kolmogorov-Smirnov test and most fit with 95% confidence. Hence, the logarithm of effluent concentration is normally distributed. Distributions of F were calculated for each simulation as:

$$F = \frac{\ln\left(C_e / C_{in}\right)_{het}}{\ln\left(C'_e / C_{in}\right)_{hom}} \qquad (9.6)$$

where C'_e is the median effluent concentration from a 1 m thick PRB in a homogeneous aquifer that has a hydraulic conductivity equal to $\overline{K}_g$ (i.e., the geometric mean hydraulic conductivity obtained from simulated pumping tests on the heterogeneous aquifer), C_{in} is the maximum influent concentration to the PRB (i.e., 1000 ppb), and C_e is the effluent concentration from simulation of the same

PRB in a heterogeneous aquifer. A distribution of F is obtained by using Eq. 9.6 and the distribution of C_e obtained from simulation (e.g., F for the 90th cumulative density is obtained by using C_e for the 90th percentile of effluent concentration in Eq. 9.6). Repeating this procedure for all C_e allows the distributions of F to be constructed. These distributions are normally distributed since C_e is log-normally distributed, and the denominator in Eq. 9.6 is constant.

The distribution of F can be defined using a mean (μ_F) and standard deviation (σ_F) because F is normally distributed. These moments were determined for all simulations, producing a table of μ_F and σ_F with their associated aquifer and PRB descriptors (i.e., $\overline{K}_g$, s_{lnK}, λ_x, λ_y, σ_K, and σ_k). This information was then used to derive empirical equations for μ_F and σ_F as a function of $\overline{K}_g$, s_{lnK}, λ_x, λ_y, σ_K, and σ_k via regression. The regression was performed using Statview® software, Abacus Concepts, Inc. Equations for μ_F and σ_F allow estimates of F to be made based on measured properties of a heterogeneous aquifer ($\overline{K}_g$, s_{lnK}, λ_x, λ_y) and properties of the PRB (σ_K and σ_k).

Reliability is incorporated into the design method by choosing the F corresponding to a desired probability of failure (or percentile of effluent concentration). The probability of failure is equal to the mass of the F distribution above the F chosen for design. Since F is normally distributed, a standard Z-score (Z) for a normal distribution can be used to determine the number of σ_F's above μ_F corresponding to a desired probability of failure as:

$$F_Z = \mu_F + Z\sigma_F \quad (9.7)$$

where F_Z is F associated with the probability of failure used to select Z. Probabilities of failure and their corresponding Z are given in Table 9-2, with the probability of failure defined as the percentage of effluent from the PRB that is expected to exceed C_e.

Table 9-2 Z for Several Probabilities of Failure

Prob. of Failure	Z-score (Z)
50%	0.000
25%	0.674
20%	0.842
15%	1.036
10%	1.282
5%	1.645
1%	2.326
0.5%	2.576
0.1%	3.090

9.4.2 Using the Proposed Design Method

The preceding section explains how a normally distributed scaling factor (F) is calculated. Distributions of F were calculated for all simulations performed in this study and a mean (μ_F) and standard deviation (σ_F) were calculated. Finally, equations for μ_F and σ_F were derived empirically as functions of $\overline{K}_g$, s_{lnK}, λ_x, λ_y, σ_K, and σ_k.

The objective of this model is to determine the F that is needed to account for aquifer and PRB heterogeneity. Median effluent concentration for a given PRB in a homogeneous aquifer is calculated using a deterministic or numerical model.

Then, F is calculated and used to scale the size of the PRB (designed assuming the aquifer is homogeneous) to account for aquifer and PRB heterogeneity.

There are four steps to using the proposed design method. The first step is to calculate μ_F and σ_F using the appropriate empirical equations:

a) HFPRB (9.8a)

$$\mu_F = -0.181(\ln(\overline{K}_g)) + 0.67 s_{\ln K} + 0.024\lambda_x - 0.87$$

$$\sigma_F = 0.127(\ln(\overline{K}_g))^2 + 2.49(\ln(\overline{K}_g)) + 3.94(s_{\ln K})^2 - 1.8 s_{\ln K} + 0.077\lambda_x + 12.8$$

b) FGPRB (9.8b)

$$\mu_F = -0.102(\ln(\overline{K}_g))^2 - 1.99(\ln(\overline{K}_g)) - 0.039(s_{\ln K})^3 - 8.7$$

$$\sigma_F = 0.05(\ln(\overline{K}_g))^2 - 0.326(s_{\ln K})^2 + 1.20(s_{\ln K}) + 6.38$$

c) CPRB (9.8c)

$$\mu_F = -0.045(\ln(\overline{K}_g)) - 0.33(s_{\ln K})^2 + 0.44(s_{\ln K}) - 0.02(\lambda_x) + 0.5$$

$$\sigma_F = -0.9(s_{\ln K})^2 + 2.7(s_{\ln K}) - 0.35$$

Other parameters (i.e., λ_y, σ_K, and σ_k) did not significantly affect μ_F or σ_F.

Table 9-3 P-Value and R^2 Statistic for Regression Analysis.

PRB Type	Dependant Variables	Independent Variables							R^2
		$(\ln(\overline{K}_g))^2$	$\ln(\overline{K}_g)$	$(s_{\ln K})^3$	$(s_{\ln K})^2$	$(s_{\ln K})$	λ_x	Int.	
HFPRB	μ_F	-	<0.0001	-	-	<0.0001	<0.0001	<0.0001	0989
	σ_F	0.0007	0.0013	-	<0.0001	<0.0001	<0.0001	0.0017	.998
FGPRB	μ_F	<0.0001	<0.0001	<0.0001	-	-	-	<0.0001	.918
	σ_F	<0.0001	-	-	<0.0001	<0.0001	-	<0.0001	.974
CPRB	μ_F	-	<0.0001	-	<0.0001	<0.0001	<0.0001	<0.0001	.904
	σ_F	-	-	-	<0.0001	<0.0001	-	<0.0001	.958

Once μ_F, σ_F, and λ_x are estimated, the second step is to choose an acceptable probability of failure for the PRB and Z that corresponds to the probability of failure from Table 9-2. Then F_Z is calculated using Eq. 9.7, with μ_F and σ_F from Eq. 9.8 and Z from Table 9-2.

Third, the average discharge velocity (v) of groundwater through a PRB in a homogeneous aquifer is calculated from:

$$v = Q_p / A_p \tag{9.9}$$

where Q_p is the volumetric flow rate of groundwater through the PRB and A_p is the area of the PRB perpendicular to Q_p. For the HFPRB, v can be calculated as the product of $\overline{K}_g$ and hydraulic gradient (i). For a FGPRB or CPRB, v is affected by the width of the funnel and the PRB (and also PRB thickness and openings size for the CPRB). Thus, v may have to be calculated using simulation or a flow net (e.g., Sedivy et al. 1999). It should be noted that v changes with funnel and gate widths for the FGPRB, but does not change significantly with the thickness of the gate. Thus, v will not change much once funnels and a gate of sufficient widths have been designed to capture a plume. Likewise, funnel width, PRB thickness, and CPRB opening size affect v, but v is not significantly affected by the height of reactive media in the CPRB. Thus, the design method works for FGPRBs and CPRBs because F scales the thickness of a FGPRB and height of reactive media in a CPRB. These dimensions of the reactive media are parallel to flow and, when

changed, do not significantly affect flow through the PRB because the hydraulic conductivity of the reactive media is much higher than $\overline{K}_g$.

Fourth, with v (Eq. 9.9) and F_Z (Eq. 7.7) known, the design length of reactive media (L_d) needed for the PRB in the heterogeneous aquifer can be calculated as:

$$L_d = \frac{-v F_Z}{k_r n} \ln\left(\frac{C_{e,z}}{C_{in,max}}\right) \tag{9.10}$$

where $C_{e,z}$ is the desired effluent concentration from the PRB that has a probability of failure associated with Z, $C_{in,max}$ is the maximum influent concentration to the PRB, k_r is the average reaction rate for the media, and n is effective porosity. Equation 9.10 can be used for HFPRBs, FGPRBs, and CPRBs with the assumption that L_d is the length of reactive media parallel to flow. Thus, L_d is the thickness of the reactive media for HFPRBs and FGPRBs and is the height of the reactive media for CPRBs.

Equation 9.10 is useful for determining the design length for PRBs. However, the method may also be used to predict the distribution of effluent concentrations for an existing system. Solving Eq. 9.10 for $C_{e,Z}$ provides an equation for the effluent concentration from a PRB in a heterogeneous aquifer. The entire distribution of effluent concentrations can be determined by calculating $C_{e,Z}$ for all F_Z (i.e., probabilities of failure) as:

$$C_{e,z} = C_{in,max} \exp\left(\frac{-k_r L_d n}{v F_z}\right) \quad (9.11)$$

where L_d is the *in-situ* length of the reactive media.

The advantage of this method is that it is similar to the current design method because it uses a first order equation and plug-flow model, and applies a factor of safety to account for heterogeneity. However, the proposed method is an improvement on the current method because it relates F to parameters describing aquifer and PRB heterogeneity, and incorporates reliability into the design process, which allows F to reflect variability in the system as well as giving designers and regulators an estimate of the failure potential of the PRB. Finally, the method may be used for all types of PRBs. Currently, there are no other design models for FGPRB or CPRBs.

The method does have limitations. Empirical equations for μ_F and σ_F are based on the range of $\overline{K}_g$, s_{lnK}, λ_x, λ_y, σ_K, and σ_k that were tested. Therefore, the method should not be used for more heterogeneous aquifers than those used in this study (i.e., those shown in Table 9-1).

9.4.3 Verification of the Proposed Design Method

9.4.3.1 Backwards Modeling

The proposed method for designing PRBs was verified by comparing effluent concentrations obtained by simulation with effluent concentrations predicted using the method (i.e., backwards modeling). Ten new aquifers with a

μ_{lnK} = –9.5 (7.5 x 10^{-5} m/s), σ_{lnK} = 1.25, and λ_x = 5 m, and λ_x = 1.67 m were created using the turning bands program. Most of the input parameters selected for this simulation are unique to the simulation but within the range of those previously investigated. Pumping tests were simulated on these aquifers and yielded $\overline{K}_g$ = 8.2 x 10^{-5} m/s and s_{lnK} = 0.38. A HFPRB as shown in Fig. 5.5, FGPRB as shown in Fig 6.3, and CPRB as shown in Fig. 7.4, were simulated in the aquifer. The PRBs were homogeneous with a hydraulic conductivity of 2.5 x 10^{-3} m/s and k_r = 1.0 d^{-1}.

From the stated aquifer and PRB parameters, μ_F and σ_F were calculated for the HFPRB (μ_F = 1.21, σ_F = 0.89), FGPRB (μ_F = 0.99, σ_F = 0.63), and CPRB (μ_F = 0.94, σ_F = 0.55) using Eq. 9.8. Given these μ_F and σ_F, F_Z for probabilities of failure between 50% and 0.5% were calculated for all types of PRB using Eq. 9.7. Next, v was calculated for each PRB. For the HFPRB, v was calculated using a plug-flow model (i.e., $v = \overline{K}_g i$) whereas v for the FGPRB and CPRB was calculated by simulating the PRB in a homogeneous aquifer with a hydraulic conductivity equal to $\overline{K}_g$. The maximum influent concentrations were assumed to equal the source concentration of 1000 ppb, which is consistent with the results presented in Sections 5, 6, and 7. Using these inputs, $C_{e,Z}$ were calculated for each PRB and the associated probability of failure using Eq. 9.10. Effluent concentrations obtained from simulations of the PRBs in the heterogeneous aquifers are shown with $C_{e,Z}$ predicted from the design method in Fig. 9.4.

Effluent concentrations calculated using the method match the effluent concentrations from simulation reasonably well. The method predicts slightly

a) HFPRB

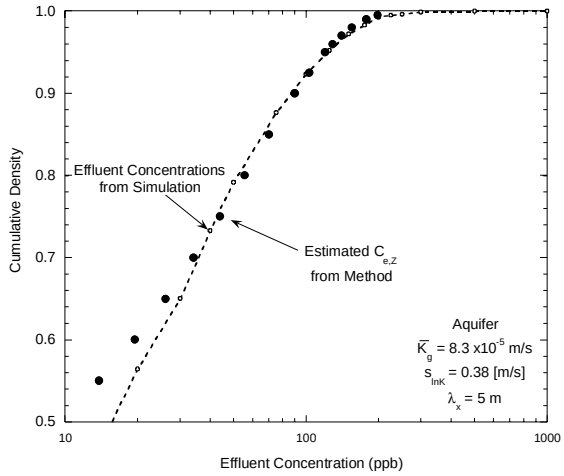

b) FGPRB

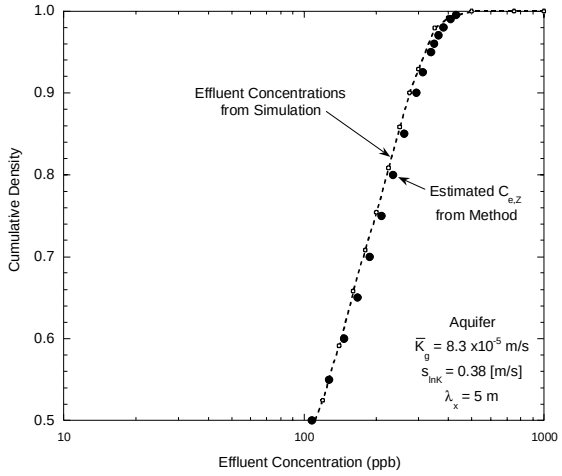

c) CPRB

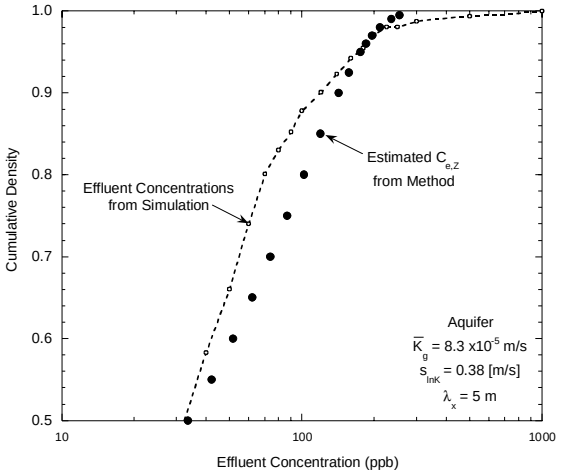

Fig. 9.4 Comparison of Effluent Concentration Obtained from Simulation and the Design Method.

higher concentrations at percentiles less than 85% to 90%, except for the HFPRB at percentiles below 70%. Thus, the method is slightly conservative below percentiles of 90% (i.e., probability of failure > 10%). Predicted and measured effluent concentrations overlap between cumulative densities of 85% to 90%, indicating that the method matches simulation data well at a probability of failure of about 10%. Above the 90^{th} percentile, the model is slightly unconservative, predicting effluent concentrations that are slightly lower than measured effluent concentrations. However, the difference in these concentrations is usually minor except at percentiles greater than 98% (i.e., probabilities of failure < 2%) where the difference is about half an order of magnitude. Nonetheless, the method yields reasonable predictions of effluent concentration, particularly for percentiles below 98%. The method is a poorer match to effluent concentrations in the tail of the distributions, so designers and regulators should be wary of method results at probabilities of failure less than 2%.

9.4.3.2 Forward Modeling

The proposed design method was also verified using a forward modeling exercise. That is, the method was used to design a HFPRB, FGPRB, and CPRB for a given aquifer and target effluent concentration. Then these PRBs were simulated in the heterogeneous aquifer to see if they achieved the desired performance. A single realization of a new aquifer was used for the test. Properties of the aquifer and reactive media are given in Table 9-4.

Table 9-4 Aquifer and PRB Inputs.

Aquifer		PRB	
μ_{lnK}	-11.25 [m/s]	Hyd. Cond.	$2.5x10^{-3}$ m/s
σ_{lnK}	1.75	σ_K	0 m/s
λ_x	4 m	Reaction Rate	1 d^{-1}
λ_y	3 m	σ_k	0 d^{-1}
gradient	0.0025		
porosity	30%		

Three pumping tests were performed at x = 33.9 m, 22.3 m; x = 32.9 m, y = 12.3 m; and x = 36.2 m, y = 27.3 m using a flow rate of 2 m^3/d. These tests yielded a $\overline{K}_g$ of $2.0x10^{-5}$ m/s and s_{lnK} of 0.62, which were input into Eq. 9.8 to calculate μ_F and σ_F for each type of PRB. It was assumed that λ_x = 4 m for these calculations. The μ_F and σ_F for each type of PRB are given in Table 9-5.

The design specification chosen for the site is that no more than 10% of the effluent from the PRB can exceed 5 ppb. For this probability of failure, Z is 1.282 (Table 9-2) and μ_F and σ_F calculated with Eq. 9.8 are given in Table 9-5 along with F_{10}, calculated with Eq. 9.7. Thus, F_{10} for the HFPRB = 3.43, F_{10} for the FGPRB = 1.75, and F_{10} for the CPRB = 2.30.

Table 9-5 Scaling Factors for Each Type of PRB.

PRB Type	μ_F	σ_F	F_{10}*
HFPRB	1.60	1.43	3.42
FGPRB	0.88	0.68	1.75
CPRB	1.05	0.97	2.30

*probability of failure = 10% corresponds to a Z = 1.282

Next, v was calculated for each type of PRB in a homogeneous aquifer with a hydraulic conductivity equal to 2.0×10^{-5} m/s (i.e., $\overline{K}_g$). For the HFPRB, v was calculated as the product of $\overline{K}_g$ and the hydraulic gradient. For the FGPRB and CPRB, v was calculated by simulation. This calculation requires the size of the funnel and PRB to be defined. Reasonably sized PRBs were chosen based on simulation in the homogeneous aquifer and judgment gained from previous simulations (i.e., knowing that funnels are longer in heterogeneous aquifers than in a homogeneous aquifer). Sizing the FGPRB and CPRB systems in a homogeneous aquifer required several trials until a reasonable PRB configuration was obtained. Then longer funnels were used because plumes are larger in heterogeneous aquifers and the capture zone of the funnels is smaller. The final system is a 3 m wide gate in the FGPRB and a 5 m wide by 1 m thick caisson in the CPRB, both PRBs are located in the center of the aquifer. The FGPRB has two 21 m long walls constituting the funnel, and the CPRB has two 22.5 m walls constituting the funnel.

Once v for each style of PRB was calculated, Eq. 9.10 was used to calculate L_d for $C_{e,10}$ = 5 ppb, given C_{in} = 1200 ppb (Eq. 9.10). For the HFPRB and FGPRB, L_d is the thickness of the PRB whereas L_d is the height of the reactive media for the CPRB. A design summary for the three types of PRB is summarized in Table 9-6. The designed PRBs were then simulated in the heterogeneous aquifer and distributions of influent and effluent concentration were calculated. Concentrations

for the three PRBs along with the target concentration (i.e., $C_{e,10}$ = 5 ppb) are shown in Fig. 9.5.

Table 9-6 Design Summary for a HFPRB, FGPRB, and CPRB

	v (m/d)	F_{10}	L_d (m)*	PRB Size
HFPRB	0.0043	3.42	0.267	25 m wide and 10 m deep
FGPRB	0.0191	1.75	0.609	2 m wide and 10 deep gate with two 21 m funnels
CPRB	0.0930	2.30	3.91	5 m wide by 1 m thick CPRB that has 5 m wide by 2.5 m tall openings and surrounded by two 22.5 m funnels

* for $C_{e,10}$ = 5 ppb and C_{in} = 1200 ppb, i = 0.0025, n = 0.3, and k_r = 1 d^{-1}

As expected, the maximum influent concentration equals the source concentration of 1200 ppb. Also, the 90th percentile of effluent concentration nearly intercepts 5 ppb for all three of PRBs, indicating that the design method produces an appropriate F to account for heterogeneity. However, effluent concentrations for the FGPRB are slightly higher than desired, perhaps because only results for a single realization are shown. Nonetheless, the results shown in Fig. 9.4 and 9.5 indicate that the proposed design method properly accounts for heterogeneity and provides a reasonable estimate of the probability of failure. These features make the proposed method a better tool for designing PRBs by quantifying risk, avoiding over-design in more homogeneous aquifers (e.g., $\sigma_{lnK} < 1.0$), and avoiding under-designed PRBs in more heterogeneous aquifers (e.g., $\sigma_{lnK} > 1.0$).

a) Influent Concentrations

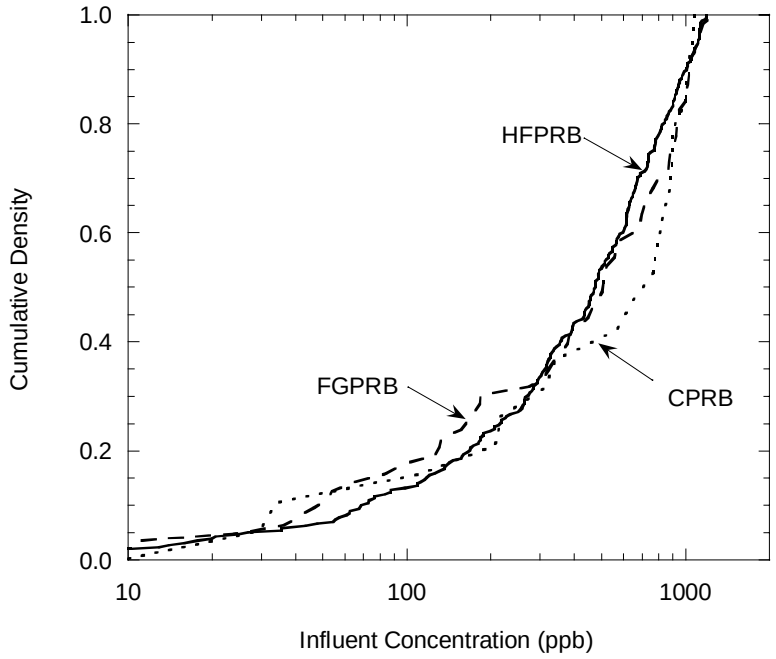

b) Effluent Concentrations

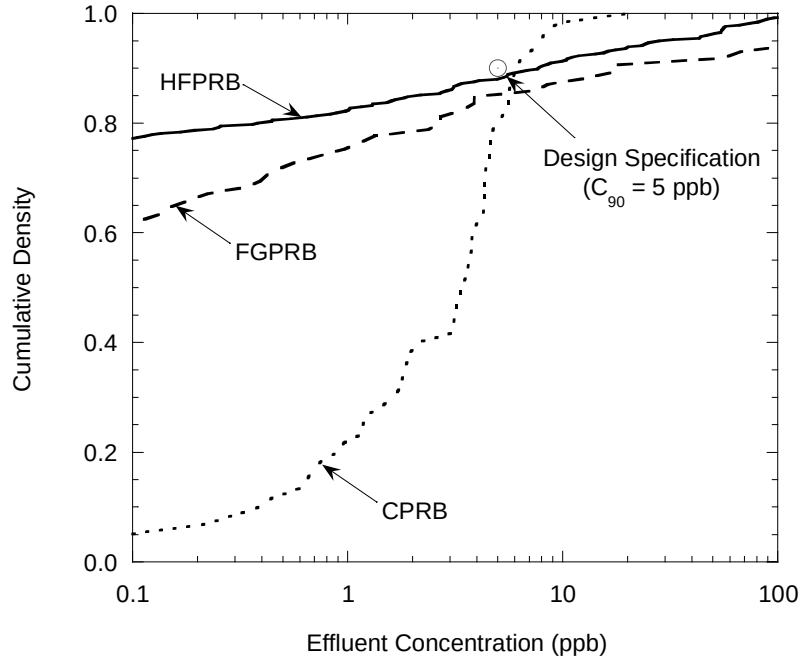

Fig. 9.5 Influent (a) and Effluent (b) Concentrations from PRBs Designed Using the Design Model.

9.5 Summary

The design of PRBs in heterogeneous aquifers has been evaluated in this section. The current method that relies on a factor of safety equal to two was considered in Section 9.3. It was found that a factor of safety equal to two was adequate in more homogeneous aquifers, but a factor of safety as large as twelve may be needed in more heterogeneous aquifers. An adaptation of the current method was suggested in Section 9.4. The new method uses empirical equations to calculate the mean and standard deviation for the distribution of scaling factors (F). The scaling factor is similar to a factor of safety but only accounts for uncertainty in the hydraulic conductivity of the aquifer, hydraulic conductivity of the PRB, and reaction rate constant of the PRB. Since F is normally distributed, the percentage of effluent from a PRB that exceeds a target effluent concentration is equal to the probability density of the F distribution greater than the F chosen for design. For example, if having 5% of the effluent from a PRB exceed an MCL is considered an acceptable probability of failure, then an F corresponding to the 95% percentile of the F distribution (i.e., 1.645 standard deviations above the mean) is used for design along with an effluent concentration equal to the MCL. This method provides the scaling factor that increases as heterogeneity increases or the probability of failure decreases. The method was verified for the three types of PRBs using simulation. Verification of the method in aquifers with moderate and moderately high heterogeneity shows that the method can predict effluent concentrations from PRBs well and correctly estimates the required design thickness for PRBs.

SECTION 10

MONITORING SYSTEMS FOR PRBs

Conclusions are made in the preceding sections of this report with the assumption that designers and regulators have knowledge of all effluent concentrations from a PRB. However, such information is unlikely to be available. Instead, designers and regulators will judge the performance of a PRB based on a limited number of point measurements of concentration obtained from monitoring wells. From these data, the entire distribution of effluent concentrations will be extrapolated and decisions regarding the safety of down-gradient receptors will be made.

The objective of this section is to determine the ability of several monitoring schemes for HFPRBs, FGPRBs, and CPRBs to detect the 50^{th}, 75^{th}, and 90^{th} percentile of effluent concentration. The monitoring schemes range from a single well screen to several multilevel monitoring wells. Once the ability of many systems at detecting higher effluent concentrations is known, the system with the maximum probability of detection per well screen will be identified. Monitoring well spacing and monitoring screen separation will be recommended for each type of PRB along with the expected probability of detecting higher effluent concentrations.

10.1 CURRENT MONITORING SYSTEMS FOR PRBS

A competent monitoring system is needed around a PRB to evaluate the effectiveness of the PRB and ensure that down-gradient receptors are not exposed

to contaminated groundwater. Currently, there are few guidelines for the number and location of monitoring wells around a PRB. Gavaskar et al. (1998) and Powell et al. (1998) recommend locating monitoring wells up-gradient and down-gradient of a PRB. Up-gradient monitoring wells are used to assess the distribution of concentration entering the PRB, whereas down-gradient wells are used to assess the effluent from the PRB. Gavaskar et al. (1998) also recommend placing monitoring wells on either side of the PRB to determine if the plume circumvents the PRB.

Monitoring wells are typically located slightly outside of the reactive media or immediately inside the reactive media. If a pea-gravel zone is placed on either side of the PRB, monitoring wells are often located in the gravel zones. Gavaskar et al. (1998) summarize the monitoring schemes used for 13 full-scale and pilot-scale PRBs. Eleven of these PRBs are HFPRBs. Three of the HFPRBs have monitoring wells located within a few inches of the effluent face, three have monitoring wells located in a narrow pea-gravel zone immediately down-gradient of the PRB, and the remaining five have monitoring wells located throughout the PRB (Gavaskar et al. 1998). When monitoring wells are located throughout the PRB, some of the wells are probably along the effluent face of the PRB. Fifty millimeter PVC monitoring wells are common and screen lengths vary from 1 m to over 3 m (Powell et al. 1998). Multilevel monitoring wells with shorter screen lengths allow more localized measurement of concentration (Robbins 1989).

Well spacings for existing PRBs differ significantly. Government sites and pilot scale PRBs have closer well spacing than full-scale PRBs at industrial sites.

For example, the FGPRB at Lowry Air Force Base in Denver, Colorado has a 3.05 m wide gate located between two 4.27 m wide walls in a funnel. The gate is instrumented with 15 monitoring wells, three of which are down gradient of the PRB. The wells are spaced approximately one meter apart with the outside wells having a single 3.05 m well screen and the center well having two, 0.305 m screens at the bottom of the well and 1.52 m from the bottom of the well. In contrast, a 750 m long FGPRB at an aircraft manufacturing facility in Oregon has two 15.2 m gates and three 240 m long funnel walls. Each gate is instrumented with two monitoring wells. For the designer, such contrasts in existing monitoring schemes make it difficult to propose monitoring schemes for PRBs, and there are no data on the effectiveness of any particular scheme.

Micropurging is recommended for obtaining groundwater samples from monitoring wells around a PRB (Warner et al. 1998, Powell et al. 1998). Micropurging involves purging only the pump and effluent line prior to sampling. The pumping rate should be slow and steady (100 to 500 mL/min), and a pump should be dedicated to each monitoring well (Kearl et al. 1992, 1994). This method differs from traditional sampling in which three to five bore-volumes are purged from the monitoring well prior to sampling (Barcelona et al. 1994). Traditional sampling is not recommended for PRBs because contaminants can be drawn through the PRB to the well by the gradient caused by purging (Warner et al. 1998), which decreases the residence time of contaminants in the PRB and biases measurements toward higher concentration (Powell et al. 1998).

There are few guidelines for the horizontal and vertical spacing of monitoring wells around a PRB. In general, the number of monitoring wells should increase with greater heterogeneity (Gavaskar et al. 1998, Powell et al. 1998, Warner et al. 1998), but specific guidelines for the frequency and spacing of monitoring wells do not exist. However, effective placement of monitoring wells is critical to ensure satisfactory effluent is obtained from the PRB, down-gradient receptors are safe, and costs are minimized. Thus, a protocol for monitoring PRBs that has a scientific basis needs to be developed. Such a protocol will provide regulators with assurance that a PRB is operating properly, reduce the cost of monitoring systems and sampling, and provide a standardized design for designers with less experience building PRBs.

10.2 METHOD FOR EVALUATING MONITORING SYSTEMS

Twenty-five monitoring schemes were investigated for the HFPRB, twenty-four monitoring schemes were investigated for the FGPRB, and twelve monitoring schemes were investigated for the CPRB. Monitoring schemes differ in the number of monitoring wells and the number of well screens per monitoring well. Monitoring points are located symmetrically around the lateral and vertical centerlines of the effluent face of the PRB. For all systems, well screens were 1 m long and the screens were assumed to measure the average concentration for a square meter of soil around the well and across the depth of the well screen. Monitoring schemes were evaluated in all aquifers for a homogeneous PRB with K_p

= 2.5×10^{-3} m/s and $k_r = 1\ d^{-1}$. Details about the monitoring schemes tested for each type of PRB are given in subsequent sections.

The measure of effectiveness for judging the monitoring schemes is the probability that any well screen for a scheme detects a concentration greater than or equal to a threshold concentration. For this study, three threshold concentrations were considered, the median (C_{50}), 75th percentile (C_{75}), and 90th percentile (C_{90}) concentration at the effluent face of the PRB. These concentrations are shown for the HFPRB in Fig. 10.1. Using relative concentrations for evaluating the monitoring schemes makes the results more general than if absolute concentrations were used because relative concentrations do not have to be adjusted for the shift and spread of distributions caused by changing μ_{lnK}, σ_{lnK}, λ_x, and λ_y.

The magnitude of effluent concentration is a function of aquifer and PRB heterogeneity. However, the location of higher or lower effluent concentration is a random variable and independent of μ_{lnK}, σ_{lnK}, λ_x, and λ_y because the aquifers are random fields of hydraulic conductivity. Thus, probabilities of a monitoring scheme detecting a target concentration at all μ_{lnK}, σ_{lnK}, λ_x, and λ_y were averaged to yield the average probability of detecting C_{50}, C_{75}, or C_{90} for a particular monitoring scheme and PRB in a heterogeneous aquifer.

Detection for this study (i.e., measuring a concentration above the threshold concentration) is assumed to be a Bernoulli random variable with a value of zero or one. If any monitoring well for a given scheme detects a concentration greater than the threshold concentration, detection for the realization is assigned a

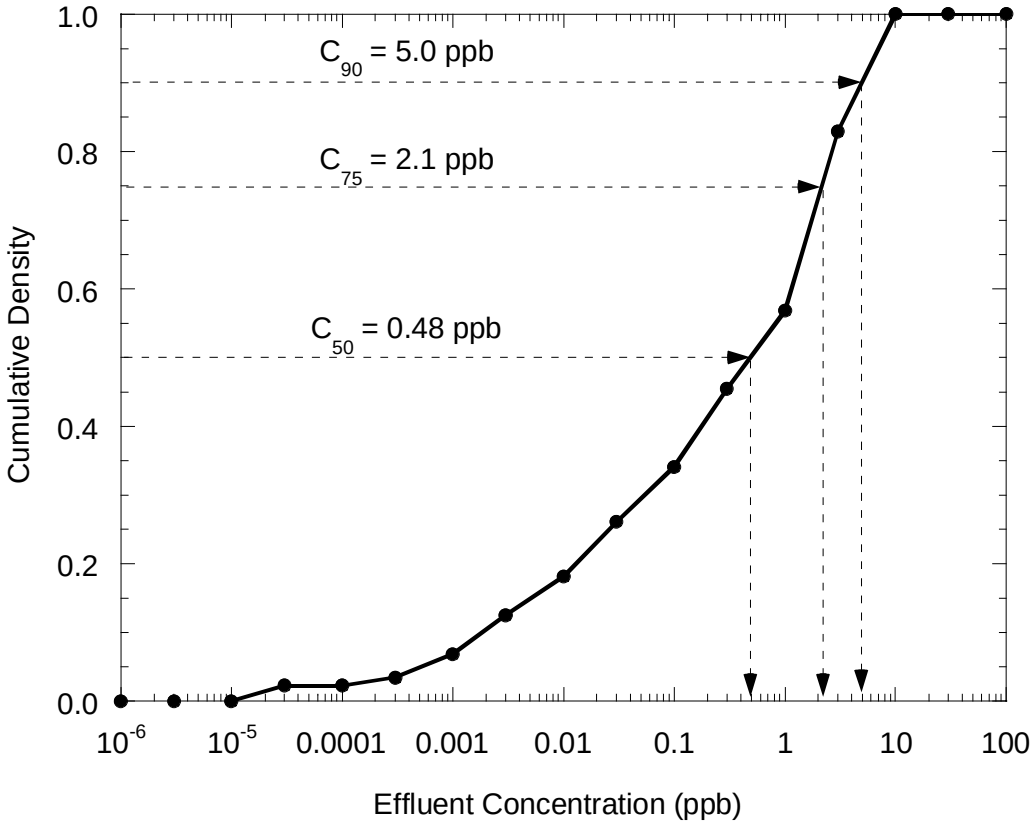

Fig. 10.1 Sample of C_{50}, C_{75}, and C_{90} That are Used for Judging the Effectiveness of Monitoring Schemes.

Bernoulli value of one. If none of the monitoring wells for a given scheme detect a concentration greater than the threshold concentration, detection for the realization is assigned a Bernoulli value of zero. The probability of a given well scheme detecting a concentration greater than the threshold concentration is calculated as the sum of Bernoulli random variables for all realization divided by the number of realizations tested. Average probabilities of detecting C_{50}, C_{75}, and C_{90} for each monitoring scheme and PRB type at all μ_{lnK}, σ_{lnK}, λ_x, and λ_y are reported.

10.3 MONITORING HFPRBs

The probability of twenty-five monitoring schemes detecting C_{50}, C_{75}, and C_{90} for a HFPRB was calculated for all realizations of all aquifers and then averaged. The monitoring schemes that were tested for the HFPRB are summarized in Table 10.1. Schemes with different lateral spacing between monitoring wells (Δy) are arranged across the table and the vertical spacing between the centers of well screens (Δz) are listed down the table. Below the chart is a schematic of the effluent face of the HFPRB for reference.

The probability of the twenty-five monitoring schemes at detecting C_{50}, C_{75}, and C_{90} from a HFPRB is shown in Fig. 10.2. Monitoring schemes are presented in terms of Δy and Δz between the centers of the well screens. The densest lateral spacing (i.e., smaller Δy) is shown near the origin of Fig. 10.2 (6 wells with Δy = 5 m) and the coarsest spacing (a single well located at the lateral centerline of the PRB) is shown at the right side of Fig. 10.2. Lines connect schemes with constant vertical spacing.

Table 10-1 Monitoring Schemes Used for a HFPRB.

		Lateral Location of the Well Screen (m)				
		10.5, 15.5, 20.5, 24.5 29.5, 34.5	15.5, 20.5, 24.5 29.5	16.5, 22.5, 28.5	18.5, 26.5	22.5
Vertical Location of the Center of the Well Screen (m)	1.5, 3.5, 5.5, 7.5, 9.5	MW1 Δy=5 m, Δz=2 m (30 Screens)	MW2 Δy=5 m, Δz=2 m (20 Screens)	MW3 Δy=6 m, Δz=2 m (15 Screens)	MW4 Δy=8 m, Δz=2 m (10 Screens)	MW5 one well, Δz=2 m (5 Screens)
	2.5, 4.5, 6.5, 8.5	MW6 Δy=5 m, Δz=2 m (24 Screens)	MW7 Δy=5 m, Δz=2 m (16 Screens)	MW8 Δy=6 m, Δz=2 m (12 Screens)	MW9 Δy=8 m, Δz=2 m (8 Screens)	MW10 one well, Δz=2 m (4 Screens)
	2.5, 5.5, 7.5	MW11 Δy=5 m, Δz=3 m (18 Screens)	MW12 Δy=5 m, Δz=3 m (12 Screens)	MW13 Δy=6 m, Δz=3 m (9 Screens)	MW14 Δy=8 m, Δz=3 m (6 Screens)	MW15 one well, Δz=3 m (3 Screens)
	2.5, 7.5	MW16 Δy=5 m, Δz=5 m (12 Screens)	MW17 Δy=5 m, Δz=5 m (8 Screens)	MW18 Δy=6 m, Δz=5 m (6 Screens)	MW19 Δy=8 m, Δz=5 m (4 Screens)	MW20 one well, Δz=5 m (2 Screens)
	5.5	MW21 Δy=5 m, one screen (6 Screens)	MW22 Δy=5 m, one screen (4 Screens)	MW23 Δy=6 m, one screen (3 Screens)	MW24 Δy=8 m, one screen (2 Screens)	MW25 one well, one screen (1 Screen)

Δy is lateral monitoring well spacing
Δz is vertical well screen spacing

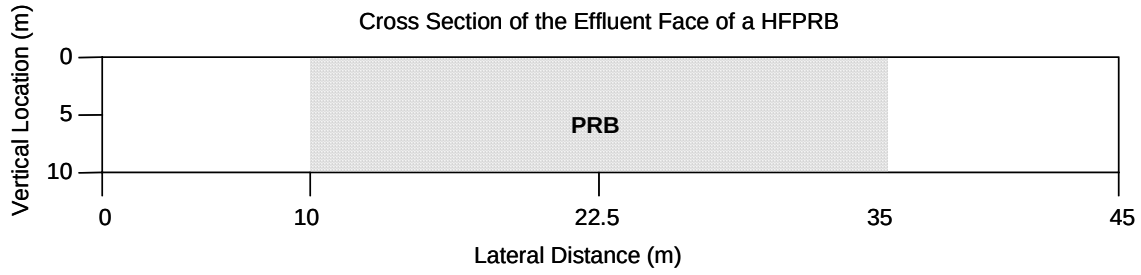

The probability of detecting C_{50} is nearly 100% if multiple monitoring wells are used and these wells are screened every other meter. The maximum probability of detecting C_{50} decreases to less than 90% if a single monitoring well is used. The probability of detecting C_{50} is greater than 85% provided $\Delta z \leq 3$ m. For multilevel wells with $\Delta z > 3$ m, the probability of detecting C_{50} decreases by 15 to 20% for each additional two meters of vertical well screen separation. Increasing

a) Probability of Detecting C_{50}

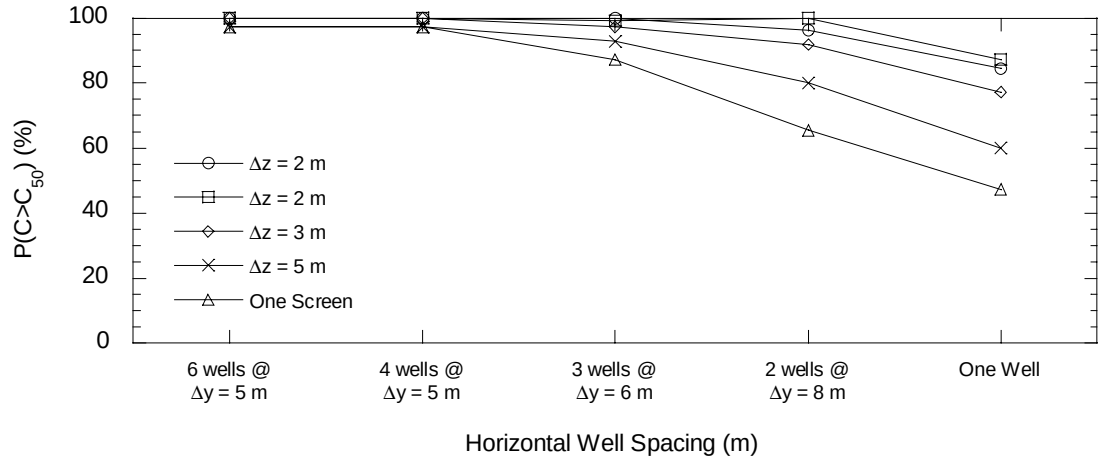

b) Probability of Detecting C_{75}

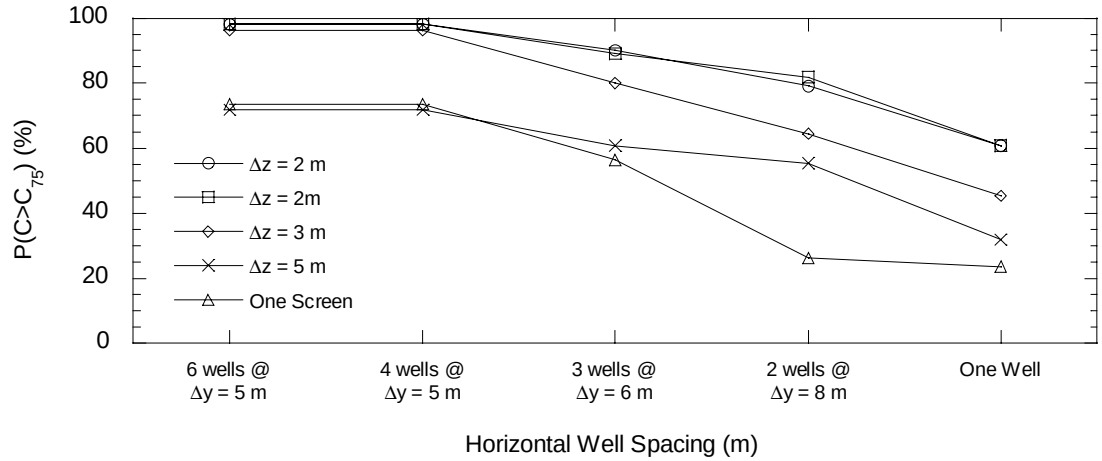

c) Probability of Detecting C_{90}

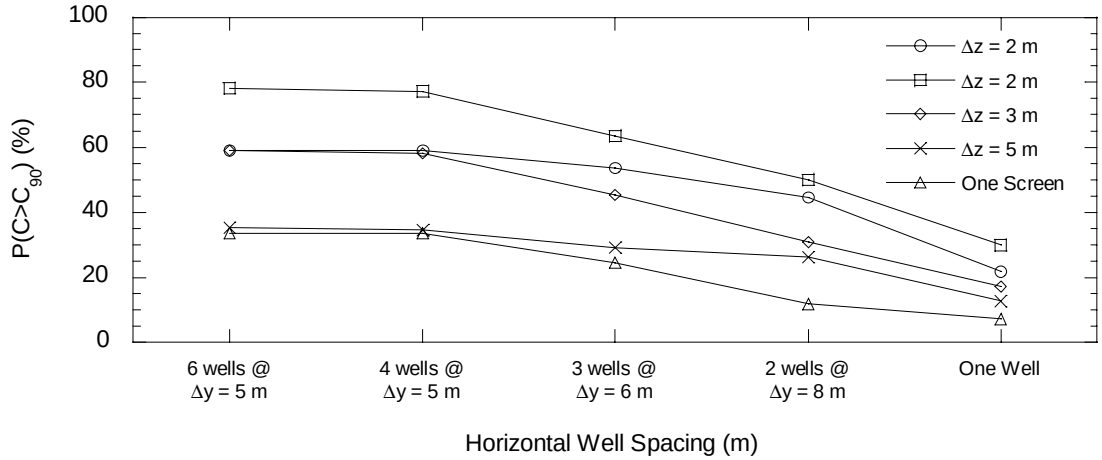

Fig. 10.2 Probability of Detecting C_{50} (a), C_{75} (b), and C_{90} (c) of Concentration as a Function of Horizontal and Vertical Well Screen Spacing.

Δy past 6 m causes a 10 to 15% decrease in the probability of detecting C_{50} per additional meter of lateral well separation. Thus, the probability of detecting C_{50} decreases more for a unit increase in Δz than for a unit increase in Δy. Therefore, multilevel monitoring wells with finer vertical resolution should be used for HFPRBs even if this results in fewer monitoring wells at greater Δy.

The probability of detecting C_{75} follows a similar trend as the probability of detecting C_{50}. The probability of detecting C_{75} is greater than 95% when $\Delta z \leq 3$ m and $\Delta y \leq 5$ m, or greater than 90% when $\Delta z \leq 2$ m and $\Delta y \leq 6$ m. The probability of detecting C_{75} decreases by about 10% with each additional meter of lateral separation and about 15% with each additional two meters of vertical well screen separation. Thus, as with C_{50}, the probability of detecting C_{75} decreases faster with increasing Δz than with increasing Δy, and better performance is achieved when $\Delta z \leq 3$m.

The probabilities of detecting C_{90} are 20 to 35% lower than the probabilities of detecting C_{50} or C_{75}. With the densest monitoring, the probability of detecting C_{90} is 80% and only about 50% for the schemes recommended for detecting C_{50} and C_{75}. Better performance (i.e., $P(C > C_{90}) > 50\%$) is achieved if $\Delta y \leq 5$ m and $\Delta z \leq 3$ m. At greater Δy or Δz, the probability of detecting C_{90} decreases by about 10% per meter of additional Δy or Δz.

In summary, a monitoring scheme with wells located 5 to 6 m apart and well screens separated by 2 to 3 m appears to yield the highest probability of detecting C_{50}, C_{75}, and C_{90} with the fewest well screens. Such a system is expected to have

about a 90% chance of detecting C_{50}, 80% chance of detecting C_{75}, and 50% chance of detecting C_{90}. Systems with greater well separation will have a 10 to 15% lower probability of detection for each additional meter of lateral separation beyond 6 m, and 15 to 20% lower probabilities of detection for each additional meter of vertical well screen separation beyond 3 m.

The most efficient monitoring scheme, on a basis of cost, can be determined by considering the number of well screens versus the probability of detection. The twenty-five schemes that were considered are shown in Fig. 10.3a in terms of the number of well screens for each scheme (across a 25 m wide by 10 m deep PRB). As with Fig. 10.2, the probability of detecting C_{50}, C_{75}, and C_{90} are shown for each scheme. Also shown on Fig. 10.2a are trendlines fit to the data.

The probability of detecting the C_{50}, C_{75}, and C_{90} increases sharply as the number of well screens increases from one to five. There is less benefit gained by using more than five to ten well screens. This is consistent with the aforementioned recommendation of using nine well screens for an efficient monitoring program of a 25 m long, 10 m deep PRB (i.e., three multi-level monitoring wells at a horizontal spacing of 6 m and vertical screen spacing of 3 m). Figure 10.3a can also be used to determine the appropriate number of well screens to achieve a given probability of detection.

The probability of detection gained by adding an additional monitoring well is calculated by differentiating the functions fit to the data shown on Fig. 10.3a. The derivative can then be evaluated for any number of well screens to yield the benefit gained by adding one more well screen (Fig. 10.3b). As expected, the benefit of an

a) Probability of Detection versus the Number of Well Screens

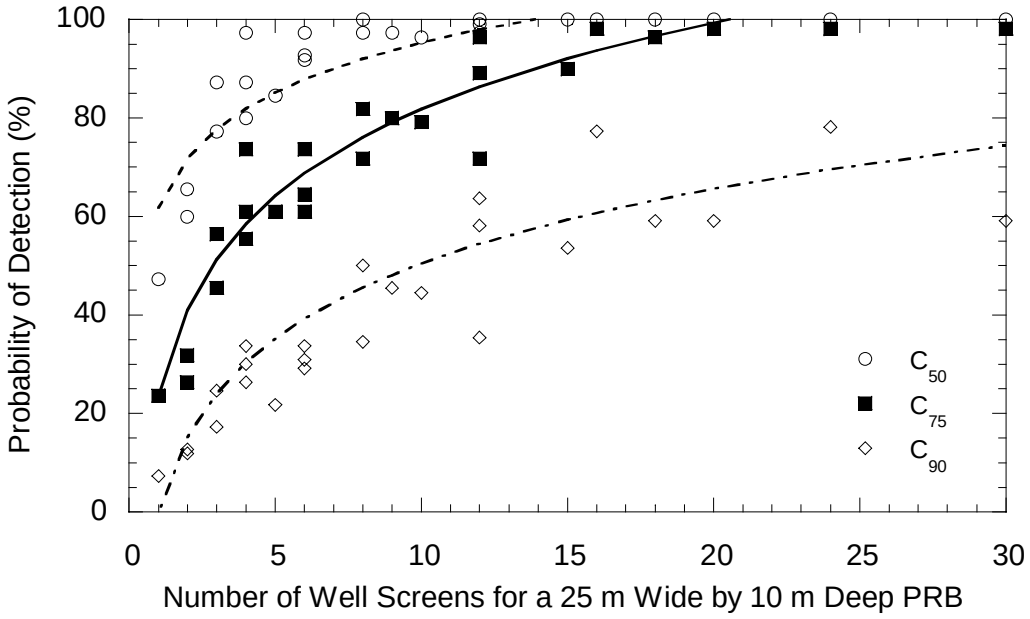

b) Additional Probability of Detection Gained By Adding a Well Screen

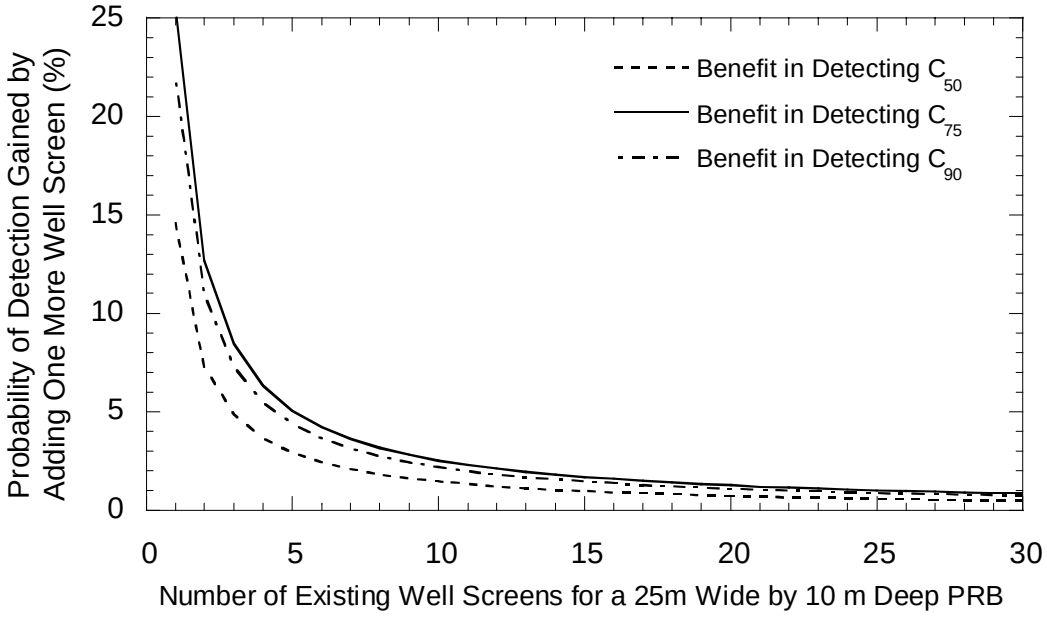

Fig. 10.3 Probability of Detecting the C_{50}, C_{75}, and C_{90} as a Function of the Number of Well Screens (a), and the Benefit Gained by Adding an Additional Well Screen to a Monitoring Scheme (b) for a HFPRB.

additional well is greatest for systems with less than five well screens and little benefit is gained by adding a screen to a system with more than ten well screens.

Based on these results, an effective monitoring design for a 10 m deep by 25 m long PRB has at least three multi-level monitoring wells located symmetrically around the centerline of the PRB and plume. Monitoring wells should be spaced 6 m apart (horizontally) and have a vertical center-to-center screen spacing of 3 m. Such a system has about 90% probability of detecting C_{50}, 80% probability of detecting C_{75}, and 50% probability of detecting C_{90}. These recommendations are for a 25 m wide by 10 m deep PRB that has a 15 m wide source located 20 m up-gradient from the PRB. Larger plumes and PRBs may require more monitoring wells; however, the horizontal and vertical spacing between well screens is not expected to change.

10.4 MONITORING FGPRBS

Twenty-four monitoring schemes were tested for the FGPRB. The Δy and Δz for these schemes are given in Table 10-2. Schemes with different Δy are arranged across the chart and schemes with different Δz are listed down the chart. Below the chart is a schematic of the effluent face of the FGPRB for reference. The densest monitoring system has three monitoring wells with well screens located every other meter. The coarsest scheme has a single well screen centered at the back of the gate. The probabilities of detecting C_{50}, C_{75}, and C_{90} for the twenty-four monitoring well schemes are shown in Fig. 10.4.

Table 10-2 Monitoring Schemes Considered for a FGPRB.

		Lateral Location of the Well Screen (m)		
		30.5, 32.5, 34.5	31.5, 33.5	32.5
Vertical Location of the Center of the Well Screen (m)	1.5, 3.5, 5.5, 7.5, 9.5	MW1 Δy=2 m, Δz=2 m (15 Screens)	MW9 Δy=2 m, Δz=2 m (10 Screens)	MW17 one well, Δz=2 m (5 Screens)
	0.5, 2.5, 4.5, 6.5, 8.5	MW2 Δy=2 m, Δz=2 m (15 Screens)	MW10 Δy=2 m, Δz=2 m (10 Screens)	MW18 one well, Δz=2 m (5 Screens)
	1.5, 4.5, 7.5	MW3 Δy=2 m, Δz=3 m (9 Screens)	MW11 Δy=2 m, Δz=3 m (6 Screens)	MW19 one well, Δz=3 m (3 Screens)
	2.5, 5.5, 8.5	MW4 Δy=2 m, Δz=3 m (9 Screens)	MW12 Δy=2 m, Δz=3 m (6 Screens)	MW20 Δy=2 m, Δz=3 m (3 Screens)
	2.5, 6.5	MW5 Δy=2 m, Δz=4 m (6 Screens)	MW13 Δy=2 m, Δz=4 m (4 Screens)	MW21 one well, Δz=4 m (2 Screens)
	3.5, 5.5	MW6 Δy=2 m, Δz=5 m (6 Screens)	MW14 Δy=2 m, Δz=5 m (4 Screens)	MW22 one well, Δz=5 m (2 Screens)
	4.5	MW7 Δy=2 m, one screen (3 Screens)	MW15 Δy=2 m, one screen (2 Screens)	MW23 one well, one screen (1 Screens)
	5.5	MW8 Δy=2 m, one screen (3 Screens)	MW16 Δy=2 m, one screen (2 Screens)	MW24 one well, one screen (1 Screens)

Δy is lateral monitoring well spacing
Δz is vertical well screen spacing

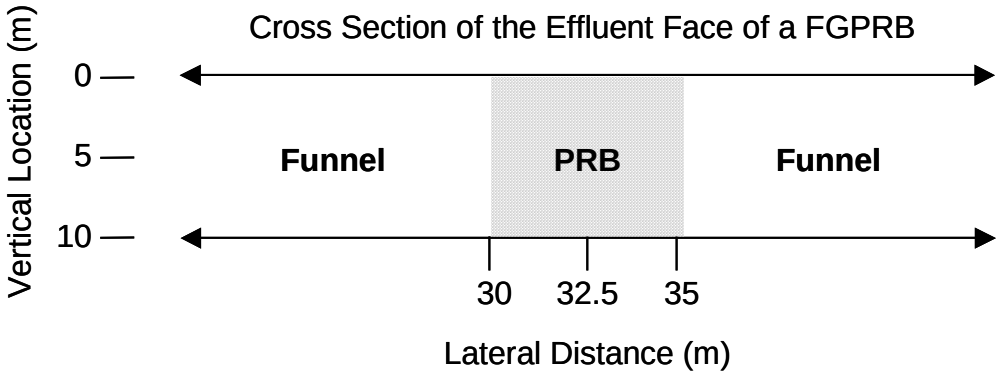

The probability of detecting C_{50} is greater than 90% provided multiple monitoring wells with $\Delta z \leq 4$ m are used and $\Delta y \leq 2$ m. In contrast, a single monitoring well only has a 50 to 80% probability of detecting C_{50}. Probabilities of

a) Probability of Detecting C_{50}

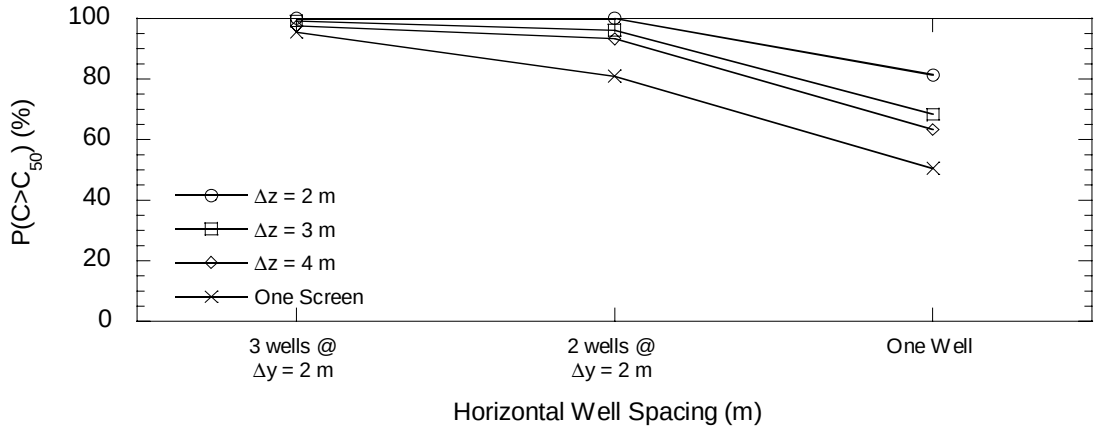

b) Probability of Detecting C_{75}

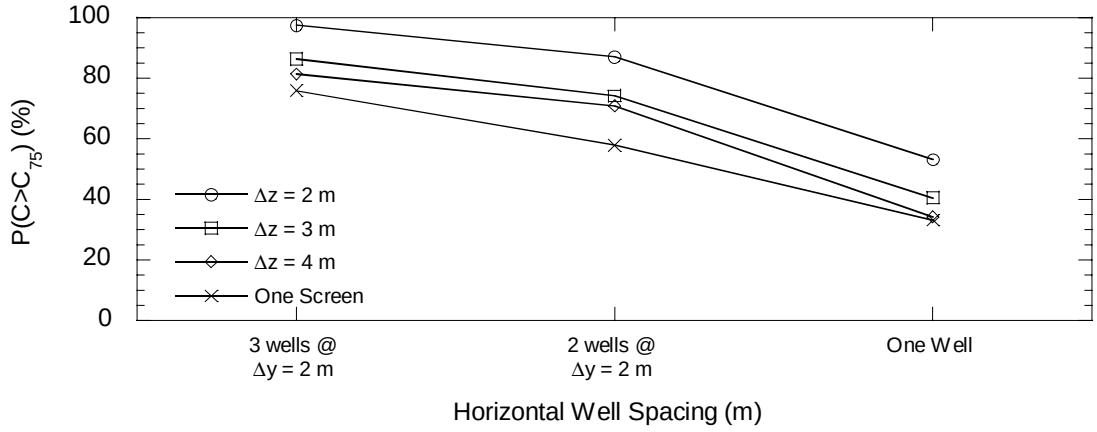

c) Probability of Detecting C_{90}

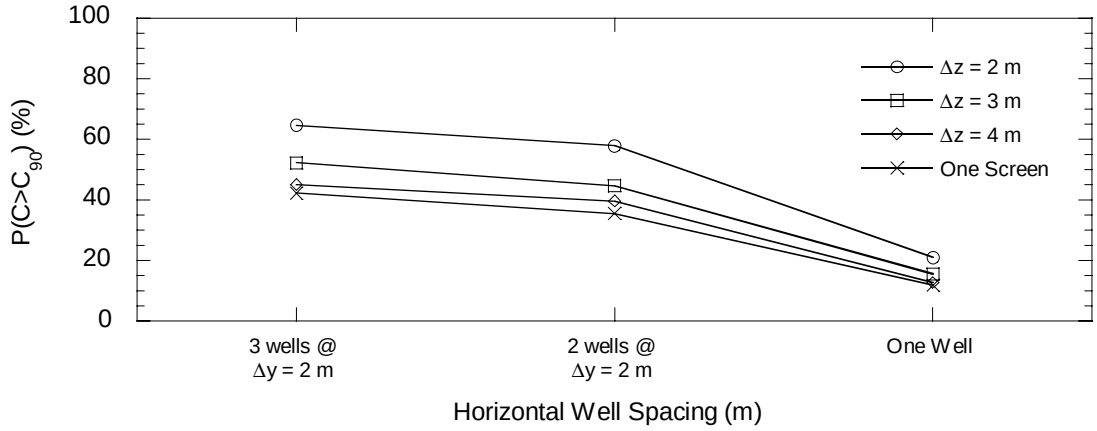

Fig. 10.4 Probability of Detecting C_{50} (a), C_{75} (b), and C_{90} (c) of Concentration as a Function of Horizontal and Vertical Well Screen Spacing.

detecting C_{75} are about 15% lower than the probabilities of detecting C_{50}. As with C_{50}, the probability of detecting C_{75} is about 20% higher if multiple monitoring wells are used.

Increasing Δz has a greater impact on the probability of detecting C_{75} than on the probability of detecting C_{50}. Probabilities of detecting C_{50} are similar provided multilevel sampling is used. However, increasing Δz from 2 to 3 m causes a 10% decrease in the probability of detecting C_{75}. The probability of detecting C_{75} changes little for Δz from 3 to 4 m, but decreases an additional 5 to 10% when a single well screen is used.

Probabilities of detecting C_{90} are about 25% lower then the probabilities of detecting C_{75} and about 40% lower then the probabilities of detecting C_{50}. Probabilities of detecting C_{90} follow a similar trend as probabilities for C_{50} and C_{75}. Probabilities of detecting C_{90} are much better provided concentrations at the edges of the plume are measured (i.e., more than a single monitoring well is used). Probability of detecting C_{90} is also higher for $\Delta z = 2$ m and decreases about 10% when Δz increases to 3 m but changes less for $\Delta z > 3$ m.

In summary, FGPRBs appear to require denser lateral monitoring than HFPRBs to achieve the same probability of detection. For example, there is an 80% probability of detecting C_{75} from a HFPRB when 9 well screens are used (i.e., $\Delta y = 6$ m, $\Delta z = 3$ m). To achieve the same probability of detecting C_{75} from a FGPRB requires four wells with $\Delta y = 2$ m and screens at 4 m intervals. The FGPRB may use slightly greater Δz than the HFPRB, but a much smaller Δy.

However, since the effluent face of the gate is much smaller than a HFPRB, the number of monitoring wells required for the FGPRB may be less despite being more closely spaced. The recommended monitoring system for a FGPRB is $\Delta y \leq 2$ m and $\Delta z \leq 4$ m. Such a system is expected to have about 90% chance of detecting C_{50}, 70% chance of detecting C_{75}, and 40% chance of detecting C_{90}.

Probabilities of detecting C_{50}, C_{75}, and C_{90} as a function of the number of well screens are shown in Fig. 10.5a. Curves are fit to these data, and the derivatives of these curves are plotted in Fig 10.5b. The functions shown in Fig. 10.5b give the additional probability of detecting C_{50}, C_{75}, or C_{90} that is gained by adding a well screen to an existing system. Diminishing returns (i.e., the probability of detection < 5%) occur for C_{50} and C_{90} for systems with more than 4 to 5 well screens and 5 to 6 well screens when detecting C_{75}. These results are consistent with the data shown in Fig. 10.4 and support the recommendation that efficient monitoring systems for a FGPRB use multilevel monitoring wells spaced no more than 2 m apart with 1 m screens located at 3 m intervals. Monitoring wells and screens should be oriented symmetrically around the center of the effluent face of the gate.

10.5 MONITORING CPRBs

Twelve monitoring schemes were tested for the CPRB. The Δy and Δz for these schemes are given in Table 10-3. Schemes with different Δy are arranged across the chart and schemes with different Δz are listed down the chart. Below

a) Probability of Detection versus the Number of Well Screens

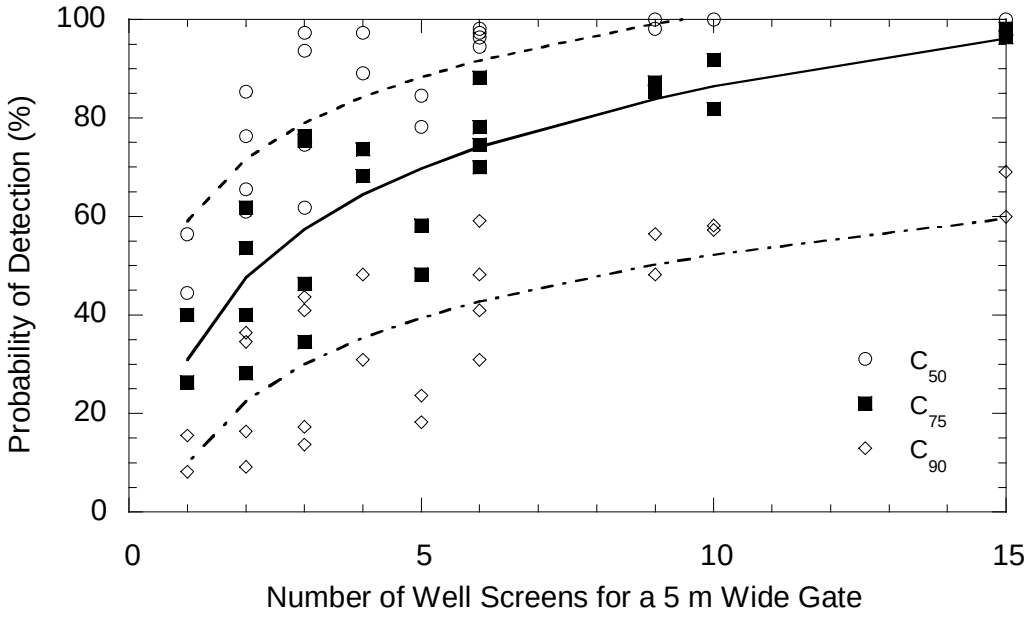

b) Additional Probability of Detection Gained By Adding a Well Screen

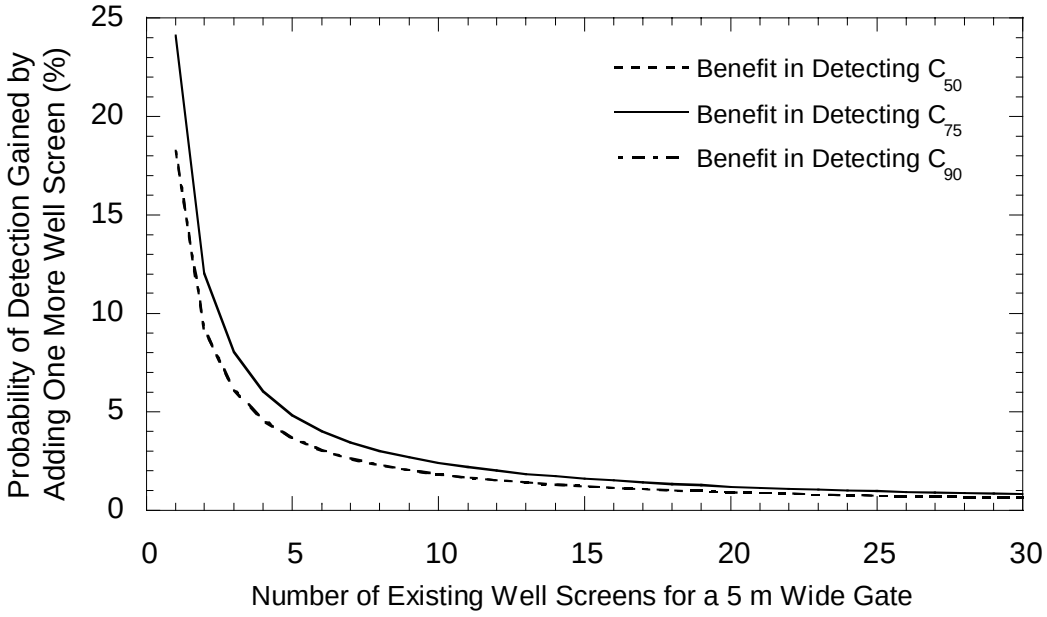

Fig. 10.5 Probability of Detecting the C_{50}, C_{75}, and C_{90} as a Function of the Number of Well Screens (a), and the Benefit Gained by Adding an Additional Well Screen to a Monitoring Scheme (b) for a FGPRB.

the chart is a schematic of the effluent face of the FGPRB for reference. The densest monitoring system has five monitoring wells with well screens located every meter. Six monitoring schemes use a single well screen. Three of these have screens near the bottom of the effluent opening (z = 1.5 m) and three have the screens near the top of the effluent opening (z = 0.5 m). Average probabilities of detecting C_{50}, C_{75}, and C_{90} for the two CPRBs are shown in Fig. 10.6.

Table 10-3 Monitoring Schemes Considered for a CPRB.

		Lateral Location of the Well Screen (m)			
		20.5, 21.5, 22.5, 23.5, 24.5 and 40.5, 41.5, 42.5, 43.5, 44.5	20.5, 22.5, 24.5 and 40.5, 42.5, 44.5	21.5, 23.5 and 41.5, 43.5	22.5 and 42.5
Vertical Location of the Center of the	1.5, 0.5	MW1 Δy=1 m, Δz=1 m (20 Screens)	MW4 Δy=2 m, Δz=1 m (12 Screens)	MW7 Δy=2 m, Δz=1 m (8 Screens)	MW10 one well, Δz=1 m (4 Screens)
	1.5	MW2 Δy=1 m, one screen (10 Screens)	MW5 Δy=2 m, one screen (6 Screens)	MW8 Δy=2 m, one screen (4 Screens)	MW11 one well, one screen (2 Screens)
	0.5	MW3 Δy=1 m, one screen (10 Screens)	MW6 Δy=2 m, one screen (6 Screens)	MW9 Δy=2 m, one screen (4 Screens)	MW12 one well, one screen (2 Screens)

Δy is lateral monitoring well spacing
Δz is vertical well screen spacing

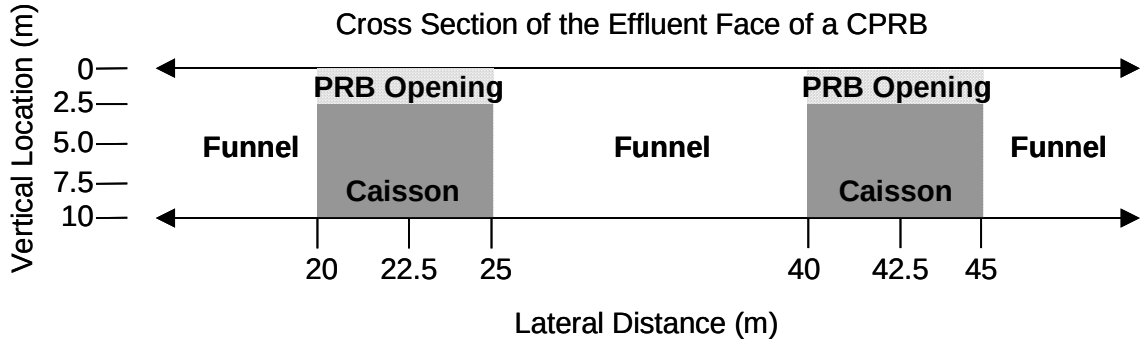

The probabilities of detecting C_{50}, C_{75}, and C_{90} are higher for the CPRB than for the HFPRB or FGPRB. Placing wells across the bottom of the effluent opening

a) Probability of Detecting C_{50}

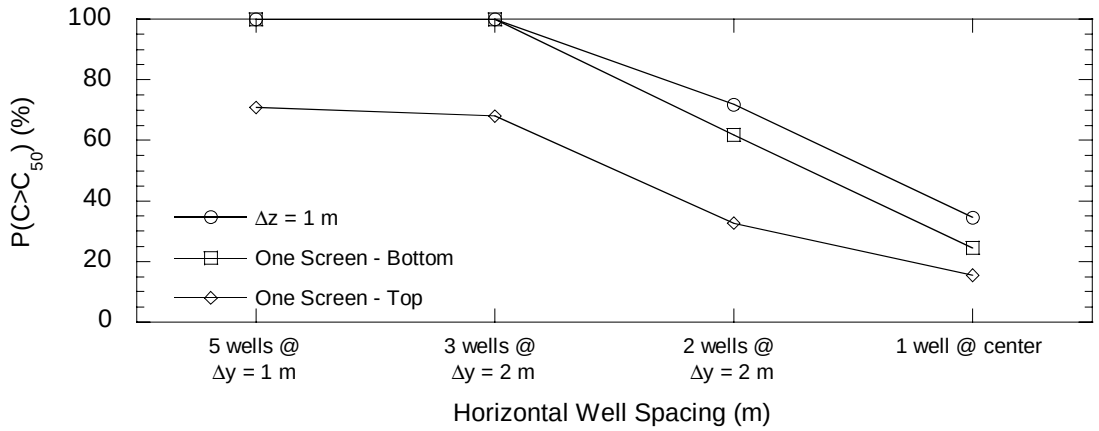

b) Probability of Detecting C_{75}

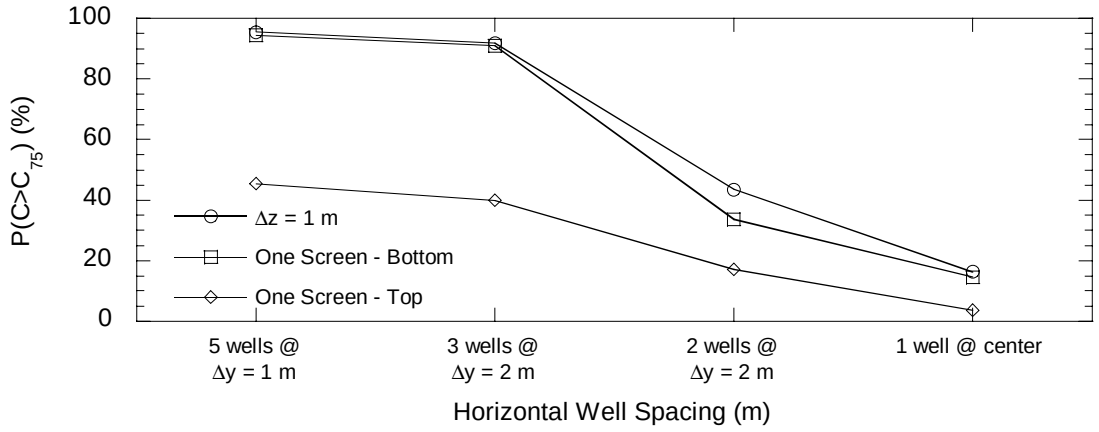

c) Probability of Detecting C_{90}

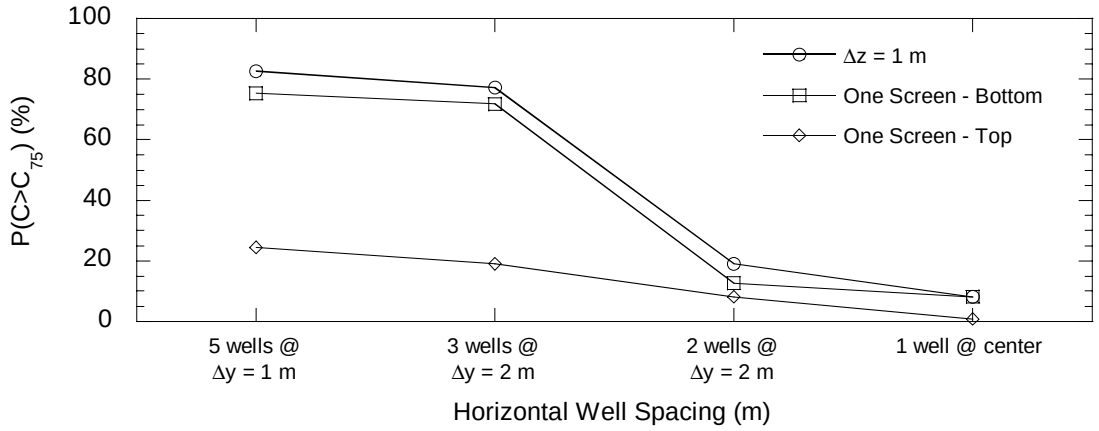

Fig. 10.6 Probability of Detecting C_{50} (a), C_{75} (b), and C_{90} (c) of Concentration as a Function of Horizontal and Vertical Well Screen Spacing.

appears to be the key to effective monitoring of a CPRB. Probabilities of detection decrease if only a single well screen or two well screens located at 1/3 points across the effluent opening are used (i.e., 1 well or wells at y = 21.5, 23.5, 41.5, and 43.5 m). The probability of detection is about 30% higher when a third monitoring well is added to the system so that monitoring wells are located at the edges and center of the effluent openings. Furthermore, the probability of detection is 30 to 50% higher when well screens are placed near the bottom of the effluent opening than when well screens are only placed at the top of the opening nearer the water surface. The CPRB is the only PRB that can be effectively monitored with single-screened wells.

Monitoring of a CPRB should use $\Delta y \leq 2$ m and wells should be positioned near the sides of CPRB outlet. Only a single well screen located near the base of the outlet is needed. Such a system is expected to have almost a 100% chance of detecting C_{50}, nearly a 90% chance of detecting C_{75}, and a 70% chance of detecting C_{90}. These probabilities are 10 to 30% higher than those achieved bya single screened monitoring systems for HFPRBs and FGPRBs.

The benefit of adding additional well screens to a monitoring system was evaluated. Probabilities of detecting C_{50}, C_{75}, and C_{90} were plotted versus the number of well screens in a system (Fig. 10.7a), functions were fit to these data, and the derivatives of these functions plotted (Fig. 10.7b). The derivative (i.e. Fig. 10.7b) is the additional probability of detection that is gained by adding one more well screen to an existing monitoring system.

a) Probability of Detection versus the Number of Well Screens

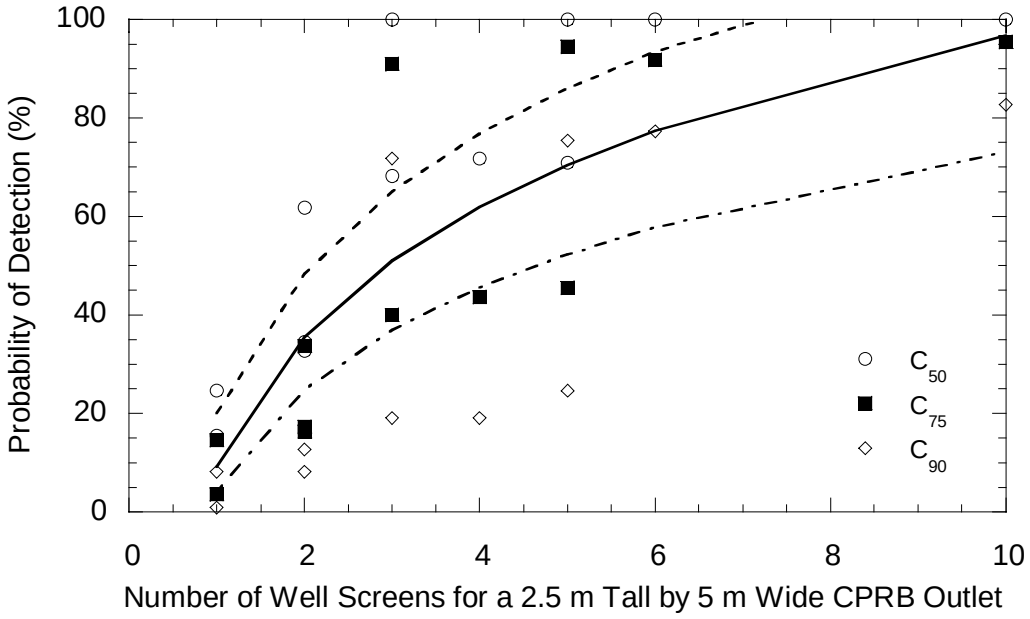

b) Additional Probability of Detection Gained By Adding a Well Screen

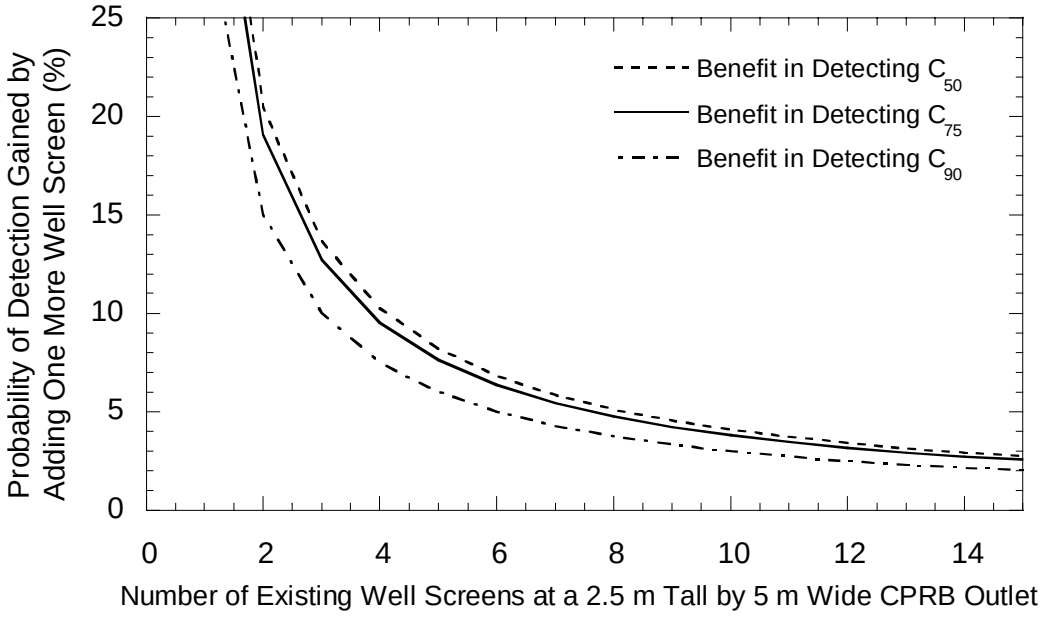

Fig. 10.7 Probability of Detecting the C_{50}, C_{75}, and C_{90} as a Function of the Number of Well Screens (a), and the Benefit Gained by Adding an Additional Well Screen to a Monitoring Scheme (b) for a CPRB.

The curves in Fig. 10.7b begin to flatten after about three well screens are used. There is a 10 to 30% increase in the probability of detection when a well screen is added to system that has one or two well screens, but less than a 10% increase in probability of detection for systems with three or more well screens. This result supports the previous recommendation that CPRBs are efficiently monitored using closely spaced wells that have a single well screen located near the base of the CPRB outlet (i.e., single-screened wells at $\Delta y \leq 2$ m with wells located at the edges of the effluent opening).

10.6 RECOMMENDATIONS FOR MONITORING PRBS

Monitoring systems for HFPRBs, FGPRBs and CPRBs were evaluated. Monitoring systems that yield the highest probability of detecting C_{50}, C_{75}, and C_{90} with the fewest monitoring well screens were determined for each type of PRB. The recommended lateral well spacing (Δy) and vertical well screen spacing (Δz) for each type of PRB are listed in Table 10.4 along with the expected probabilities of detecting C_{50}, C_{75}, and C_{90} for the recommended systems.

Table 10-4 Recommended Monitoring Systems for PRBs.

	Lateral Monitoring Well Spacing (Δy)	Well Screen Separation (Δz)[1]	Expected Prob. of Detection		
			C_{50}	C_{75}	C_{90}
HFPRB	5 m	3 m	95%	80%	45%
FGPRB	2 m	4 m	90%	70%	40%
CPRB	2 m[2]	None[3]	~100%	90%	70%

1 – center to center spacing of 1 m long well screens
2 – monitoring wells should be placed at the edges of the effluent opening
3 – well screens should extend to the bottom of the CPRB opening

SECTION 11

ADDITIONAL DESIGN CONSIDERATIONS

Previous sections of this report dealt with design thickness and monitoring systems for PRBs. This section briefly addresses two additional design questions that have arisen during this study. The first half of this section addresses the effectiveness of installing gravel zones immediately up-gradient and down-gradient of a PRB. Gravel zones are intended to induce mixing of groundwater and more uniform flow through the PRB. The effectiveness of gravel zones at producing more uniform influent, more uniform residence time, and lower effluent concentrations will be assessed in Section 11.1.

The second design consideration that is discussed in this section is the distribution of concentrations down-gradient of the PRB. Previous results have assumed that the effluent face of the PRB is the point at which compliance of the PRB is judged. However, the choice of this compliance point raises concerns about the distribution of concentration down-gradient of the PRB at locations where perhaps a property line or sensitive receptor is located. To assess changes in concentration throughout the aquifer, influent, effluent concentrations at the back of the PRB, concentrations 10 m beyond the back of the PRB, and concentrations 20 m beyond the back of the PRB will be presented and discussed for several simulations that cover the range of aquifer heterogeneity.

11.1 GRAVEL ZONES

Gravel zones before and after a PRB have been used at several field sites (e.g., Moffett Naval Air Station) with the intent of creating more uniform flow through the PRB (NFESC, 1998). More uniform flow is expected to yield more uniform residence times for contaminants in the PRB and consequently a more uniform distribution of concentration exiting the PRB. In essence, gravel zones on either side of a PRB are expected to dampen fluctuations in flow entering and exiting the PRB so that plug flow models are more appropriate for design.

The effectiveness of gravel zones at producing more uniform residence time of groundwater in the PRB was investigated by simulating a HFPRB, FGPRB, and CPRB with and without gravel zones. Simulations were performed for each type of PRB in a moderately heterogeneous aquifer, very heterogeneous aquifer, and aquifer with longer correlation lengths. Results from simulations of homogeneous PRBs with gravel zones were then compared with results from simulations of the identical PRB without gravel zones. Results were compared using two measures of effectiveness, the distribution of travel time for particles crossing the PRB and the distributions of influent and effluent concentration.

11.1.1 Gravel Zones for HFPRBs

A plan view of the conceptual model that is used for simulating a HFPRB with gravel zones is shown in Fig. 11.1. This is the same conceptual model used in Section 5 for the HFPRB except that one-half meter wide, fully penetrating

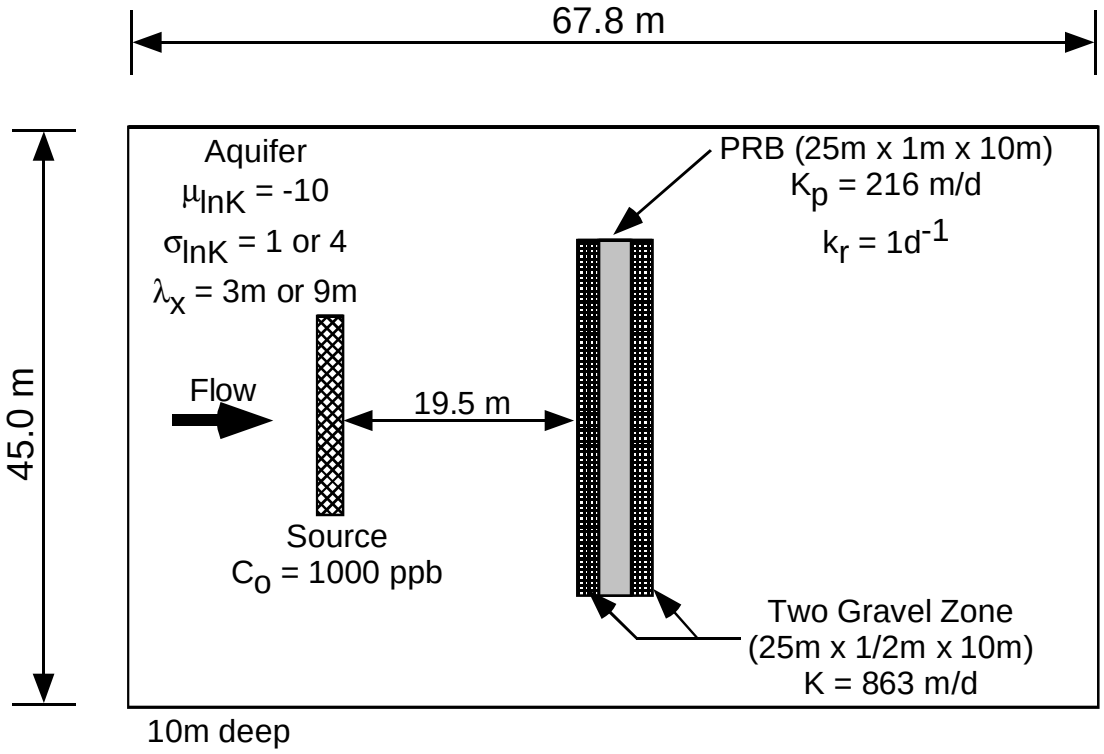

Fig. 11.1 Conceptual Model of a HFPRB with Gravel Zones.

gravel zones are placed in front and behind the PRB. The gravel zones are homogeneous with a hydraulic conductivity of 863 m/d, which is four times greater than the hydraulic conductivity of the PRB. The thickness and hydraulic conductivity of the gravel zones were selected to be consistent with the gravel zones used at Moffett Naval Air Station (NFESC, 1998). Aquifers with moderate heterogeneity (σ_{lnK} = 1.0 and 2.25, λ_x = 3 m, λ_y = 1 m), high heterogeneity (σ_{lnK} = 4.0, λ_x = 3 m, λ_y = 1 m), and longer correlation lengths (σ_{lnK} = 1.0, λ_x = 9 m, λ_y = 3 m) were used for evaluating the impact of gravel zones. All simulations have a homogeneous PRB ($K_p = 2.5 \times 10^{-3}$ m/s, $k_r = 1.0\ d^{-1}$) in aquifers with μ_{lnk} = -10.

Cumulative distributions of residence time for particles to pass through a HFPRB with and without gravel zones are shown in Fig. 11.2. The addition of gravel zones causes the distribution of residence times to become narrower, indicating that flow through the wall is more uniform. The residence time at the upper tail of the distribution decreases by about 2.5 days when gravel zones are used. In contrast, the median residence time for particles to pass through the PRB is unaffected by the gravel zones.

An analysis of residence time alone may be misleading unless concentrations entering the PRB are uniform. A better evaluation of the effect of gravel zones should consider the distributions for influent concentrations and the resulting distribution of effluent concentrations. Distributions of influent and effluent concentration for a HFPRB with and without gravel zones are shown in Fig. 11.3.

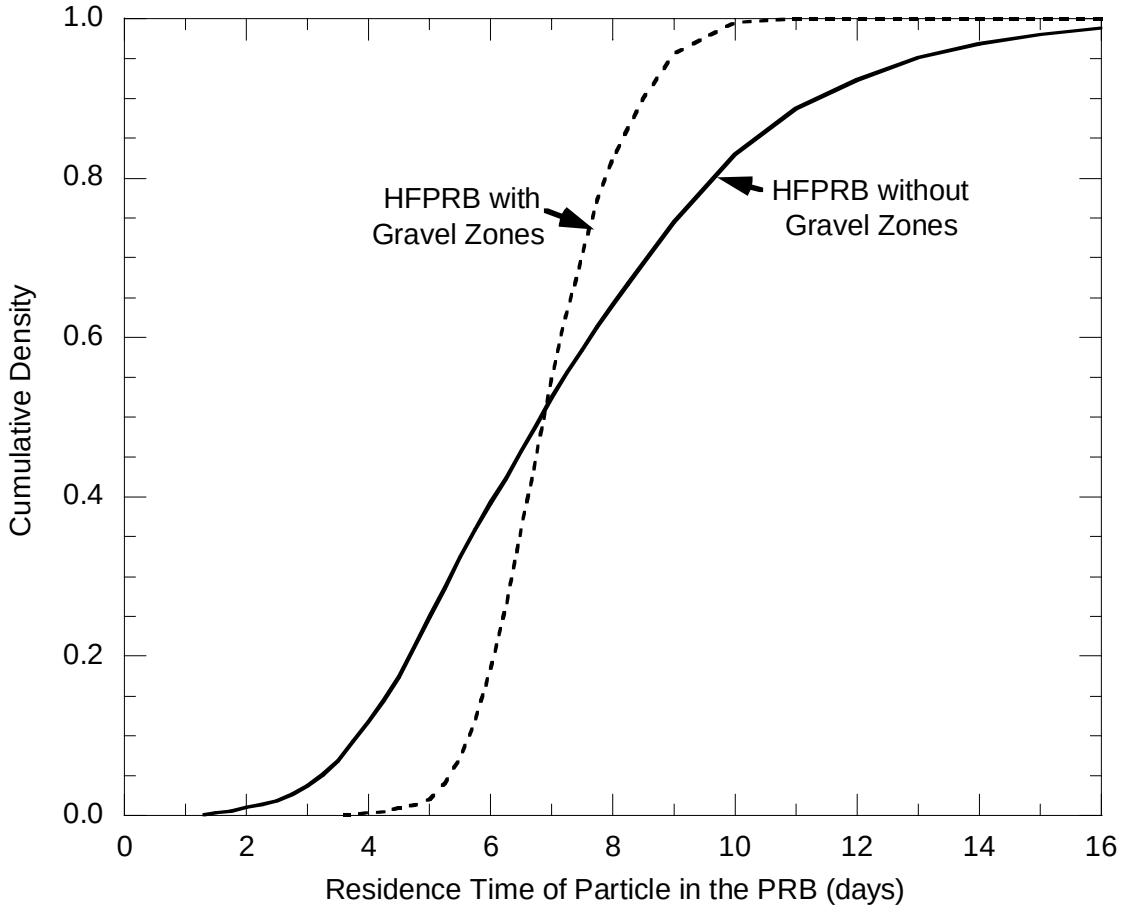

Fig. 11.2 Cumulative Distributions of Transit Time for Particles to Travel through HFPRBs With and Without Gravel Zones (σ_{lnK} = 1.0).

a) Influent Concentration

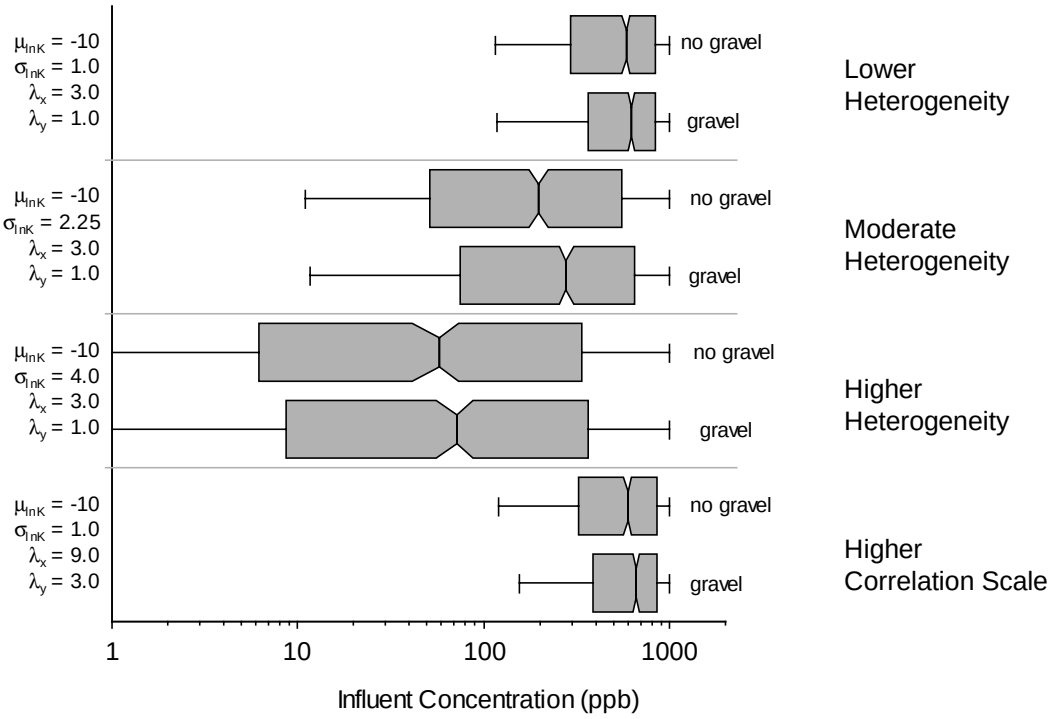

b) Effluent Concentration

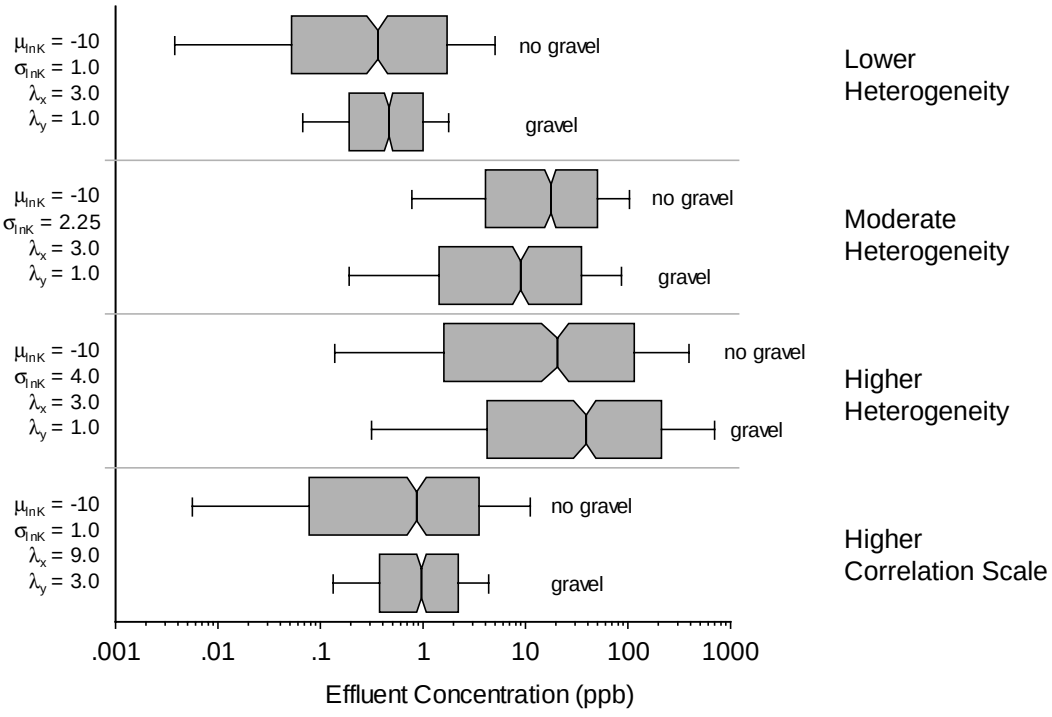

Fig. 11.3 Distributions of Influent (a) and Effluent (b) Concentration from HFPRBs With and Without Gravel Zones.

Gravel zones increase the median and 75th percentile of influent concentration by less than 20%, but do not significantly change the range or 90th percentile of influent concentration. Influent concentrations increase slightly because there is less mixing at the influent face of the PRB when gravel zones are not used. As will be shown subsequently, PRBs without gravel zones have a significant amount of vertical flow through the reactive media, particularly at higher σ_{lnK}. This vertical component of flow induces some mixing and dilutes concentrations slightly. Flow is more horizontal through HFPRBs with gravel zones; consequently, there is less mixing and some influent concentrations are slightly higher.

Gravel zones do cause effluent concentrations to become more uniform and higher effluent concentrations to decrease in lower to moderately heterogeneous aquifers (i.e., $\sigma_{lnK} \leq 1.0$). The benefit gained by the gravel zones is about a two-fold decrease in the 90th percentile of effluent concentration when $\sigma_{lnk} = 1.0$. This is a more modest benefit than that predicted based on travel time (i.e., a 2 to 2.5 day increase in residence time corresponds to an order of magnitude decrease in effluent concentration). The more modest benefit gained from the gravel zones is caused by not making assumptions about the distribution of concentration entering the PRB.

The results for PRBs with and without gravel zones located in aquifers that have higher σ_{lnK} are not immediately intuitive. At $\sigma_{lnK} = 4.0$, there is a factor of 2 increase in effluent concentrations between the HFPRB with gravel zones and HFPRB without gravel zones and the range of effluent concentrations are similar.

The gravel zones appear to have the opposite effect to that intended and are detrimental to the performance of the PRB.

To understand why gravel zones are detrimental to HFPRB in aquifers with higher σ_{lnK}, flow through the gravel zones and PRB has to be understood. Gravel zones have higher hydraulic conductivities than the PRB and provide paths of less headloss for water flow. That is, groundwater prefers to move diagonally through the gravel zones and horizontally through the PRB to minimize energy lost between more permeable units on either side of the PRB. The result of horizontal flow rather than diagonal flow through the reactive media is a shorter residence time for groundwater in the PRB. Shorter residence times of groundwater in the PRB cause higher effluent concentrations to occur in more heterogeneous aquifers for PRBs with gravel zones. The σ_{lnK} where gravel zones become detrimental varies depends on the percentile of the effluent distribution chosen for analysis; for the 90^{th} percentile of effluent concentration, HFPRBs with and without gravel zones yield nearly equal effluent concentrations at σ_{lnK} of approximately 2.3 (Fig. 11.3b). Gravel zones increase effluent concentrations for σ_{lnK} greater than 2.3 and decrease effluent concentrations for σ_{lnK} less than 2.3.

Diagonal flow through the gravel zone and horizontal flow through the reactive media is illustrated in Fig. 11.4, which shows particle trajectories through a PRB surrounded by gravel zones (Fig. 11.4a) and a PRB without gravel zones (Fig. 11.4b). Without gravel zones, particles pass through the PRB diagonally between permeable units. With gravel zones, particles pass through the PRB more

a) HFPRB without Gravel Zones

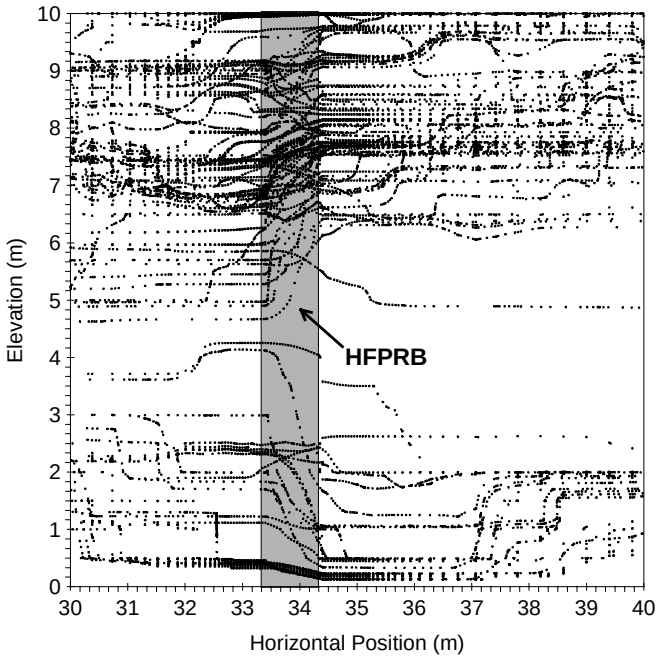

b) HFPRB with Gravel Zones

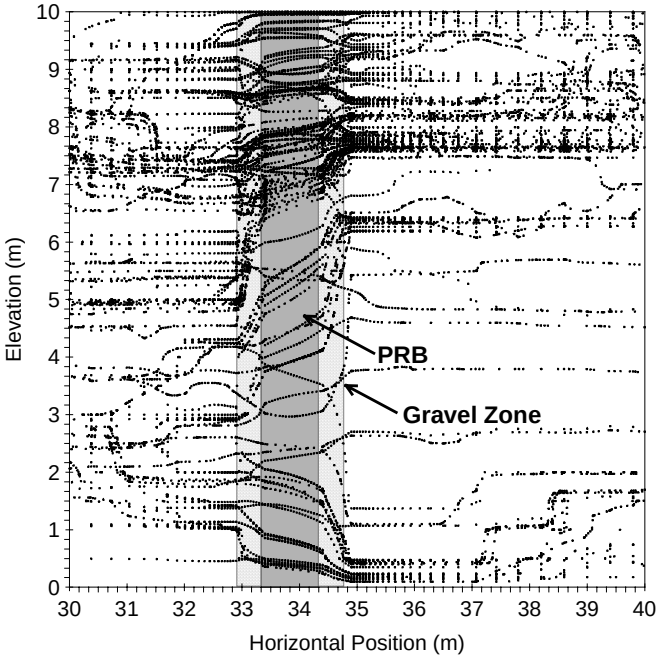

Fig. 11.4 Particle Trajectories through a HFPRB With Gravel Zones (a) and Without Gravel Zones (b) in Aquifers with $\sigma_{lnK} = 4$.

horizontally. The angle and distance of particle trajectory across the PRB are shown in Fig. 11.5. When gravel zones are located on either side of the PRB, particle trajectories through the PRB are more horizontal (Fig. 11.5a). More horizontal particle paths cause shorter travel distance for particles across the PRB (Fig. 11.5b), and thus, lower residence time and less mass conversion, assuming similar gradients.

In summary, the benefits of gravel zones around a HFPRB are questionable. In aquifers with σ_{lnK} less than 2.3, gravel zones yield a modest decrease in peak effluent concentration, but in aquifers with σ_{lnK} greater than 2.3, gravel zones may result in uniformly higher effluent concentrations.

11.1.2 Gravel Zones for FGPRBs

The impact of adding gravel zones up and down gradient of a FGPRB is investigated in this section. Gravel zones that are one-half meter thick with a hydraulic conductivity of 863 m/d were simulated directly in front and behind the gate of a FGPRB. FGPRBs with and without gravel zones were compared in a moderately heterogeneous aquifers (σ_{lnK} = 1.0, λ_x = 3 m, λ_y = 1 m), very heterogeneous aquifers (σ_{lnK} = 4.0, λ_x = 3 m, λ_y = 1 m), and aquifers with longer correlation lengths (σ_{lnK} = 1.0, λ_x = 9 m, λ_y = 3 m). All simulations are for homogeneous PRBs ($K_p = 2.5 \times 10^{-3}$ m/s, $k_r = 1.0\ d^{-1}$) in aquifers with μ_{lnk} = -10.

a) Average Angle of Particle Trajectory through the Reactive Media

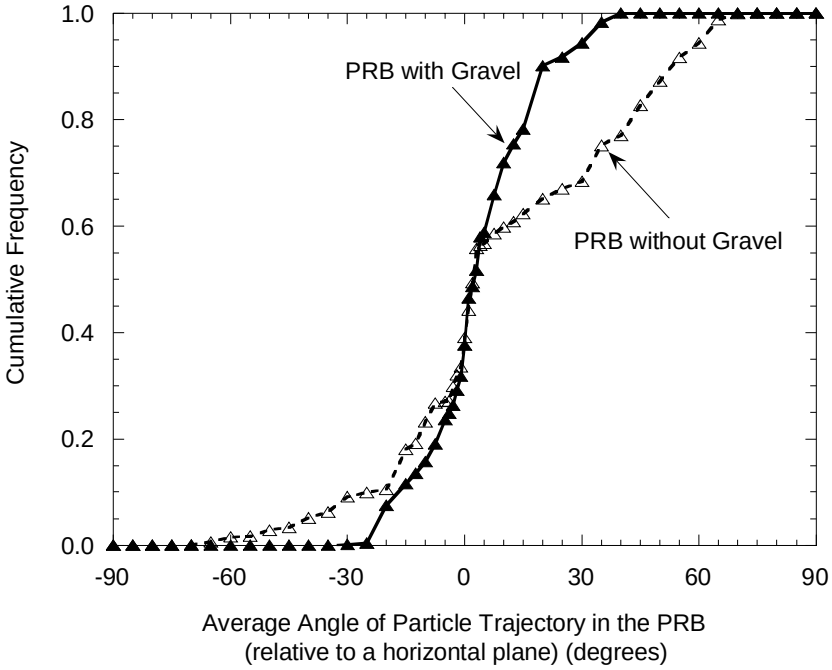

b) Travel Distance of Particles through the Reactive Media

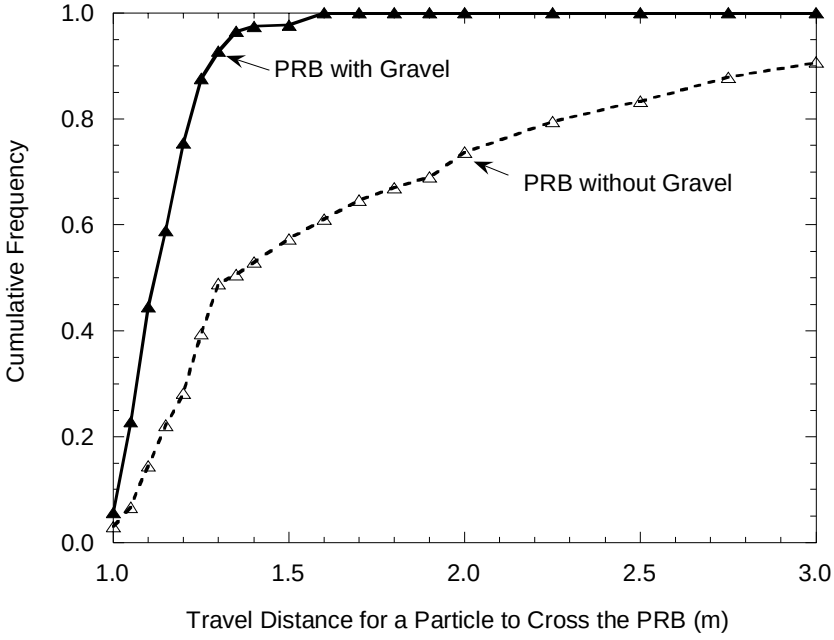

Fig. 11.5 Average Vertical Angle (a) and Travel Distance (b) of Particle Trajectory in HFPRBs With Gravel Zones and Without Gravel Zones in Aquifers with $\sigma_{lnK} = 4$.

Distributions of influent and effluent concentrations for a FGPRB with and without gravel zones are shown in Fig. 11.6. Influent concentrations are more broadly distributed and slightly lower when gravel zones are used. Median influent concentrations are 15% to 25% lower and the 10^{th} percentile of influent concentration decreases by 30% to 50% when gravel zones are used.

Despite having lower influent concentrations, FGPRBs with gravel zones have slightly higher effluent concentrations (Fig. 11.6b). Distributions of effluent concentration are also narrower when gravel zones are used. Differences in flow through the gate are the cause for more broadly distributed, slightly lower influent concentrations and higher, more uniform effluent concentrations for FGPRB with gravels zones. The trajectories of 75 particles passing through gates with and without gravel zones are shown in Fig. 11.7.

When gravel zones are not used, particles enter the gate and move through the gate between zones of higher hydraulic conductivity on either side of the PRB. The paths taken by particles are often diagonal because zones of higher hydraulic conductivity may not be aligned on either side of the gate. However, when gravel zones are used, the gravel zones have a hydraulic conductivity that is four times greater than the hydraulic conductivity of the reactive media. Thus, particle paths with the lowest head loss change from a diagonal path through the reactive media to a diagonal path through the gravel zones and a horizontal path across the PRB. This type of trajectory, which was observed at higher σ_{lnK} for the HFPRB, occurs even at σ_{lnK} of 1.0 for the FGPRB.

a) Influent Concentration

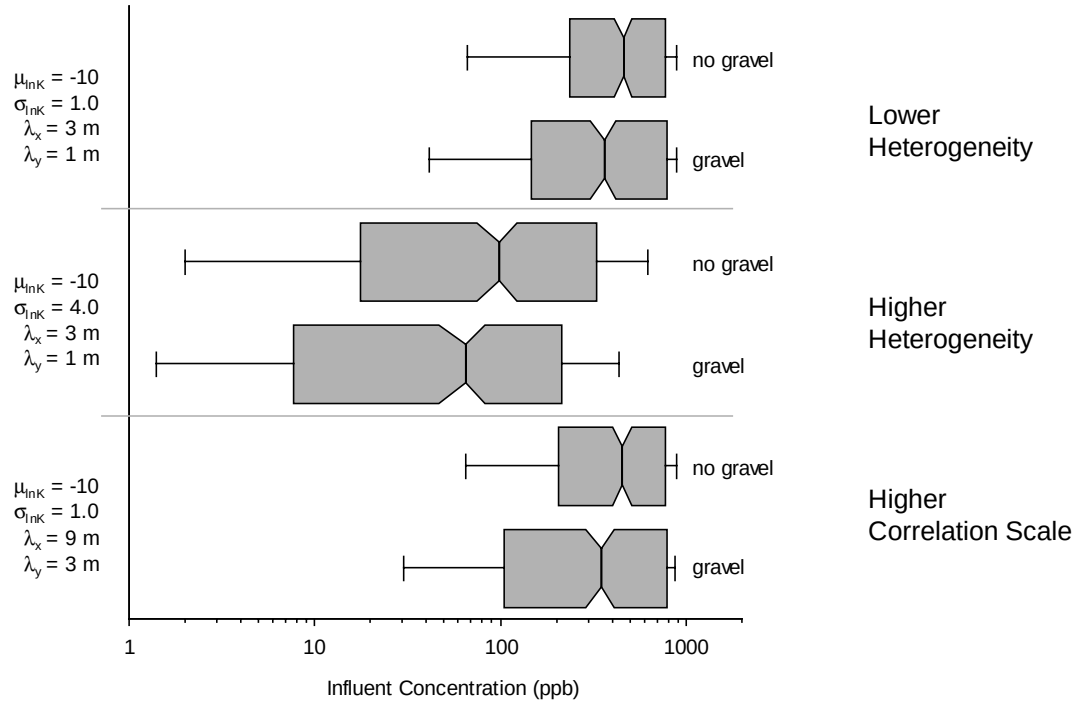

b) Effluent Concentration

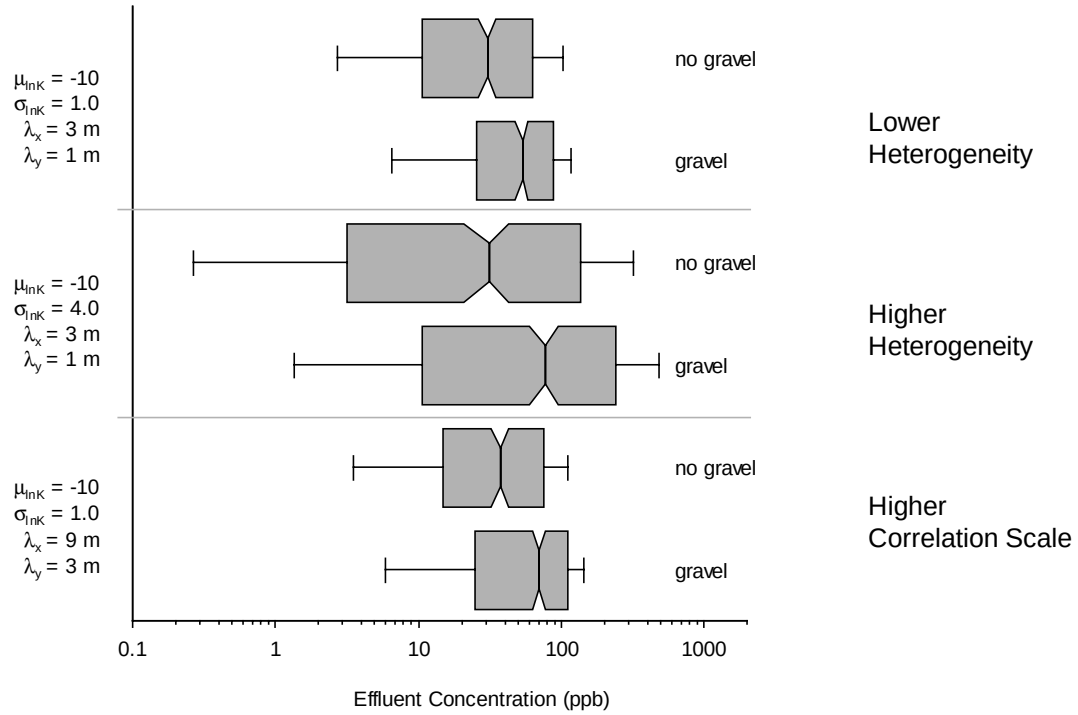

Fig. 11.6 Influent (a) and Effluent (b) Concentrations through FGPRBs with and without Gravel Zones.

Differences in flow through the PRB with gravel zones versus the PRB alone explain the changes that were observed in influent and effluent concentrations (Fig. 11.6). Diagonal flow through the up-gradient gravel zone results in greater mixing of the groundwater prior to entering the PRB. As a result, slightly lower and more broadly distributed influent concentrations occur when gravel zones are used. This is a benefit of using the gravel zones.

A disadvantage of using gravel zones is the horizontal flow that occurs. When groundwater passes through the gate horizontally, contaminants take the shortest possible path through the reactive media (Fig. 11.5). The gravel zones produce more uniform groundwater velocities through the reactive media and more uniform residence times (Fig. 11.8); however, the average velocity of groundwater with and without the gravel zones is similar because the PRB and gravel zones represent such a small amount of headloss for the system (Fig. 11.8a). Thus, the shorter path which occurs when gravel zones are used causes shorter residence times for contaminants in the reactive media (Fig. 11.8b) and higher effluent concentrations.

In summary, more horizontal particle trajectories occur when gravel zones are used for FGPRBs in aquifers with modest and higher heterogeneity, and at shorter and longer correlation lengths; this result only occurs in highly heterogeneous aquifers for the HFPRB. Since this type of flow yields shorter contact time for contaminants in the reactive media and higher effluent concentrations, gravel zones are not recommended for FGPRBs.

a) Without Gravel Zones

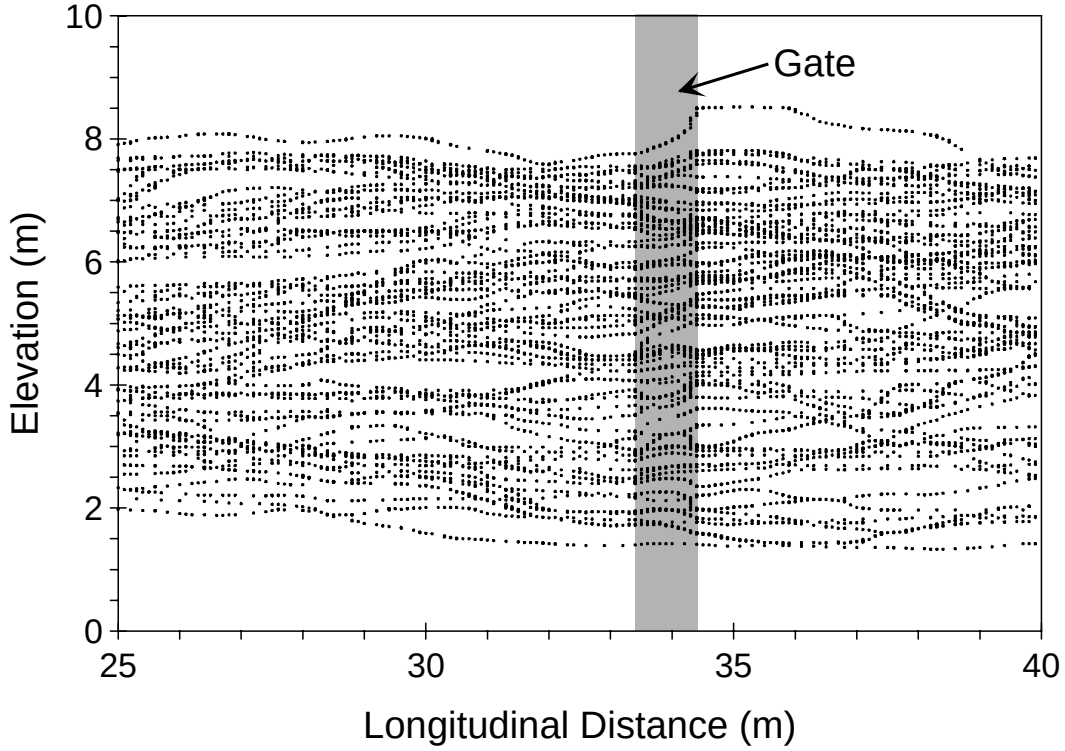

b) With Gravel Zones

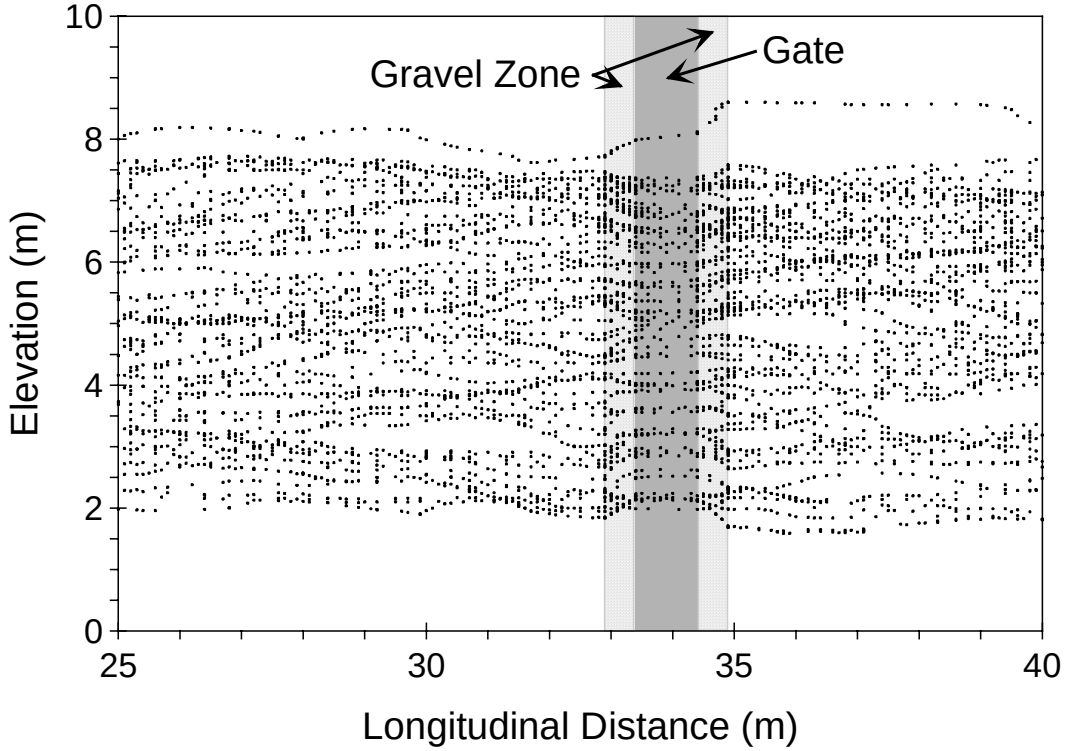

Fig. 11.7 Trajectory of Particles Passing through a FGPRB without Gravel Zones (a) and with Gravel Zones (b) (σ_{lnK} = 1.0).

a) Average Horizontal Velocity

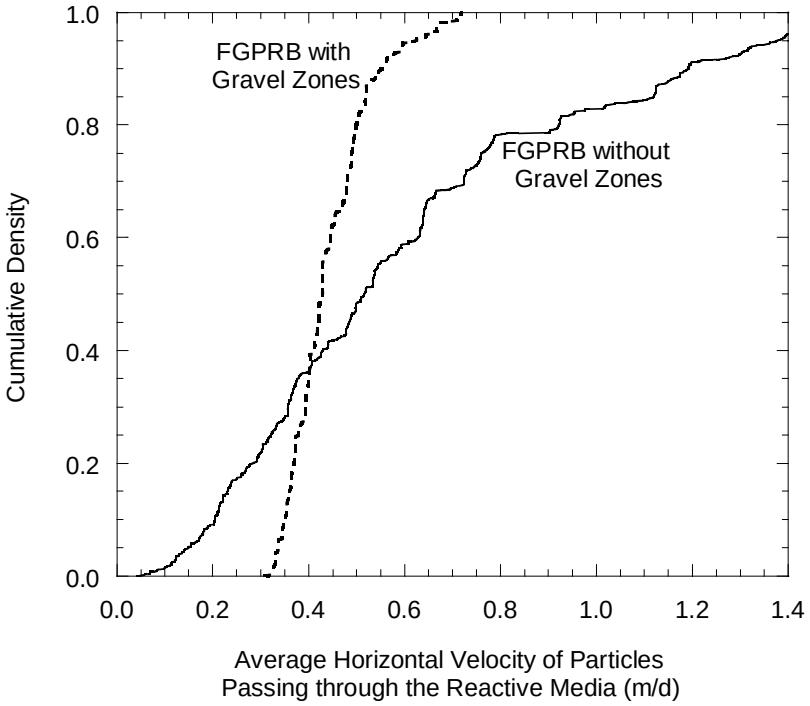

b) Residence Time

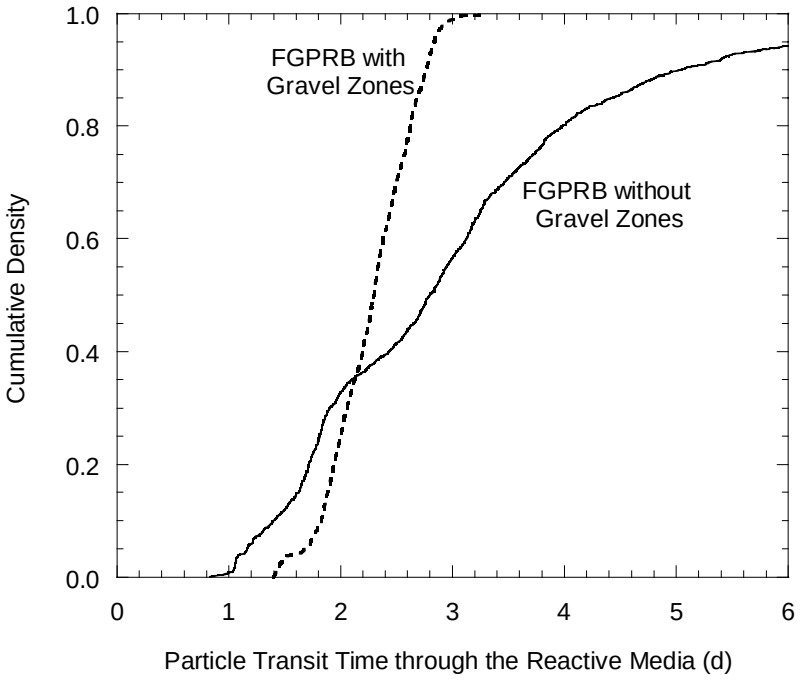

Fig. 11.8 Cumulative Distributions for the Average Horizontal Velocity (a) and Residence Time (b) of Particles in the Reactive Media.

11.1.3 Gravel Zones for CPRBs

The impact of adding gravel zones up and down gradient of a CPRB is investigated in this section. Gravel zones that are one-half of a meter thick were simulated directly in front and behind the caisson of a CPRB. The gravel zones extend the entire thickness of the aquifer, but are not located in front of the funnels. CPRBs with and without gravel zones were compared in a moderately heterogeneous aquifer (σ_{lnK} = 1.0, λ_x = 3 m, λ_y = 1 m), very heterogeneous aquifer (σ_{lnK} = 4.0, λ_x = 3 m, λ_y = 1 m), and aquifer with longer correlation lengths (σ_{lnK} = 1.0, λ_x = 9 m, λ_y = 3 m). All simulations are for homogeneous PRBs ($K_p = 2.5 \times 10^{-3}$ m/s, $k_r = 1.0\ d^{-1}$) in aquifers with μ_{lnk} = -10.

Distributions of influent and effluent concentrations for a CPRB with and without gravel zones are shown in Fig. 11.9. Influent concentrations are similar for CPRBs with and without gravel zones. The 25th and 75th percentile of influent concentration changes slightly when σ_{lnK} = 4.0 and gravel zones are used, but the median influent concentration and range of influent concentrations are unchanged. Thus, gravel zones induce some mixing of influent to a CPRB, but do not significantly change the range or median influent concentration.

Effluent concentrations change significantly when gravel zones are added to a CPRB, especially at lower σ_{lnK}. In moderately heterogeneous aquifers (σ_{lnK} = 1.0), effluent concentrations increase by three fold when gravel zones are added (Fig. 11.9b). The change in effluent concentration can be explained by considering

a) Influent Concentration

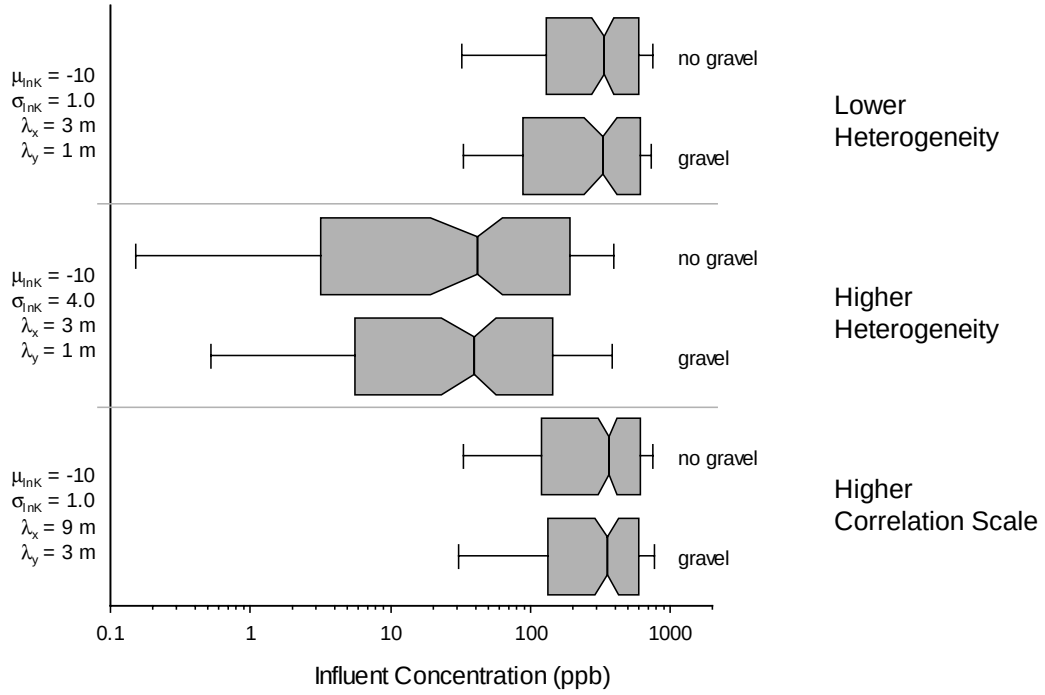

b) Effluent Concentration

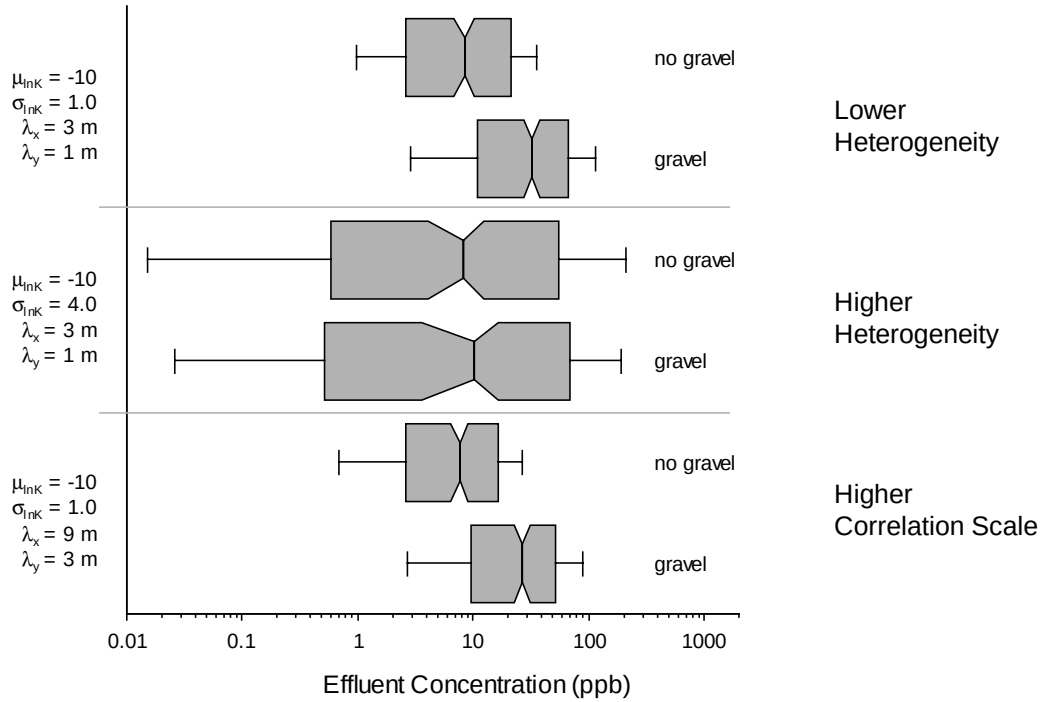

Fig. 11.9 Distributions of Influent (a) and Effluent (b) Concentrations for CPRBs with and without Gravel Zones

the quantity of water captured by the funnels and the flow rate of water through the reactive media. In moderately heterogeneous aquifers, CPRBs with gravel zones have higher effluent concentrations because the velocity of groundwater flowing through the PRB is higher, causing residence time of contaminants in the reactive media to be shorter. Cumulative distributions of average velocity and residence time for particle in the reactive media are shown in Fig. 11.10. Median velocity through the CPRB increases by about 35% when gravel zones are used (Fig. 11.10a), which causes the residence time of groundwater in the reactive media to decrease (Fig. 11.10b).

In aquifers with (σ_{lnK} = 1.0), the median residence time decreases from 3.2 days to 2.1 days. For an influent concentration of 200 ppb (median influent for σ_{lnK} = 1.0 in Fig. 11.9a) and k_r = 1 d^{-1}, these residence times yield effluent concentrations of 8.15 ppb and 24.5 ppb respectively, a three-fold increase due to the gravel zones. A three-fold increase in effluent concentration is approximately equal to the shift in distributions of effluent concentration for aquifers with σ_{lnK} = 1.0 in Fig. 11.9b. In aquifers with σ_{lnK} = 4.0, the change in residence times are more modest (median residence time are 0.25 days and 0.45 days with and without gravels zones respectively). For a median influent concentration of 40 ppb, these residence times yield effluent concentrations of 31 ppb with gravel zones and 26 ppb without gravel zones. This is only a 20% increase in effluent concentration, significantly less than the 300% increase in aquifers where σ_{lnK} = 1. However, the 20% increase in effluent concentration is similar to the increase in the median and 75th percentile of effluent concentration shown in Fig. 11.9b.

a) Particle Velocity

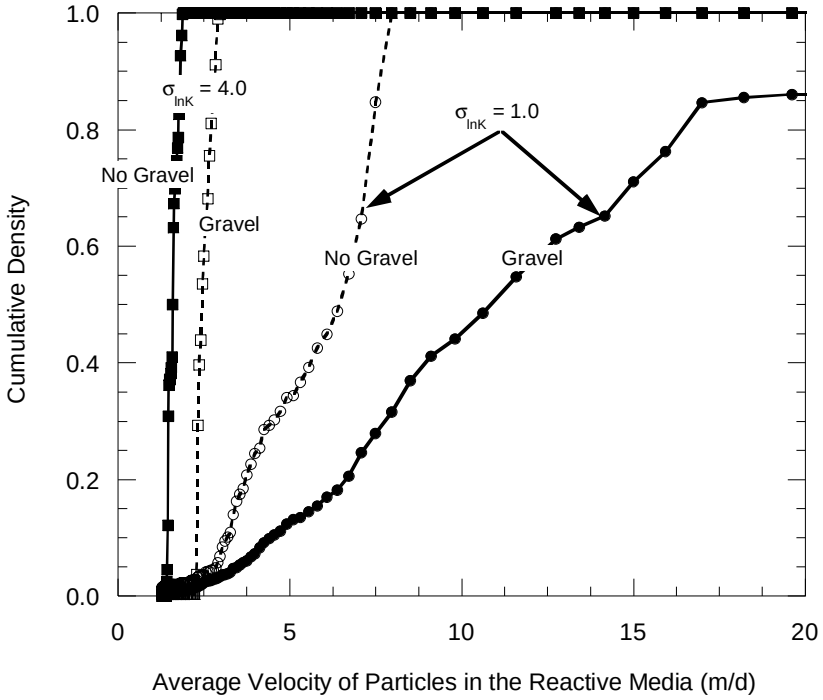

b) Residence Time

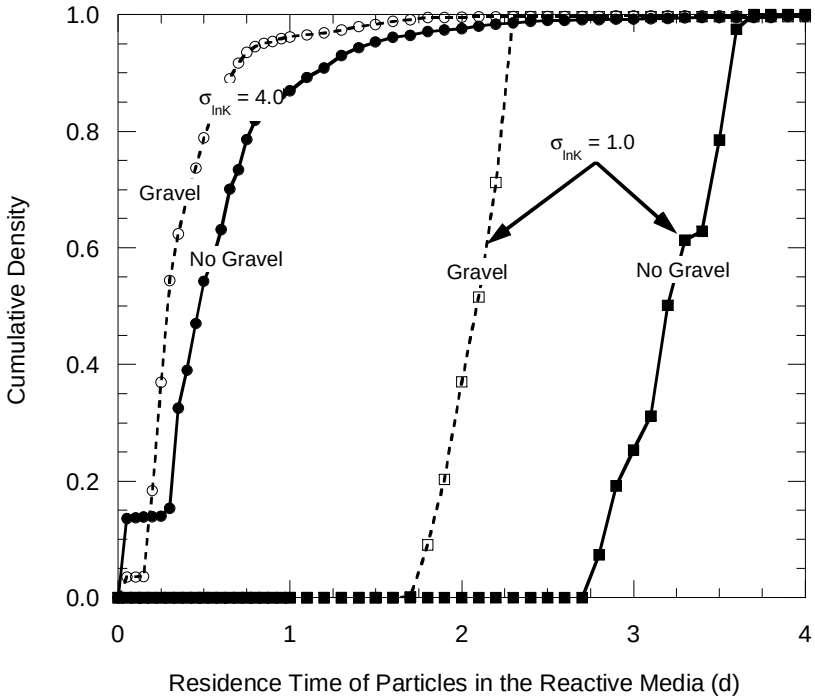

Fig. 11.10 Cumulative Distributions of Velocity (a) and Residence Time (b) for Particle in a CPRBs with and without Gravel Zones

Despite the magnitude of the change in effluent concentration, the result of using gravel zones is the same. Gravel zones increase the velocity of groundwater through the reactive media and decrease residence times of contaminants in the media which causes higher effluent concentrations. The gravel zones appear to increase median residence time by 35% to 50%, which has a greater impact on CPRBs in more homogeneous aquifers that have larger residence times.

The cause for velocities increasing and residence times decreasing when gravel zones are used is related to the quantity of water captured by the funnels and forced through the CPRB. For CPRBs without gravel zones, groundwater converges and moves downward as it approaches the CPRB because it has to flow through the opening at the base of the CPRB (Fig. 11.11a). However, when gravel zones are used, groundwater flows horizontally through the aquifer toward the PRB and then vertically in the gravel zone to the opening (Fig. 11.11b). By following this path, groundwater travels a shorter distance in the aquifer, which has a hydraulic conductivity more than two orders of magnitude less than gravel zones. Groundwater then flows through the higher hydraulic conductivity gravel zones and through the PRB. Vertical flow through the gravel zone and horizontal flow through the aquifer also occurs on the effluent side of the CPRB.

Groundwater minimizes travel through the aquifer by moving vertically through the gravel zones because this path has a higher effective hydraulic conductivity than a path diagonally across the aquifer. As a result, under a similar gradient, more water can flow through the CPRB when gravel zones are used. The

a) Without Gravel Zones

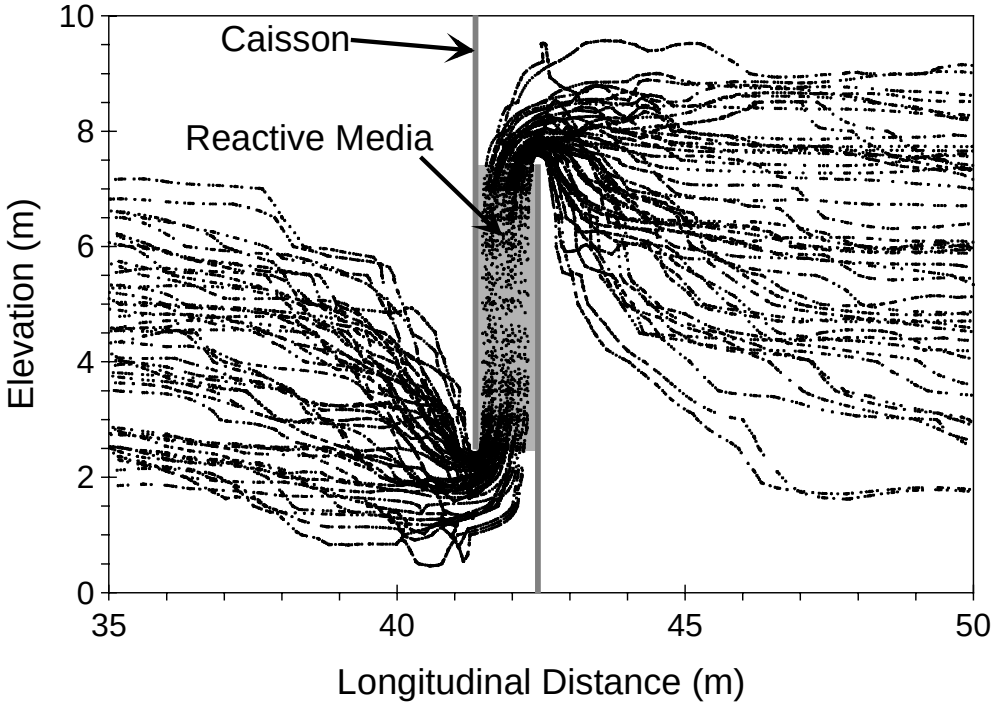

b) With Gravel Zones

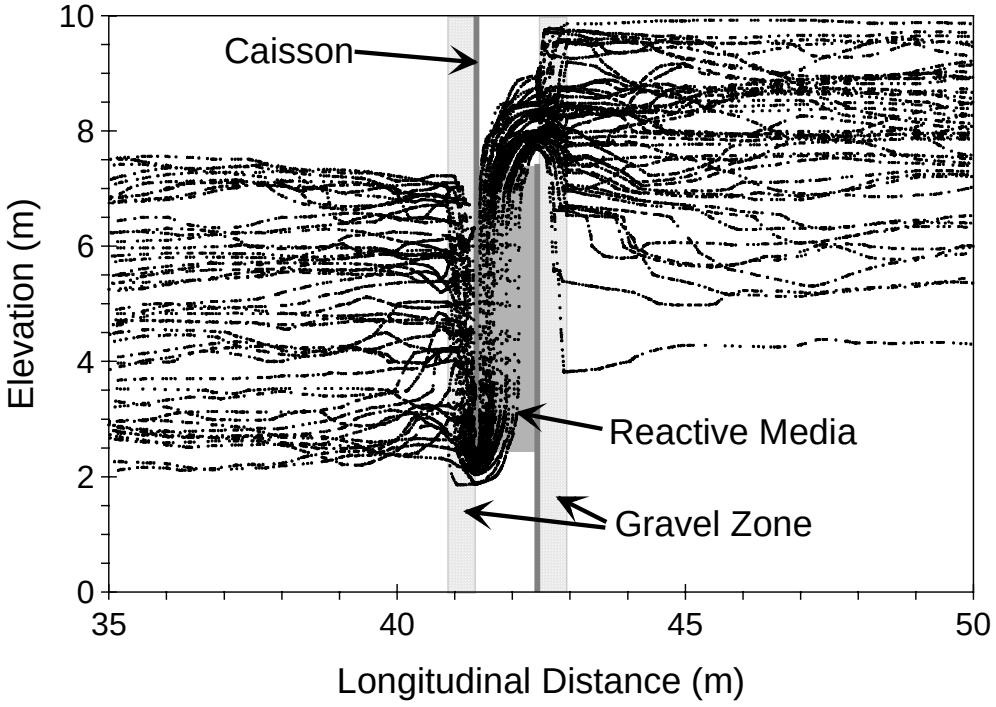

Fig. 11.11 Particle Trajectory Into, Through, and Out of CPRBs without (a) and with Gravel Zones.

larger flow rate caused by a more conductive path increases the velocity of water flowing through the reactive media and increases the capture zone of the funnels.

Capture zones of CPRB systems with and without funnels are shown in Fig. 11.12 for aquifers with $\sigma_{lnK} = 1.0$. Plumes captured by the funnels (i.e., the size of the area in which particles eventually travel through the CPRBs) are approximately 20% wider when the CPRBs have gravel zones (e.g., 17.5 m compared to 22.5 m). The wider plumes cause more water to flow through the PRBs. However, the size of the CPRBs is fixed, meaning that water must flow through the reactive media faster.

The 20% increase in the size of the capture zones shown in Fig. 11.12 does not account for the 35% decrease in residence time shown in Fig. 11.10b. However, the width of the capture zone for a CPRB system is not uniform with depth. Rather the capture zone will be larger at the base of the aquifer closer to the CPRB opening and smaller at the top of the aquifer. The capture zones shown in Fig. 11.12 are for a mid-depth in the aquifer and therefore larger volumes of water captured at other depths is believed to cause the additional decrease in residence times.

In summary, gravel zones for CPRBs are useful for increasing the capture zone of the funnel. The gravel zones do not accomplish their objective of creating more uniform residence times or lower effluent concentrations. Instead, the gravel zones draw a larger quantity of water into the PRB, decreasing the residence time of contaminants in the reactive media and causing effluent concentrations to increase.

a) CPRB Without Gravel Zones

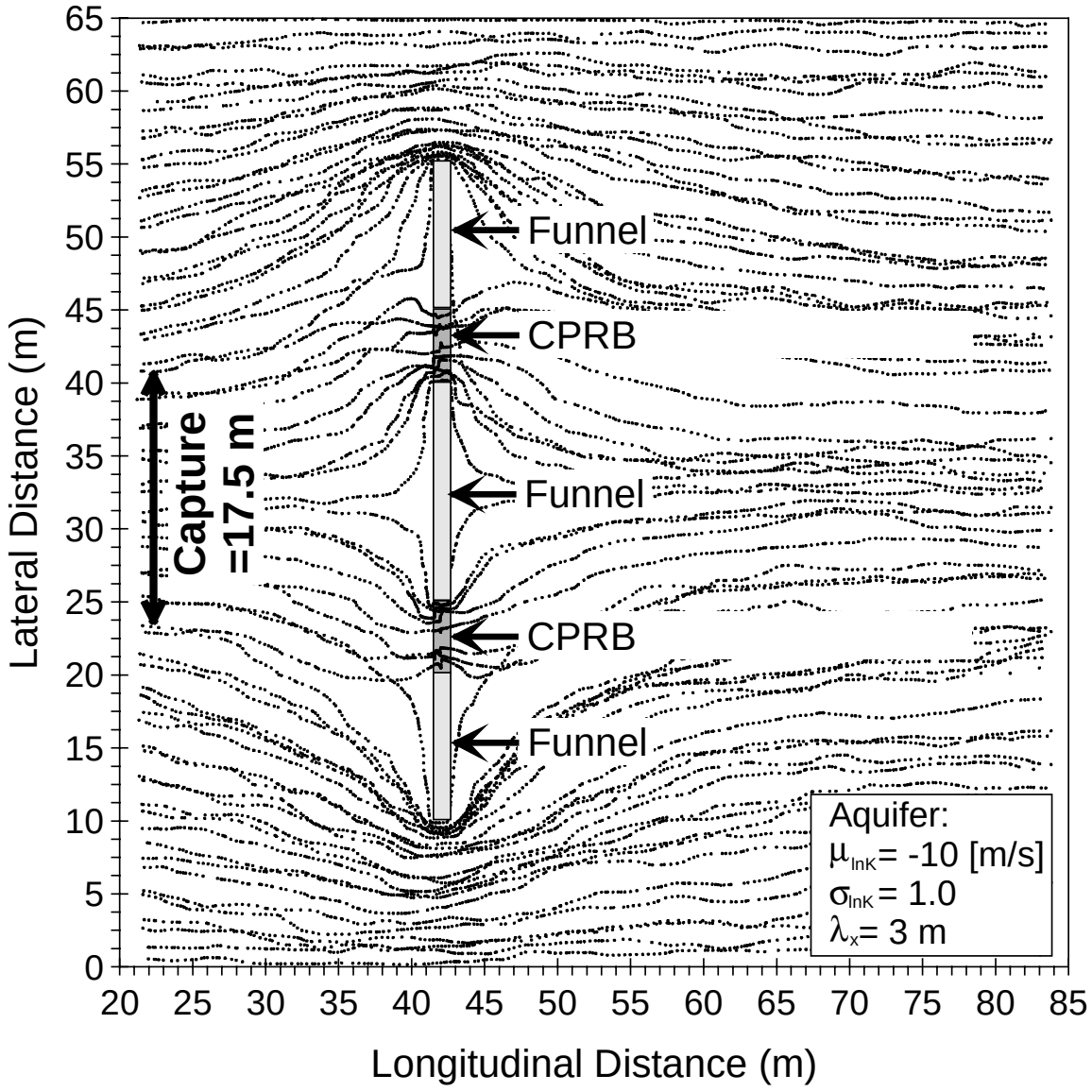

b) CPRB With Gravel Zones

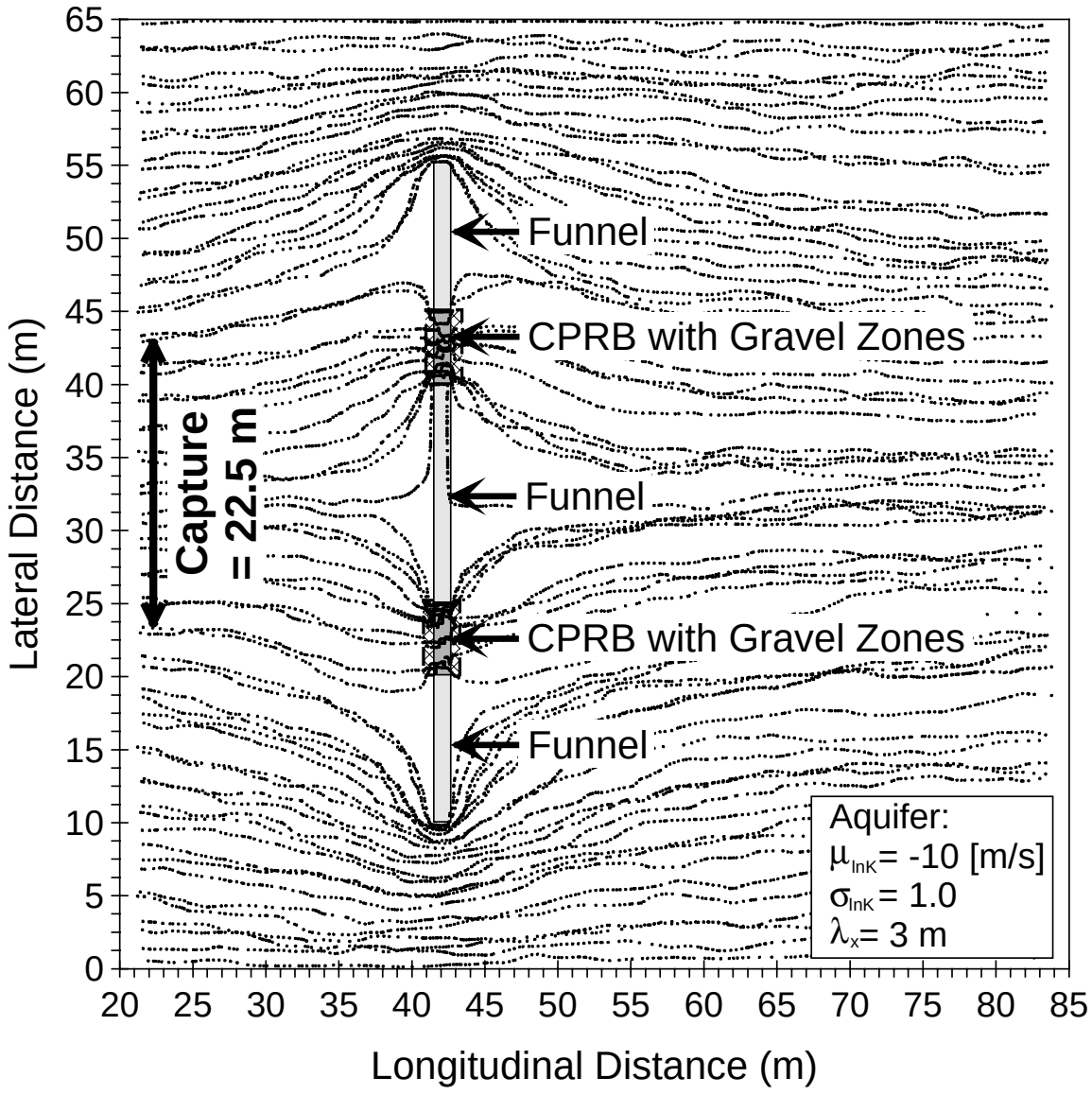

Fig. 11.12 Capture Zone of CPRB Systems (a) without and (b) with Gravel Zones.

11.1.4 Summary of Gravel Zones

Overall, gravel zones do not appear to be beneficial for PRBs. The only condition where gravel zones yield lower effluent concentrations is for a HFPRB in aquifers with σ_{lnK} less than 2.3. For the HFPRB, in aquifers with σ_{lnK} greater then 2.3, or any FGFPRB or CPRB, gravel zones cause higher effluent concentrations. The best use for gravel zones appears to be for increasing the capture zone of funnels. In some cases gravel zones may be used with funnels and a PRB as part of a containment system, but in general, there is little evidence supporting the use of gravel zones adjacent to PRBs.

11.2 DOWN-GRADIENT CONCENTRATIONS

Concentrations 10 m and 20 m down-gradient from a HFPRB, FGPRB, and CPRB were evaluated to investigate the role of dispersion at reducing concentrations beyond the effluent face of the PRB. This topic was investigated because the previous analyses only considered effluent concentrations at the back of the PRB. However, plumes increase in size down-gradient of a PRB (e.g., Fig. 8.1), particularly for the FGPRB and CPRB, which results in lower concentrations down-gradient of the PRB.

Influent and effluent concentrations along with effluent concentrations 10 m and 20 m down-gradient of the PRB are shown in Fig. 11.13. Concentrations are shown for all three types of PRB in moderately heterogeneous aquifers (σ_{lnK} = 1.0, λ_x = 3 m, λ_y = 1 m), very heterogeneous aquifers (σ_{lnK} = 4.0, λ_x = 3 m, λ_y = 1 m), and aquifers with greater spatial correlation (σ_{lnK} = 1.0, λ_x = 9 m, λ_y = 3 m). All

a) HFPRB

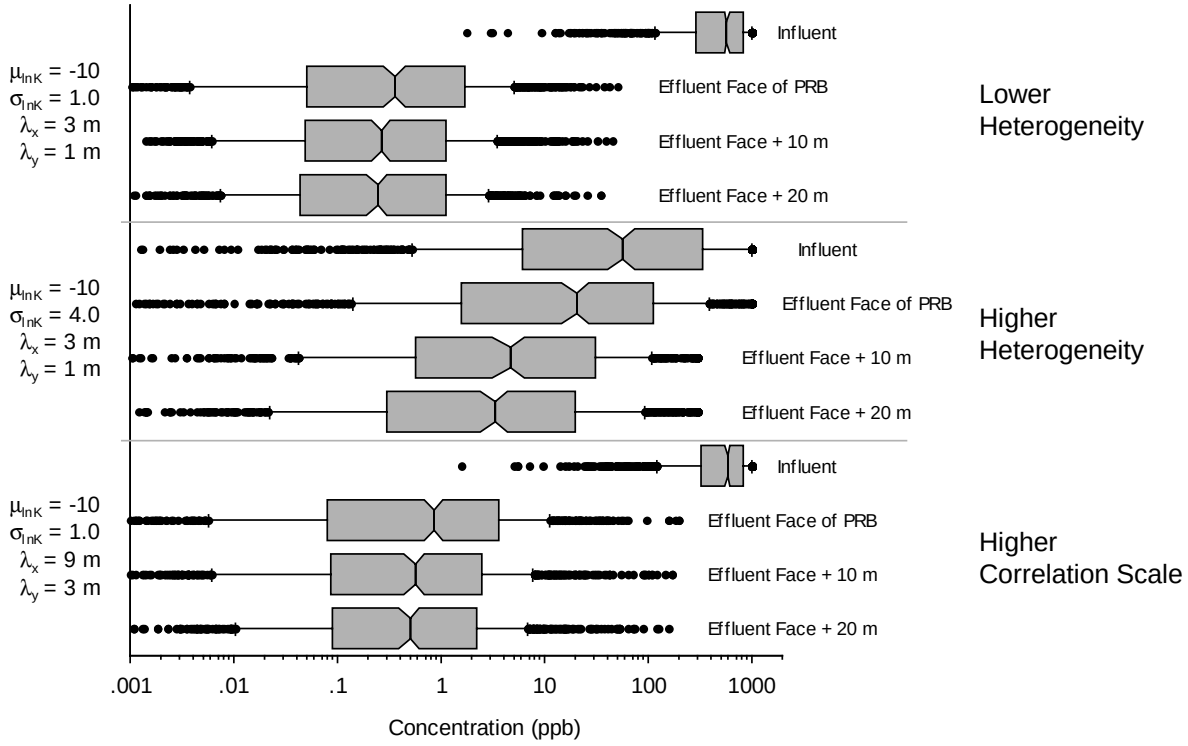

b) FGPRB

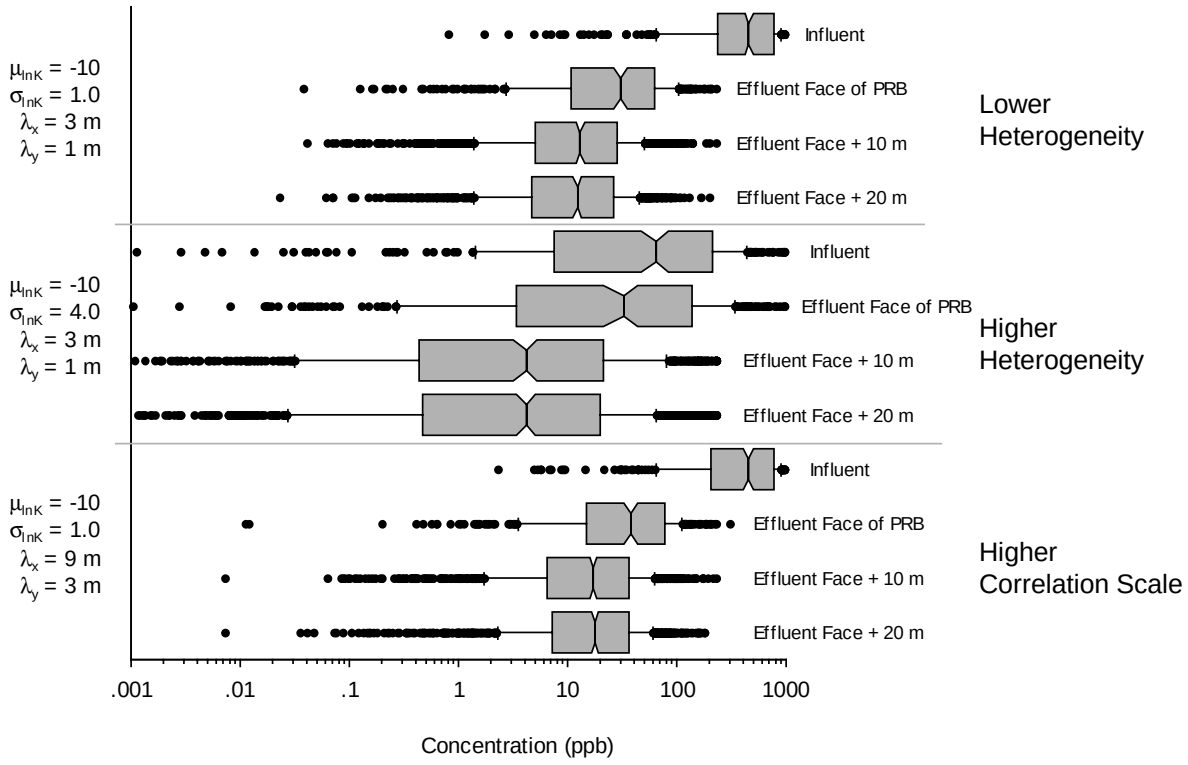

c) CPRB

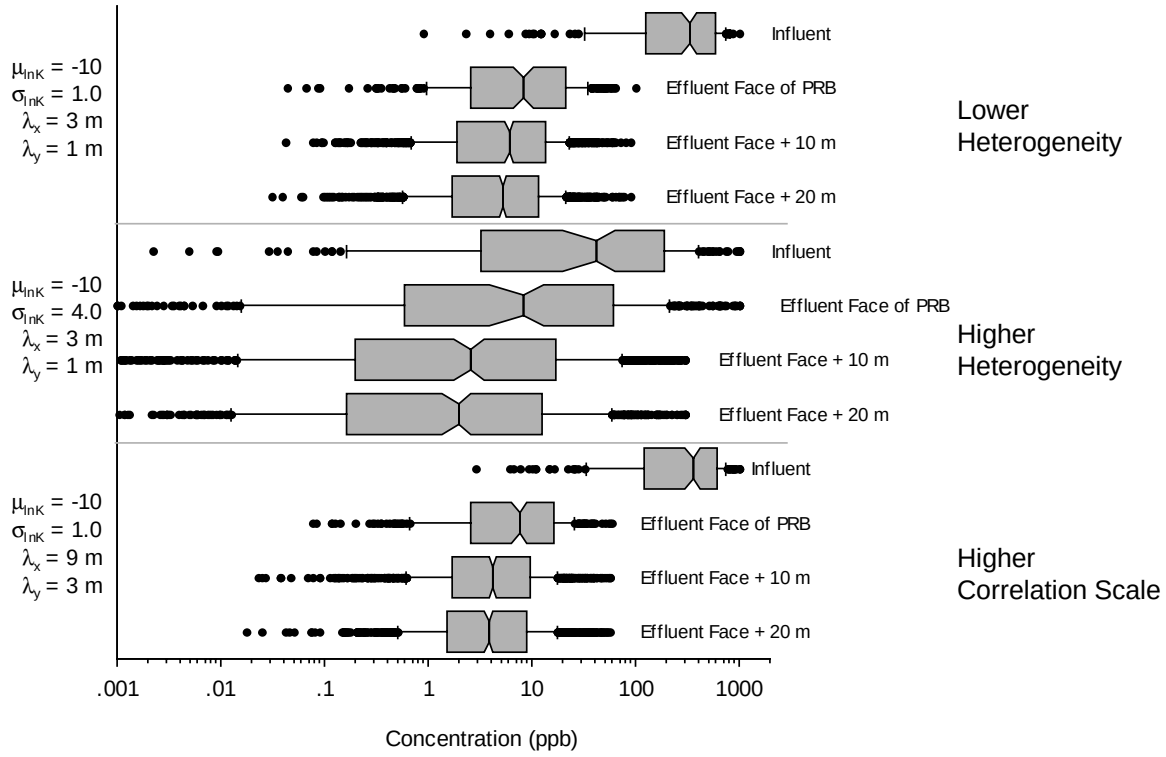

Fig. 11.13 Influent, Effluent, and Concentrations 10 m and 20 m Down-Gradient of a HFPRB (a), FGPRB (b), and CPRB (c).

simulations are for homogeneous PRBs (K_p = 2.5x10^{-3} m/s, k_r = 1.0 d^{-1}) in aquifers with μ_{lnk} = -10.

Trends observed for all PRBs are that concentrations decrease with distance from the PRB, but decreases in concentration after the PRB are small compared to the concentration change in the PRB. Concentration decreases are greater for the FGPRB and CPRB than for the HFPRB because plumes widen more after exiting the FGPRB and CPRB than after exiting the HFPRB. This result will be discussed in greater detail subsequently. Nonetheless, concentrations decrease down-gradient of PRBs.

The greatest change in concentration occurs in the upper and lower tails of the distribution (i.e., concentrations greater than the 90th percentile and below the 10th percentile). In moderately heterogeneous aquifers, the range between the 10th and 90th percentile decreases with distance, but the overall range of the distribution remains constant or increases. This result indicates that peak concentrations in the center of the plume and lower concentrations at the edges of the plume are diluted as the plume moves through the aquifer, because the plume grows in size as it travels (Fig. 8.1). As the plume widens and thickens, mixing between uncontaminated groundwater and lower concentrations at the edge of the plume decrease concentrations that compose the lower 10$^{\%}$ of the distribution. Also, peak concentrations that exist in the central portions of the plume (i.e., above the 90th percentile) mix with lower concentration or uncontaminated groundwater and are diluted.

Decreases in concentrations are greater in the first 10 m following the PRB than in the subsequent 10 m. Concentrations decrease more immediately down-gradient of the PRB because groundwater flow paths change most as water exits the PRB and returns to the aquifer. Consequently, more dispersion occurs as groundwater returns to the aquifer from the PRB. Between 10 m and 20 m after the PRB, less dispersion occurs because groundwater flow through the aquifer is no longer influenced by the PRB that is located more than a correlation length up-gradient.

Changes in concentrations after the PRB are greatest in more heterogeneous aquifers. As shown in Fig. 6.14, plumes are larger in aquifers with larger σ_{lnK}. Greater variation in flow for aquifers with larger σ_{lnK} was discussed previously, and it was also shown that PRBs in these aquifers perform worse than PRBs in more homogeneous aquifers. Thus, dilution compensates for poor PRB performance in more heterogeneous aquifers by diluting higher effluent concentrations down-gradient of the PRB. However, regulators and designers should also consider that plumes are larger in more heterogeneous aquifers and require wider containment and monitoring systems.

Using the effluent concentration at the back of the PRB for evaluating the effectiveness of a PRB is a reasonable and conservative choice. Effluent concentrations at the back of the PRB are higher than down-gradient concentrations. Thus, groundwater that complies with a target concentration at the effluent face of the PRB will comply with target concentrations down-gradient of the PRB. Also, plumes are smaller at the effluent face of the PRB than down gradient

of the PRB, so that fewer monitoring wells are required to monitor plumes closer to the PRB (assuming the same monitoring density). Thus, conclusions made in the preceding section regarding monitoring well placement still hold true. A 30 to 50% decrease in concentration in the 10 to 20 m following the PRB is likely to occur; however, designers and regulators should not depend on this decrease in concentration because it is minimal relative to the change in concentration within the PRB. For example, influent concentrations are reduced 99.96% between the influent face and 20 m past the effluent face of a 1 m thick HFPRB in an aquifer with σ_{lnK} = 1.0; 99.94% of this reduction is due to the PRB and only 0.02% is due to dilution after the PRB.

The median and 90th percentile of concentration 10 m and 20 m down-gradient of each type of PRB are shown in Fig. 11.14. Concentrations are normalized by the effluent concentration at the back of the PRBs so that Fig. 11.14 shows the decrease in concentration due to dilution for each PRB in the three aquifers. As previously mentioned, the greatest change in concentration occurs in the initial 10 m following the PRB. In this 10 m, concentrations decrease by 30% to 70% with larger decreases in aquifers with larger σ_{lnK}. In the subsequent 10 m, concentrations decrease an additional 5% to 10%, with larger decreases occurring in aquifers with longer correlation lengths.

PRBs that use funnels have the largest change in concentration. This result is expected because plumes exiting a FGPRB or CPRB widen significantly in the 10 m following the PRB (Fig. 8.1). The greatest change in concentration due to

a) 50th Percentile of Concentration

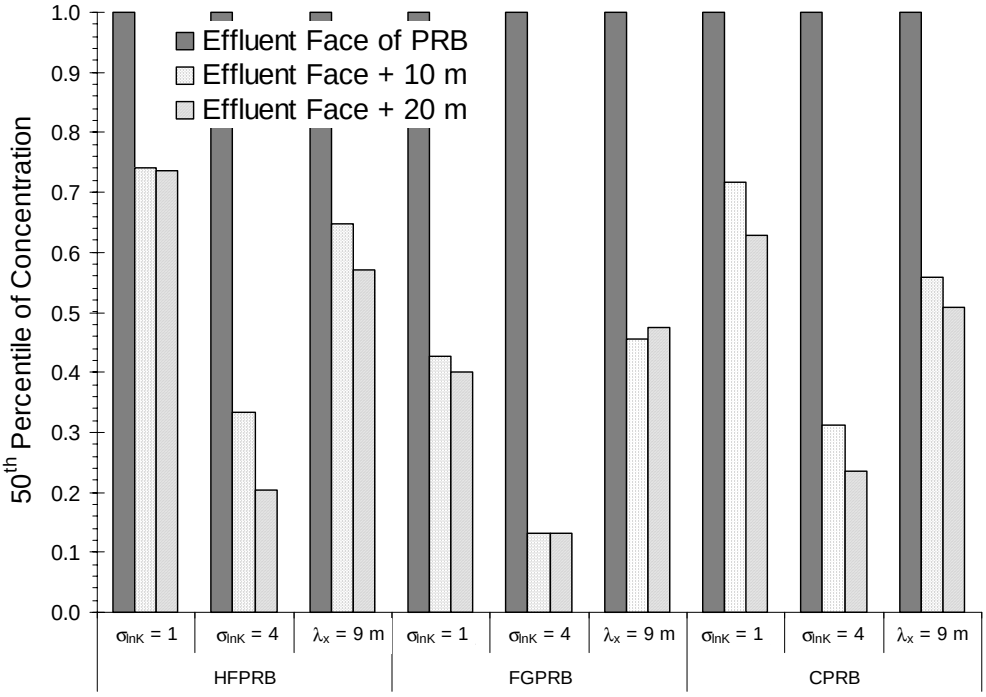

b) 90th Percentile of Concentration

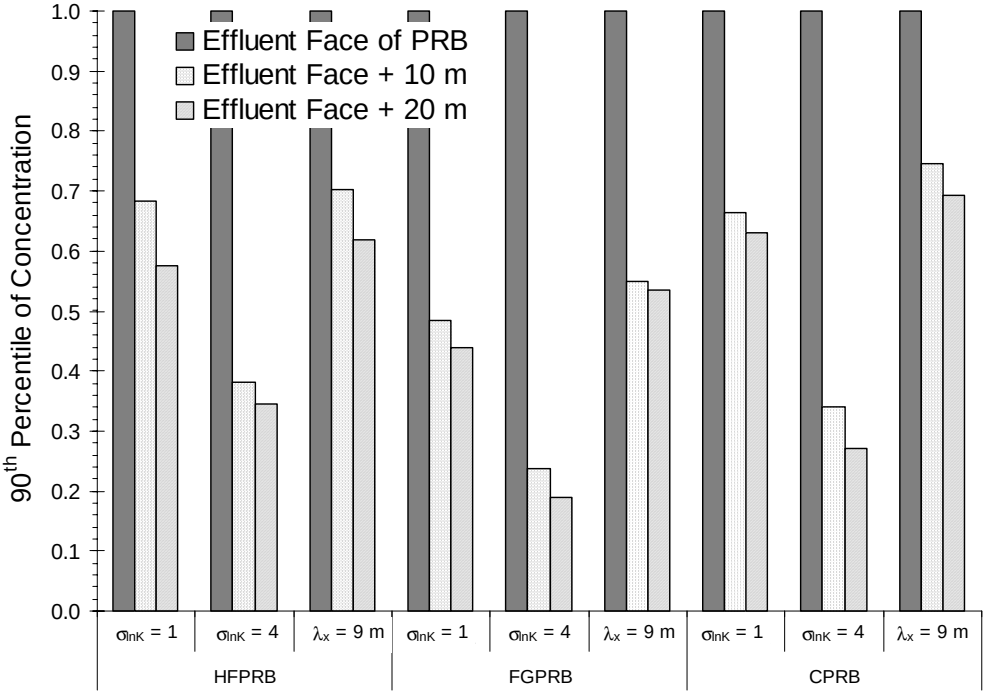

Fig. 11.14 Relative 50th (a) and 90th (b) Percentile of Concentration Down-Gradient of a HFPRB, FGPRB, and CPRB.

dilution occurs for the FGPRB. The FGPRB has the largest change in concentration down-gradient of the PRB because the FGPRB captures more water than the CPRB. Both PRBs have 40 m of funnel; however, the gate of the FGPRB has a greater cross-sectional area (i.e., 50 m^2) than the opening for the CPRB (i.e., 10 m^2). As a result, a greater quantity of water flows through the FGPRB than the CPRB for a similar gradient and hydraulic conductivity. Thus, concentrations down-gradient of the FGPRB are diluted more than concentrations down-gradient of the CPRB. Results will vary if funnel sizes are changed, but the general conclusion remains the same, more dilution will occur down-gradient of funnel systems with larger capture zones, all other factors being equal.

In summary, plumes down-gradient of a PRB increase in size and decrease in concentration due to the irregular flow of water through a heterogeneous aquifer. As the plume moves through the aquifer, mechanical mixing dilutes extremes in concentration resulting in a broader range of slightly lower concentrations. Concentrations change most as groundwater flow returns to the aquifer from the PRB and less once flow through the aquifer has been reestablished. Changes in concentration are larger for systems with funnels, and the decreases in concentration are proportional to the capture zone of the funnel. However, designers and regulators should also bear in mind that changes in concentration due to dispersion in the aquifer may be small relative to decreases in concentration within the PRB.

SECTION 12

SUMMARY AND CONCLUSIONS

The purpose of this study was to understand how permeable reactive barriers (PRBs) operate in heterogeneous aquifers and to recommend improvements for their design and monitoring. Three types of PRBs were investigated, a horizontal flow PRB (HFPRB), funnel and gate PRB (FGPRB), and caisson PRB (CPRB). Each type of PRB was simulated in heterogeneous aquifers, and influent and effluent concentrations were calculated. Aquifers varied with respect to the mean (μ_{lnK}), standard deviation (σ_{lnK}), and correlation length for the logarithm of hydraulic conductivity (lnK), and PRBs varied with respect to their hydraulic conductivity and reaction rate constant.

Currently, the design of PRBs uses a plug-flow model that assumes the aquifer and PRB are homogeneous and isotropic, which rarely occurs in natural deposits. The results of this study show that zones of higher hydraulic conductivity conduct groundwater and contaminants into and through a PRB faster than predictions made using Darcy's Law with the geometric mean hydraulic conductivity of the aquifer. Effluent concentrations change considerably as the hydraulic conductivity of the aquifer varies and little with variations in the hydraulic conductivity and reaction rate constant of the PRB.

Table 12-1 summarizes the median and 90^{th} percentile of effluent concentration from the three types of PRBs in most of the aquifers considered. For

all simulations, the maximum influent concentration is approximately 1000 ppb, and the average reaction rate constant for the PRB is 1 d^{-1}.

Table 12-1 Median and 90th Percentile of Effluent Concentration from PRBs in Heterogeneous Aquifers.

		Median and 90th Percentile of Effluent Concentration*(ppb)					
Aquifer		**HFPRB**		**FGPRB**		**CPRB**	
Homogeneous $\mu_{lnK} = -10$		0.04	0	31.0	47.5	7.0	11.2
Heterogeneous Aquifers	**Base Case** $\mu_{lnK} = -10$ $\sigma_{lnK} = 1$ $\lambda_x = 3m$, $\lambda_y = 1m$	0.37	5.1	31.1	101.2	9.0	35
	$\mu_{lnK} = -10$ **$\sigma_{lnK} = 0.25$** $\lambda_x = 3m$, $\lambda_y = 1m$	0.05	0.14	24.3	40.4	6.8	12.3
	$\mu_{lnK} = -10$ **$\sigma_{lnK} = 4$** $\lambda_x = 3m$, $\lambda_y = 1m$	20.5	415.5	39.7	497.5	8.3	415.0
	$\mu_{lnK} = -9$ $\sigma_{lnK} = 1$ $\lambda_x = 3m$, $\lambda_y = 1m$	27.7	98.1	169.1	342.5	91.4	235.2
	$\mu_{lnK} = -12$ $\sigma_{lnK} = 1$ $\lambda_x = 3m$, $\lambda_y = 1m$	2.3×10^{-17}	7.5×10^{-9}	7.2×10^{-5}	0.04	3.5×10^{-9}	1.7×10^{-6}
	$\mu_{lnK} = -10$ $\sigma_{lnK} = 1$ **$\lambda_x = 9m$ $\lambda_y = 3m$**	0.88	11.3	38.6	112.2	7.8	36.7

* for a maximum influent concentration = 1000 ppb

Increasing σ_{lnK} increases the median effluent concentration and causes the 90th percentile effluent concentration to be much higher; thus, PRBs in aquifers with greater variability in hydraulic conductivity yield a broader range of higher effluent concentrations. As σ_{lnK} decreases, the median effluent concentration decreases

and the concentration distribution becomes more uniform. Decreasing μ_{lnK} yields lower and more broadly distributed effluent concentrations, whereas aquifers with higher μ_{lnK} cause higher and more uniform effluent concentrations. Increasing the correlation scale of the aquifer increases the median effluent concentration slightly but causes very little change in the range of effluent concentrations.

The second half of this study focused on recommendations for the design and monitoring of PRBs. The three types of PRBs were compared on the basis of equivalent cost and equivalent performance. FGPRBs were found to be the most economical PRB design and the HFPRB the least economical design. The factor of safety that should be used when PRBs are designed with a plug-flow model were back-calculated. Required factors of safety for 90% of effluent concentrations to meet a target concentration ranged from 1.5 in more homogeneous aquifers ($\sigma_{lnK} < 1.0$) to 12 in very heterogeneous aquifers ($\sigma_{lnK} = 4.0$). Equations for calculating a scaling factor that can be used with the plug-flow model were suggested for each type of PRB. The equations estimate the mean and standard deviation for the scaling factor as a function of aquifer heterogeneity. The mean and standard deviation for the scaling factor can then be used to calculate a scaling factor for design once an acceptable probability of failure is chosen.

Several monitoring systems for each type of PRB were tested. Systems that provide the maximum probability of detection per monitoring well screen were determined. For the HFPRB, a monitoring system with 5 m well spacing and 3 m wells screen spacing is recommended. For the FGPRB, a monitoring system with 2 m well spacing and 4 m screen spacing is recommended, and for a CPRB, 2 m

well spacing with a well screen located at the base of the effluent opening is recommended. All systems assume well screens are 1 m long and well screens are symmetrically located around the horizontal and vertical centerlines of the effluent face of the PRB.

Finally, the use of thin gravel-filled trenches up and down gradient of the PRB was evaluated in terms of changing the residence time and effluent concentrations. Gravel zones are designed to induce mixing so that influent concentrations and velocities through the PRB are more uniform. Gravel zones typically yield more uniform flow and residence time in the reactive media, but they also provide more conductive paths for ground water flow between the aquifer and reactive media. Thus, in most cases, gravel zones caused residence times to be lower and effluent concentrations to be higher. The only condition where gravels zones were beneficial was for a HFPRB in aquifers with σ_{lnK} less than 2.3.

In summary, PRBs are effective at reducing the concentration of groundwater contamination provided groundwater has a sufficient residence time in the reactive media for rate limited reactions to occur. Understanding aquifer heterogeneity is key to achieving the desired effluent concentration economically. Guidelines are provided in this report for designing and monitoring PRBs, but these models depend on accurate site information. Thus, designers and regulators must recognize that the system in which the PRB will operate is likely the single greatest factor affecting PRB performance, and expend the necessary effort to accurately characterize the aquifer in which a PRB will be placed.

SECTION 13

TOPICS FOR FUTURE RESEARCH

The goal of this project was to evaluate permeable reactive barriers in heterogeneous aquifers and make design recommendations for their use. While studying this topic, several related areas of interest that are outside the scope of this project but warrant further study became apparent. The purpose of this section is to identify these areas and provide preliminary suggestions regarding a course of investigation.

13.1 FUTURE STUDIES FOR PRBS

13.1.1 Cultural Heterogeneity

Cultural heterogeneities are man-made structures such as buried pipes, parking lots, or drainage ditches that change recharge or the natural flow of groundwater. The current study did not consider the impact of cultural heterogeneity on the performance of PRBs. However, PRBs are typically used at industrial sites where groundwater flow may be affected by cultural heterogeneity. Thus, an investigation of the impact of common sources of cultural heterogeneity is pertinent and would have direct implications on the design of PRB and other containment systems.

13.1.2 Temporal Variability

Simulations performed for this study were steady-state and the PRBs were aligned perpendicular to regional groundwater flow. However, temporal variations

in the magnitude and direction of the hydraulic gradient have been observed at field sites (e.g., Benner et al. 1997). Therefore, a study of the response of PRBs to seasonal changes in the hydraulic gradient is advised. Such a study may reveal that portions of a PRB are overwhelmed when groundwater enters the PRB at an angle or the PRB fails during wetter seasons. Also, the performance of PRBs with funnels versus a HFPRB may yield interesting results that support the use of one style of PRB over another.

13.1.3 Defects

PRBs and funnels in this study were assumed to be free of defects; however, field-scale PRBs are likely to have defects. Defects may be as simple as regions where the PRB is thinner because the reactive media compress under the lateral pressure of the surrounding soil (e.g., Puls et al. 1999), to fully penetrating defects caused by sloughing of soil during emplacement. Depending on the size and hydraulic conductivity of these defects, the effectiveness of the PRB may be significantly compromised. A study of PRB defects could be undertaken using the method of Tachavises (1998) as a guide. Tachavises (1998) investigated defects in vertical cut-off walls and found that small flaws can drastically reduce the effectiveness of vertical cut-off walls. Since more economical construction methods are typically faster and have less opportunity for inspection, the consequence of defects in a PRB that may occur during or after installation should be understood as new placement methods are developed.

13.1.4 Physical Modeling

Numerical simulation has provided insight of PRB performance in heterogeneous aquifers. A logical next step for PRB research is to construct large and well-controlled laboratory or field-scale PRBs to verify the results of the current study. A reasonable approach would be to construct a pit for testing that is large enough to remove and replace the soil using smaller construction equipment (e.g., a bobcat), but small enough so that units of varying hydraulic conductivity or defects in the PRB can be built by hand and steady flow can be established in a reasonable period of time. Also, an inert but easily measured tracer would be advisable, perhaps a salt solution or florescent dye. The PRB could then be constructed from any granular media that reacts with the chosen contaminant. Systems with chlorinated solvents and iron media are common in the field, but a model system that uses safer and less volatile contaminants probably exists.

13.2 Funnel and Gate Systems

Using a FGPRB or CPRB requires the design of funnels for channeling contaminated groundwater into the reactive barrier. Funnels for this study were designed by trial and error, which is a tedious and time-consuming process. Starr and Cherry (1994) and Edwards et al. (1997) recommend the configuration of funnels and Garron et al. (1998) and Sedivy et al. (1999) provide design charts for sizing funnels in homogeneous aquifers. However, to the author's knowledge, there has been no study recommending design widths for funnels in heterogeneous aquifers, although it is known that dispersion is greater and

contaminant plumes are wider in more heterogeneous aquifers. The lack of understanding about funnels in heterogeneous aquifers could result in incomplete containment of plumes or higher than expected groundwater velocities through a PRB.

An evaluation of the capture zone for funnels in heterogeneous aquifers needs to be undertaken. Research should start with design recommendations made by Starr and Cherry (1994), Edwards et al. (1997), Garron et al. (1998) and Sedivy et al. (1999) for homogeneous aquifers and see if they apply to heterogeneous aquifers. Next, design lengths for funnels in heterogeneous aquifers should be determined. A model similar to the one used for calculating scaling factors for PRBs thickness (i.e., Section 9) could be developed. Such a model would likely improve our understanding of containment systems in aquifers that are more typical of natural deposits and aid in the design of FGPRBs and CPRBs.

SECTION 14

REFERENCES

Aiken, J. (1993), “A Three-Dimensional Characterization of a Coarse Glacial Outwash Deposit Used for Modeling Contaminant Movement,” MS Thesis, Department of Geology, University of Wisconsin - Madison.

Alabert, F. (1987), “The Practice of Fast, Conditional Simulation through Lower Upper Decomposition of the Covariance Matrix,” *Mathematical Geology*, 19(5), 369-387.

Arnold, W and Roberts, A. (1998), “Pathways of Chlorinated Ethene and Chlorinated Acetylene Reaction with Zn(0),” *Environmental Science and Technology*, 32(19), 3017-3025.

Bakr, A., Gelhar, L., Gutjahr, A., and MacMillan, J. (1978), “Stochastic Analysis of Spatial Variability in Subsurface Flows: 1. Comparison of One- and Three-Dimensional Flows,” Water Resources Research, 14 (2), 263-271.

Bakr, A., Gelhar, L., Gutjahr, A., and MacMillan, J. (1978), “Stochastic Analysis of Spatial Variability in Subsurface Flows: 2. Evaluation and Application,” Water Resources Research, 14 (5), 953-959.

Barcelona, M., Wehrmann, H., and Varljen, M. (1994), "Reproducible Well-Purging Procedure and VOC Stabilization Criteria for Ground-Water Sampling," *Ground Water*, 32 (1), 12-22.

Bear, J. (1979), *Hydraulics of Groundwater*, McGraw-Hill Inc., New York.

Benson, C. (1993), "Probability Distributions for Hydraulic Conductivity of Compacted Soil Liners," *Journal of Geotechnical Engineering*, 119(3), 471-486.

Benson, C. and Daniel, D. (1994), “Minimum Thickness of Compacted Soil Liners: 1. Stochastic Models,” *Journal of Geotechnical Engineering*, 120 (1), 129-152.

Benner, S., Blowes, D., and Ptacek, C. (1997), "A Full-Scale Porous Reactive Wall for Prevention of Acid Mine Drainage," *Ground Water Monitoring and Remediation*, 17 (3), 99-107.

Blowes, D., Ptacek, C., Cherry, J., Gillham, R., and Robertson, W. (1995), "Passive Remediation of Groundwater Using In Situ Treatment Curtains,"

Geoenvironment 2000: Characterization, Containment, Remediation, and Performance in Environmental Geotechnics (2), Daniel, D. and Acar, Y. (Eds.), ASCE, GSP 46, 1588-1607.

Boggs, J., Young, S., Benton, D., and Chung, Y. (1990), "Hydrogeologic Characterization of the MADA Site, *Electrical Power Research Institute*, EPRI EN-6915, Palo Alto , CA.

Box, G. and Muller, M. (1958), “A Note on the Generation of Random Normal Deviates,” Statistical Techniques Research Group Contract Number DA 36-034-ORD 2297, Princeton University.

Burris, D., Allen-King, R., Manoranjan, V., Campell, T., Loraine, G., and Deng, B. (1998), “Chlorinated Ethene Reduction by Cast Iron: Sorption and Mass Transfer,” *Journal of Environmental Engineering*, 124(10), 1012-1019.

Burris, D., Delcomyn, C., Smith, M., and Roberts, A. (1996), “Reductive Dechlorination of Tetrachloroethylene and Trichloroethylene Catalyzed by Vitamin B12 in Homogeneous and Heterogeneous Systems,” *Environmental Science and Technology*, 30(10), 3047-3052.

Byers, E. and Stephens, D. (1983), "Statistical and Stochastic Analysis of Hydraulic Conductivity and Particle Size in Fluvial Sands,"*Soil Science Society of America Journal*, 47, 1072-1081.

Campell, T., Burris, D., Roberts, A., and Wells, J. (1997), “Trichloroethylene and Tetrachloroethylene Reduction in a Metallic Iron-Water-Vapor Batch System,” *Environmental Toxicology and Chemistry*, 16(4), 625-630.

Cantrell, K., Martin, P., and Szecsody, J. (1994), “Clinoptilolite as an In Situ Permeable Barrier to Strontium Migration in Ground Water”, In Situ Remediation: Scientific Basis for Current and Future Technologies, G. Gee and N. Wing, Eds., Battelle Press, Columbus OH, 839-850.

CERCLA (1980), The Comprehensive Environmental Responsibility, Compensation and Liability Act (Superfund), 42 USC 9601.

Charlet, L., Liger, E., and Gerasimo, P. (1998), "Decontamination of TCE- and U-Rich Waters by Granular Iron: Role of Sorbed Fe(II)," *Journal of Environmental Engineering*, 124(1), 25-30.

Christensen, R. (1999), Personal Correspondence, December 30.

Christakos, G. (1992), *Random Field Models in Earth Sciences*, Academic Press, Inc., San Diego, 326-328.

Cooke, R., Mostaghimi, S., and Woeste, F. (1995), "Effect of Hydraulic Conductivity Probability Distribution Function on Simulated Solute Leaching," *Water Environment Research*, 67(2), 159-168.

Dagan, G. (1979), “Models of Groundwater Flow in Statistically Homogeneous Porous Formations,” *Water Resources Research*, 15 (1), 47-63.

Dagan, G. (1982a), “Stochastic Modeling of Groundwater Flow by Unconditional and Conditional Probabilities, 1. Conditional Simulation and the Direct Problem,” *Water Resources Research*, 18 (4), 813-833.

Dagan, G. (1982b), “Analysis of Flow through Heterogeneous Random Aquifers, 2. Unsteady Flow in Confined Formations,” *Water Resources Research*, 18 (5), 1571-1585.

Das, B. (1998), *Principles of Geotechnical Engineering*, PWS Publishing Co., Boston.

Day, S., O’Hannesin, S., and Marsdon, L. (1999), “Geotechnical Techniques for the Construction of Reactive Barriers,” *Journal of Hazardous Materials*, (67) 285-297.

DeGroot, D. (1996), "Analyzing Spatial Variability of In Situ Soil Properties," *Uncertainty in the Geologic Environment: From Theory to Practice (1)*, Shackelford, C., Nelson, P., and Roth, M. (Eds.), ASCE, GSP 58, 210-238.

Devroye, L. (1986), *Non-Uniform Random Variate Generation*, Springer-Verlag, New York, 564-566.

Dykaar, B. and Kitanidis, P. (1992), “Determination of the Effective Hydraulic Conductivity for Heterogeneous Porous Media Using a Numerical Spectral Approach, 2. Results,” *Water Resources Research*, 28(4), 1167-1178.

Edwards, D., Little, J., Dick, V., and Walker, S., (1997), “Concepts For Refractive Flow and Treatment,” In-Situ Remediation of the Geoenvironment, Evans, J. (ed.), GSP 71, ASCE, Minneapolis, MN, Oct. 5-7.

El-Kali, A. (1986), “A Computer Program for Generating Two-Dimensional Random Fields of Autocorrelated Parameters,” *Ground Water*, 24 (5), 663-667.

EPA (1995), “In Situ Remediation Technology Status Report: Treatment Walls,” United States Environmental Protection Agency Office of Solid Waste and Emergency Response, EPA 542-K-94-004, Washington DC.

EPA (1997), “Permeable Reactive Subsurface Barriers for the Interception and Remediation of Chlorinated Hydrocarbons and Chromium (VI) Plumes in Groundwater,” National Risk Management Research Laboratory, EPA 600/F-97/008, Ada, OK.

Eykholt, G. and Sivavec, T. (1995), "Contaminant Transport Issues for Reactive-Permeable Barriers," *Geoenvironment 2000: Characterization, Containment, Remediation, and Performance in Environmental Geotechnics (2),* Daniel, D. and Acar, Y. (Eds.), ASCE, GSP 46, 1608-1621.

Eykholt, G. (1999), “Analytical Solution for Networks of Irreversible First-Order Reactions,” *Water Research*, 33(3), 814-826.

Eykholt, G. (1997), “Uncertainty Based Scaling of Iron Reactive Barriers,” In-Situ Remediation of the Geoenvironment, Evans, J. (ed.), GSP 71, ASCE, Minneapolis, MN, Oct. 5-7, 41-55.

Eykholt, J., Elder, C., and Benson, C. (1999), “Effects of Aquifer Heterogeneity and Reaction Mechanism Uncertainty on a Reactive Barrier,” *Journal of Hazardous Materials* 58(1-2), 73-96.

Eykholt, G. and Li, L. (2000), “Solute Transport and Linear Reaction Networks: Semi-Analytical Solution for Species with Different Retardation Coefficients,” *Journal of Hydrology*, accepted.

Farrell, J., Bostick, W., Jarabek, R, and Fiedor, J. (1999), “Uranium Removal From Ground Water Using Zero Valent Iron Media,” *Ground Water*, 37(4), 618-624.

Fennelly, J. and Roberts, A. (1998), “Reaction of 1,1,1-Trichloroethane with Zero-Valent Metals and Bimetallic Reductants,” *Environmental Science and Technology*, 32(13), 1980-1988.

Fenton, G. and Vanmarcke, E. (1990), “Simulation of Random Fields via Local Average Subdivision,” *Journal of Engineering Mechanics*, 116 (8), 1733-1749.

Fenton, G. and Griffiths, D. (1993), “Statistics of Block Conductivity Through a Simple Bounded Stochastic Medium,” *Water Resources Research*, 26 (6), 1825-1830.

Fenton, G. (1994), “Error Evaluation of Three Random Field Generators,” *Journal of Engineering Mechanics*, 120 (12), 2478-2497.

Fisher, A., Barnhill, M., and Revenaugh, J. (1998), "The Relationship Between Hydrogeologic Properties and Sedimentary Facies: An Example from Pennsylvanian Bedrock Aquifers, Southwestern Indiana," *Ground Water*, 36(6), 901-912.

Foose (1997), “Leakage Rates and Chemical Transport through Composite Landfill Liners,” Ph.D. Dissertation, Department of Civil and Environmental Engineering, University of Wisconsin - Madison.

Fort, J. (2000), “Long-Term Hydraulic Performance of Permeable Reactive Barriers,” MS Thesis, Department of Civil and Environmental Engineering, University of Wisconsin - Madison.

Freeze, R. (1975), "A Stochastic-Conceptual Analysis of One-Dimensional Groundwater Flow in Nonuniform Homogeneous Media," *Water Resources Research*, 11(5) 725-741.

Garron, K. Schultz, D, and Landis, R. (1998), “Modeling of Plume Capture by Continuous, Low-Permeability Barriers,” *Groundwater Monitoring and Remediation*, 18(2), 82-87.

Gavaskar, A., Gupta, N., Sass, B., Fox, T., Janosy, R., Cantrell, K., and Olfenbuttel, R. (1997), “Design Guidance for Application of Permeable Barriers to Remediate Dissolved Chlorinated Solvents,” Armstrong Laboratory/Environics Directorate (AL/EQ), Contract No. F08637-95-D-6004, DO 5501.

Gavaskar, A., Gupta, N., Sass, B., Janosy, R., O'Sullivan, D. (1998), *Permeable Barriers for Groundwater Remediation: Design Construction, and Monitoring*, Battelle Press, Columbus, OH.

Gelhar, L. (1993), *Stochastic Subsurface Hydrogeology*, Prentice Hall, Englewood Cliffs, New Jersey.

Gelhar, L., Wierenga, K., Rehfeld, C., Duffy, M., Simonett, M., Yeh, T., and Strong, W. (1983), "Irrigation Return Flow Water Quality Monitoring, Modeling, and Variability in the Middle Rio Grande Valley, New Mexico,” U.S. EPA Report, EPA-600-S2-83-072.

Georgakakos, A., Kitanidis, P., Loaiciga, H., Olea, S., Yates, S., and Rouhani, S. (1990), “Review of Geostatistics in Geohydrology. I.: Basic Concepts,” *Journal of Hydraulic Engineering*, 116(5), 612-658.

Gierke, J. and Powers, S. (1997), "Increasing Implementation of In Situ Treatment Technologies Through Field-Scale Performance Assessment," *Water Environment Research*, 69(2), 196-205.

Gillham, R. and O'Hannesin, S. (1994), "Enhanced Degradation of Halogenated Aliphatics by Zero-Valent Iron," *Ground Water*, 32(6), 958-967.

Griffiths, D., Fenton, G., and Paice, G. (1996), "Reliability-Based Exit Gradient Design of Water Retaining Structures," *Uncertainty in the Geologic Environment: From Theory to Practice (1)*, Shackelford, C., Nelson, P., and Roth, M. (Eds.), ASCE, GSP 58, 518-534.

Grimmett, G. and Stirzaker, D. (1995), *Probability and Random Processes*, Oxford Science Publications, Oxford.

Hald, A. (1952), *Statistical Tables and Formulas*, John Wiley & Sons, New York.

Harter, T. (1998), "Uncertainty and Risk Analysis of Contaminant Transport," Proc. 21st Biennial Ground Water Conf., DeVries, J. and Woled, J. (ed.), Water Resources Center Report 95, Davis, CA, 97-107.

Hassan, A., Cushman, J., and Delleur, J. (1997), "Monte Carlo Studies of Flow and Transport in Fractal Conductivity Fields: Comparison with Stochastic Perturbation Theory," *Water Resources Research*, 33(11), 2519-2534.

Hastings, N. and Peacock, J. (1975), *Statistical Distributions*, Butterworth Group, London.

Hathhorn, W. (1997), "Simplified Approach to Particle Tacking Method for Contaminant Transport," *Journal of Hydraulic Engineering*, 123(12) 1157-1160.

Herbert, R., Benner, S., and Blowes, D. (1998), "Reactive Barrier Treatment of Groundwater Contaminated with Acid Mine Drainage: Sulphur Accumulation and Sulphide Formation," *Proc. of Groundwater '98*, Herbert, M. and Kovar, K. (eds), Sept. 21-25, Tubingen, Germany, 451-457.

Hess, K. (1989), "Use of Borehole Flowmeter to Determine Spatial Heterogeneity of Hydraulic Conductivity and Macrodispersion in a Sand and Gravel Aquifer, Cape Cod, MA," *Proceeding of the Conference on New Field Techniques for Quantifying the Physical and Chemical Properties of Heterogeneous Aquifers*, Molz, F., Melville, J., and Guvan, O. (Eds.), National Water Well Assoc., Dublin, OH, 497-508.

Hoban, J. and Vasko, S. (1998), “An In Situ Method for Groundwater Remediation: A Permeable Iron Reactive Wall,” Senior Design Project, Geological Engineering Program, University of Wisconsin – Madison.

Hocking, G., Wells, S., and Ospina, R. (1998), “Design and Construction of Vertical Hydraulic Fracture Placed Iron Reactive Walls,” Designing and Applying Treatment Technologies, *Proc. of First International Conference on Remediation of Chlorinated and Recalcitrant Compounds*, May 18-21, Monterey, CA, 103-108.

Hoeksema, R. and Kitanidis, P. (1985), “Analysis of Spatial Structure of Properties of Selected Aquifers,” *Water Resources Research*, 21(4), 563-572.

Hufschmied, P. (1986), "Estimation of Three-Dimensional, Statistical Anisotropic Hydraulic Conductivity Field by Means of Single Well Pumping Tests combined with Flowmeter Measurements," *Hydrogeologie*, 2, 163-174.

ITRC (1999), “Regulatory Guidance for Permeable Reactive Barriers Designed to Remediate Chlorinated Solvents,” Interstate Technology Regulatory Cooperation Work Group Permeable Reactive Barriers Work Team.

Jarre, P. and Kociolok, P. (1999), “Examples of the Use of Reactive Treatment Barriers,” *Conferenze Di Geotecnica Di Torino XVII CICLO*, Italian Geotechnical Society, Torino, Italy, Nov. 23-25.

Johnson, N. and Dreiss, S. (1989), "Hydrostratigraphic Interpretation Using Indicator Geostatistics," *Water Resources Research*, 25(12), 2501-2510.

Johnson, T., Scherer, M., and Tratnyk, P. (1996), “Kinetics of Halogenated Organic Compound Degradation by Iron Metal,” *Environmental Science and Technology*, 30(8), 2634-2640.

Journel, A. G. (1989), “Fundamentals of Geostatistics in Five Lessons,” presented at the 28th International Geological Congress, American Geophysical Union, Washington, D.C

Jussel, P., Stauffer, F., and Dracos, T. (1994a), “Transport Modeling in Heterogeneous Aquifer: 1. Statistical Description and Numerical Generation of Gravel Deposits,” *Water Resources Research*, 30(6), 1803-1817.

Jussel, P., Stauffer, F., and Dracos, T. (1994b), “Transport Modeling in Heterogeneous Aquifer: 2. Three-Dimensional Transport Model and Stochastic Numerical Tracer Experiments,” *Water Resources Research*, 30(6), 1819-1831.

Kachigan, S. (1982), *Multivariate Statistical Analysis: A Conceptual Introduction*, Radius Press, New York.

Kearl, P., Korte, N., Stites, M., and Baker, J. (1994), "Field Comparison of Micropurging vs. Traditional Ground Water Sampling," *Ground Water Monitoring and Remediation*, 14(4), 183-190.

Kearl, P., Korte, N, and Cronk, T. (1992), "Suggested Modifications to Ground Water Sampling Procedures Based on Observations from the Colloidal Borescope," *Ground Water Monitoring and Review*, 12 (2), 155-161.

Kershaw, D., and Pamucku, S. (1997), “Ground Rubber: Reactive Permeable Barrier Sorption Media,” *In Situ Remediation of the Geoenvironment*, Evans, J. (Ed.), ASCE, GSP 71, 26-40.

Kolmorov, A. (1933), “Sulla determinazione Empirica di Una Legga di Distribuzione,” Giorn. Inst. Ital. Actuari, 4, 83-91.

Kulhawy, F. and Phoon, K. (1996), “Engineering Judgement in the Evolution from Deterministic to Reliability-Based Design,” *Uncertainty in the Geologic Environment: From Theory to Practice*, GSP 58, C. Shackelford, P. Nelson, and M. Roth, eds., ASCE, 29-48.

Lacasse, S. and Nadim, F. (1996), “Uncertainty in Characterizing Soil Properties,” *Proc. Uncertainty in the Geologic Environment: From Theory to Practice*, GSP 58, C. Shackelford, P. Nelson, and M. Roth, eds., ASCE, 49-75.

Loague, K. and Gander, G. (1990), "Spatial Variability of Infiltration on a Small Ranchland Catchment," *Water Resources Research*, 26(5), 957-971.

Lowry, G. (1995), “Kinetics of the Enhanced Dechlorination of Trichloroethylene Using Zero-Valent Iron,” M.S. Thesis, Department of Civil and Environmental Engineering, University of Wisconsin – Madison.

Lumb, P. (1974), “Applications of Statistics in Soil Mechanics – Chapt. 3,” *Soil Mechanics – New Horizons*, Lee, I. (Ed.), American Elsevier, New York.

MacKenzie, P., Horney, D., and Sivavec, T. (1999), “Mineral Precipitation and Porosity Losses in Granular Iron Columns,” *Journal of Hazardous Materials*, 68, 1-17.

Maldonado, M. (1996), “Brownfields Boom,” *Civil Engineering*, ASCE, 66(5), 36-40.

MacDonald, M. and Harbaugh, A. (1988), A Modular Three-Dimensional Finite-Difference Ground-Water Flow Model, *Techniques of Water-Resources*

Investigations of the United States Geologic Survey, United States Government Printing Office, Washington, D.C.

Matheson, L. and Tratnyek, P. (1994), “Reductive Dehalogenation of Chlorinated Methanes by Iron Metal,” *Environmental Science and Technology*, 28(11), 2045-53.

McGregor, R., Blowes, D., Jambor, J., and Robertson, W. (1998), “Mobilization and Attenuation of Heavy Metals within a Nickel Mine Tailings Impoundment Near Sudburry, Ontario, Canada,” *Environmental Geology*, 36(4) 305-319.

McMahon, P., Dennehy, K., and Sandstrom, M. (1999), “Hydraulic and Geochemical Performance of a Permeable Reactive Barrier Containing Zero-Valent Iron, Denver Federal Center,” *Ground Water*, 37(3), 396-404.

Mejia, J. and Rodriguez-Iturbe, I. (1974), “On the Synthesis of Random Field Sampling from the Spectrum: An Application to the Generation of Hydrological Spatial Processes,” *Water Resources Research*, 10 (4), 705-711.

Meyer, P., Rockhold, M., and Gee, G. (1997), “Uncertainty Analysis of Infiltration and Surface Flow and Transport for SDMP Sites,” US Nuclear Regulatory Commission, NUREG/CR-6565, PNNL-11705.

Mantoglou, A. and Wilson, J. (1982), “The Turning Bands Method for Simulation of Random Fields Using Line Generation by a Spectral Method,” *Water Resources Research*, 18 (5), 1379-1394.

Moo-Young, H. and Zimmie, T. (1998), “Geotechnical Properties of Paper Mill Sludges for Use in Landfill Covers,” *Journal of Geotechnical and Geoenvironmental Engineering*, 122 (9), 768-775.

Moreno, L. and Tsang, C. (1994), "Flow Channeling in Strongly Heterogeneous Porous Media: A Numerical Model," *Water Resources Research*, 30(5), 1421-1430.

Naval Facilities Engineering Service Center (1998), “Performance Evaluation of a Pilot-Scale Permeable Reactive Barrier at Former Naval Air Station Moffett Field, Mountain View, CA,” Battelle Press, Columbus, OH.

O'Hannesin, S. and Gillham, R. (1998), "Long-Term Performance of an In Situ "Iron Wall" for Remediation of VOCs," *Ground Water*, 36(1), 164-170.

O’Hannesin, S. (1999) Personal Correspondence, EPA Innovative Remediation Conference, 11/2/99.

Olea, R. (1991), *Geostatistical Glossary and Multilingual Dictionary*, Oxford University Press, Oxford.

Pankow, J., Johnson, R, and Cherry, J. (1993), “Air Sparging in Gate Wells in Cutoff Walls and Trenches for Control of Plumes of Volatile Organic Compounds (VOCs),” *Ground Water*, 31 (4), 654-662.

Payne, F., Rogers, D., and Buehlman, M. (1996), “Chlorinated Solvent Reduction Induced by an Aquifer Sparge Fence,” *Proceedings of the First International Symposium on In Situ Air Sparging for Site Remediation*, Oct. 24-25, Las Vegas.

Phoon, K. and Kulhawy, F. (1999), “Characterization of Geotechnical Variability,” *Canadian Geotechnical Journal*, 36, 612-624.

Porter, J. (1998), “Greener Process,” *Ground Engineering*, July, 32-33.

Powell, R., Blowes, D., Gillham, R., Schultz, D., Sivavec, T., Puls, R., Vogan, J., Powell, P., and Landis, R. (1998), “Permeable Reactive Barrier Technologies for Contaminant Remediation,” EPA/600/R-98/125, Washington DC.

Press , W., Vetterling, W., Teukolsky, S., and Flannery, B. (1992), *Numerical Recipes in Fortran 77: The Art of Scientific Computing*, Cambridge University Press, New York.

Prickett, T., Naymik, T. and Lonnquist, C. (1981), “A Random Walk Solute Transport Model for Selected Groundwater Quality Evaluation,” Illinois State Water Survey Bulletin 65, Urbana, Ill.

Priestley, M. (1981), *Spectral Analysis and Time Series, Vol. 1. Univariate Series*, Academic Press, NY.

Puls, R., Blowes, D., and Gillham, R. (1999), “Long-Term Performance Monitoring for a Permeable Reactive Barrier at the U.S. Coast Guard Support Center, Elizabeth City, NC,” *Journal of Hazardous Materials*, 68, 109-24.

Rael, J., Shelton, S., and Dayaye, R. (1995), "Permeable Barriers to Remove Benzene: Candidate Media Evaluation," *Journal of Environmental Engineering*, 121(5), 411-415.

Rajaram and McLaughlin (1990), “Identification of Large-Scale Spatial Trends in Hydrologic Data,“ *Water Resources Research*, 26(10), 2411-2423.

Recordon, E. (1977), “Uncertainty in Some Characteristics of Natural Soils,” *Proc. Probability Theory and Reliability Analysis in Geotechnical Engineering*, D. A-Grivas, ed., Rensselaer Polytechnic Institute, Troy, NY.

Rehfeldt, K., Gelhar, L., Southard, J., and Dasinger, A. (1989), "Estimates of Macrodispersivity Based on Analysis of Hydraulic Conductivity Variability at the MADA Site," *Electric Power Research Institute Report*, EPRI EN-6405, Palo Alto, CA.

Reinhart, D., Clausen, C., Geiger, C., Ruiz, N., and Afiourny, G. (1996), “Enhancement of In Situ Zero-Valent Metal Treatment of Contaminated Groundwater,” *Proceedings of Non-Aqueous Phase Liquids (NAPLs) in Subsurface Environment: Assessment and Remediation*, Reddi, L. ed., ASCE, Nov. 12-14, Washington, D.C., 323-332.

Rice, S. (1954), “Mathematical Analysis of Random Noise,” *Selected Papers on Noise and Stochastic Processes*, Wax, N. ed., Dover, Mineola, N.Y.

Riemersma, P. (1996), “Geostatistical Characterization of Heterogeneity, Simulations of Advective Transport, and Evaluation of Pump-and-Treat Systems in Braided Stream Deposits,” Ph.D. Dissertation, Department of Geology, University of Wisconsin - Madison.

Riemersma, P., Bahr, J., and Anderson, M. (1996), “A Comparison of Geological and Stochastic Approaches to Characterization of Heterogeneity and their Effects on Simulations of Pump-and-Treat Systems,” *Proceeding of Uncertainty ‘96, Uncertainty in the Geologic Environment: From Theory to Practice (1)*, July 31 - Aug. 3, Madison, Wisconsin, 1003-1018.

Robbins, G. (1989), "Influence of Using Purged Partially Penetrating Monitoring Wells on Contaminant Detection, Mapping, and Modeling," *Ground Water*, 27 (2), 155-162.

Roberts, A., Totten, L., Arnold, W., Burris, D., and Campbell, T. (1996), "Reductive Elimination of Chlorinated Ethylenes by Zero-Valent Metals," *Environmental Science and Technology*, 30(8), 2654-2659.

Robin, M., Sudicky, E., Gillham, R., and Kachanaski, R. (1991), "Spatial Variability of Strontium Distribution Coefficients and Their Correlation with Hydraulic Conductivity in the Canadian Forces Base Bordon Aquifer," *Water Resources Research*, 27(10) 2619-2632.

Ross, S. (1997), *Introduction to Probability Models*, Academic Press, San Diego, CA.

Rubin, Y. and Dagan, G. (1988), “Stochastic Analysis of Boundaries Effects on Head Spatial Variability in Heterogeneous Aquifers: 1. Constant Head Boundaries,” *Water Resources Research*, 24 (10), 1689-1697.

Rubin, Y. and Dagan, G. (1989), “Stochastic Analysis of Boundaries Effects on Head Spatial Variability in Heterogeneous Aquifers: 2. Impervious Head Boundaries,” *Water Resources Research*, 25 (4), 707-712.

Scheibe, T. and Cole, C. (1994), "Non-Gaussian Particle Tracking: Application to Scaling of Transport Processes in Heterogeneous Porous Media," *Water Resources Research*, 30(7), 2027-2039.

Schlimm, C., and Heitz, E. (1996), “Development of a Wastewater Treatment Process: Reductive Dehalogenation of Chlorinated Hydrocarbons by Metals,” *Environmental Progress*, 15(1), 38-47.

Schreiber, M., Moline, G., and Bahr, J. (1999), “Using Hydrochemical Facies to Delineate Ground Water Flowpaths in Fractured Shale,” *Ground Water Monitoring and Remediation*, 19(4) 95-109.

Sedivy, R., Shafer, J. and Bilbrey, L. (1999), “Design Screening Tools for Passive Funnel and Gate Systems,” *Ground Water Monitoring and Remediation*, 19(4), 125-133.

Shinozuka, M. and Jan, C. (1972), “Digital Simulation of Random Processes and Its Application,” *Journal of Sound and Vibration*, 25 (1) 111-128.

Shoemaker, S., Greiner, J., and Gillham, R., (1995), “Permeable Reactive Barriers,” *Assessment of Barrier Containment Technologies: A Comprehensive Treatment for Environmental Remediation Application*, Rumer, R. and Mitchell, J. Eds., International Containment Technology Workshop, Baltimore, Maryland, August 29-31, 301-353.

Siegrist, R., Lowe, K., Murdoch, L., Case, T. and Pickering, D. (1999), “In-Situ Oxidation by Fractive Emplaced Reactive Solids,” *Journal of Environmental Engineering*, 125(5), 429-440.

Sims, J. Suflita, J. and Russel, H. (1991) “Reductive Dehalogenation of Organic Contaminants in Soils and Groundwater,” Superfund Technology Support Center for Groundwater, Kerr Environmental Research Laboratories, Ada, OK, EPA 540/4-90/054.

Sisson, J. and Wierenga, P. (1981), "Spatial Variability of Steady-State Infiltration Rates as a Stochastic Process,"*Soil Science Society of America Journal*, 45, 699-704.

Smirnov, N. (1930), “On the Estimation of the Discrepancy Between Empirical Curves for Two Independent Samples,” *Bulletin Mathmatique de l‘Universite de Moscou*, 2.

Smith, L. and Freeze, A. (1979a), "Stochastic Analysis of Steady-State Groundwater Flow in Bounded Domain: One-Dimensional Simulations," *Water Resource Research*, 15(3), 521-528.

Smith, L. and Freeze, A. (1979b), "Stochastic Analysis of Steady-State Groundwater Flow in Bounded Domain: Two-Dimensional Simulations," *Water Resource Research*, 15(6), 1543-1559.

Srivastava, R. (1996), "Describing Spatial Variability Using Geostatistical Analysis," *Geostatistics for Environmental and Geotechnical Applications*, Rouhani, S., Srivastava, R., Desbarats, A., Cromer, M., and Johnson, A. (Eds.), ASTM, STP 1283, 13-19.

Starr, R. and Cherry, J. (1994), "In Situ Remediation of Contaminated Ground Water: The Funnel-and-Gate System," *Ground Water*, 32(3) 465-476.

Sudicky, E. (1986), "A Natural Gradient Experiment on Solute Transport in a Sand Aquifer: Spatial Variability of Hydraulic Conductivity and Its Role in the Dispersion Process," *Water Resources Research*, 22(13), 2069-2082.

Tachavises, C. (1997), “Flow Rate Past Vertical Groundwater Cut-Off Walls: Influential Factors and Their Impact on Wall Selection,” Ph.D. Dissertation, Department of Civil and Environmental Engineering, University of Wisconsin - Madison.

Terzaghi, K. and Peck, R. (1948), *Soil Mechanics in Engineering Practice*, John Wiley & Sons, New York.

Tompson, A., Ababou, R., and Gelhar, L. (1989), “ Implementation of the Three-Dimesional Turning Bands Random Field Generator,” *Water Resources Research*, 25 (10) 2227-2243.

Tompson, A. and Gelhar, L. (1990), "Numerical Simulation of Solute Transport in Three-Dimensional, Randomly Heterogeneous Porous Media," *Water Resources Research*, 26(10), 2541-2562.

Tratnyk, P., Johnson, T., Scherer, M., and Eykholt, G. (1997), “Remediating Groundwater with Zero-Valent Metals: Chemical Considerations in Barrier Design,” *Ground Water Monitoring and Remediation*, 17(4), 108-114.

Vanmarcke, E. (1984), *Random Fields: Analysis and Synthesis*, MIT Press, Cambridge, MA.

Viera, S., Nielson, D., and Bigger, J. (1981), "Spatial Variability of Field Measured Infiltration Rate,"*Soil Science Society of America Journal*, 45, 1040-1048.

Vollmayr, H., Kleint, F., and Schuurmann, G. (1997), “Discrete Modeling of Water and Pesticide Movement in Soil,” *Water Resources Research*, 33 (7), 1743-1747.

Warner, S., Yamane, C., Gallinatti, J. and Hankins, D. (1998), "Considerations for Monitoring Permeable Ground-Water Treatment Walls," *Journal of Environmental Engineering*, 124(6), 524-529.

Warren, K., Arnold, R., Bishop, T., Lindholm, L, and Betterton, E (1995), “Kinetics and Mechanisms of Reductive Dehalogenation of Carbon Tetrachloride Using Zero Valent Metals,” *Journal of Hazardous Materials*, 41, 217-227.

Webb, E. (1992), “Simulation of Spatial Heterogeneity of Sedimentological and Hydrological Characteristics for Braided Stream Deposits,” Ph.D. Dissertation, Department of Geology, University of Wisconsin - Madison.

Webb, E. (1995), "Simulation of Braided Channel Topology and Topography," *Water Resources Research*, 31(10), 2603-2611.

Webb, E. and Anderson, M. (1996), “Simulation of Preferential Flow in Three-Dimensional, Heterogeneous Conductivity Fields with Realistic Internal Architecture,” *Water Resources Research*, 32(3), 533-545.

Wilson, N. (1995), *Soil, Water, and Groundwater Sampling*, Lewis Publishers, Boca Raton, FL.

Woodbury, A. and Sudicky, E. (1991), "The Geostatistical Characteristics of the Borden Aquifer," *Water Resources Research*, 27(4), 533-546.

Wu, T. (1973), “Probabilistic Analysis of Seepage,” *Journal of Soil Mechanics and Foundation Division*, ASCE, SM4, April, 323-340.

Yarus, J. and Chambers, R. (1994), *Stochastic Modeling and Geostatistics; Principles, Methods, and Case Studies*, American Society of Petroleum Geologists, Tulsa OK.

Zhang, Y., Zheng, C., Neville, C., and Andrews, C. (1995), ModIME, An Integrated Modeling Environment for MODFLOW, PATH3D, and MT3D, Version 1.0, S.S. Papadopulos & Associates, Inc., Bethesda, MD.

Zheng, C. (1992), MT3D, A Modular Three-Dimensional Transport Model for Simulation of Advection, Dispersion and Chemical Reactions of Contaminants in Groundwater Systems, S.S. Papadopulos & Associates, Inc., Bethesda, MD.

Zwiren, W. and Woodford, J. (1997), "Evaluation of Oxygen Delivery Systems for a Downgradient Treatment Zone in a High Groundwater Velocity Aquifer," *Proc. Petroleum Hydrocarbons and Organic Chemicals in Ground Water: Prevention*, Detection, and Remediation Conference, Houston, Nov. 12-14, 656-667.

APPENDIX I

METHOD FOR CALCULATING CONCENTRATION

Consider a representative element of width Δx and cross sectional area A so that the volume of the element is $A\Delta x$ (Fig A1a). Also consider stream tubes entering the face of the element, each adding mass to the element at a rate of $\dot{M}_i$. Under steady-state conditions, the concentration of the representative element is equal to:

$$C = \frac{\sum_i \dot{M}_i(\Delta x / v_{xi})}{V n} = \frac{\sum_i \dot{M}_i / v_{xi}}{A n} \qquad \text{(A1)}$$

where $\dot{M}_i$ is a mass loading rate of stream tube i ($\dot{M}_i$ is always positive for a steady input), v_{xi} is the velocity of the stream tube normal to A (i.e., the seepage velocity of groundwater through the element), V is volume of the element, and n is porosity. The quotient $\Delta x/v_{xi}$ is the residence time of mass in the volume from stream tube I (i.e., Δt_i). Since Δx is a constant it may be moved outside of the summation and cancelled.

Now consider particles starting from a steady-state source that have a constant concentration and move through the aquifer due to advection. Particle trajectories through the aquifer are calculated by Path3D and define stream-tubes.

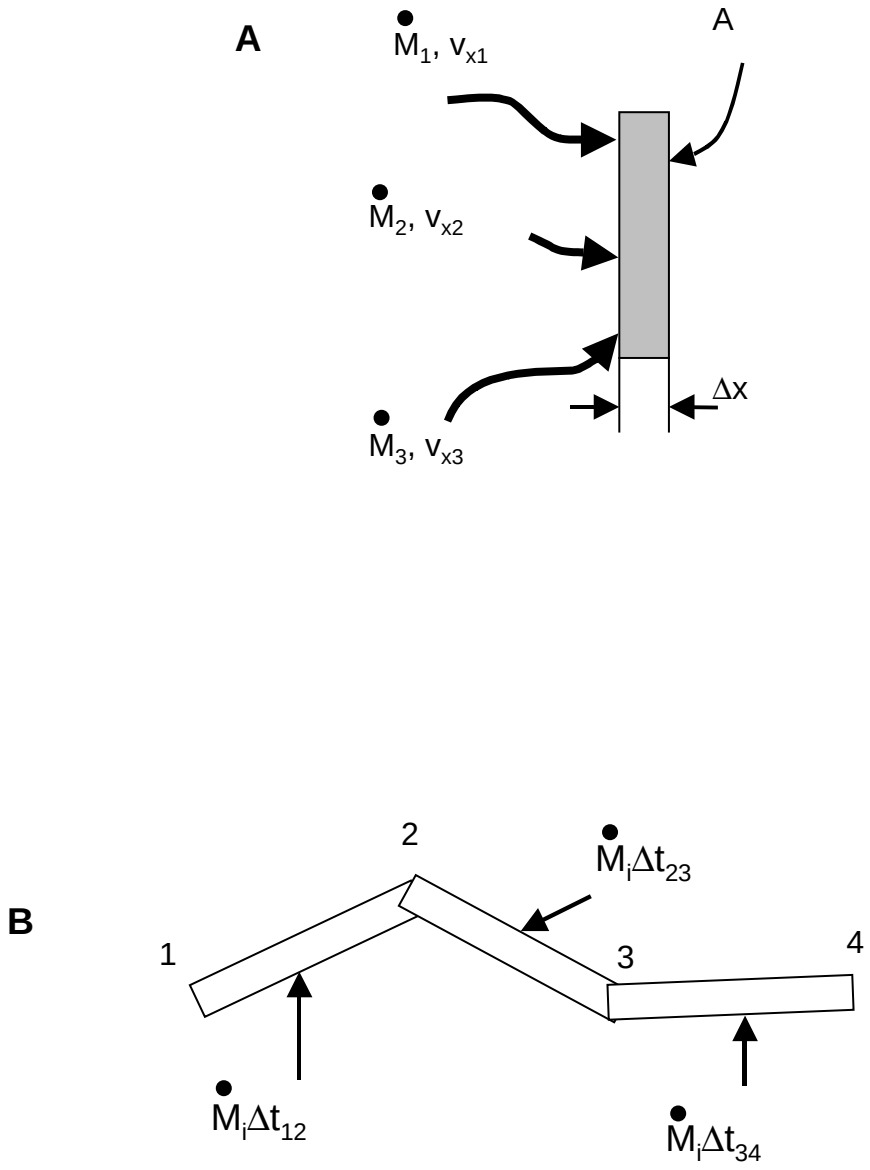

Fig. A1 Conceptual Model of a Stream Tubes Entering a Volume (A) and Passing Through a Reactive Zone (B).

Equation A1 is an expression for concentration of a representative element as a function of the mass loading rate into the element relative to the rate of groundwater entering the element. Equation A1 can also be used to calculate the rate of mass exiting an element at the source in each stream tube given a concentration of the source is known and some simplifying assumptions are made. The number of stream tubes (N) exiting the face of an element in the source zone is known because it is an input to Path3D (i.e., N = the number of particles). Each stream tube exiting the control volume is assumed to contribute an equal amount of mass to the control volume (i.e., all stream tubes are assumed to exit the element with the same velocity and mass loading rate). This assumption is valid provided that A is small so that stream tubes within A start near one another. For this study, A is 0.25 m^2. Given this assumption, the mass loading rate of each stream tube exiting the source ($\dot{M}_i$) is:

$$\dot{M}_i = \frac{C_s}{N} A n v_x \qquad \text{(A2)}$$

where C_s is a specified concentration at the source that is assumed to remain constant throughout the simulation (e.g., steady-state dissolution from a pool of DNAPL). Equation A2 is used to calculated $\dot{M}_i$ for the first N-1 stream tubes exiting an element. The $\dot{M}_i$ for the last stream tube exiting an element (i.e., $\dot{M}_N$) is adjusted using the expanded version of Eq. A1 to assure a constant source concentration.

Equation A2 defines the $\dot{M}_i$ into each stream tube exiting a representative element in the source zone. The $\dot{M}_i$ for the stream tubes can be thought of as the mass delivery rate (into or out of the volume), weighted by the velocity of the groundwater that is necessary to maintain a constant concentration at the source. In essence, $\dot{M}_i$ is the rate at which mass is carried into or out of an element by advection.

Reactions are handled by modeling increments of time using a series of plug flow models with first order reactions. When a stream tube enters a reactive zone (usually the PRB), mass is reduced according to:

$$\dot{M}_{i,t+\Delta t} \; \Delta t_{12} = \Delta t_{12} \, \dot{M}_{i,t} \exp(-k_{12} \, \Delta t_{12}) \qquad \text{(A3)}$$

where k_{12} is the reaction rate constant for the media between points 1 and 2 in Fig. A1b and Δt_{12} is the transit time of groundwater between points 1 and 2. Equation A3 is applied for each increment in time throughout the reactive zone (e.g., Δt_{23} and Δt_{34} in Fig. A1b) using the appropriate reaction rate constant (k_{23} and k_{34}, respectively). This method is prone to numerical error because errors propagate through time. To minimize errors due to rounding, double precision is used for $\dot{M}_i$ in the computer code, time steps are small, and a fourth order Runge-Kutta method is used for particle tracking.

At any point where concentration would like to be known, Eq. A1 is used to calculate the concentrations for an element around the point. The sum of $\dot{M}_i / v_{xi}$ is

calculated for all stream tubes that intersect a cross section centered on the point of interest. The sum is then divided by the product of porosity and the area of the cross section. This concentration is assigned to the point at the center of the area.

The method for assigning $\dot{M}_i$ to stream tubes and then recalculating concentration was verified by checking mass flux for a simulation. A simulation of a heterogeneous random field with a funnel and gate system was performed (Fig A2). This system yields a relatively complicated flow pattern as stream tubes pass through the funnel or around the gate. The reaction rate constant for the funnel is zero; therefore, under steady state conditions, total mass flux across any cross section of the aquifer should be equal. Mass flux through the aquifer was calculated at distances of 1 m, 2 m, 3.5 m, 4.5 m, 6 m, and 7 m from the source. Mass fluxes between cross sections were within 0.0005% of each other. This difference can be attributed to rounding and numerical error. Essentially, mass flux was constant across any cross section of the aquifer.

The stream tube method was further verified by comparing concentrations calculated with the stream tube approach to concentrations calculated by MT3D with a method of characteristics solution for several hypothetical aquifers where mass moved across the aquifers due to advection under steady-state flow. The three hypothetical aquifers used for testing are shown in Fig. A3. For each aquifer, steady-state concentrations at six cross-sections along the aquifer were obtained using each model. Concentrations across six cross-sections in the aquifers are shown in Fig. A4.

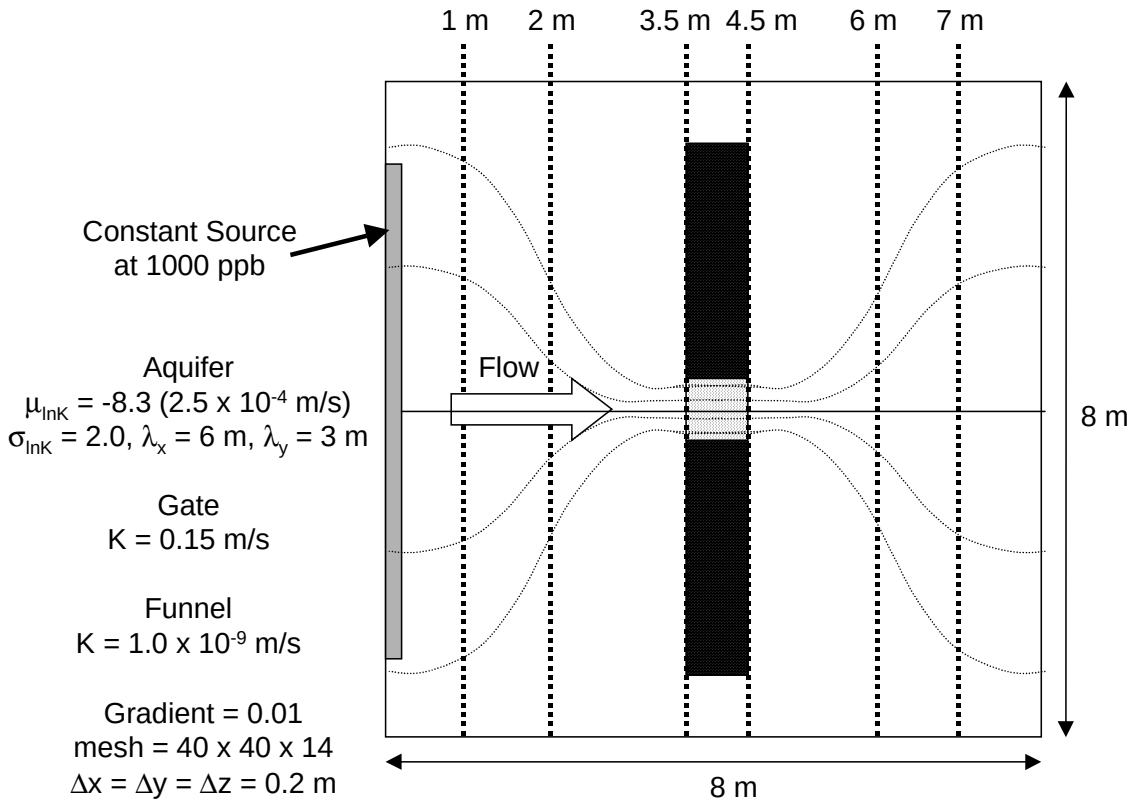

Fig. A2 Conceptual Model Used to Check Mass Flux through an Aquifer.

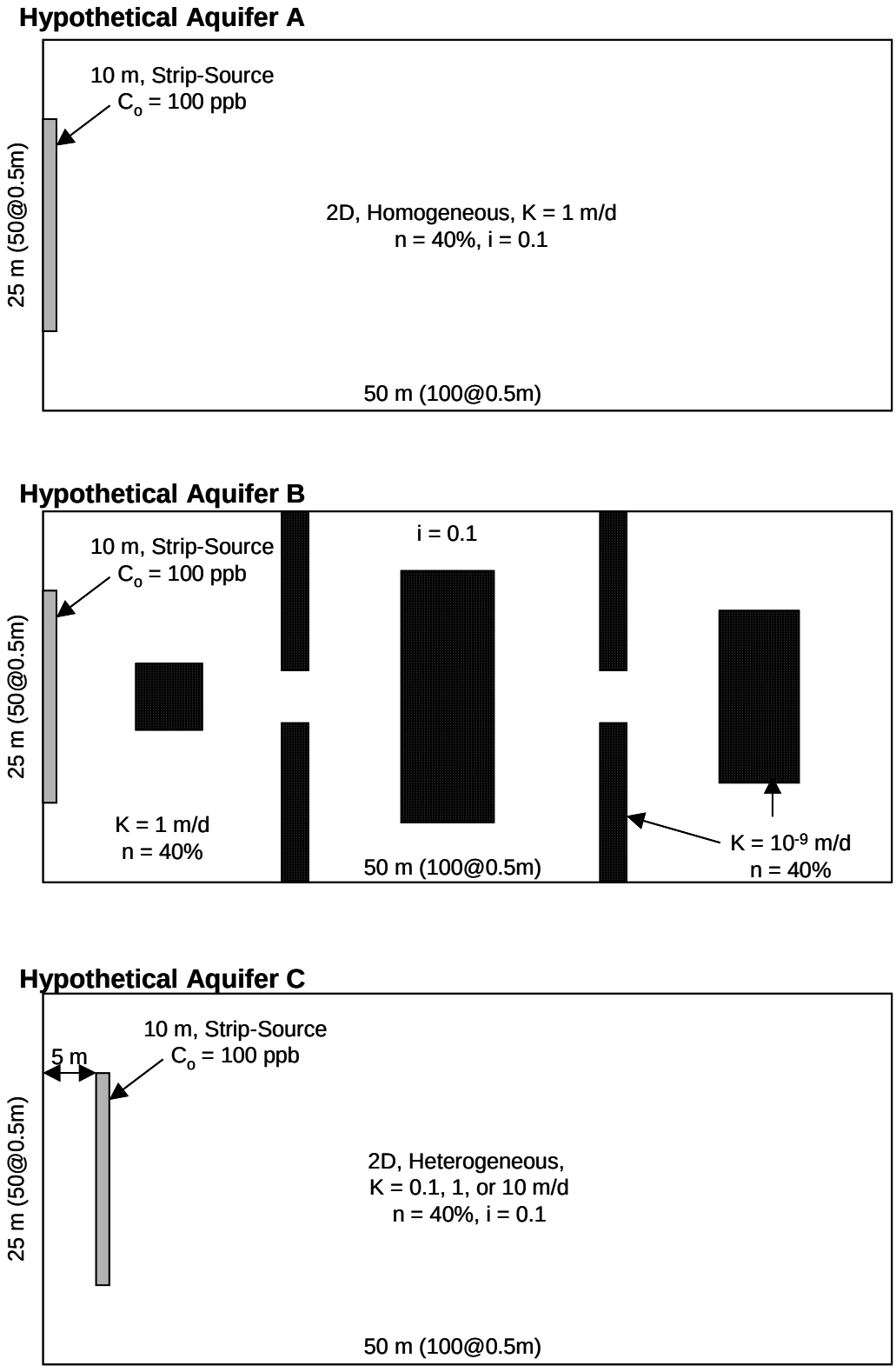

Fig. A3 Hypothetical Aquifers Used for Comparing Path3D and MT3D Results.

The stream tube method appears to capture the size and distribution of concentrations within the plume for all simulations. Results for Aquifer C have the most difference, but the MT3D solution also had the greatest mass balance error (i.e., 10.3%) and slowest run-time for Aquifer C. Differences in concentration predicted using the MT3D and stream tube methods for Aquifer C are typically less than 15% and both models make similar predictions for the size of the plume and distribution of mass. The slight differences in the solution are therefore tolerable given that a Monte-Carlo scheme is used with the stream tube method and it runs 500 to 50000 times faster than MT3D.

Hypothetical Aquifer A
(MT3D Solution Has 2.3% Mass Error)

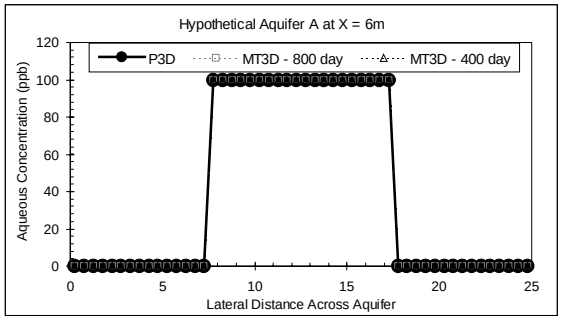

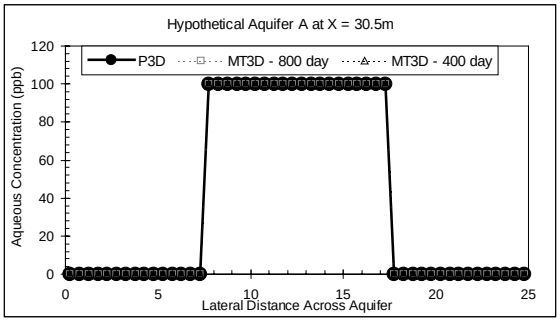

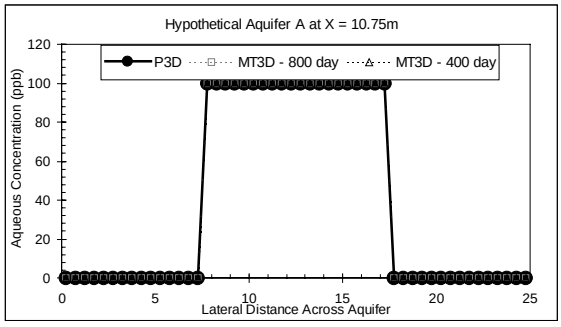

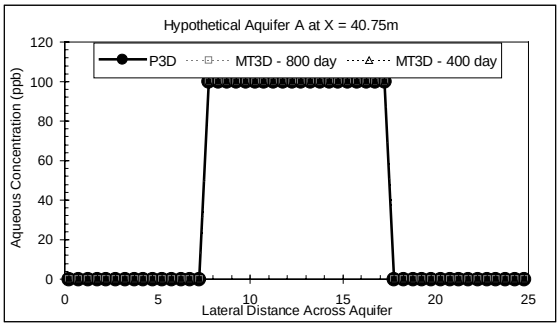

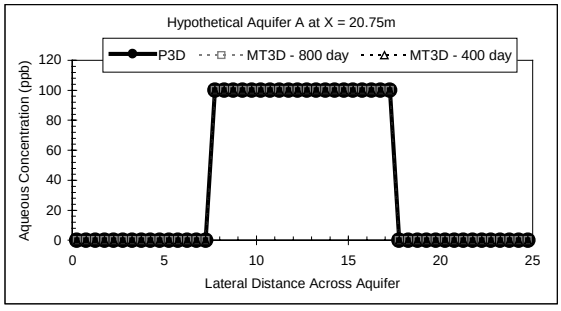

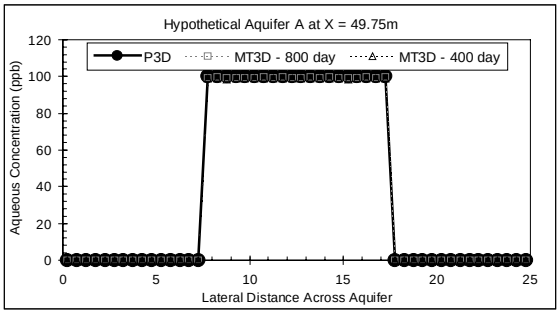

Hypothetical Aquifer B
(MT3D Solution Has 6.3% Mass Error)

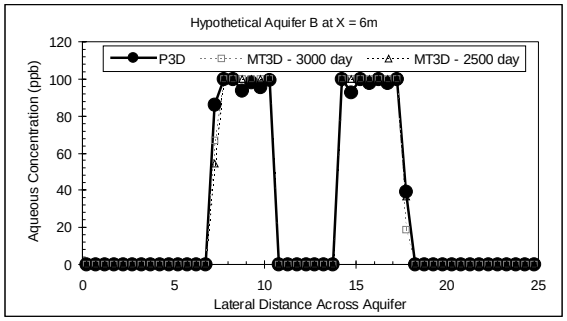

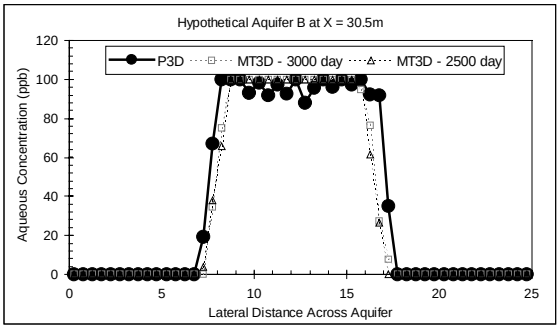

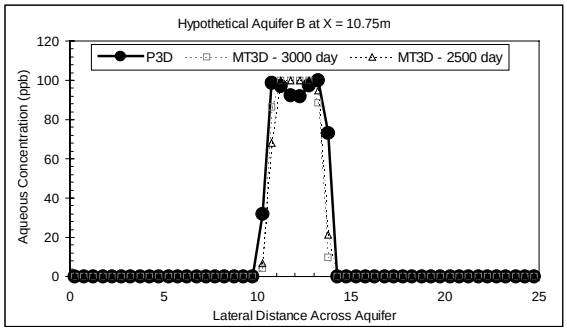

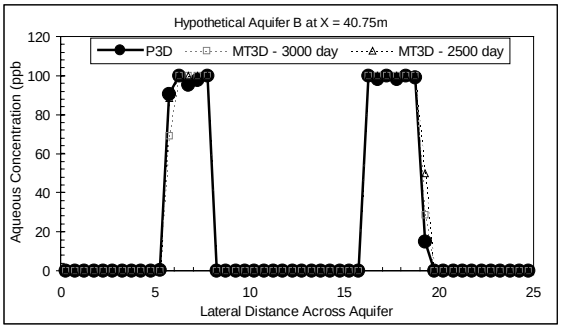

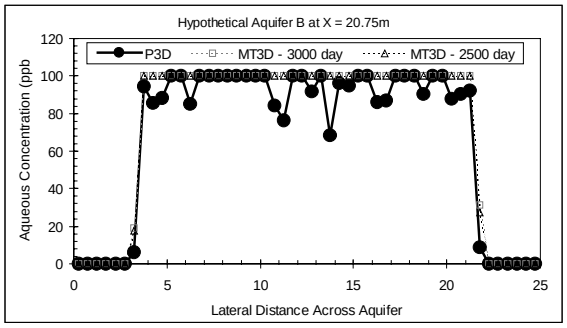

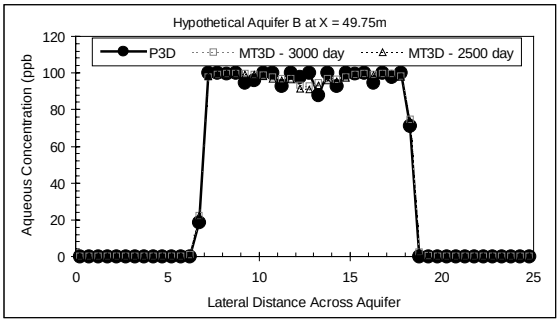

Hypothetical Aquifer C
(MT3D Solution Has 10.3% Mass Error)

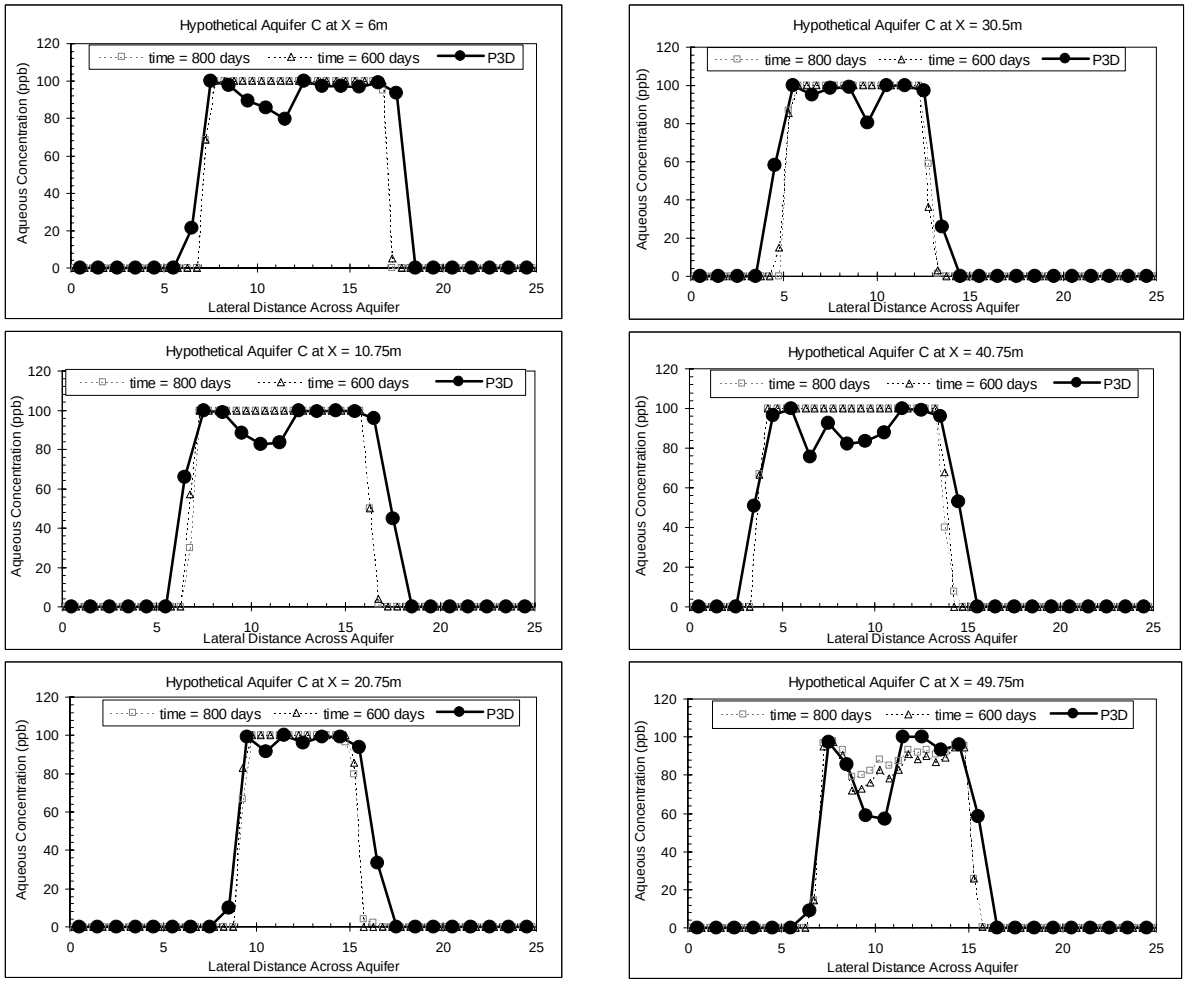

Fig. A4 Comparison of Path3D and MT3D Results for Hypothetical Aquifers.

APPENDIX II

ACCURACY OF THE EDITED P3D CODE

This project involved editing the source code for Path3D. The impact of these edits on the accuracy of the tracking algorithm is evaluated by comparing predictions of transit time made using Modime (which includes Path3D) and the edited version of Path3D. The conceptual model of the aquifer that was used for verification is shown in Fig. A2.1. For these simulations, a single particle was initially placed in the center of each finite difference element at the up-gradient constant head boundary of the aquifer (560 particles) and tracked to the down-gradient constant head boundary. Transit times were predicted using each code. Transit times predicted using the edited code were normalized by the transit time predicted using Modime and are shown in Fig. A2.2. The absolute error between estimates made using the two versions of the program is less than 0.015%; thus, edits made to Path3D for this study do not significantly affect the particle tracking algorithm.

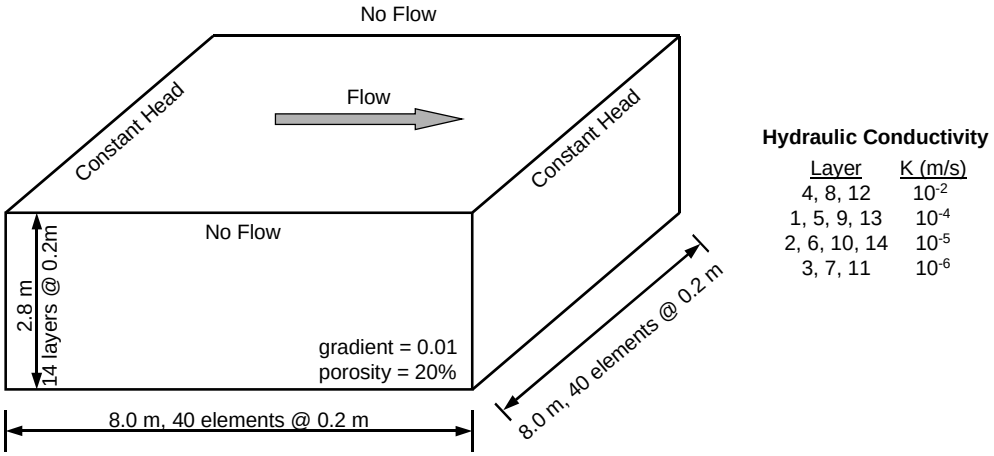

Fig. A5 Conceptual Model for Verifying Edits to Path3D.

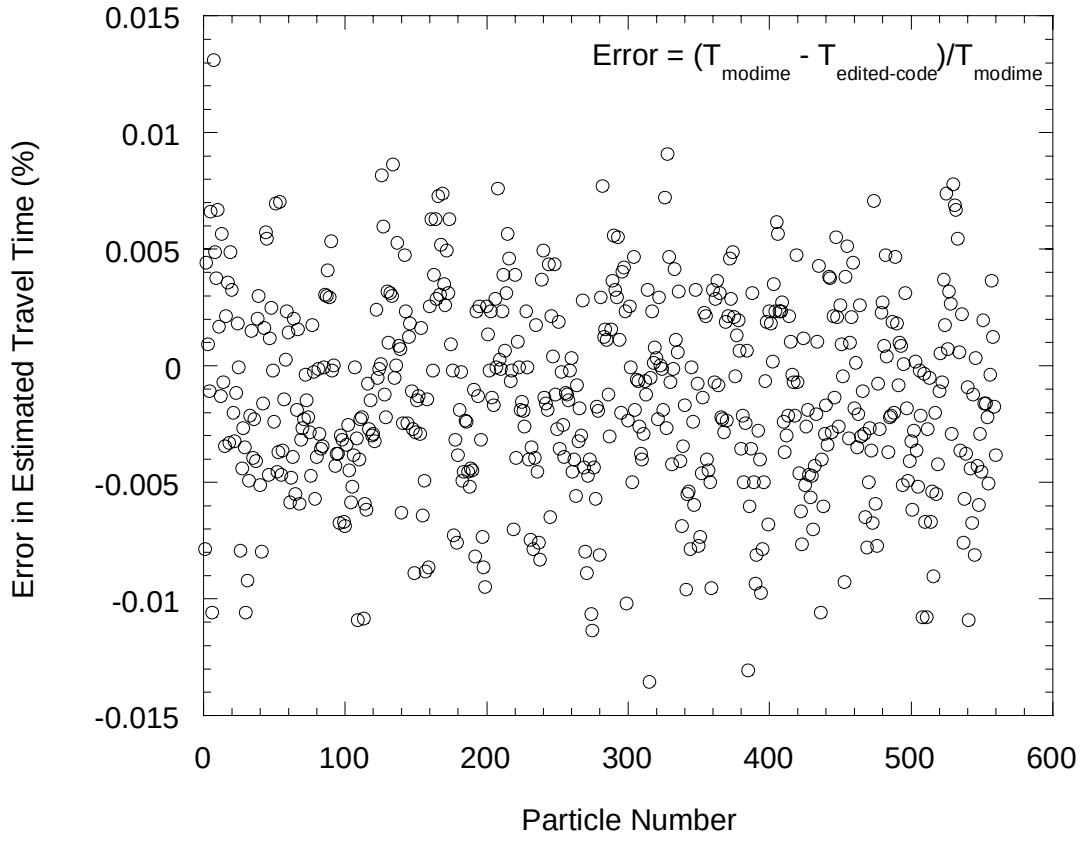

Fig. A6 Error in Predicted Transit Time Between Path3D from Modime and the Edited Source Used for this Study.